University of California, Santa Barbara

Department of Electrical and Computer Engineering

Mode-Locked Vertical-Cavity Semiconductor Lasers

by

Wenbin Jiang

A Dissertation submitted in partial satisfaction

of the requirements for the degree of

Doctor of Philosophy

in

Electrical and Computer Engineering

November 1993

Committee Members

Professor John E. Bowers, Chair

Professor Larry A. Coldren

Professor Yoshihisa Yamamoto (Stanford University)

Professor Pochi Yeh

Mode-Locked Vertical-Cavity Semiconductor Lasers

Electrical and Computer Engineering Department

University of California

Santa Barbara, CA 93106

Acknowledgments

Upon the completion of this dissertation, I would like to express my deep appreciation to Professor Bowers for his enthusiastic support and insightful advises during the last several years. I have gained enormously from his knowledgeable guidance.

I would like to acknowledge Professor Coldren, Professor Yamamoto and Professor Yeh for being on my Ph.D committee and for having provided very constructive suggestions on my researches. All of the ECE faculties deserve credits for having created such a wonderful environment for studies and researches. I have benefited a lot from taking their classes.

The Bowers group members have been very supportive to me since the first day I arrived at UCSB. I acknowledge Richard Mirin for having taken up his time and efforts to grow the wafers I requested, Dr. Mitsuaki Shimizu for the extremely useful discussions and the amiable collaborations, and Tom Reynolds for the AR coatings, device mountings and many other technical supports. Mode-locking group people have always been very helpful. The discussions with Dennis Derickson helped me understand more of the laser pulse chirping. Roger Helkey provided very important assistance in the electronics part of the laser mode-locking, as well as many other insightful comments on my writings. Alan Mar is always there to give you good suggestions. I acknowledge Dubravko Babic and Radha Nagarajan for the device design. Radha provided me very important data on the GaAs MQW structure when I was designing the first optically pumped mode-locked GaAs VCSEL. Dubravko generously offered me his programs for the DBR mirror evaluation and the current distribution modeling, which have been very important in designing the electrically

pumped mode-locked VCSEL. I acknowledge Judy Karin for having kindly let me share many of the equipment she needed herself at the time of my experiments. Her expertise in the laser maintenance guaranteed the smooth running of the femto lab when I was working on the optically pumped VCSELs. I acknowledge Gary Wang for having provided me the convenience of using the streak camera, Jim Dudley and Dan Tauber for having shown me how to use the streak camera, Gang Jia for having helped me to take the autocorrelation data, Paul Humphley for the computer data taking programs.

Thanks go to many other of my fellow graduate students whom I cannot name one by one. I have received a lot of encouragement and assistance from them.

I would like to acknowledge Dr. Stephen R. Friberg at NTT for having created opportunities for me to start the mode-locked VCSEL project while I was at NTT, and for having provided me with constant and sincere advises in every aspects.

Finally I acknowledge the support of this work from QUEST during my first year in the Ph.D program and from ARPA and Rome Laboratories during the rest of my years as a Ph.D student.

To Jianwen & Carrie

VITA

July, 1985:	B.S., Physics, Fudan University
July, 1988:	M.S., Optics, Fudan University
1989 - 1990:	Invited researcher, NTT Basic Research Labs
1990 - 1993:	Research Assistant, ECE Department
	University of California, Santa Barbara

PUBLICATIONS

1. Diechi Sun, Wenbin Jiang, and Fuming Li, " A 75 fsec pulse generated from a CPM dye laser", ACTA Optica Sinica, Vol. 10, 865 (1986). Chinese

2. Wenbin Jiang, Diechi Sun and Fuming Li, "Influence of colliding pulses on the chirp production of a saturable absorber", Opt. Comm., Vol. 64, 449 (1987)

3. Wenbin Jiang, Diechi Sun and Fuming Li, " Particle behavior of femtosecond optical pulses", Opt. Comm. Vol. 66, 152 (1988)

4. Wenbin Jiang, Diechi Sun and Fuming Li, " Transition Radiation of femtosecond optical pulses", Proc. Laser Materials & Laser Spectroscopy, (World Scientific Publishing, Singapore, 1988) P. 328

5. Wenbin Jiang, Diechi Sun and Fuming Li, "Observation of DFWM in the saturable absorber inside the CPM ring dye laser cavity", Proc. Laser

Materials & Laser Spectroscopy, (World Scientific Publishing, Singapore, 1988) P.333

6. Wenbin Jiang, Diechi Sun and Fuming Li, "The distortion of femtosecond optical pulses with Gaussian spatial distribution when propagating in free space", Chinese Phys. Lasers, Vol. 16, 96 (1989). Chinese

7. Wenbin Jiang, Diechi Sun and Fuming Li, "The distortion of femtosecond optical pulses with Gaussian spatial distribution when propagating in free space", Chinese Phys. (a translation journal of the American Institute of Physics), Vol. 10, N1: P.168 (1990)

8. Stephen R. Friberg and Wenbin Jiang, "Ultrafast switching using two-color soliton collisions", Photonic Switching II (K. Tada, and H. S. Hinton, eds., Springer-Verlag, Berlin 1990), P. 138

9. Stephen R. Friberg, Wenbin Jiang, Yoshitaka Sakai and Raymond J. Hawkins, "Observation of two-color soliton collisions in optical fiber", Ultrafast Phenomena VII, C.B. Harris, E.P. Ippen, G.A. Mourou and A. H. Zewail, eds. (Springer-Verlag, Berlin, 1990), P.184

10. Wenbin Jiang, Stephen R. Friberg, Hidetoshi Iwamura and Yoshihisa Yamamoto, "High powers and subpicosecond pulses from an external-cavity surface-emitting InGaAs/InP multiple quantum well laser", Appl. Phys. Lett. Vol. 58, 807 (1991)

11. Wenbin Jiang, Stephen R. Friberg, Hidetoshi Iwamura and Yoshihisa Yamamoto, "Collision-induced pulse shortening in a mode-locked linear-cavity NaCl color-center laser with an InGaAs/InP multiple-quantum-well saturable absorber", Opt. Lett. Vol. 16, 1165 (1991)

12 Wanghua Xiang, Stephen R. Friberg, Kimitaka Watanabe, Susumu Machida, Wenbin Jiang, Hidetoshi Iwamura, and Yoshihisa Yamamoto, "Femtosecond

external-cavity surface-emitting InGaAs/InP multiple-quantum-well laser", Opt. Lett. Vol. 16, 1394 (1991)

13. Wanghua Xiang, Wenbin Jiang and Yuzo Ishida, "Femtosecond pulses generated from non-colliding pulse mode-locked ring dye lasers", Opt. Comm., Vol. 86, 70 (1991)

14. Wenbin Jiang, Richard Mirin, and John E. Bowers, "Mode-locked GaAs vertical cavity surface emitting lasers", Appl. Phys. Lett., Vol. 60, 677 (1992)

15. Dennis J. Derickson, Roger J. Helkey, Alan Mar, John G. Wasserbauer, Wenbin Jiang, and John E. Bowers, "Modelocked semiconductor lasers: Short pulse, small package", Opt. & Photon. News, Vol. 3, 14 (1992)

16. J. J. Dudley, M. Ishikawa, B.I. Miller, D. I. Babic, R. Mirin, W. B. Jiang, J. E. Bowers, and E.L. Hu, "144 C operation of 1.3 μm InGaAsP vertical cavity lasers on GaAs substrates," Appl. Phys. Lett., Vol. 61, 3095 (1992)

17. Wenbin Jiang, Mitsuaki Shimizu, Richard P. Mirin, Thomas E. Reynolds and John E. Bowers, "Femtosecond periodic gain vertical-cavity lasers", Photo. Tech. Lett., Vol. 5, 23 (1993)

18 Wenbin Jiang, Mitsuaki Shimizu, Richard P. Mirin, Thomas E. Reynolds and John E. Bowers, "Femtosecond periodic gain vertical-cavity semiconductor lasers", OSA Proc. Ultrafast Electronics and Optoelectronics, Vol.14, 21 (1993)

19. Wenbin Jiang, Dennis J. Derickson, and John E. Bowers, "Analysis of laser pulse chirping in mode-locked vertical cavity surface emitting lasers", J. Quantum Electron., QE-29, 1309 (1993)

20. M. Shimizu, D. I. Babic, J. J. Dudley, W. B. Jiang and J. E. Bowers, "Thermal resistance of 1.3-μm InGaAsP vertical cavity lasers," Microwave Opt. Technol. Lett., Vol. 6, 455 (1993)

21. Wenbin Jiang, Mitsuaki Shimizu, Richard P. Mirin, Thomas E. Reynolds and John E. Bowers, "Electrically pumped mode-locked vertical cavity semiconductor lasers", Opt. Lett., Vol. 18, Nov. 15 (1993)

PRESENTATIONS

1. Wenbin Jiang, Diechi Sun and Fuming Li, "Influence of colliding pulses on the chirp production of a saturable absorber", 1987 International Conference of Lasers, Xiamen, China, November 1987

2. Wenbin Jiang, Diechi Sun and Fuming Li, "Observation of DFWM in saturable absorber inside the CPM ring dye laser cavity", Topical Meeting on Optical Pulses and Ultrafast Phenomena, Guangzhou, China, January 1988

3. Wenbin Jiang, Diechi Sun and Fuming Li, "Transition radiation of femtosecond optical pulses", 1988 Topical Meeting on Laser Materials & Laser Spectroscopy (IQEC'88 satellite meeting), Shanghai, China, July 1988

4. Wenbin Jiang, Diechi Sun and Fuming Li, "Observation of DFWM in saturable absorber inside the CPM ring dye laser cavity", 1988 Topical Meeting on Laser Materials & Laser Spectroscopy (IQEC'88 satellite meeting), Shanghai, China, July, 1988

5. Diechi Sun, Wenbin Jiang, and Fuming Li, "Fabrication of high Tc superconductor thin films using YAG lasers", Topical Meeting on High Tc Superconductor Materials, Zhejiang, China, November, 1988

6. Stephen R. Friberg, Wenbin Jiang, Yoshitaka Sakai, and Raymond Hawkins, "Observation of soliton collisions in optical fibers", Ultrafast Phenomena 1990, Monterey, California, May 1990

7. Stephen R. Friberg, Wenbin Jiang, "Ultrafast switching using two-color soliton collisions", International Topical Meeting on Photonic Switching, Kobe, Japan, 1990

8. Wenbin Jiang, Stephen R. Friberg, Hidetoshi Iwamura, and Yoshihisa Yamamoto, "External-cavity surface-emitting InGaAs/InP MQW lasers: high powers and subpicosecond pulses", Quantum Optoelectronics, WB3, Salt Lake City, Utah, March, 1991

9. Wenbin Jiang, Richard Mirin and John E. Bowers, "Mode-locked GaAs vertical cavity surface emitting lasers", LEOS Annual Meeting, PD2, San Jose, California, November, 1991

10. Wenbin Jiang, Dennis J. Derickson, Richard Mirin, and John E. Bowers, "Importance of laser cavity length detuning in mode-locked vertical cavity surface emitting lasers", CLEO '92, JThE2, Anaheim, California, May, 1992

11. J. J. Dudley, M. Ishikawa, B.I. Miller, D. I. Babic, R. Mirin, W. B. Jiang, M. Shimizu, J. E. Bowers, and E.L. Hu, "InGaAsP (1.3 μm) vertical cavity lasers using GaAs/AlAs mirrors", OSA Annual, FKK7, Albuquerque, NM, Sept. 1992

12. Wenbin Jiang, Dennis J. Derickson, and John E. Bowers, "Analysis of laser pulse chirping in mode-locked vertical cavity surface emitting lasers", High Speed Optoelectronic Devices and Circuits, Banff, Canada, August, 1992

13. Wenbin Jiang, Mitsuaki Shimizu, Richard P. Mirin, Thomas E. Reynolds and John E. Bowers, "Femtosecond periodic gain vertical-cavity semiconductor lasers", Ultrafast electronics & optoelectronics, MA4, San Francisco, CA, Jan. 1993

14. M. Shimizu, J.J. Dudley, D. I. Babic, W. B. Jiang and J. E. Bowers, "Conditions for continuous wave operation of 1.3 μm InGaAsP vertical cavity laser", OFC'93, WH18, San Jose, CA, Feb., 1993

15. J. E. Bowers, D. I. Babic, G. Wang, D. Tauber, W. B. Jiang, and R. Nagarajan, "Vertical cavity laser high speed dynamics and modeling", Integrated Photonics Research Topical Meeting, Palm Spring, CA, March, 1993

16. Wenbin Jiang, Mitsuaki Shimizu, Richard P. Mirin, Thomas E. Reynolds and John E. Bowers, "Electrically pumped mode-locked vertical cavity semiconductor lasers", LEOS Summer Topical Meeting/Optical Microwave Interactions, PD1, Santa Barbara, CA, July, 1993

17. Wenbin Jiang, and John E. Bowers, "Effect of carrier transport on mode-locked vertical-cavity semiconductor lasers," OSA annual, MWW3, Toronto, Canada, Oct., 1993

Abstract

Mode-Locked Vertical Cavity Semiconductor Lasers

by

Wenbin Jiang

In-plane semiconductor lasers can be mode locked to generate ultrashort pulses, but the output power is small because of the gain saturation limitation. Vertical cavity surface emitting lasers (VCSEL), on the other hand, have a large gain saturation energy because of the large active area. High power ultrashort optical pulses can thus be generated by mode locking a VCSEL. Optically pumped external cavity VCSELs have been synchronously mode locked to generate subpicosecond pulses with a peak power two orders of magnitude higher than that from an in-plane laser. However, pulses generated from the mode locked VCSEL are broadened because of the pulse chirping. The cause of this pulse chirping is analyzed. Carrier transport effect is identified as another cause of the pulse broadening. A periodic gain structure has been used to limit the carrier transport so that pulses with an intensity autocorrelation width of 300 fs have been directly generated from the mode-locked VCSEL. To make the mode-locked VCSEL compact, devices for electrical pumping have been designed and fabricated. Active mode locking of such devices has yielded pulses with a pulsewidth of 80 ps and a pulse energy of 4.6 pJ at a repetition rate of 1 GHz. This is the first electrically pumped mode locked VCSEL.

Table of Contents

Chapter 1 Introduction

1.1 Mode-locked lasers

Mode-locking was at first demonstrated in mid-1960s using He-Ne Lasers [1], Ruby lasers [2], and Nd^+ glass lasers [3]. Theories on both active mode-locking and passive mode-locking were developed in 1970s [4 - 6], and, by the end of the decade, subpicosecond pulses were generated from passive mode-locked dye lasers [7 - 9]. Colliding pulse mode-locking (CPM) of dye lasers in early 1980s [10] made sub-100 femtosecond pulses routinely available, and additive pulse mode-locking (APM) of color center lasers that was originated from the idea of a soliton laser pushed the wavelength of the sub-100 femtosecond pulses from the visible to the infrared [11, 12]. Kerr lens mode-locking of Ti: sapphire lasers was discovered in 1990 [13 - 14] and produced the shortest laser pulses [15] directly from the laser cavity without any additional external cavity pulse compression.

The rapid development of ultrashort pulse generation ignites applications in various areas of physics, chemistry and biology [16 - 18]. Under picosecond and femtosecond pulses, the optical damage threshold of most materials is greatly enhanced, thus making possible the observation of higher order nonlinear effects. The short pulses allow the investigation of the instantaneous nonlinear interactions between field and materials, such as instantaneous stimulated Raman scattering and instantaneous self-focusing. Those nonlinear processes are usually in the range of 100 fs to 100 ps. The measurements of those effects provide us with important information on dynamics of ultrashort pulses propagating within nonlinear mediums. Ultrafast time spectroscopy reveals enormous information on the rapid relaxation processes within liquids, solids and plasmas. Those time decay measurements

usually involve the interactions between light and exitons, phonons, plasmas or molecular oscillations. Other interests are such as the investigation of molecular polarization relaxation in liquids, energy exchange between molecules, and electron transitions. Ultrafast spectroscopy has also become a useful tool in biological measurements. Experiments have been performed in understanding the mechanisms of DNA, blood protein and other organic molecules.

Not only are ultrashort pulses important for optical measurements, but also useful for information processing and transmission. 80 Gbit/s solitons can transmit 80 km in the optical fiber at a bit-error-rate (BER) less than 10^{-9} [19] and 10 Gbit/s solitons can in principle transmit over unlimited distance [20], which is a very good alternative for optical communications. All optical switching has also been demonstrated with ultrashort pulses and solitons [21].

There are lots of other applications of ultrashort pulses, such as electro-optic sampling [22], terahertz electromagnetic wave generations [23], and time-resolved photo-luminescence spectroscopy [24].

1.2 Mode-locked edge emitting semiconductor lasers

Semiconductor lasers were demonstrated in 1962 by four groups almost simultaneously [25-28] only two years after the demonstration of the first laser [29]. Efforts have since been made in generating short optical pulses with semiconductor laser mode-locking. Limited success were reported with active mode locking by Harris [30] and passive mode locking by Morozov *et al*. [31], who observed deep modulations at a frequency of cavity roundtrip with GaAs p-n junction structure lasers in external cavities. Semiconductor laser mode-locking, however, had not gained very much success until the late 1970s.

The first successful operation of semiconductor laser mode locking was reported by Ho *et al*. [32], who actively mode locked a GaAlAs double heterojunction (DH) laser in an external cavity at a wavelength of 810 nm. Similar results were reported thereafter with either different diode lasers or different current bias schemes [33 - 35]. The pulse duration from an actively mode locked semiconductor laser was typically dozens of picoseconds. Passive mode locking with saturable absorbers was necessary in order to generate pulses of several picoseconds [36] or even subpicoseconds [37].

The pulses generated with the above techniques usually had substructures due to the reflection from the diode facet facing the external cavity. One approach to eliminate such an effect was to include a bandwidth limiting etalon in the laser cavity and/or to antireflectively (AR) coat the facet [38 - 41]. An electro-optic tuner (EOT) could be used in the cavity instead of the etalon for the bandwidth control as well as wavelength tuning as reported by Olsson *et al*. [42] in either a linear cavity or a ring cavity configuration.

A poor AR coating would induce multiple pulses [43]. The simulation by Morton *et al*. [44] indicated that multiple pulses would be induced even with an AR coating of only 0.1% reflectivity. The imperfect AR coating was also the origin of the instability for an actively mode locked semiconductor laser with strong pulse current injection [45]. Such a stringent requirement to AR coatings makes it imperative to look for other approaches to overcome the defects of AR coatings. Holbrook *et al*. [46, 47] actively mode locked an angled stripe laser in an external cavity. Bandwidth-limited pulses of 16 ps duration at a peak power of 1 W and a time-bandwidth product $\Delta\upsilon\Delta t$ of 0.36 were obtained. Chen *et al*. [48] and Chang *et al*. [49] reported Brewster-angled semiconductor diode lasers to be actively mode locked in external cavities. Mar *et al*. [50] eliminated multiple pulsing by using long laser chips to delay the reflected pulses into the off-region of the modulation. Helkey *et al*. [51]

demonstrated a curved waveguide diode laser to reduce the reflection from an AR coated facet and mode locked the laser in an external cavity. Derickson *et al*. [52] suppressed the multiple pulses caused by the imperfect AR coating using the intra-waveguide saturable absorber for a two-section diode laser in an external cavity. A saturated traveling-wave laser amplifier (TWA) could also be used to remove unwanted secondary pulses while amplifying and limiting the amplitudes of pulses from an actively mode-locked semiconductor laser [53].

Some applications require that the mode locked pulse sources to be tunable in wavelength. Although an EOT or a narrow band filter could be used in the cavity for the wavelength tuning [42, 54], the most widely used scheme is to replace the external cavity mirror by a grating [48, 49, 55 - 63]. The wavelength tunability is typically around 20 nm. A wider tuning range from 1.26 - 1.32 μm with a pulsewidth shorter than 6 ps was achieved with the combination of a mode locked laser terminated by a reflective grating in the external cavity and a grating-pair compressor [64].

Mode locked semiconductor lasers with higher repetition rate are useful in high bit rate optical communications and high speed optical computing. To increase the repetition rate, one approach is to mode lock the laser at the harmonic frequency of the cavity fundamental mode [40, 65 - 72]. A repetition rate of 20 GHz (tenth harmonic of the cavity fundamental mode) at a wavelength of 1.55 μm with a pulsewidth of 5 ps was generated in this way [66]. A compact external resonator using a Selfoc rod lens [73 - 75] or an optical-fiber [65 - 67, 76 - 78] is another approach to generate GHz repetition rate pulses. A more feasible approach to generate high repetition rate pulses is, however, to mode lock a monolithic diode laser. The monolithic diode laser can be actively mode locked, passively mode locked, or hybridly mode locked, owing to an earlier idea of a segmented-contact

device with independent current control to effect a localized absorbing region in the cavity [79]. Lau *et al*. [80] reported the passive mode-locking at 18 GHz by operating the single contact monolithic buried DH GaAlAs laser close to the catastrophic damage. Hybrid mode-locking was also demonstrated when a RF signal was applied to the laser. Higher repetition rate results were reported thereafter with active mode locking, passive mode locking or hybrid mode locking [81 - 96]. The highest repetition rate of 350 GHz was obtained with a monolithic colliding pulse mode locked (CPM) InGaAsP multiple quantum well (MQW) laser structure [92].

Efforts have also been made in generating the shortest possible pulses from mode locked semiconductor lasers. The typical pulsewidths from actively or passively mode locked semiconductor lasers are a few picoseconds, although there are also reports of subpicosecond pulse generation from either passive mode locking [37, 43] or active mode locking [69, 70]. A drawback of passive mode locking is the large timing jitter between pulses [97]. Hybrid mode locking [98, 99] is a good compromise that generates pulses of comparable pulsewidth to passive mode locking with small timing jitter between pulses [97]. CPM [10] is another important technique to generate subpicosecond pulses from semiconductor lasers. The first semiconductor CPM laser was reported by Van der Ziel *et al*. [100] in an external cavity with a saturable absorber at one facet of the device introduced by proton bombardment. Bursts of pulses of 0.56 ps FWHM at a repetition rates of 625 MHz were obtained. Vasil'ev *et al*. [101] reported a linear cavity CPM laser with a three-segment device in which the saturable absorber was located between the two gain sections. Pulses of 0.8 ps at a repetition rate of 710 MHz were generated. Wu and Chen *et al*. [90 - 92] monolithically incorporated the CPM technique in quantum well lasers. Pulses of 0.64 ps at a repetition rate of 350 GHz were generated. The fundamental limit to the pulsewidth from a mode locked semiconductor laser is the

gain bandwidth, which is typically around 50 fs. The actual pulsewidths from all the mode locked semiconductor lasers are substantially longer. Carrier variation induced pulse chirping [59, 102] is the main cause of the long pulses. Various chirp compensation techniques [62, 64, 103 - 106] can be used to compress the pulses. Subpicosecond pulses can routinely be generated by pulse compression outside of the laser cavity.

Table 1.2.1 Comparison of Different Mode-Locked Lasers

Laser Type	Dye	Ti:Al_2O_3	F - Center	Semiconductor
Pump Scheme	Optical	Optical	Optical	Electrical
Wavelength (μm)	0.35 - 1.0	0.68 - 1.05	0.8 - 3	0.5 - 10
Temperature	Room	Room	77 K	Room
Pulsewidth	~ 30 fs	~ 20 fs	~ 100 fs	~ 1 ps
Ave. Output Power (mW)	~ 10	~ 300	~ 100	~ 1
Peak Output Power (W)	~ 3 k	~ 100 k	~ 10 k	~ 1
Output Pulse Energy	~ 0.1 nJ	~ 2 nJ	~ 1 nJ	~ 1 pJ
Intra-Cavity Pulse Energy	~ 3 nJ	~ 40 nJ	~ 10 nJ	~ 1 pJ

Due to the small gain saturation energy, the output power from a mode locked semiconductor laser is small. The peak power is limited to a few Watts in the best cases [46, 47, 57, 106]. Applications such as soliton optical communications, optical switching, optical clock distribution, etc., require high power pulses. Amplification using traveling wave amplifiers (TWA) [53, 107 -109] is an attractive way in boosting the pulse energy. A peak power of 165 W at the pulsewidth of 200 fs was

obtained in this way [110]. High CW output power can be generated from phase-locked diode array lasers. Mode locking of those array lasers looks promising in generating high energy pulses [94, 111 - 115].

Comparing with other mode locked solid state lasers and mode locked dye lasers (Table 1.2.1), semiconductor lasers are still low in output power and long in pulsewidth. They have, however, the advantage of being electrically pumped. Mode-locked semiconductor lasers are compact, easy to use and cost-effective. They can be applied in the areas that do not require high powers. For example, those lasers can be used in fiber optical communications for data transmission [116]. They can be used for electro-optic sampling [117], optical computing [118], gyroscopes [119], etc. Modern epitaxial techniques can tailor the materials for the wavelength ranging from the visible to the infrared, which gives mode-locked semiconductor lasers an extra advantage to be applied where other types of lasers do not work.

1.3 Vertical-cavity surface-emitting lasers

In the late 1970s, Iga *et al.* [120] proposed to have the semiconductor laser oscillating perpendicular to the plane of the device surface [Fig. 1.3.1(a)] to overcome the difficulties facing the cleaved in-plane semiconductor lasers. VCSELs offer many advantages over in-plane lasers. First, the monolithic fabrication process and wafer scale probe test will substantially reduce the manufacturing cost since only good devices will be kept for further packaging [121]. Second, a densely packed two-dimensional laser array can be fabricated since the device occupies no larger area than commonly used electronic devices [122]. This is very important for applications in optoelectronic integrated circuits. Third, the microcavity length allows inherently single longitudinal cavity mode operation because of its large mode spacing.

Temperature-insensitive devices can be fabricated with an offset between the wavelength of the cavity mode and the active gain peak [123]. Finally, the device can be designed with a low numerical aperture, circular output beam to match the optical mode of an optical fiber, thereby permitting efficient coupling without additional optics [124].

A conventional in-plane semiconductor laser [Fig.1.3.1(b)] utilizes its cleave edges as the laser cavity reflectors since the length of the active layer is usually several hundred micrometers, which provides enough gain to overcome the cavity reflector loss. A VCSEL, however, needs both of its surfaces to be highly reflective to decrease the cavity mirror loss since its active layer is usually less than 1 μm thick. The first VCSEL was demonstrated with GaInAsP/InP in 1979, which was operating pulsed at 77 K with the annealed Au at both sides as reflectors [120]. A room temperature pulsed operating VCSEL was demonstrated with a GaAs active region in 1984 [125]. Room temperature CW operating GaAs VCSELs succeeded by improving both the mirror reflectivity and current confinement [126].

At present, the highest output power is obtained from an InGaAs/GaAs VCSEL with GaAs/AlAs monolithic diffractive Bragg reflectors (DBR) mounted on a diamond heat sink [127]. Lasing threshold of sub-mA or high wall-plug efficiency have also been reported with the same material-based VCSELs [128, 129]. Room temperature CW InGaAsP/InP VCSELs have met some difficulties primary due to a low index difference between GaInAsP and InP, which causes difficulty in preparing highly reflective monolithic DBR [130]. Nevertheless, a CW InGaAsP VCSEL was recently reported operating at 15 ˚C with dielectric mirrors [131]. Record low threshold current of 9 mA at room temperature has been demonstrated in InGaAsP VCSELs using GaAs/AlAs DBR mirrors [132].

Two dimensional (2-D) arrayed VCSELs can find important applications in stacked planar optics, such as the simultaneous alignment of a tremendous number of optical components used in parallel multiplexing lightwave systems and parallel optical logic systems, etc. High output powers are also possible from phase-locked 2-D arrayed VCSELs. There have been some demonstrations of 2-D arrayed devices [122, 133]. Coherent coupling of these arrayed lasers has been reported [134].

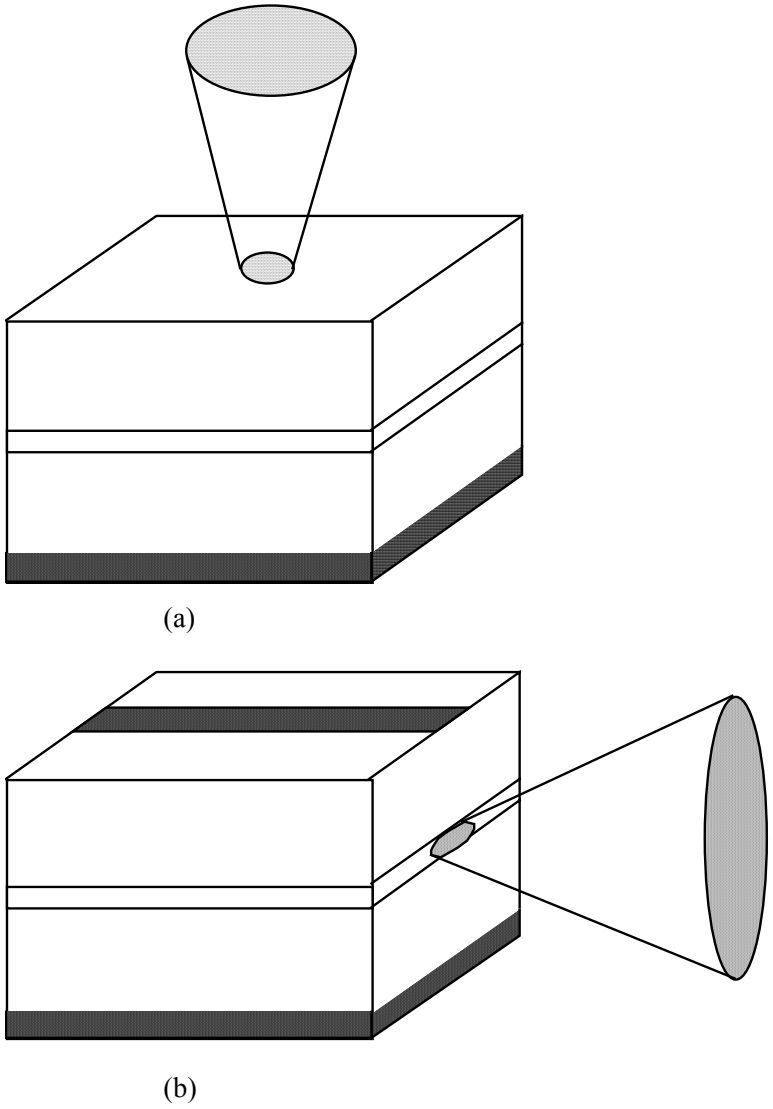

(a)

(b)

Figure 1.3.1 (a) A vertical-cavity surface-emitting laser, and (b) an edge emitting laser.

1.4 Surface-emitting laser mode-locking

Many applications require sub-picosecond pulses with high peak powers from mode-locked semiconductor lasers. The peak power of a mode-locked in-plane semiconductor laser is, however, less than one percent of that of the dye lasers or other solid state lasers (See Table 1.2.1), and so is the pulse energy. Is there any way to generate high peak power laser pulses from semiconductor lasers? External cavity amplification of those low power pulses with a traveling waveguide amplifier is certainly an approach [53, 107 - 110], but the amplified spontaneous emission (ASE) accompanied with the amplified laser pulses will deteriorate the laser quality. Extra chirping will also be brought to the pulses during the amplification, and an external chirp compensation set-up will thus be imperative. Sometimes this additional chirp is not linear, and the chirp compensation becomes difficult. Phase-locked array laser mode-locking is another approach [94, 111 - 115], but the external cavity coupling is difficult. The peak powers are also limited to several Watts at present.

Is there any alternative to generate high power pulses directly from mode-locked semiconductor lasers? Look at the gain saturation energy of active mediums, as expressed by

$$\varepsilon_s = \frac{h\nu\sigma}{\Gamma\, dg/dN} \tag{1.4.1}$$

where $h\upsilon$ is the laser photon energy, σ is the gain cross sectional area, Γ is the transverse mode confinement factor, and dg/dN is the differential gain. For a semiconductor laser with $\sigma = 0.1 \times 1\ \mu m^2$, $\Gamma = 0.3$, $\lambda = 0.88\ \mu m$, and $dg/dN = 3 \times 10^{-16}\ cm^2$, the gain saturation energy is $\varepsilon_S = 2.5$ pJ, a typical value for the intracavity

pulse energy in mode-locked semiconductor lasers (See Table 1.2.1). In order to generate high energy pulses, the gain saturation energy ε_s has to be increased. Both the differential gain *dg/dN* and the lasing frequency υ in the expression (1.4.1) are intrinsic to materials and hard to change, but the gain cross sectional area σ is an easily variable parameter. For a VCSEL with $\sigma = 10 \times 10\ \mu m^2$, for example, the gain saturation energy ε_s will be 750 pJ if Γ is taken as unity. The intracavity laser pulse energy from a VCSEL can therefore be at least two orders of magnitude larger than that from an in-plane semiconductor laser. The area of a VCSEL could be $50 \times 50\ \mu m^2$ or even larger. To this end, it becomes clear that the VCSEL mode-locking will be a good approach to generate ultrashort pulses with high pulse energy. The better beam quality from such a mode locked VCSEL will also be more useful in applications.

Table 1.4.1 List of Mode-locking Techniques

	Mode-Locking Method	Examples	
	Sychronous Optical Pumping	YAG Laser Pumped Color Center Laser	
	Active Modulation	Mode-locked YAG Laser	
	Saturable Absorber	CPM Dye Laser	
	Additive Pulse Mode-locking (APM)	Mode-locked Color Center Laser	
	Kerr Lens Effect	Mode-locked Ti:Saphire Laser	
	A Combination of Active and Passive Mode-locking	Coherent Satori Dye Laser	

Up to now mode-locking has frequently been mentioned. Simply speaking, mode-locking is a technique to generate ultrashort optical pulses from a laser. Detailed analysis on mode-locking techniques can be found in text books [135, 136]. Mode-locking is generally classified into three categories --- active mode-locking, passive mode-locking and hybrid mode-locking. More detailed categorization of mode-locking is shown in Table 1.4.1. Active mode-locking with RF current modulation or synchronous electrical pulse pumping and passive mode-locking with saturable absorbers are the two commonly used methods to generate ultrashort pulses from in-plane semiconductor lasers. To demonstrate the mode-locking of VCSELs, optical pumping similar to synchronous pumping of a dye laser or a color center laser was initially used.

Synchronous optical pumping has the advantage of higher pump efficiency at reduced heat generation, as well as the simple laser cavity configuration. The laser wavelength from a synchronously mode-locked laser is generally tunable. Two synchronized pulse trains at different wavelengths (one pump, one laser) are good sources for certain pump-probe measurements. Synchronous optical pumping shows effectiveness in mode locking a VCSEL to generate ultrashort optical pulses with high peak power or high pulse energy. Actually almost any direct bandgap semiconductor materials can be used for this purpose, thus ultrashort pulses with a wavelength ranging from visible to the far infrared can in principle be obtained simply by using different bandgap semiconductor materials. Synchronous mode locking of a semiconductor laser was earlier reported with a bulk GaAs crystal of 4 × 5 × 10 mm as the gain in the external cavity using two photon absorption pumping [137, 138]. Tunable picosecond pulses covering a wavelength range of 840 - 885 nm was generated over a temperature range from 97 to 260 K. Peak power of 1 MW at 97 K was achieved because of the large active volume involved. Synchronous mode

locking of platelet lasers, the prototype of VCSEL mode locking, was reported with CdS, CdSe, CdSSe, InGaAsP, and ZnCdS semiconductor materials as gain mediums when pumped by either a mode locked Ar^+ laser or a mode locked YAG laser [139 - 142]. Those semiconductor platelets of generally a few micrometer thick were kept at liquid nitrogen temperature during the laser operation. The output pulsewidths from those mode locked lasers were several picoseconds and the highest peak power was 50 W from the InGaAsP platelet laser. All mode locked platelet lasers were tunable in wavelength, ranging from 490 nm to 2 μm [141, 143].

VCSEL gain switching, an alternative to the mode-locking, is another approach in generating short optical pulses with high peak powers. An earlier version of a gain switched VCSEL was an optically pumped film laser made of single-crystal GaAs film of 1 - 2 μm thick sandwiched between highly reflective dielectric mirrors. The VCSEL could generate 1 ps pulses with a peak power of 1 - 10 W [144 - 145]. The film laser was tunable in wavelength from 890 nm to 770 nm by using the wedged cavity [146]. Thin-film $In_{1-x}Ga_xAs_yP_{1-y}$ lasers of different compositions, including InP and $In_{0.53}Ga_{0.47}As$, were made to lase between 0.77 and 1.65 μm [147, 148]. Pulses from film lasers were chirped and could be compressed in a dispersive fiber [149, 150]. All of those gain switched film lasers were pumped at low repetition rate to prevent device heating. With the improvement of semiconductor epitaxial techniques, better heat dissipation has been achieved by replacing dielectric mirrors with monolithic semiconductor DBR mirrors and gain-switched periodic-gain VCSELs were able to generate 4 ps pulses by optical pumping at 80 MHz [151 -153]. Electrically gain-switched VCSELs have also been reported, but at wider pulsewidths and lower peak powers [154 -157].

This dissertation concludes the work performed on mode-locked vertical-cavity lasers. Mode locked GaAs VCSEL at room temperature will be demonstrated with

synchronous optical pumping. Pulses of 320 fs with a peak power of 64 W are achieved after chirp compensation with a grating-pair compressor (Chapter 2). The use of a periodic gain structure enables pulses with a correlation width of 300 fs directly generated from the mode locked VCSEL (Chapter 3). 1.5 μm is an important wavelength for optical communications and soliton transmissions. The synchronously mode locked InGaAs/InP VCSEL research was conducted while I was at NTT. The mode-locked laser produced pulses with an average output power of 190 mW. Subpicosecond pulses were generated with chirp compensation. The laser wavelength was tunable over 70 nm around 1.5 μm (Chapter 2).

One of the advantages of a semiconductor laser is its ability to be electrically pumped. Electrical pumping will ensure the mode locked VCSEL to be compact and cost effective. An electrically pumped actively mode locked VCSEL was demonstrated in this dissertation. Chapter 4 will discuss the electrically pumped device processing and characterization, as well as the mode locking operation. More work remains to be done in optimizing the design of the device structure and in searching for the better mode-locking technique for this type of laser.

Chirping is usually accompanied with the high energy pulses from the mode locked VCSEL with optical pumping. The chirping is sometimes very linear. Theoretical analysis reveals that pulse chirping comes from the pump induced cross-phase-modulation (XPM) and gain saturation induced self-phase-modulation (SPM) (Chapter 5). Carrier transport because of the spatial hole-burning also broadens the laser pulsewidth. Appropriate gain structure design can control pulse chirping and carrier transport, resulting in the generation of subpicosecond pulses directly from the mode-locked VCSEL (Chapter 6).

In short, mode locked VCSELs have shown the ability of generating subpicosecond pulses with high peak powers. Future work especially with electrically pumped mode-locked VCSEL will be discussed in the Conclusions (Chapter 7).

References

[1] L. E. Hargrove, R. L. Fork, and M. A. Pollack, "Locking of He-Ne laser modes induced by synchronous intracavity modulation," *Appl. Phys. Lett.*, **5**, 4 (1964)

[2] H. W. Mocker, R. J. Collins, "Mode competition and self-locking effects in a Q-switched ruby laser," *Appl. Phys. Lett.*, **7**, 270 (1965)

[3] A. J. De Maria, D. A. Stetser, H. Heynau, "Self mode-locking of lasers with saturable absorbers," *Appl. Phys. Lett.*, **8,** 174 (1966)

[4] H. A. Haus, "A theory of forced modelocking," *IEEE J. Quantum Electron.*, **QE-11**, 323 (1975)

[5] H. A. Haus, "Theory of modelocking with a fast saturable absorber," *J. Appl. Phys.*, **46**, 3049 (1975)

[6] H. A. Haus, "Theory of modelocking with a slow saturable absorber," *IEEE J. Quantum Electron.*, **QE-11**, 736 (1975)

[7] C. V. Shank, and E. P. Ippen, "Subpicosecond kilowatt pulses from a mode-locked cw dye laser," *Appl. Phys. Lett.*, **24**, 373 (1974)

[8] I. S. Ruddock, and D. J. Bradley, "Bandwidth-limited subpicosecond pulse generation in mode-locked cw dye lasers," *Appl. Phys. Lett.*, **29**, 296 (1976)

[9] J. C. Diels, E. W. Van Stryland and G. Benedict, "Generation and measurement of pulses of 0.2 psec duration," *Opt. Comm.*, **25**, 93 (1978)

[10] R. L. Fork, B. I. Greene, and C. V. Shank, "Generation of optical pulses shorter than 0.1 ps by colliding pulse mode-locking," *Appl. Phys. Lett.*, **38**, 671 (1981)

[11] L. F. Mollenauer, and R. S. Stolen, "The soliton laser," *Opt. Lett.*, **9**, 13 (1984)

[12] K. J. Blow and B. P. Nelson, "Improved mode locking of an F-center laser with a nonlinear nonsoliton external cavity," *Opt. Lett.*, **13**, 1026 (1988)

[13] D. E. Spence, P. N. Kean, and W. Sibbett, "60-fsec pulse generation from a self-mode-locked Ti-sapphire laser," *Opt. Lett.*, **16**, 42 (1991)

[14] N. Sarukura, Y. Ishida, and H. Nakano, "Generation of 50-fsec pulses from a pulse-compressed, cw, passively mode-locked Ti-sapphire laser," *Opt. Lett.*, **16**, 153 (1991)

[15] M. T. Asaki, C. P. Huang, D. Garvey, J. P. Zhou, H. C. Kapteyn, and M. M. Murnane, "Generation of 11-fs pulses from a self-mode-locked Ti-sapphire laser," *Opt. Lett.*, **18**, 977 (1993)

[16] N. Bloembergen, "*Nonlinear Optics*" (Benjamin, New York, 1965, 1977 printing)

[17] S. L. Shapiro, "*Ultrashort Light Pulses*," (Springer-Verlag, 1977)

[18] *Ultrafast Phenomena I - VIII* (1978 - 1992), Springer Series in Chemical Physics, (Springer-Verlag, Berlin)

[19] K. Iwatsuki, K. Suzuki, S. Nishi, and M. Saruwatari, "80 Gb S optical soliton transmission over 80 km with time polarization division multiplexing," *IEEE Photon. Tech. Lett.*, **5**, 245 (1993)

[20] M. Nakazawa, K. Suzuki, E. Yamada, H. Kubota, Y. Kimura, and M. Takaya, "Experimental demonstration of soliton data transmission over unlimited distances with soliton control in time and frequency domains," *Electron. Lett.*, **29**, 729 (1993)

[21] S. R. Friberg, A. M. Weiner, Y. Silberberg, B. G. Sfez, and P. S. Smith, "Femtosecond switching in a dual-core-fiber nonlinear coupler," *Opt. Lett.*, **13**, 904 (1988); K. J. Blow, N. J. Doran, and B. K. Nayar, "Experimental demonstration of optical soliton switching in an all-fiber nonlinear Sagnac interferometer," *Opt. Lett.*, **14**, 754, 1989

[22] B. H. Kolner, D. M. Bloom, and P. S. Cross, "Electro-optic sampling with picosecond resolution," *Electron. Lett.*, **10**, 574 (1983)

[23] L. Xu, X. C. Zhang, and D. H. Auston, "Terahertz beam generation by femtosecond optical pulses in electro-optic materials," *Appl. Phys. Lett.*, **61**, 1784 (1992)

[24] S. Charbonneau, "Picosecond photoluminescence spectroscopy in highly excited semiconductors," *Opt. Eng.*, **28**, 1101 (1989)

[25] R. N. Hall, G. E. Fenner, J. D. Kingsley, T. J. Soltys, and R. O. Carlson, "Coherent light emission from GaAs junctions," *Phys. Rev. Lett.*, **9**, 366 (1962)

[26] M. I. Nathan, W. P. Dumke, G. Burns, F. H. Dills, and G. Lasher, "Stimulated emission of radiation from GaAs p-n junctions," *Appl. Phys. Lett.*, **1**, 62 (1962)

[27] N. Holonyak, and S. F. Bevacqua, "Coherent (visible) light emission from $Ga(As_{1-x}P_x)As$ junctions," *Appl. Phys. Lett.*, **1**, 82 (1962)

[28] T. M. Quist, R. J. Keyes, W. E. Krag, B. Lax, A. L. McWhorter, R. H. Rediker, and H. J. Zeiger, "Semiconductor maser of GaAs," *Appl. Phys. Lett.*, **1**, 91 (1962)

[29] T. H. Maiman, "Stimulated optical radiation in ruby," *Nature*, **187**, 493 (1960)

[30] E. P. Harris, "Spiking in current-modulated CW GaAs external cavity lasers," *J. Appl. phys.*, **42,** 892 (1971)

[31] V. N. Morozov, V.V. Nikitin, and A. A. Sheronov, "Self-synchronization of modes in a GaAs semiconductor injection laser," *JETP Lett.* **7,** 256 (1968)

[32] P. T. Ho, L. A. Glasser, E. P. Ippen, and H. A. Haus, "Picosecond pulse generation with a CW GaAlAs laser diode," *Appl. Phys. Lett.*, **33**, 242 (1978)

[33] L. A. Glasser, "CW mode locking of a GaInAsP diode laser," *Electron. Lett.*, **14**, 725 (1978)

[34] H. Ito, H. Yokoyama, S. Murata, H. Inaba, "Picosecond optical pulse generation from an R. F. modulated AlGaAs D. H. diode laser," *Electron. Lett.*, **15**, 738 (1979)

[35] J. P. van der Ziel and R. M. Mikulyak, "Mode locking of strip buried heterostructure (AlGa)As lasers using an external cavity," *J. Appl. Phys.*, **51**, 3033 (1980)

[36] E. P. Ippen, D. J. Eilenberger, and R. W. Dixon, "Picosecond pulse generation by passive mode locking of diode lasers," *Appl. Phys. Lett.*, **37**, 267 (1980); "Picosecond pulse generation with diode lasers," *Picosecond Phenomena II*, P. 21 (Ed. R. M. Hochstrasser, W. Kaiser, and C. V. Shank, Springer-Verlag, 1980)

[37] H. Yokoyama, H. Ito, and H. Inaba, "Generation of subpicosecond coherent optical pulses by passive mode locking of an AlGaAs diode laser," *Appl. Phys. Lett.*, **40**, 105 (1982)

[38] P. T. Ho, "Coherent pulse generation with a GaAlAs laser by active mode locking," *Electron. Lett.*, **15**, 527 (1979)

[39] H. Ito, H. Yokoyama, H. Inaba, "Bandwidth limited picosecond optical pulse generation from actively mode-locked AlGaAs diode laser," *Electron. Lett.*, **16**, 620 (1980)

[40] J. P. van der Ziel, "Active mode locking of double heterostructure lasers in an external cavity," *J. Appl. Phys.*, **52**, 4435 (1981)

[41] J. C. AuYeung and A. R. Johnston, "Picosecond pulse generation from a synchronously pumped mode-locked semiconductor laser diode," *Appl. Phys. Lett.*, **40**, 112 (1982)

[42] A. Olsson and C. L. Tang, "Active mode locking of linear and ring external-cavity semiconductor lasers," *IEEE J. Quantum Electron.*, **QE-17**, 1977 (1981)

[43] J. P. van der Ziel, W. T. Tsang, R. A. Logan, R. M. Mikulyak, and W. M. Augustyniak, "Subpicosecond pulses from passively mode-locked GaAs buried optical guide semiconductor lasers," *App. Phys. Lett.*, **39**, 525 (1981)

[44] P. A. Morton, R. J. Helkey, and J. E. Bowers, "Dynamic detuning in actively mode locked semiconductor lasers," *IEEE J. Quantum Electron.*, **25**, 2621 (1989)

[45] J. Chesmoy, M. C. Klein, L. Chusseau and J. M. Lourtioz," Period doubling and period quadrupling for an actively mode locked laser diode with extended cavity," *J. Appl. Phys.*, **67**, 7615 (1990)

[46] M. B. Holbrook, W. E. Sleat, and D. J. Bradley, "Bandwidth-limited picosecond pulse generation in an actively mode-locked GaAlAs diode laser", *Appl. Phys. Lett.*, **37**, 59 (1980)

[47] D. J. Bradley, M. B. Holbrook, and W. E. Sleat, "Bandwidth-limited picosecond pulses from an actively mode-locked GaAlAs diode laser," *IEEE J. Quantum Electron.*, **QE-17**, 658 (1981)

[48] J. Chen, W. Sibbett and J. I. Vukusic, "Tunable mode-locked semiconductor lasers incorporating Brewster-angled diodes," *Opt. Comm.*, **48**, 427 (1984)

[49] J. T. K. Chang, and J. I. Vukusic, "Active mode locking of InGaAsP Brewster angled semiconductor lasers," *IEEE J. Quantum Electron.*, **QE-23**, 1329 (1987)

[50] A. Mar, D. J. Derickson, R. J. Helkey, J. E. Bowers, R. T. Huang, and D. Wolf, "Actively mode-locked external-cavity semiconductor lasers with transform-limited single pulse output," *Opt. Lett.*, **17**, 868 (1992)

[51] R. J. Helkey, W. X. Zou, A. Mar, D. B. Young, and J. E. Bowers, "Curved and tapered waveguide mode-locked InGaAs/AlGaAs semiconductor lasers

fabricated by impurity induced disordering," (*51st Annual Device Research Conference*, IIB-4, Santa Barbara, CA, 1993)

[52] D. J. Derickson, R. J. Helkey, A. Mar, J. R. Karin, J. E. Bowers, and R. L. Thornton, "Suppression of multiple pulse formation in external cavity mode locked semiconductor lasers using intrawaveguide saturable absorbers," *IEEE Photon. Tech. Lett.*, **4**, 333 (1992)

[53] A. J. Lowery, and I. W. Marshall, "Stabilization of mode locked pulses using traveling wave semiconductor laser amplifier," *Electron. Lett.*, **26**, 104 (1990)

[54] M. Serenyi and J. Kuhl, E. O. Göbel, "Pulse shortening of actively mode-locked diode lasers by wavelength tuning," *Appl. Phys. Lett.*, **50,** 1213 (1987)

[55] Yu. L. Bessonov, A. P. Bogatov, P.P. Vasil'ev, V. N. Morozov, and A. B. Sergeev, "Generation of picosecond pulses in an injection laser with an external selective resonator," *Sov. J. Quantum Electron.*, **12**, 1510 (1982)

[56] S. Lundqvist, T. Andersson, and S. T. Eng, "Generation of tunable single-mode picosecond pulses from an AlGaAs semiconductor laser with grating feedback," *Appl. Phys. Lett.*, **43**, 715 (1983)

[57] A. P. Bogatov, P.P. Vasil'ev, V. N. Morozov, and A. B. Sergeev, "Direct detection of picosecond pulses emitted by an injection laser with active mode locking," *Sov. J. Quantum Electron.*, **13**, 1303 (1984)

[58] J. E. Epler, G. S. Jackson, N. Holonyak, Jr., M. Weinstein, R. D. Burnham and T. L. Paoli, "Mode-locked coupled-stripe quantum well laser operation ($\lambda \sim$ 7350 Å) in a tunable ($\Delta\hbar\omega \sim 37meV > kT$) external grating cavity," *Appl. Phys. Lett.*, **47**, 1022 (1985)

[59] P.P. Vasil'ev, V. N. Morozov, G. T. Pak, Yu. M. Popov, and A. B. Sergeev, "Measurement of the frequency shift of a picosecond pulse from a mode-locked injection laser," *Sov. J. Quantum Electron.*, **15**, 859 (1985)

[60] P. Kempf and B. K. Garside, "Dynamics of mode-locked laser diodes employing a repetitive short pulse drive current," *Appl. Opt.*, **26,** 4522 (1987)

[61] D. M. Bird, R. M. Fatah, M. K. Cox, P. D. Constantine, J. C. Regnault, K. H. Cameron, "Miniature packaged actively mode locked semiconductor laser with tunable 20 ps transform limited pulses," *Electron. Lett.*, **26**, 2086 (1990)

[62] A. S. Hou, R. S. Tucker, and G. Eisenstein, "Pulse compression of an actively modelocked diode laser using linear dispersion in fiber," *IEEE Photon. Tech. Lett.*, **2**, 322 (1990)

[63] M. S. Ozyazici, and M. S. Demokan, "Actively mode locked 1.3 and 1.55 μm InGaAsP diode lasers," *Opt. and Quantum Electron.*, **23**, 1169 (1991)

[64] J. M. Wiesenfeld, M. Kuznetsov, and A. S. Hou, "Tunable, picosecond pulse generation using a compressed, modelocked laser diode source," *IEEE Photon. Tech. Lett.*, **2**, 319 (1990)

[65] R. S. Tucker, G. Eisenstein, and I. P. Kaminow, "10 GHz active mode-locking of a 1.3 μm ridge-waveguide laser in an optical-fiber cavity," *Electron. Lett.*, **19**, 552 (1983)

[66] R. S. Tucker, S. K. Korotky, G. Eisenstein, U. Koren, L. W. Stulz, and J. J. Veselka, "20 GHz active mode-locking of a 1.55 μm InGaAsP laser," *Electron. Lett.*, **21**, 239 (1985)

[67] G. Eisenstein, R. S. Tucker, U. Koren, And S. K. Korotky, "Active mode-locking characteristics of InGaAsP-single mode fiber composite cavity lasers," *IEEE J. Quantum Electron.*, **QE-22**, 142 (1986)

[68] M. Kuznetsov, D. Z. Tsang, J. N. Walpole, Z. L. Liau, and E. P. Ippen, "Multistable mode locking of InGaAsP semiconductor lasers," *Appl. Phys. Lett.*, **51**, 895 (1987)

[69] S. W. Corzine and J. E. Bowers, G. Przybylek, U. Koren, B. I. Miller, and C. E. Soccolich, "Actively mode-locked GaInAsP laser with subpicosecond output," *Appl. Phys. Lett.*, **52,** 348 (1988)

[70] J. E. Bowers, P. A. Morton, A. Mar and S. W. Corzine, "Actively mode locked semiconductor lasers," *IEEE J. Quantum Electron.*, **QE-25**, 1426 (1989)

[71] N. Onodera, Z. Ahmed, R. S. Tucker, and A. J. Lowery, "Stability of harmonically driven mode locked semiconductor lasers," *Appl. Phys. Lett.*, **59**, 3527 (1991)

[72] S. Sanders, A. Yariv, J. Paslaski, J. E. Ungar, and H. A. Zarem, "Passive mode locking of a two section multiple quantum well laser at harmonics of the cavity round-trip frequency," *Appl. Phys. Lett.*, **58**, 681 (1991)

[73] S. Akiba, G. E. Williams and H. A. Haus, "High rate pulse generation from InGaAsP laser in selfoc lens external resonator," *Electron. Lett.*, **17**, 527 (1981)

[74] Y. Tada, H. Yokoyama, H. Ito and H. Inaba, " Ultrashort optical pulse generation from microwave modulated AlGaAs diode laser with Selfoc rod resonator," *Opt. Comm.*, **47**, 187 (1983)

[75] T. E. Dimmick, P. T. Ho, and G. L. Burdge, "Coherent pulse generation by active modelocking of a GaAlAs laser in a Selfoc lens extended resonator," *Electron. Lett.*, **20**, 831 (1984)

[76] G. Eisenstein, R. S. Tucker, I. P. Kaminow, T. P. Lee, C. A. Burrus, "InGaAsP 1.3 μm optical amplifier modulator integrated with a fibre-resonator mode-locked laser," *Electron. Lett.*, **20** , 624 (1984)

[77] G. Eisenstein, R. S. Tucker, S. K. Korotky, U. Koren, J. J. Veselka, L. W. Stulz, R. M. Jopson, K. L. Hall, "Active mode-locking of an InGaAsP 1.55 μm laser in a fibre resonator with an integrated single-mode-fibre output port," *Electron. Lett.*, **21**, 173 (1985)

[78] K. Y. Lau, A. Yariv, "Direct modulation and active mode locking of ultrahigh speed GaAlAs laser at frequencies up to 18 GHz," *Appl. Phys. Lett.*, **46**, 326 (1985)

[79] C. Harder, J. S. Smith, K. Y. Lau, and A. Yariv, "Passive mode locking of buried heterostructure lasers with nonuniform current injection," *Appl. Phys. Lett.*, **42**, 772 (1983)

[80] K. Y. Lau, I. Ury, and A. Yariv, "Passive and active mode locking of a semiconductor laser without an external cavity, "*Appl. Phys. Lett.*, **46**, 1117 (1985)

[81] K. Y. Lau, "Efficient narrow band direct modulation of semiconductor injection lasers at millimeter wave frequencies of 100 GHz and beyond," *Appl. Phys. Lett.*, **52**, 2214 (1988)

[82] K. Y. Lau, "Short pulse and high frequency signal generation in semiconductor lasers," *J. Lightwave Tech.*, 7, 400 (1989)

[83] K. Y. Lau, "Narrow band modulation of semiconductor lasers at millimeter wave frequencies (>100 GHz) by mode locking," *IEEE J. Quantum Electron.*, **26**, 250 (1990)

[84] S Sanders, L. Eng, J. Paslaski, and A. Yariv, "108 GHz passive mode locking of a multiple quantum well semiconductor laser with an intracavity absorber," *Appl. Phys. Lett.*, **56**, 310 (1989)

[85] R. S. Tucker, U. Koren, G. Raybon, C.A. Burrus, B. I. Miller, T. L. Koch, and G. Eisenstein, "40 GHz active mode locking in a 1.5 μm monolithic extended cavity laser," *Electron. Lett.*, 25, 621 (1989)

[86] P.P. Vasil'ev, and A. B. Sergeev, "Generation of bandwidth limited 2 ps pulses with 100 GHz repetition rate from multisegmented injection laser," *Electron. Lett.*, **25**, 1049 (1989)

[87] P.A. Morton, J. E. Bowers, L. A. Koszi, M. Soler, J. Lopata and D. P. Wilt, "Monolithic hybrid mode locked 1.3 μm semiconductor lasers," *Appl. Phys. Lett.*, **56**, 111 (1990)

[88] S. Sanders, L. Eng, and A. Yariv, "Passive mode locking of monolithic InGaAs/AlGaAs double quantum well lasers at 42 GHz repetition rate," *Electron. Lett.*, **26**, 1087 (1990)

[89] S. Sanders, L. Eng, J. Paslaski, and A. Yariv, "108 GHz passive mode locking of a multiple quantum well semiconductor laser with an intracavity absorber," *Appl. Phys. Lett.*, **56**, 310 (1990)

[90] M. C. Wu, Y. K. Chen, T. Tanbun-Ek, R. A. Logan, M. A. Chin, and G. Raybon, "Transform-limited 1.4 ps optical pulses from a monolithic colliding-pulse mode-locked quantum well laser," *Appl. Phys. Lett.*, **57**, 759 (1990)

[91] M. C. Wu, Y. K. Chen, T. Tanbun-Ek, R. A. Logan, M. A. Chin, "Subpicosecond optical pulse generation at 350 GHz in monolithic passive CPM MQW lasers," *IEEE IEDM*, 137 (1990)

[92] Y. K. Chen, M. C. Wu, T. Tanbun-Ek, R. A. Logan, and M. A. Chin, "Subpicosecond monolithic colliding-pulse mode-locked multiple quantum well lasers," *Appl. Phys. Lett.*, **58**, 1253 (1991)

[93] P. G. May, and M. Bierbaum, "Monolithic mode locking of long cavity GaAs-AlGaAs semiconductor lasers," *IEEE Photon. Tech. Lett.*, **3**, 296 (1991)

[94] J. H. Zarrabi, E. L. Portnoi and A. V. Chelnokov, "Passive mode locking of a multistripe single quantum well GaAs laser diode with an intracavity saturable absorber," *Appl. Phys. Lett.*, **59**, 1526 (1991)

[95] D. J. Derickson, R. J. Helkey, A. Mar, J. R. Karin, J. G. Wasserbauer, and J. E. Bowers, "Short pulse generation using multisegment mode locked semiconductor lasers," *IEEE J. Quantum Electron.*, **QE-28**, 2186 (1992)

[96] P. B. Hansen, G. Raybon, M. D. Chien, U. Doren, B. I. Miller, M. G. Young, J. M. Verdiell, and C. A. Burrus, "A 1.54 μm monolithic semiconductor ring laser: cw and mode locked operation," *IEEE Photon. Tech. Lett.*, **4**, 411 (1992)

[97] D. J. Derickson, P.A. Morton, J. E. Bowers, and R. L. Thornton, "Comparison of timing jitter in external and monolithic cavity mode locked semiconductor lasers," *Appl. Phys. Lett.*, **59**, 3372 (1991)

[98] J. P. Ryan, L. S. Goldberg, and D. J. Bradley, " Comparison of synchronous pumping and passive mode-locking of cw dye lasers for the generation of picosecond and subpicosecond light pulses," *Opt. Comm.*, **27**, 127 (1978)

[99] Y. Ishida, T. Yajima, and K. Naganuma, "Generation of broadly tunable subpicosecond light pulses from a synchronously and passively mode-locked cw dye laser," *Japan. J. Appl. Phys.*, **19**, L717 (1980)

[100] J. P. van der Ziel, R. A. Logan, and R. M. Mikulyak, "Generation of subpicosecond pulses from an actively mode locked GaAs laser in an external ring cavity," *Appl. Phys. Lett.*, **39**, 867 (1981)

[101] P. P. Vasil'ev, V. N. Morzov, Y. M. Popov, And A. B. Sergeev, "Subpicosecond pulse generation by a tandem-type AlGaAs DH Laser with colliding pulse mode locking," *IEEE J. Quantum Electron.*, **QE-22**, 149 (1986)

[102] J. P. van der Ziel, and R. A. Logan, "Dispersion of the group velocity refractive index in GaAs double heterostructure lasers," *IEEE J. Quantum Electron.*, **QE-19**, 164 (1983)

[103] Y. Silberberg And P. W. Smith, "Subpicosecond pulses from a mode-locked semiconductor laser," *IEEE J. Quantum Electron.*, **QE-22** , 759 (1986)

[104] J. Kuhl, M. Serenyi, and E. O. Göbel, "Bandwidth-limited picosecond pulse generation in an actively mode-locked GaAs laser with intracavity chirp compensation," *Opt. Lett.*, **12** , 334 (1987)

[105] G. M. Carter, L. Zheng, and K. Y. Huang, "Compression of pulses from a mode locked GaAs laser diode in an extended cavity with a fiber grating reflector," *Appl. Phys. Lett.*, **61**, 379 (1992)

[106] C.F. Lin and C. L. Tang, "Colliding pulse mode locking of a semiconductor laser in an external ring cavity," Appl. Phys. Lett., **62**, 1053 (1993)

[107] J. R. Andrews, R. D. Burnham, "High peak power and gateable picosecond optical pulses from a diode array traveling-wave amplifier and a mode-locked diode laser," *Appl. Phys. Lett.*, **49**, 1004 (1986)

[108] P. J. Delfyett, C. H. Lee, G. A. Alphonse and J. C. Connolly, "High peak power picosecond pulse generation from AlGaAs external cavity mode locked semiconductor laser and traveling-wave amplifier," *App. Phys. Lett.*, **57**, 971 (1990)

[109] P. J. Delfyett, C. H. Lee, L. T. Florez, N. G. Stoffel, T. J. Gmitter, and N. C. Andredakis, G. A. Alphonse and J. C. Connolly, "Generation of subpicosecond high-power optical pulses from a hybrid mode-locked semiconductor laser," *Opt. Lett.*, **15**, 1371 (1990)

[110] P. J. Delfyett, L. Florez, N. Stoffel, T. Gmitter, N. Andreadakis, G. Alphonse, and W. Ceislik, "200-fs optical pulse generation and intracavity pulse evolution in a hybrid mode-locked semiconductor diode-laser/amplifier system," *Opt. Lett.*, **17**, 670 (1992)

[111] J. P. van der Ziel, H. temkin, R. D. Dupuis, and R. M. Mikulyak, "Mode-locked picosecond pulse generation from high power phase-locked GaAs laser arrays," *Appl. Phys. Lett.*, **44,** 357 (1984)

[112] H. Masuda, A. Takada, "Picosecond optical pulse generation from mode locked phased laser diode array," *Electron. Lett.*, **25**, 1418 (1989)

[113] J. C. Kuo, C. S. Chang, and C. L. Pan, "Buildup of steady state picosecond pulses in an actively mode locked laser diode array," *Opt. Lett.*, **16**, 1328 (1991)

[114] L. Y. Pang, J. G. Fujimoto, E. S. Kintzer, "Ultrashort pulse generation from high power diode arrays by using intracavity optical nonlinearities," *Opt. Lett.*, **17**, 1599 (1992)

[115] A. Mar, R. Helkey, T. Reynolds and J. Bowers, "Mode-locked multi-segment resonant-optical-waveguide diode laser arrays," *IEEE/LEOS Summer Topical Meeting on Optical Microwave Interactions*, PD2 (Santa Barbara, CA, 1993)

[116] L. F. Mollenauer, B. M. Nyman, M. J. Neubelt, G. Raybon, and S. G. Evangelides, "Demonstration of soliton transmission at 2.4 Gbit/s over 12000 km," *Electron. Lett.*, **27**, 178 (1991)

[117] A. J. Taylor, J. M. Wiesenfeld, G. Eisenstein, R. S. Tucker, J. R. Talman, and U. Koren, "Electro-optic sampling of fast electrical signals using an InGaAsP injection laser," *Electron. Lett.*, **22**, 61 (1986)

[118] P.A. Morton, R. J. Helkey, A. Mar, D. J. Derickson and J. E. Bowers, "Monolithic mode locked laser arrays in optical computing," *SPIE Digital Optical Computing II*, **1215**, 94 (1990)

[119] W. R. Christian, and M. J. Rosker, "Picosecond pulsed diode ring-laser gyroscope," *Opt. Lett.*, **16**, 1587 (1991)

[120] H. Soda, K. Iga, C. Kitahara, and Y. Suematsu, "GaInAsP/InP surface emitting injection lasers," *Jpn. J. Appl. Phys.*, **18**, 2329 (1979)

[121] K. Iga, F. Koyama, and S. Kinoshita, "Surface emitting semiconductor lasers," *IEEE J. Quantum Electron.*, **QE-24**, 1845 (1988)

[122] M. Orenstein, A. C. Von Lehmen, C. Chang-Hasnain, N. G. Stoffel, J. P. Harbison, and L. T. Florez, "Matrix addressable vertical cavity surface emitting laser array," *Electron. Lett.*, **27**, 437 (1991)

[123] D. B. Young, J. W. Scott., F. H. Peters, B. J. Thibeault, S. W. Corzine, M. G. Peters, S. L. Lee, and L. A. Coldren, "High-power temperature-insensitive gain-offset InGaAs/GaAs vertical-cavity surface-emitting lasers," *IEEE Photon. Tech. Lett.*, **5**, 130 (1993)

[124] K. Tai, G. Hasnain, J. D. Wynn, R. J. Fischer, Y. H. Wang, B. Weir, J. Gamelin, and A. Y. Cho, "90% coupling of top surface emitting GaAs/AlGaAs quantum well laser output into 8 μm diameter core silica fibre," *Electron. Lett.*, **26**, 1628 (1990)

[125] K. Iga, S. Ishikawa, S. Ohkouchi, and T. Nishimura, "Room temperature pulsed oscillation of GaAlAs/GaAs surface emitting laser," *Appl. Phys. Lett.*, **45**, 348 (1984)

[126] F. Koyama, S. Kinoshita, and K. Iga, "Room-temperature CW operation of GaAs vertical cavity surface emitting laser," *Trans. IEICE*, **E71**, 1089 (1988)

[127] F. H. Peters, M. G. Peters, D. B. Young, J. W. Scott, B. J. Thibeault, S. W. Corzine, and L. A. Coldren, "High power vertical cavity surface emitting lasers," *Electron. Lett.*, **29**, 200 (1993)

[128] R. S. Geels and L. A. Coldren, "Submilliamp threshold current vertical-cavity laser diodes," *Appl. Phys. Lett.*, **57**, 1605 (1990)

[129] M. G. Peters, F. H. Peters, D. B. Young, J. W. Scott, B. J. Thibeault and L. A. Coldren, "High wallplug efficiency vertical-cavity surface-emitting lasers using lower barrier DBR mirrors," *Electron. Lett.*, **29**, 170 (1993)

[130] K. Iga, "Surface emitting lasers," *Opt. Quantum Electron.*, **24**, S97 (1992)

[131] T. Baba, Y. Yogo, K. Suzuki, F. Koyama, and K. Iga, "Near room temperature continuous wave lasing characteristics of GaInAsP/InP surface emitting laser," *Electron. Lett.*, **29**, 913 (1993)

[132] J. J. Dudley, D. I. Babic, R. Mirin, R. J. Ram, T. Reynolds, E. L. Hu, J. E. Bowers, L. Yang, and B. I. Miller, "Low threshold, electrically injected InGaAsP (1.3 μm) vertical cavity lasers on GaAs substrates," *51st Annual Device Research Conference*, IIIB-8 (Santa Barbara, CA, 1993)

[133] S. Uchiyama and K. Iga, "Two-dimensional array of GaInAsP/InP surface-emitting lasers," *Electron. Lett.*, **21**, 162 (1985)

[134] E. Ho, F. Koyama, and K. Iga, "Effective reflectivity from self-imaging in a talbot cavity and on the threshold of a finite 2-D surface emitting laser array," *Appl. Opt.*, **29**, 5080 (1990)

[135] H. A. Haus, "*Waves and fields in optoelectronics*," (Prentice-Hall, Inc., Englewood Cliffs, New Jersey, 1984)

[136] A. E. Siegman, "*Lasers*," (University Science Books, Mill Valley, CA, 1986)

[137] W. L. Cao, A.M. Vacher, and C. H. Lee, "Synchronously pumped mode-locked GaAs laser," *Appl. Phys. Lett.*, 38, 653 (1981)

[138] A. M. Vaucher, W. L. Cao, J. D. Ling, and C. H. Lee, "Generation of tunable picosecond pulses from a bulk GaAs laser," *IEEE J. Quantum Electron.*, **QE-18**, 187 (1982)

[139] C. B. Roxlo, and M. M. Salour, "Synchronously pumped mode-locked CdS platelet laser," *Appl. Phys. Lett.*, 38, 738 (1981)

[140] C. B. Roxlo, and M. M. Salour, "Dewar design for optically pumped semiconductor lasers," *Rev. Sci. Instrum.*, **53**, 458 (1982)

[141] C. B. Roxlo, R. S. Putnam, and M. M. Salour, "Optically pumped semiconductor platelet lasers," *IEEE J. Quantum Electron.*, **QE-18**, 338 (1982)

[142] J. Yorsz, S. G. Shevel, and E. P. Ippen, "Optically pumped ZnxCdS platelet lasers," *Opt. Comm.*, **48**, 139 (1983)

[143] R. S. Putnam, and M. M. Salour, "Modelocked picosecond pulses from 490 nm to 2 μm with optically pumped semiconductor lasers," *Proc. SPIE*, **439**, 66 (1983)

[144] J. Stone, C.A. Burrus, and J. C. Campbell, "Laser action in photopumped GaAs ribbon whiskers," *J. Appl. Phys.*, **51**, 3038 (1980)

[145] M. A. Duguay, T. C. Damen, J. Stone, J. M. Wiesenfeld, and C.A. Burrus, "Picosecond pulses from an optically pumped ribbon-whisker laser," *Appl. Phys. Lett.*, **37**, 369 (1980)

[146] T. C. Damen, M. A. Duguay, J. Shah, J. Stone, J. M. Wiesenfeld and R. A. Logan, "Broadband tunable picosecond semiconductor lasers," *Appl. Phys. Lett.*, **39**, 142 (1981)

[147] J. Stone, J. M. Wiesenfeld, A. G. Dentai, T. C. Damen, M. A. Duguay, T. Y. Chang, and E. A. Caridi, "Optically pumped ultrashort cavity $In_{1-x}GaxAsyP_{1-y}$ lasers: picosecond operation between 0.83 and 1.59 μm," *Opt. Lett.*, **6**, 534 (1981)

[148] J. M. Wiesenfeld, and J. Stone, "Picosecond pulse generation in optically pumped, ultrashort-cavity, InGaAsP, InP, and InGaAs film lasers," *IEEE J. Quantum Electron.*, **QE-22**, 119 (1986)

[149] J. M. Wiesenfeld, and J. Stone, "Chirp in picosecond film lasers and pulse compression by linear dispersion in optical fibers," *Opt. Lett.*, **8**, 262 (1983)

[150] D. Marcuse, and J. M. Wiesenfeld, "Chirped picosecond pulses: evaluation of the time-dependent wavelength for semiconductor film lasers," *Appl. Opt.*, **23**, 74 (1984)

[151] J. R. Karin, L. G. Melcer, R. Nagarajan, J. E. Bowers, S. W. Corzine, P.A. Morton, R. S. Geels, and L. A. Coldren, "Generation of picosecond pulses with a gain-switched GaAs surface-emitting laser," *Appl. Phys. Lett.*, **57**, 963 (1990)

[152] A. Mukherjee, M. Mahbobzadeh, C.F. Schaus, and S. R. J. Brueck, "Ultrafast operation of optically pumped resonant periodic gain GaAs surface emitting lasers," *IEEE Photon. Tech. Lett.*, **2**, 857 (1990)

[153] L. G. Melcer, J. R. Karin, R. Nagarajan, and J. E. Bowers, "Picosecond dynamics of optical gain switching in vertical cavity surface emitting lasers," *IEEE J. Quantum Electron.*, **27**, 1417 (1991)

[154] J. Lin, J. K. Gamelin, S. Wang, M. Hong, and J. P. Mannaerts, "Short pulse generation by electrical gain switching of vertical cavity surface emitting laser," *Electron. Lett.*, **27**, 1957 (1991)

[155] G. Hasnain, J. M. Wiesenfeld, T. C. Damen, J. Shah, J. D. Wynn, Y. H. Wang, and A. Y. Cho, "Electrically gain-switched vertical-cavity surface-emitting lasers," *IEEE Photon. Tech. Lett.*, **4**, 6 (1992)

[156] D. Tauber, G. Wang, R. S. Geels, J. E. Bowers, and L. A. Coldren, "Large and small signal dynamics of vertical cavity surface emitting lasers," *Appl. Phys. Lett.*, **62**, 325 (1993)

[157] P. Pepeljugoski, J. Lin, J. Gamelin, M. Hong, and K. Y. Lau, "Ultralow timing jitter in electrically gain-switched vertical cavity surface emitting lasers," *Appl. Phys. Lett.*, **62**, 1588 (1993)

Chapter 2 Optically pumped mode-locked vertical-cavity semiconductor lasers

2.1 Threshold Condition

A laser oscillation at steady state requires that the amplitude and the phase of the laser beam return to their initial values after each round trip inside the resonator [1, 2]. A threshold gain condition is thus the amplitude condition for the laser oscillation, which requires

$$\text{Gain} = \text{Loss} \tag{2.1.1}$$

For an in-plane semiconductor laser, this transforms into a mathematical expression

$$\Gamma g(N_{th}) = \alpha_{\text{int}} + \frac{1}{2L_a}\ln\left(\frac{1}{R_1 R_2}\right) \tag{2.1.2}$$

where $g(N_{th})$ is the threshold gain at threshold carrier density N_{th}, Γ is the confinement factor, α_{int} is the internal loss from both active and cladding layers, L_a is the active length, and R_1 and R_2 are the facet reflectivity at two ends [3].

The transverse confinement factor of a VCSEL is approximately equal to one. The gain threshold condition for an external cavity surface emitting laser can thus be expressed by

$$g(N_{th}) = \alpha_{\text{int}} + \frac{1}{2L_a}\ln\left(\frac{1}{R_1 R_2 T}\right) \tag{2.1.3}$$

for a bulk active medium, where T is introduced to account for any other linear loss from intracavity optical components other than the two end mirrors.

For an optically pumped VCSEL, the absorbed pump power is completely used to excite carriers that will recombine only through spontaneous emission at the lasing threshold. Higher order processes such as Auger recombination are ignored. The optically pumped lasing threshold can be written mathematically as

$$P_{th}\left[1-e^{-\alpha(N_{th})L_a}\right]=R_{sp}(N_{th})h\nu_p\sigma L_a \tag{2.1.4}$$

or

$$P_{th}=\frac{h\nu_p R_{sp}(N_{th})\sigma L_a}{1-e^{-\alpha(N_{th})L_a}} \tag{2.1.5}$$

where P_{th} is the threshold pump power, $\alpha(N_{th})$ is the absorption coefficient to the pump at threshold, $R_{sp}(N_{th})$ is the spontaneous emission rate at threshold with the unit of $m^{-3}s^{-1}$, $h\upsilon_p$ is the photon energy of pump, and σ is the active area.

A multiple-quantum-well (MQW) structure is preferred as the gain medium for the external cavity VCSEL in order to increase the differential gain. The threshold gain condition of Equation (2.1.3) will accordingly be modified into

$$\sum_{i=1}^{N_{QW}} g(N_i)L_w = N_{QW}\alpha_{\text{int}}(L_w+L_b)+\frac{1}{2}\ln\left(\frac{1}{R_1R_2T}\right) \tag{2.1.6}$$

where N_{QW} is the number of quantum wells, $g(N_i)$ is the gain coefficient at carrier density N_i in the i-th quantum well, L_w is the width of quantum well and L_b is the

width of barrier. The internal loss α_{int} is assumed the same in both the well and the barrier.

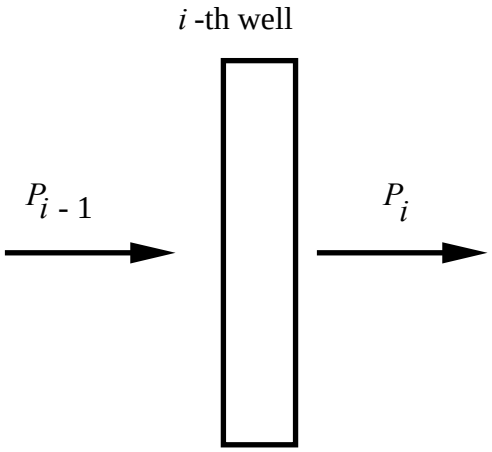

Figure 2.1.1 The *i*-th quantum well of a multiple-quantum-well (MQW) sample with the input pump P_{i}-1 and output pump P_{i}. The absorbed pump power by the well is P_{i}-1 - P_{i}.

To write down the threshold pump power, examine at Figure 2.1.1. If the input pump power to the *i*-th quantum well is P_{i}-1 and the transmitted pump power from this well is P_{i}, where $i = 1, 2, ..., N_{QW}$, the expression to P_{i}-1 and P_{i} can be written as

$$P_{i-1} = P_{th} \exp\left[-\sum_{j=0}^{i-1} \alpha(N_j) L_w\right] \qquad (2.1.7)$$

$$P_{i} = P_{th} \exp\left[-\sum_{j=0}^{i} \alpha(N_j) L_w\right] \qquad (2.1.8)$$

where $\alpha(N_j)$, j= 1, 2, ..., is the absorption coefficient to the pump at carrier density N_j in the j-th quantum well, and $\alpha(N_0)$=0 is introduced for the convenience of mathematical expression. The difference of P_{i-1} and P_i is the pump power absorbed by the i-th quantum well that is used to excite carriers in this well. The excited carriers recombine through spontaneous emission, i.e.,

$$P_i - P_{i-1} = h\nu_p R_{sp}(N_i)\sigma L_w \tag{2.1.9}$$

where $R_{sp}(N_i)$ is the spontaneous emission rate at carrier density of N_i in the i-th quantum well. With Equations (2.1.7), (2.1.8) and (2.1.9), the threshold pump power for the external cavity VCSEL with the MQW gain structure is obtained as shown by

$$P_{th} = \frac{h\nu_p R_{sp}(N_i)\sigma}{\alpha(N_i)} \prod_{j=0}^{i-1} \left[1 + \alpha(N_j) L_w\right] \tag{2.1.10}$$

where $\alpha(N_j)\, L_w << 1$ is assumed and is generally satisfied. If i = 1, the threshold pump power

$$P_{th} = \frac{h\nu_p R_{sp}(N_1)\sigma}{\alpha(N_1)} \tag{2.1.11}$$

which means that the threshold pump power will be determined as long as the carrier density in the first quantum well N_1 is known. The carrier density distribution throughout the quantum wells will also be uniquely determined according to Equation (2.1.10) by having i equal to 2 to N_{QW} one by one.

Equations (2.1.6) and (2.1.10) are used to design the MQW gain structure for an optically pumped VCSEL. Strictly speaking they are true only for a VCSEL under CW operation. When the designed laser is synchronously pumped, the threshold pump power is going to be smaller if the pump pulsewidth is shorter than the spontaneous emission lifetime and the laser round-trip time in the cavity is longer than the spontaneous emission lifetime. These conditions are satisfied in the experiments demonstrated in this chapter. For simplicity, the average absorption coefficient $\alpha(N_{th})$ is used at average threshold carrier density N_{th}, and the threshold pump power becomes

$$P_{th} = \frac{f h \nu_p N_{th} \sigma L_a}{1 - \exp\left[-\alpha\left(N_{th}\right) L_a\right]} \tag{2.1.12}$$

where L_a is the net active length and f is the pump repetition rate. No spontaneous emission rate $R_{sp}(N_{th})$ is involved in this equation as carriers have been excited to reach the lasing threshold before the spontaneous emission has a chance to start.

2.2 Mode-locked GaAs vertical cavity semiconductor lasers

2.2.1 GaAs/AlGaAs MQW gain structure for optical pumping

Equations (2.1.6) and (2.1.10) are used to determine the GaAs/AlGaAs MQW gain structure for the optically pumped mode-locked VCSELs. There are controversies over the exact expressions of $g(N)$, $\alpha(N)$ and $R_{sp}(N)$ varying with carrier density N [4]. The basic difference lies in the choice of a matrix element in the expressions.

Agrawal's expressions [3] are used for discussion in this section. For comparison, Corzine's expressions [5] will be listed in Appendix I.

The expressions of α and R_{sp} for the MQW structure are as follows [3],

$$\alpha(E) = \frac{e^2 m_r |M_b|^2}{\varepsilon_0 m_0^2 c \hbar \bar{n} E L_w} \left[1 - f_c(E_c) - f_v(E_v)\right] \tag{2.2.1}$$

$$R_{sp} = \frac{16\pi^2 \bar{n} e^2 m_r |M_b|^2}{m_0^2 \varepsilon_0 h^4 c^3 L_w} \int_{E_q}^{\infty} E f_c(E_c) f_v(E_v) dE \tag{2.2.2}$$

where

$$E_c = \frac{m_r}{m_c}(E - E_q) \qquad E_v = \frac{m_r}{m_v}(E - E_q)$$

$$m_r = \frac{m_c m_v}{m_c + m_v}$$

E_q is the separation between the levels in the conduction band and in the valence band, f_c and f_v denote the Fermi factors for the electron at energy E_c and the hole at energy E_v, m_c and m_v are the effective mass of an electron and the effective mass of a hole, respectively. The matrix element in the equation is from the Kane band model [6, 7] and given by

$$|M_b|^2 = \frac{m_0(E_g + \Delta)}{12 m_c (E_g + 2\Delta/3)} m_0 E_g = \xi m_0 E_g \tag{2.2.3}$$

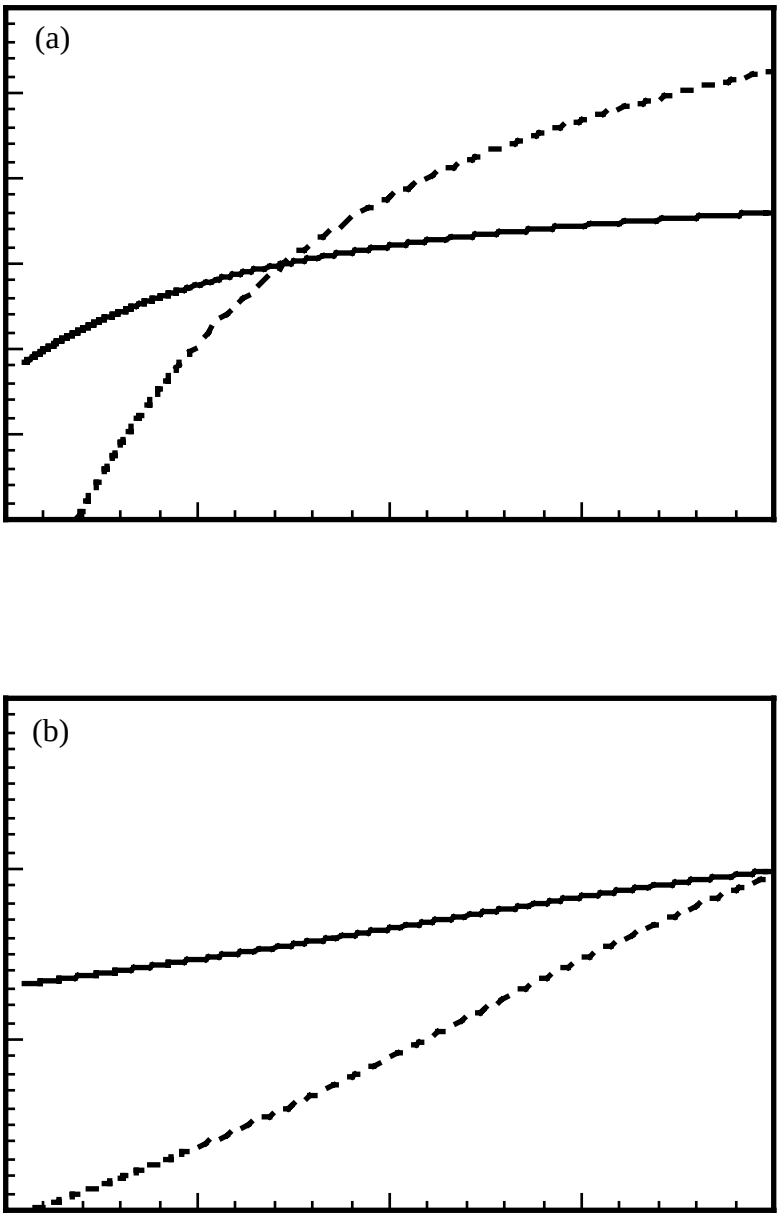

Figure 2.2.1 (a) Gain coefficient *g(N)* as a function of carrier density *N* at the lasing wavelength, and (b) absorption coefficient *α(N)* as a function of carrier density *N* at the pump wavelength for a GaAs/$Al_{0.29}Ga_{0.71}As$ MQW sample with a well width of 150 Å and a barrier width of 70 Å. The solid lines are from Agrawal's expressions, and the dashed lines are from Corzine's expressions.

Table 2.2.1 Parameters used for design of GaAs/$Al_{0.29}Ga_{0.71}As$ MQW

Parameter	Value
Eff. electron mass in well m_e	0.067
Eff. heavy hole mass in well m_{hh}	0.45
Eff. light hole mass in well m_{lh}	0.082
Eff. electron mass in barrier m_e	0.0919
Eff. heavy hole mass in barrier m_{hh}	0.543
Eff. light hole mass in barrier m_{lh}	0.1024
Bandgap in well E_g	1.424 eV
Bandgap in barrier E_g	1.798 eV
Conduction band offset	60%
Pump wavelength λ_p	800 nm
Operating temperature	288 K
Dielectric constant in well ε	13.1
Reflectivity of end mirror R_1	0.99
Reflectivity of coupler R_2	0.97
Intracavity optics transmission T	0.95
Well width L_w	150 Å
Barrier width L_b	70 Å
Active diameter d	19 μm
Spin-orbit split [2]	0.33 eV
Internal loss α_{int}	30 cm^{-1}

where m_0 is the free-electron mass, E_g is the band gap, and Δ is the spin-orbit splitting. ξ has a value between 1 and 2 for most semiconductors. The uncertainty in the value of ξ represents the accuracy of the results. E in Equation (2.2.1) denotes the photon energy. If E represents the photon energy of the VCSEL, $-\alpha(E)$ will be the $g(N)$ needed in Section 2.1, where the carrier density variable N is implicitly included in the Fermi function f_c and f_v, since the quasi-Fermi energies of both electrons and holes vary with the carrier density N. If E represents the photon energy of the pump , the summation of $\alpha(E)$ over all possible transitions between the various subbands in the conduction and valence bands will be the absorption to the pump $\alpha(N)$. A complete expression of radiative recombination rate should also include summation over all possible transitions between the various subbands in the conduction and valence bands, but the transition from the lowest level in the conduction band (level 1c) to the lowest level in the heavy-hole band (level 1hh) has the most contribution to the spontaneous emission rate $R_{sp}(N)$.

The gain medium under consideration is a MQW GaAs/$Al_{0.3}Ga_{0.7}$As structure. The well-width is 150 Å and the barrier-width is 50 Å. The pump wavelength is 800 nm. What needs to be determined is the number of quantum wells and the threshold pump power. The variation of $g(N)$ and $\alpha(N)$ against the carrier density N are shown in Figure 2.2.1. The parameters used for calculations are listed in Table 2.2.1. For comparison, the results using Corzine's expressions are also shown in the figures. It is interesting to see that the two results give the same transparent carrier density, but Agrawal's expressions give a lower differential gain, which agrees better with the experiments demonstrated in this chapter. The correspondent $R_{sp}(N)$ are shown in Figure 2.2.2. The threshold pump power and the threshold carrier density vary with the number of quantum wells are shown in Figure 2.2.3 using Equations (2.1.6) and (2.1.10).

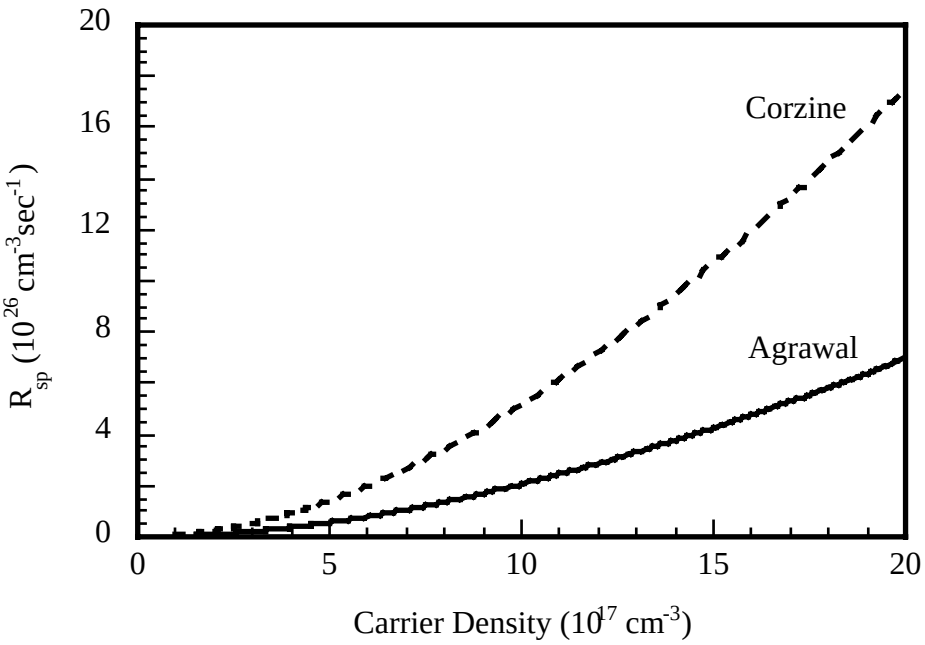

Figure 2.2.2 Spontaneous emission rate $R_{sp(N)}$ as a function of carrier density N for a GaAs/$Al_{0.29}Ga_{0.71}As$ MQW sample with a well width of 150 Å and a barrier width of 70 Å. The solid line is from Agrawal's expression, and the dashed line is from Corzine's expression.

The criteria to determine the number of quantum well for the gain of a mode-locked VCSEL is to have the lowest possible pump threshold, while keeping the carrier density in the last quantum well over the transparent carrier density. Figure 2.2.4 shows a structure of GaAs/AlGaAs MQW with a well number of 120 determined according to Figure 2.2.3. The justification to the choice has to rely on experiments. The integrated semiconductor diffractive Bragg reflector (DBR) mirror is grown between the MQWs and the semi-insulating GaAs substrate. The designed reflectivity of the DBR is shown in Figure 2.2.5(a), which is comprised of 22 pairs of $\lambda/4$ AlAs/$Al_{0.2}Ga_{0.8}As$ and an extra layer of $\lambda/4$ AlAs. The measured reflectivity of the DBR is shown in Figure 2.2.5(b). The kink at the wavelength of 900 nm is

caused by the switching of the detector during the data taking. On top of the epitaxial layer is a layer of SiN_xO_y anti-reflective (AR) coating for the VCSEL wavelength (Figure 2.2.6). The kink at λ = 900 nm in Figure 2.2.6 is again caused by the switching of the detector during the measurement.

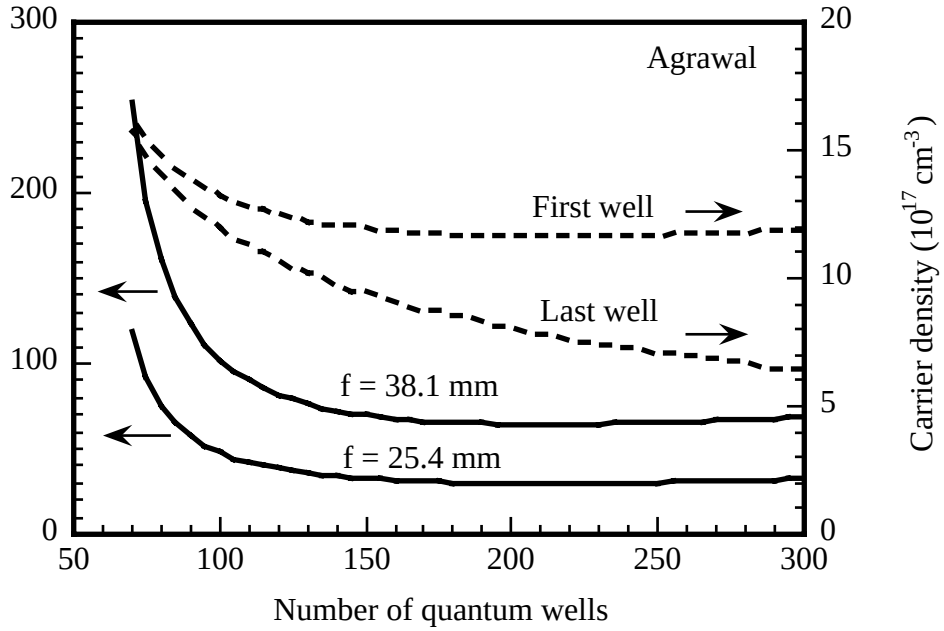

Figure 2.2.3 Threshold pump power as a function of number of quantum wells for the lens focal length of 38.1 mm and 25.4 mm, respectively (solid lines), and the corresponding carrier density in the first quantum well and the last quantum well (dashed lines).

2.2.2 GaAs/AlGaAs external cavity VCSEL

The laser cavity under study is Z-shaped as shown in Figure 2.2.7. The epitaxially grown DBR mirror integrated with the GaAs/AlGaAs MQW gain is used as one of the cavity end mirror. M1 is a dichroic mirror that is highly reflective at the lasing wavelength and highly transmissive to the pump. M2 is a total reflector. M3 is an

output coupler with a reflectivity of 97%. The focal length of the AR coated lens is 38.1 mm. A Brewster angle plate is used in the cavity to control the laser polarization. The sample is mounted on a copper heat sink that is maintained at room temperature during the laser operation. The pump comes from a synchronously mode-locked dye laser.

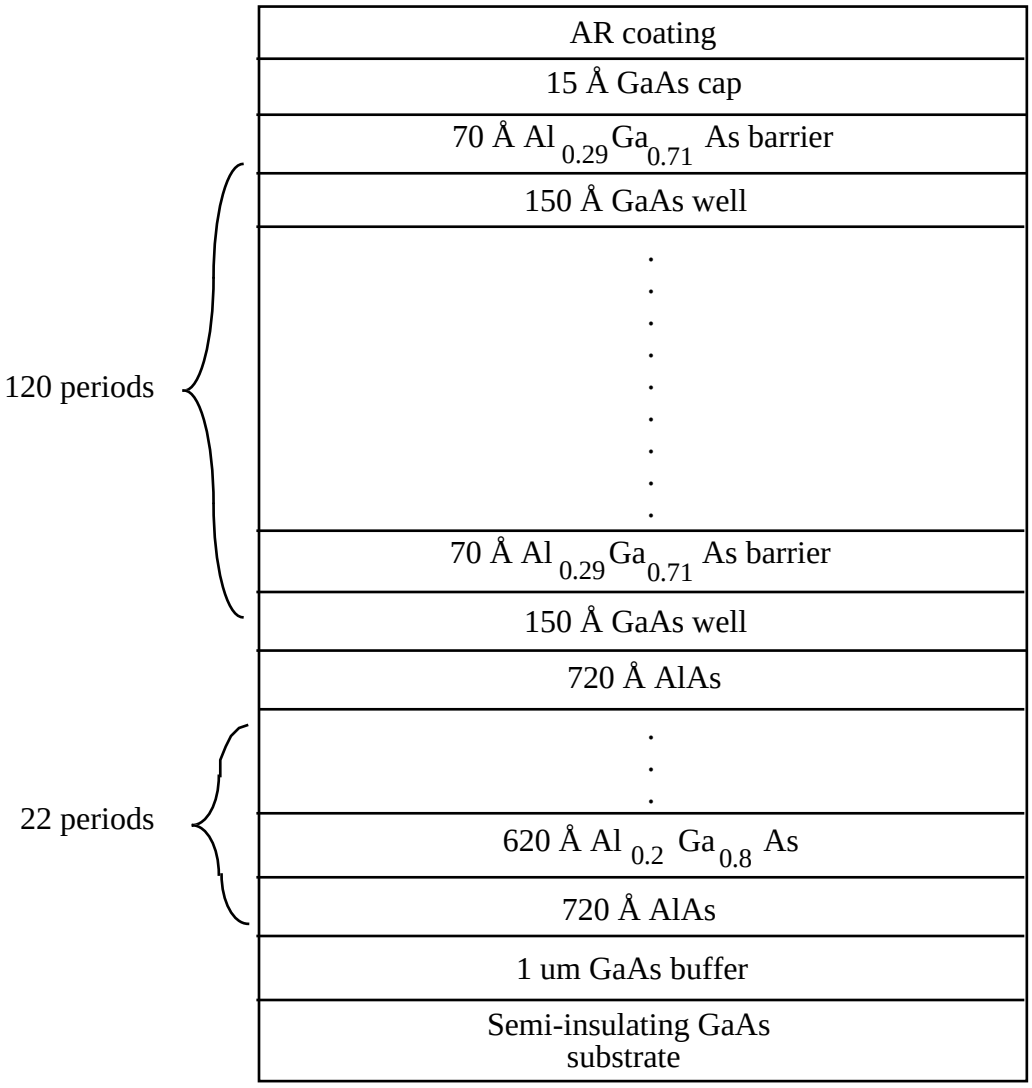

Figure 2.2.4 GaAs/$Al_{0.29}Ga_{0.71}$As MWQ structure for optical pumping.

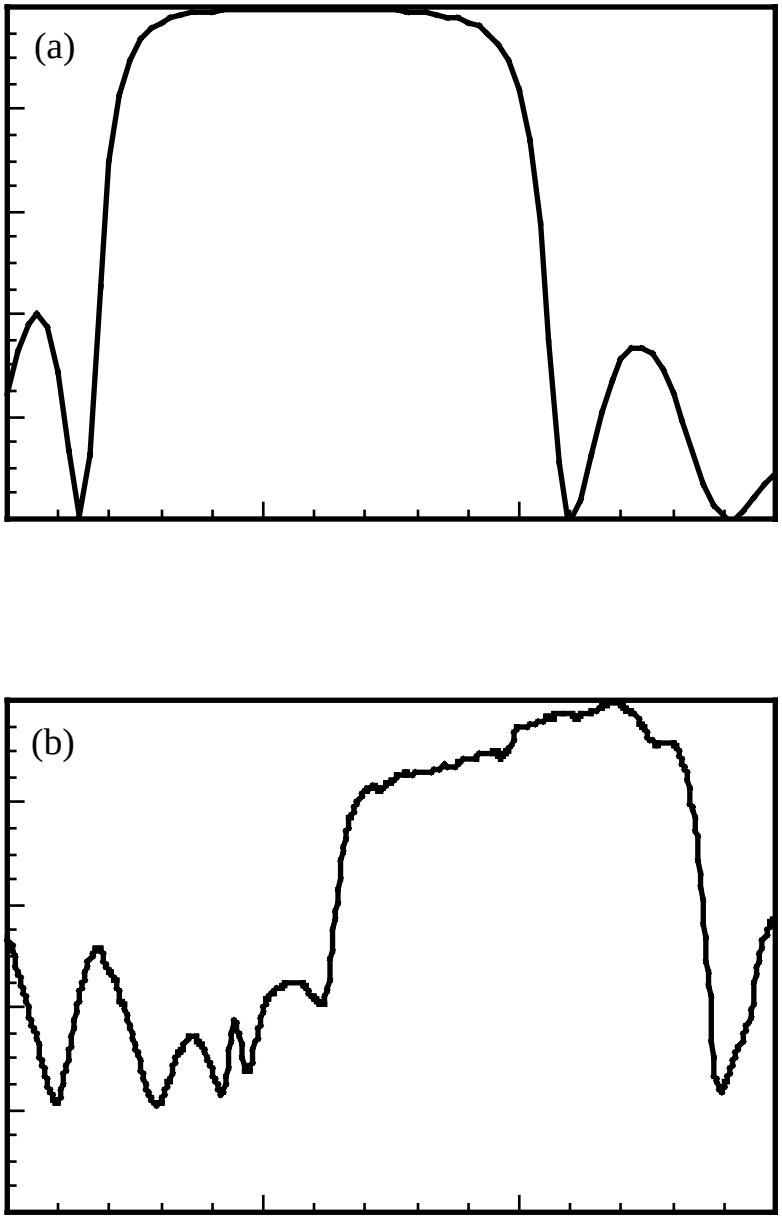

Figure 2.2.5 (a) The predicted reflectivity of DBR as designed and (b) the measured reflectivity of DBR as grown for a GaAs/AlGaAs MQW gain sample used for an optically pumped mode-locked VCSEL. The kink at 900 nm in the measured curve is caused by the switching of detectors during the measurement.

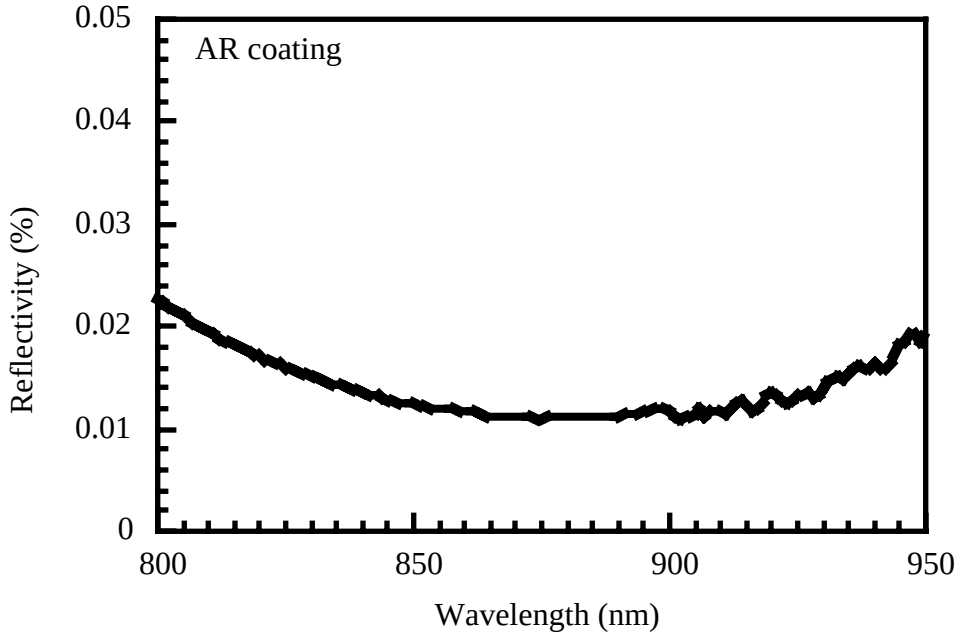

Figure 2.2.6 Measured reflectivity of the AR coating on top of the as grown GaAs/AlGaAs MQW sample.

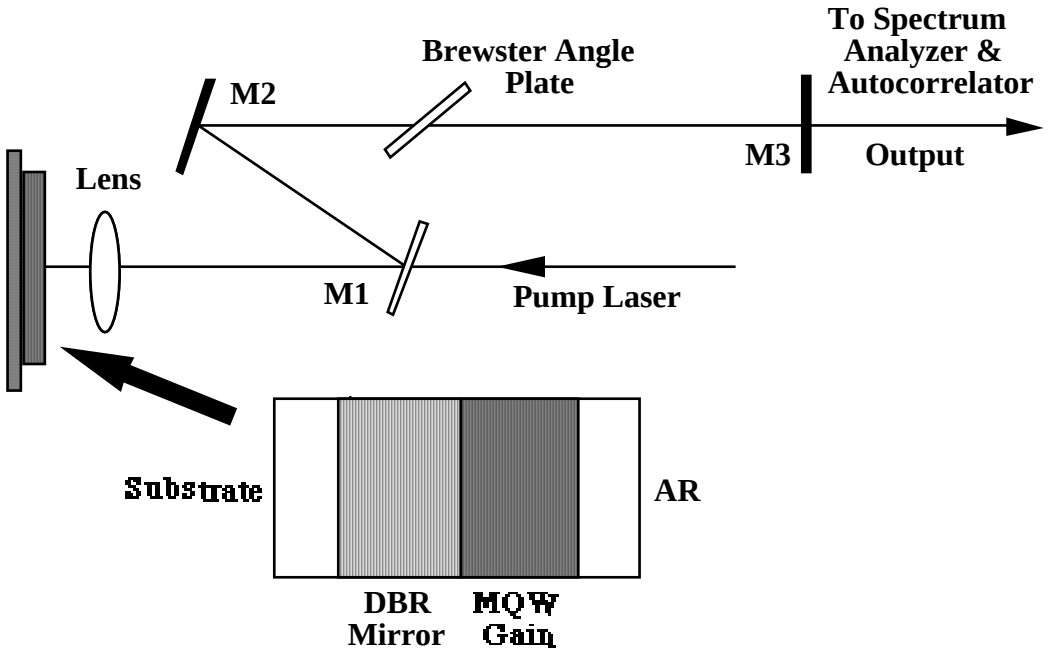

Figure 2.2.7 Cavity configuration of a GaAs mode-locked VCSEL.

To test the MQW sample, a CW Ti:sapphire laser at the wavelength of 800 nm is used to pump the external cavity surface-emitting laser. Room temperature CW operation at a pump power less than 80 mW is obtained with a 25.4 mm focal length lens and an output coupler of 99% reflectivity. It is, however, very unstable due to heating of the sample. The stability is improved by chopping the pump laser with 1:1 duty ratio, while maintaining the heat sink at 0˚C. Under these conditions, the threshold pump power becomes 90 mW with an output coupler of 97% [See curve (a) in Figure 2.2.8]. The maximum output power is 5.6 mW at the pump power of 140 mW. The decrease of the output power at high pump powers is caused by heating, which at sufficiently high level degrades the AR coating or damages the MQW sample. The material gain also decreases with the increase of the temperature. The actual lasing threshold of 90 mW pump is more than twice the predicted values (See Figures 2.2.3). The discrepancy can be attributed to the oversimplification of the theory that ignores the thermal detuning and the coupling between the wells. The actual pump area and active area are probably larger than the value assumed for predictions, too.

To mode-lock the external cavity surface-emitting laser, a synchronously mode-locked Coherent 700-series dye laser is used as the pump. The dye laser generates 5 - 10 ps pulses at a wavelength of 800 nm and a repetition rate of 80 MHz with the maximum average power of 190 mW. By matching the cavity length of the external cavity VCSEL to that of the dye laser, the VCSEL is mode-locked at room temperature.

Curve (b) in Figure 2.2.8 shows the average output power of the mode-locked external-cavity VCSEL varying with the pump power for a cavity lens with focal length of 38.1 mm and an output coupler at a reflectivity of 97%. The threshold pump power is 34 mW. Using Equation (2.1.12), the predicted threshold pump

power is 28 mW with an average threshold carrier density of 1.2 x 10^{18} cm^{-3} according to Figure 2.2.3 and thus an absorption coefficient of -3,100 cm^{-1} according to Figure 2.2.1. The actual value is in good agreement with the calculated value.

The maximum output power under synchronous pumping is 30.5 mW at a pump power of 190 mW. It is limited by the available pump power. The maximum external differential quantum efficiency is 27%. No output power saturation is observed within the available pump power. The laser can maintain operation for several hours continuously at room temperature without adjustment.

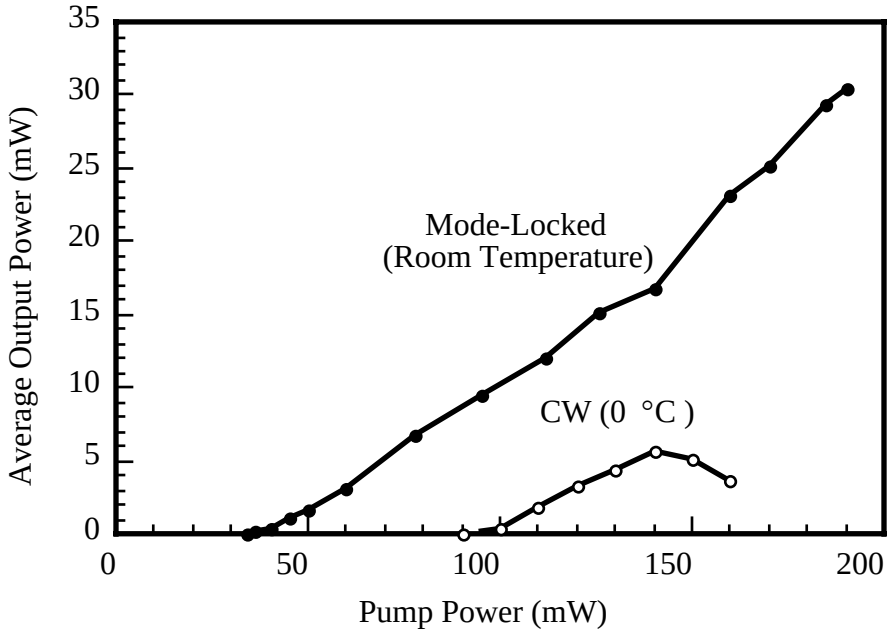

Figure 2.2.8 Average output power from an optically pumped external-cavity GaAs VCSEL as a function of input power.

2.2.3 mode-locked operation

Synchronous optical pumping is used to mode-lock the external cavity GaAs/AlGaAs VCSELs. The pump itself is a synchronously mode-locked Coherent 700-series dye laser that generates 5 - 10 ps pulses at a wavelength of 800 nm and a

repetition rate of 80 MHz when operating without the saturable absorber. Mode-locking of VCSELs is obtained by matching the VCSEL cavity length to that of the pump cavity length. The focal length of the lens in the cavity is 38.1 mm.

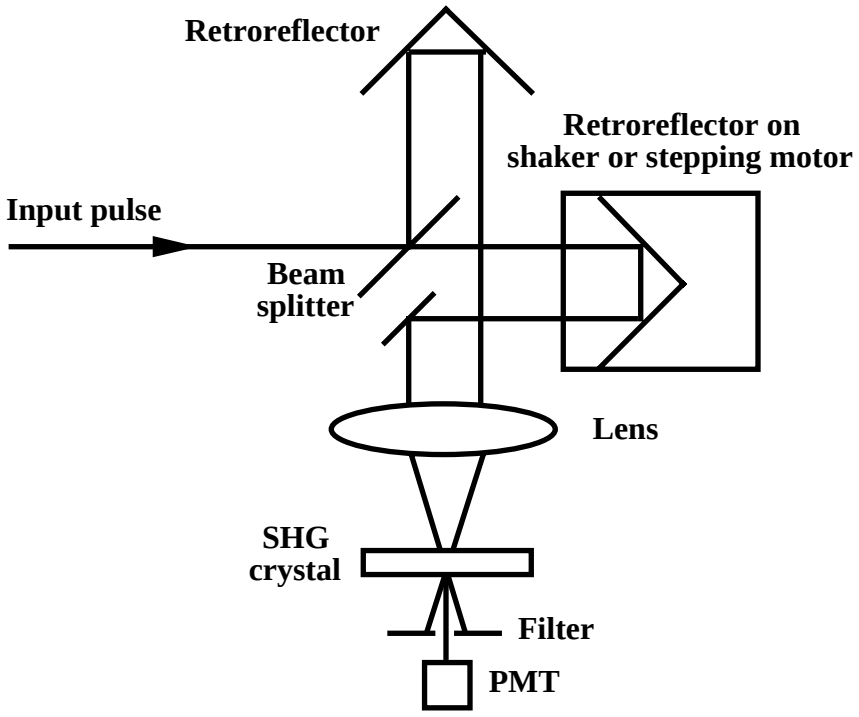

Figure 2.2.9 A noncolinear intensity autocorrelator configuration.

Autocorrelation measurement [8] is the usual way to measure the picosecond and femtosecond laser pulses. Figure 2.2.9 schematically shows a noncolinear autocorrelator. It is basically a Michelson interferometer. Two collimated beams are focused into a nonlinear crystal to generate second harmonic generation (SHG) and a photomultiply tube (PMT) is used to detect the SHG. One of the beams can be delayed during the measurement. The SHG signal as a function of the beam delay time is the intensity autocorrelation of the laser pulse. The laser pulsewidth information can be drawn from the full-width at half-maximum (FWHM) of the

intensity autocorrelation, assuming that the laser pulse shape is known. Table 2.2.2 shows the relationship between the FWHMs of laser pulse and its intensity autocorrelation for several common pulse shapes.

Table 2.2.2 Relation between FWHMs of Pulses and its Intensity Autocorrelation

$I(t)$	$\Delta\tau_{auto}/\Delta t$	$\Delta t\Delta\upsilon$
$1(0 \le t \le \Delta t)$	1	0.886
$\exp\left\{-\frac{(4\ln 2)t^2}{\Delta t^2}\right\}$	$\sqrt{2}$	0.441
$\sec h^2\left\{\frac{1.76t}{\Delta t}\right\}$	1.55	0.315
$\exp\left\{-\frac{(4\ln 2)t^2}{\Delta t^2}\right\}$ $(t \le 0)$	2	0.11

A typical autocorrelation trace of the pulse from the mode-locked GaAs VCSEL is shown in Figure 2.2.10 (a). The average power of this pulse is 14 mW. The pulsewidth is 14 ps if a Gaussian pulse shape is assumed. The coherent spike of the autocorrelation trace indicates that the spectral width of the pulse is much wider than the transform-limited pulse spectrum, which is confirmed by the measured power spectrum as shown in Figure 2.2.10 (b) with a spectral width of 6.6 nm. The time-bandwidth product of the pulse is 35.8, two orders of magnitude larger than the transform-limit.

The laser pulsewidth and the output power are dependent on the cavity length matching between the pump and the laser, as shown in Figure 2.2.11. The minimum pulsewidth is obtained at the laser cavity slightly longer than the length at which the maximum output power is obtained. The laser operation tends to be unstable when the laser cavity is shorter.

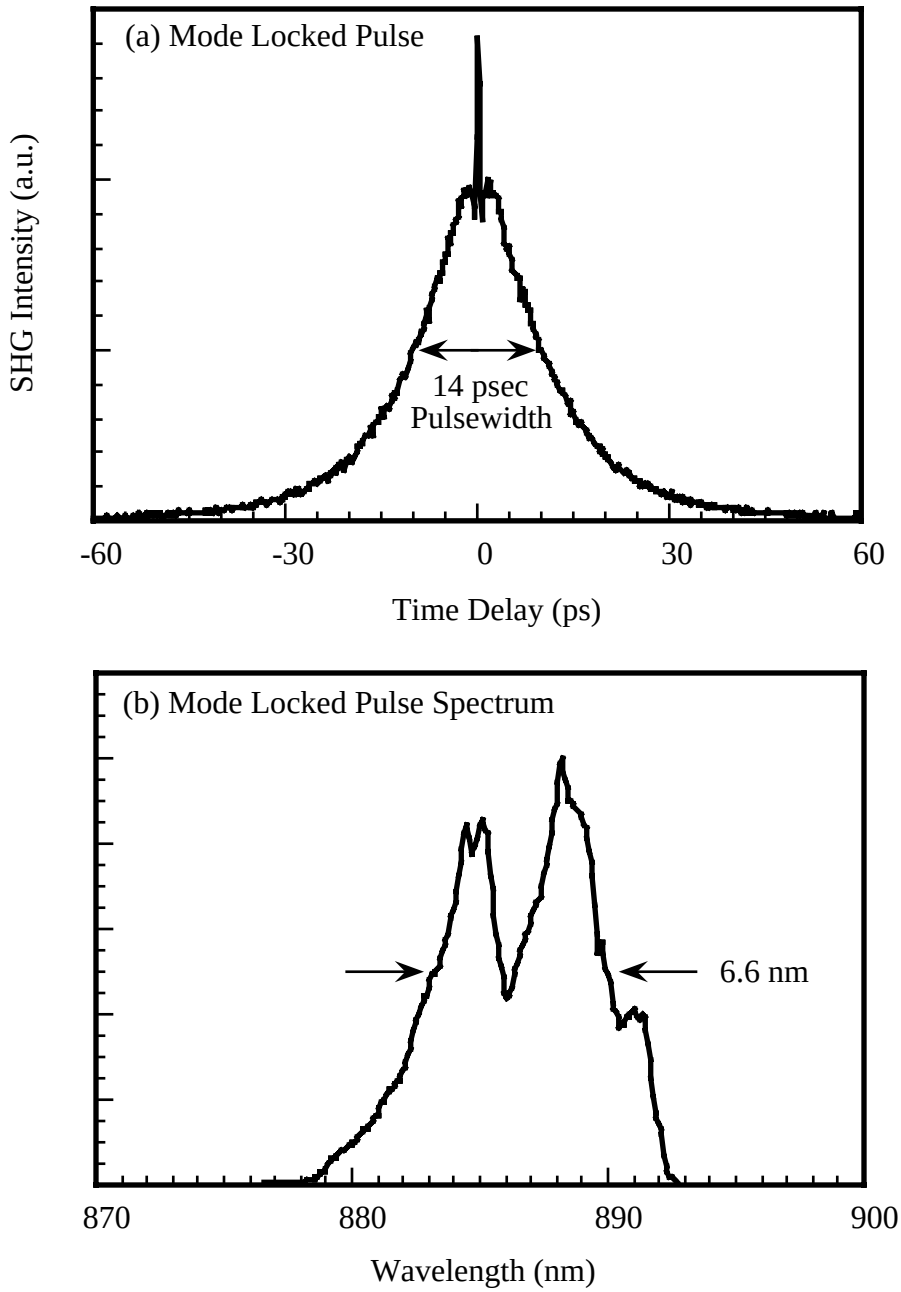

Figure 2.2.10 (a) A typical intensity autocorrelation trace of pulses from a mode-locked GaAs VCSEL. The pulsewidth at FWHM is 14 ps if assuming a Gaussian pulse shape. (b) The corresponding power spectrum.

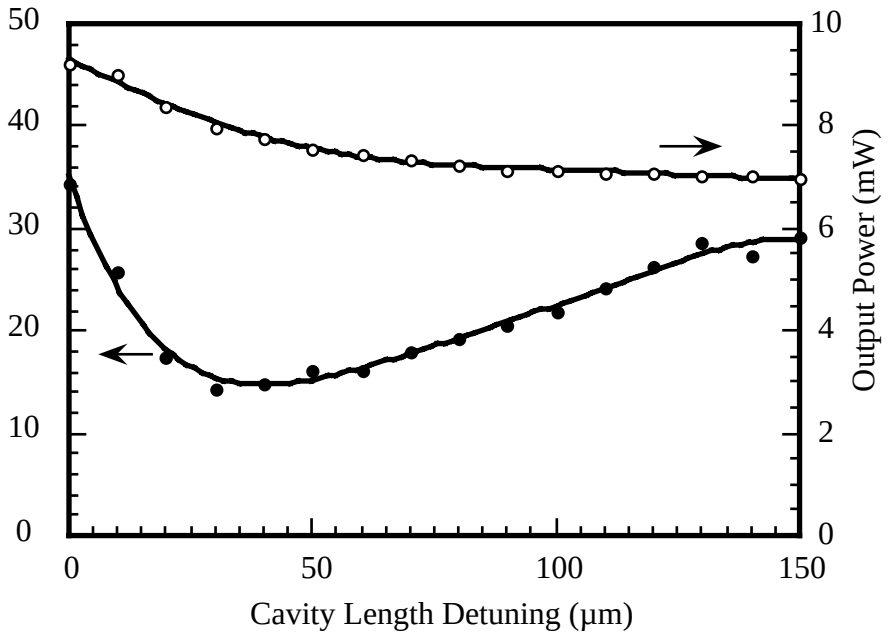

Figure 2.2.11 Pulsewidth and the corresponding average output power from a mode-locked GaAs VCSEL varying with the laser cavity length tuning.

Table 2.2.3 Comparison of Pulse Compression Techniques

	GVD sign	GVD magnitude	Loss	Application
Glass slab	variable	small	small	intra-cavity
Fiber	variable	variable	medium	intra-cavity or external cavity
Soliton fiber	negative	variable	medium	intra-cavity or external cavity
Parallel grating-pair	negative	large	large	external cavity
Grating-pair with telescope	variable	large	large	external cavity
Prism-pair	variable	small	small	intra-cavity
Gilles-Tourois Int.	variable	small	small	intra-cavity

The large time-bandwidth product of the pulses implies a large pulse chirping. Group velocity dispersion (GVD) can be introduced outside of the laser cavity to compensate for the pulse chirping [9, 10], and thus to compress the laser pulses. There are several effective ways of pulse compression, depending on the nature of pulse chirping. Some common techniques are listed in Table 2.2.3, along with their applicable ranges.

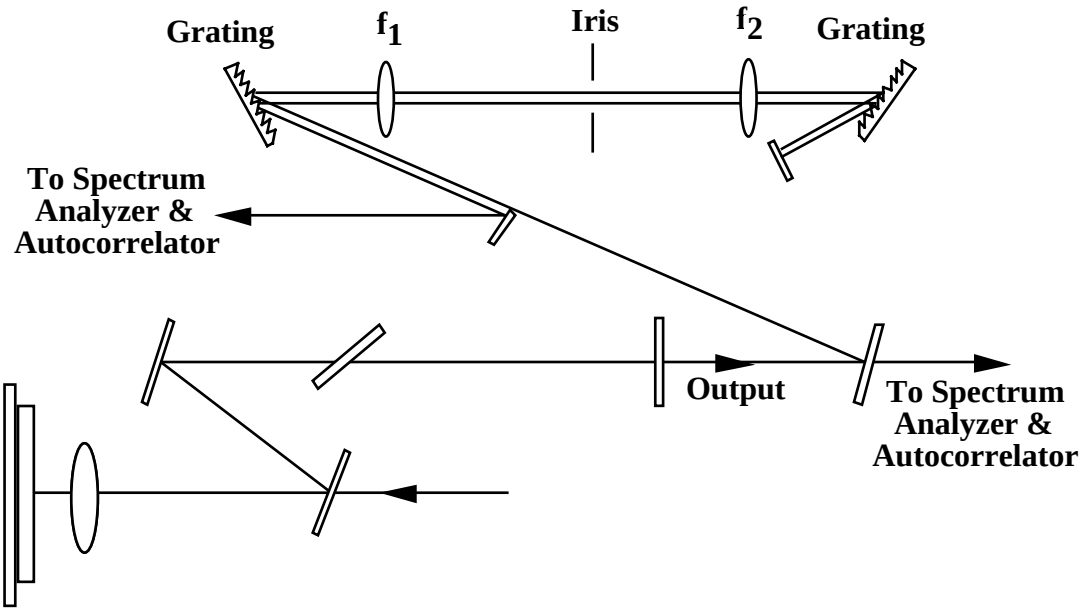

Figure 2.2.12 Pulse compressor used to compensate the chirp of the pulses from the mode-locked GaAs VCSEL.

Grating-pair compressors are among the most effective tools to compensate for the linear pulse chirping outside of the laser cavity. They are thus employed to compress the chirped pulses from the mode-locked GaAs VCSEL. A parallel grating-pair that gives only negative GVD [11] is found unable to compress the pulses. This implies that the pulses are either down-chirped or nonlinearly chirped. A more detailed analysis on the pulse chirping will be given in Chapter 5. A grating-pair with a

telescope configuration [12] can generate either positive GVD or negative GVD, depending on the distances between the two gratings and the two lenses. It is thus used for the pulse compression instead of the parallel grating-pair. Figure 2.2.12 shows the pulse compressor configuration. The gratings have a groove spacing of 1200 lines/mm. The focal length of the two lenses are f_1=175 mm and f_2 = 200 mm. The distance between the two lenses is 375 mm. Spectral windowing is used to modify the spectrum of the compressed pulses. When either or both of the gratings are moved closer to the lenses so that they are positioned between the lenses and their focal planes, the compressor is in the positive GVD region and the laser pulses are shortened, indicating the down-chirp characteristics of the pulses.

Figure 2.2.13 (a) shows the autocorrelation curve of the compressed pulses for the compressor with a slightly positive GVD. The pulsewidth would be 3.2 ps if a Gaussian pulse shape were assumed. The average power is 10 mW. The pulseshape is actually more likely a square in the main portion and falls exponentially in the tail from the autocorrelation curve. The pulses are shortened when more positive GVD is introduced as shown by the autocorrelation curve in Figures 2.2.13 (b). The pulsewidth would be 1.1 ps if a Gaussian pulse shape is again assumed. The average power of the compressed pulses is 8 mW. The pulses are further shortened when even more positive GVD is introduced as shown by the autocorrelation curve in Figures 2.2.13 (c) and (d). The pulsewidth would be 660 fs and 610 fs, respectively, if a Gaussian pulse shape is assumed. The average power is between 5 to 6 mW. Figure 2.2.14 (a) shows the autocorrelation of the pulses under optimum compression by the solid curve. The fitting to the autocorrelation by a single side exponential pulse shape

$$P(t) = P_1 \exp\left(-t / \tau_1\right) + P_2 \exp\left[-t / \tau_2\right]$$

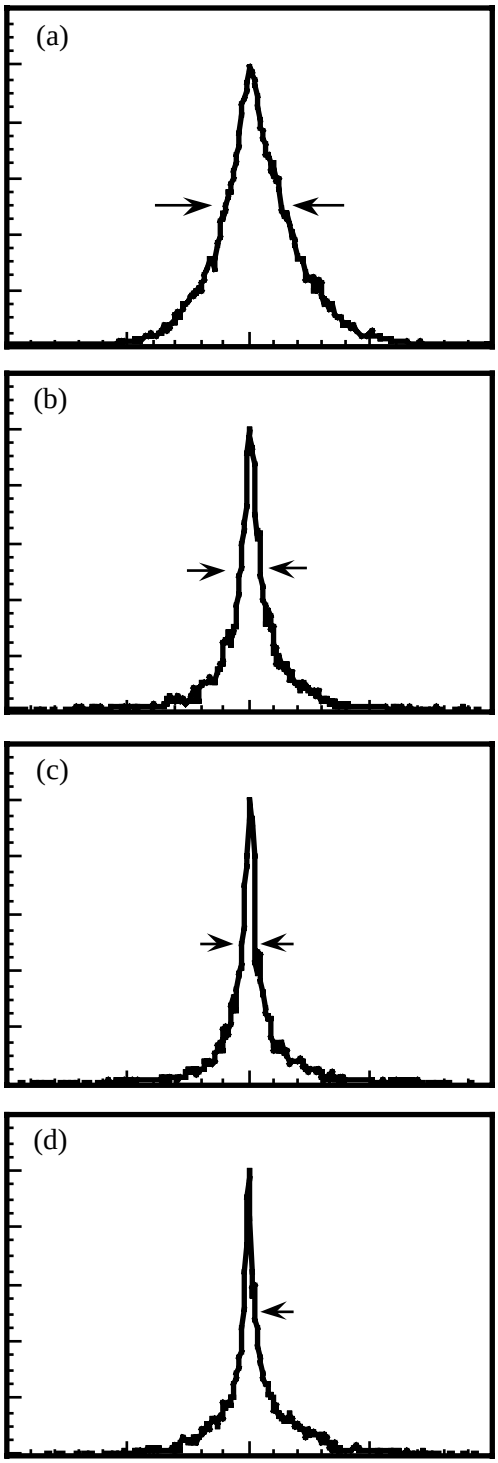

Figure 2.2.13 Intensity autocorrelation traces of compressed pulses coming out from a grating-pair compressor with the positive GVD increasing from (a) to (d).

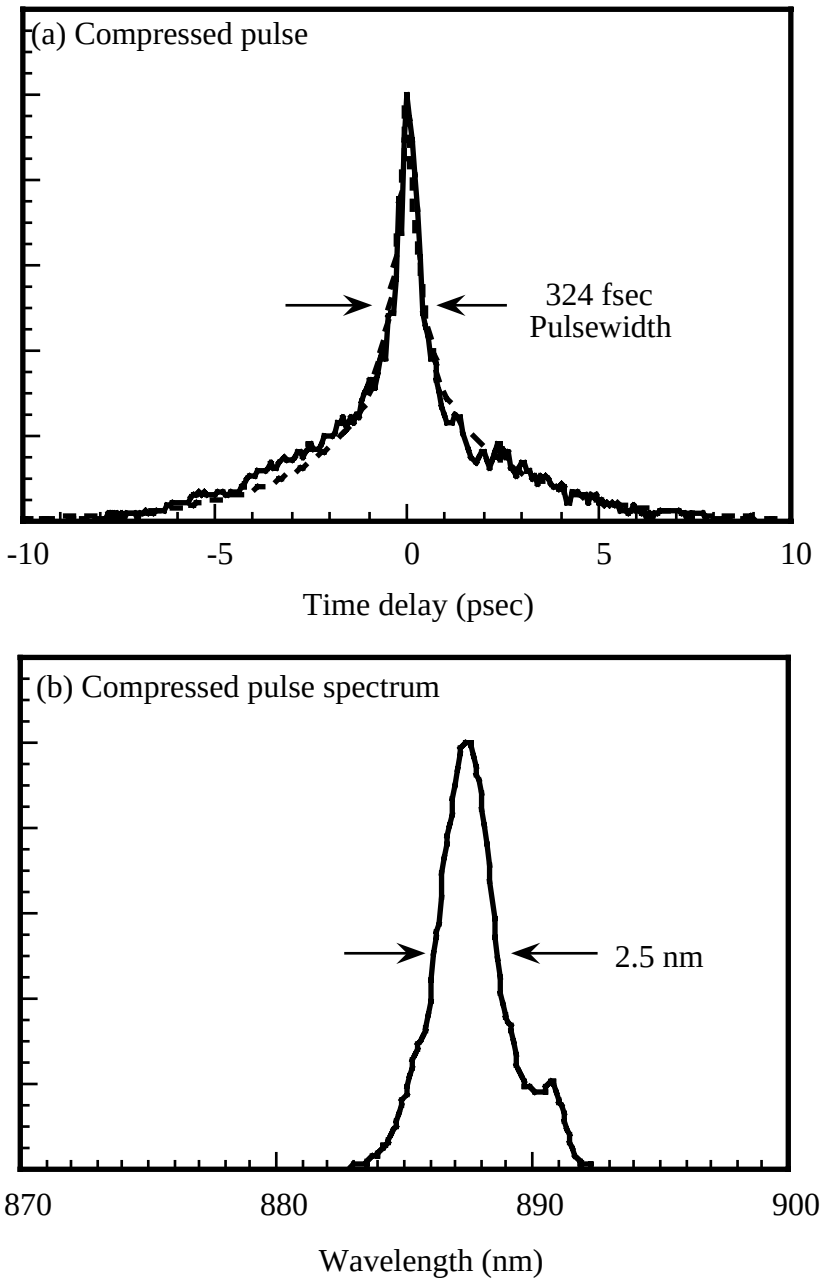

Figure 2.2.14 (a) The intensity autocorrelation trace of pulses in the optimum compression (solid line) and the fitting to the autocorrelation by single side exponential shape pulses (dashed line). (b) The corresponding power spectrum of the compressed pulses.

is shown by the dashed line, where τ_1 = 0.35 ps and τ_2 = 2.4 ps. The FWHM pulsewidth is 324 fs. The average power is 4 mW, thus P_1 = 50 W and P_2 = 14 W. The peak power of the pulses is 64 W. The correspondent spectrum of the compressed pulse is shown in Figure 2.2.14 (b). The spectral width is 2.5 nm, so the time-bandwidth product is 0.31.

An intracavity prism-pair chirp compensation technique has also been tested. The equilateral prisms are made of flint and separated by 10 cm inside of the laser cavity. When the laser gets mode-locked, the output power is 5.5 mW at the pump power of 160 mW. The pulse spectral width is around 3.2 nm, but the pulsewidth doesn't become shorter. Varying the distance between the prisms only changes the pulse spectral width, not the pulsewidth. For example, the spectral width becomes 6.0 nm when the distance is 5 cm, but the pulsewidth remain unchanged. Similar behavior is observed with SF 14 prisms instead of the flint.

2.3 Mode-locked InGaAs/InP vertical-cavity lasers

2.3.1 Gain structure

Auger nonradiative recombination is a serious problem for long wavelength semiconductor lasers [13]. To cope with the problem, the gain medium can be cooled to liquid nitrogen temperature (77K). Figure 2.3.1 shows the gain structure of InGaAs/InP MQW with 200 quantum wells grown on InP substrate of 430 μm thick. The well width is 150 Å and the barrier width is 50 Å. The epitaxial side is gold coated for serving as the cavity mirror. The gold reflectivity is 96%. The substrate side is AR-coated to reduce the intracavity loss as well as the Fabry-Perot (FP) effect.

The measured reflectivity of AR coating is shown in Figure 2.3.2. The laser is pumped by a Nd:YAG laser operating at the wavelength of 1.32 μm. To calculate the threshold pump power using Equations (2.1.6) and (2.1.10), Equations (2.2.1), (2.2.2) are first used to calculate $g(N)$, $\alpha(N)$ and $R_{sp}(N)$. They are shown in Figures 2.3.3 and 2.3.4, respectively. The parameters used for calculations are shown in Table 2.3.1. Agrawal's and Corzine's expressions again give the same transparent carrier density, but the differential gain from the Corzine's is larger. The threshold pump power varying with the number of quantum wells is shown in Figure 2.3.5, along with the threshold carrier density in the first quantum well and the last quantum well. For the quantum well number of 200, the predicted threshold pump power is 12 mW according to Figure 2.3.5.

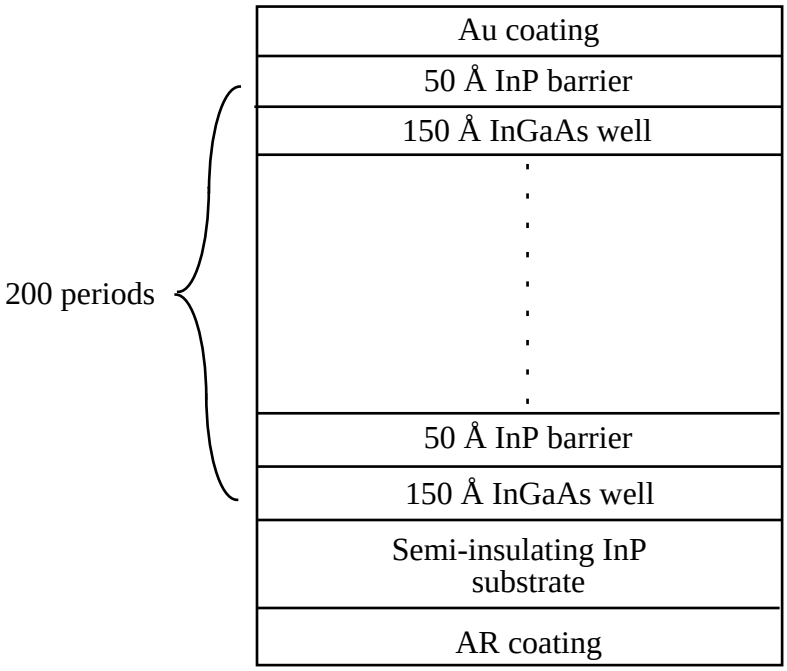

Figure 2.3.1 An InGaAs/InP MQW gain structure used for an optically pumped mode-locked VCSEL

Table 2.3.1 Parameters Used for Design of InGaAs/InP MQW

Parameter	Value
Eff. electron mass in well m_e	0.041
Eff. heavy hole mass in well m_{hh}	0.423
Eff. light hole mass in well m_{lh}	0.052
Eff. electron mass in barrier m_e	0.077
Eff. heavy hole mass in barrier m_{hh}	0.45
Eff. light hole mass in barrier m_{lh}	0.12
Bandgap in well E_g	0.817 eV
Bandgap in barrier E_g	1.403 eV
Conduction band offset	40%
Pump wavelength λ_p	1.32 μm
Operating temperature	77 K
Dielectric constant in well ε	12.62
Reflectivity of end mirror R_1	0.96
Reflectivity of coupler R_2	0.90
Intracavity optics transmission T	0.95
Well width L_w	150 Å
Barrier width L_b	50 Å
Active diameter d	22.7 μm (f = 38.1 mm)
Spin-orbit split [2]	***
Internal loss α_{int}	30 cm^{-1}

*** The data is not available and the value for GaAs is used for calculation

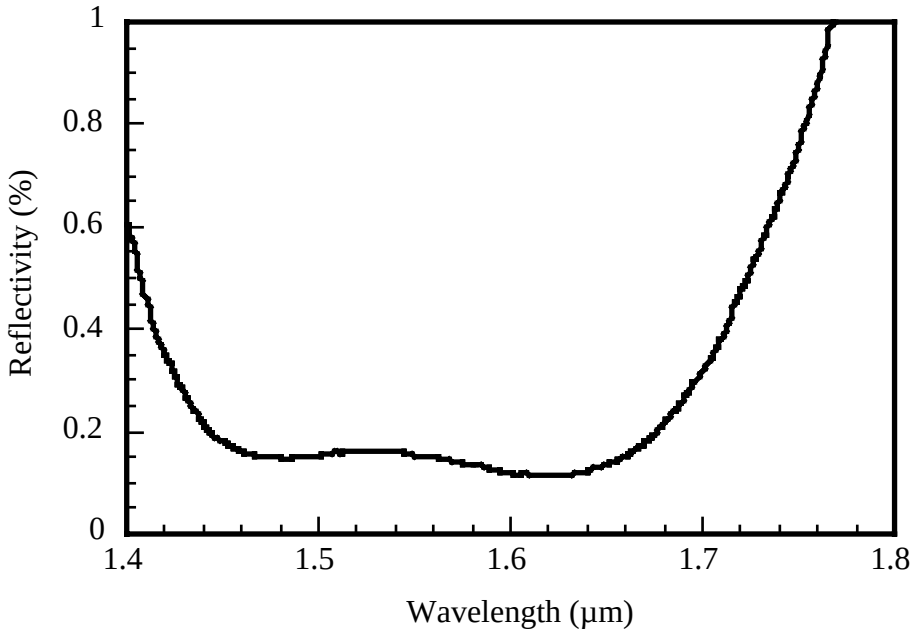

Figure 2.3.2 The measured reflectivity of AR coating on top of the InP substrate.

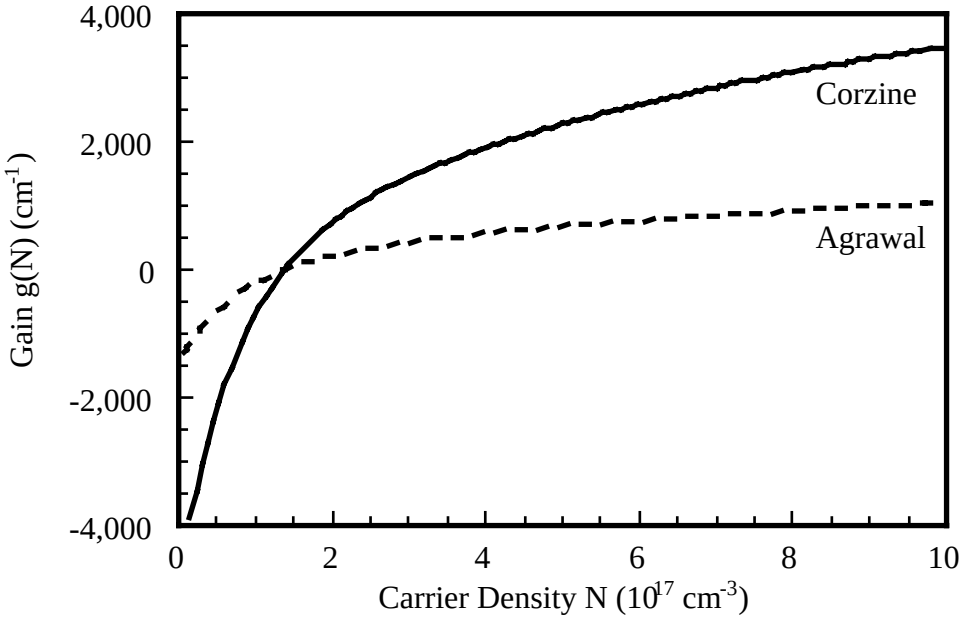

Figure 2.3.3 (a) Gain coefficient *g(N)* as a function of carrier density *N* at the lasing wavelength, for a InGaAs/InP MQW sample with a well width of 150 Å and a barrier width of 50 Å. The solid line is from Agrawal's expression, and the dashed line is from Corzine's expression.

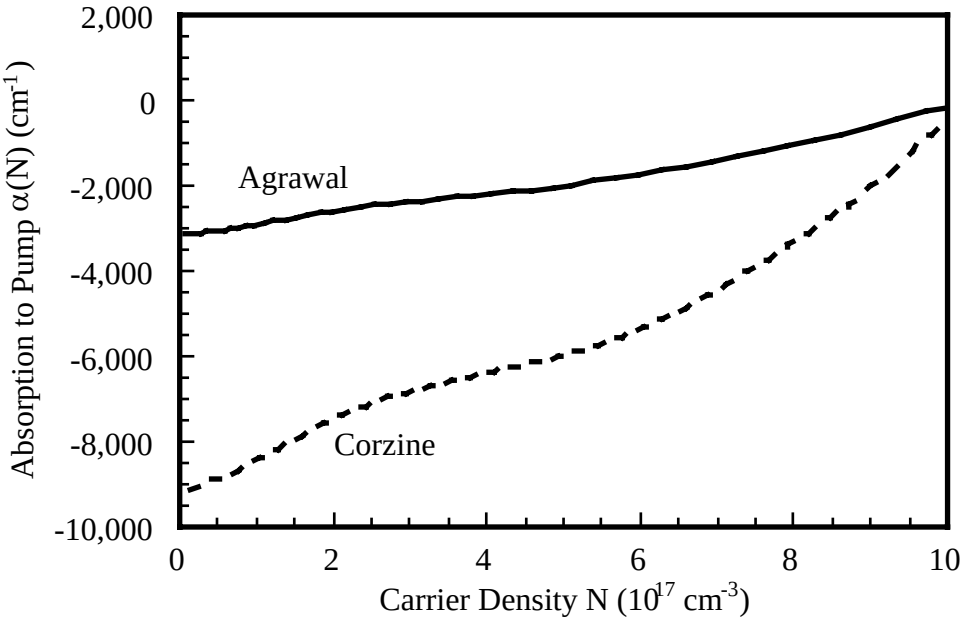

Figure 2.3.3 (b) Absorption coefficient $\alpha(N)$ as a function of carrier density N at the pump wavelength, for a InGaAs/InP MQW sample with a well width of 150 Å and a barrier width of 50 Å. The solid line is from Agrawal's expression, and the dashed line is from Corzine's expression.

2.3.2 InGaAs/InP external cavity VCSEL

The diagram of the laser cavity configuration is shown in Figure 2.3.6. The semiconductor gain medium is an InGaAs/InP MQW grown by molecular beam epitaxy, and consists of 200 periods of InGaAs (150 Å) separated by InP (50 Å). The gain is provided by the InGaAs MQW sample, which exhibits a room-temperature electron-heavy-hole (e-hh) absorption peak at 1.589 μm (Figure 2.3.7). The luminescence spectrum, obtained by cw excitation at 1.06 μm, is shown in Figure 2.3.8 (a). At operating temperatures of 77 K, the e-hh absorption peak is below 1.50 μm and the luminescence spectrum is that shown in Figure 2.3.8 (b). The substrate side of the sample is AR coated to reduce reflection and the epitaxial side is gold

coated, providing an end mirror for the laser cavity with a reflectivity of 96% and good thermal conductivity. Nonradiative Auger recombination losses are large at room temperature, so the sample is cooled to liquid-nitrogen temperatures in a cryostat with AR-coated windows. The laser cavity is completed by a 10% output coupler, a 1-mm-thick quartz birefringent tuning element (with a bandwidth of 30 nm) to tune the lasing frequency, and an AR-coated lens (focal length of 38.1 mm) focused on the MQW sample. A dichroic steering mirror coupled optical pump light from the 1.32 μm Nd:YAG pump laser into the 1.5 m cavity.

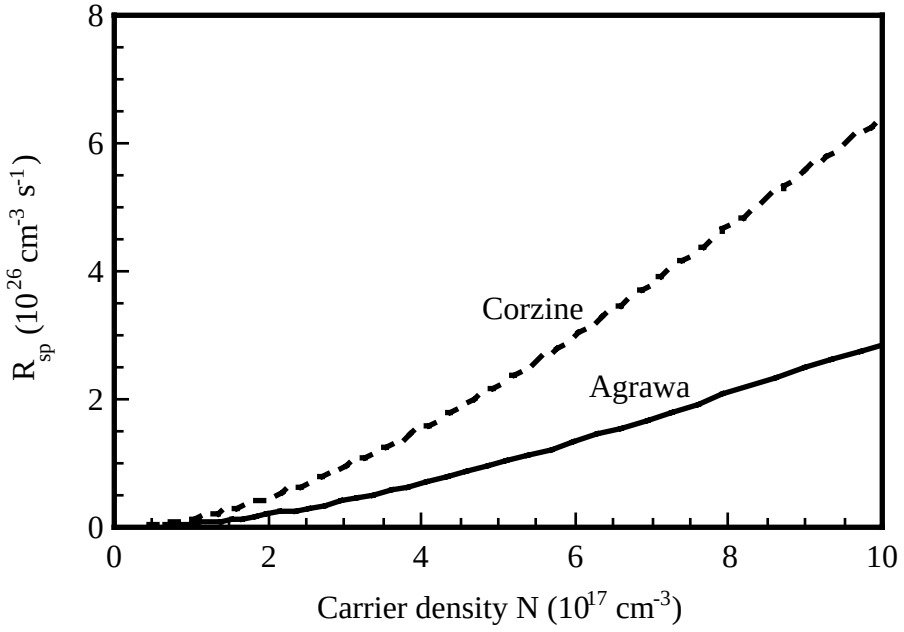

Figure 2.3.4 Spontaneous emission rate $R_{sp}(N)$ as a function of carrier density N for a InGaAs/InP MQW sample with a well width of 150 Å and a barrier width of 70 Å. The solid line is from Agrawal's expression, and the dashed line is from Corzine's expression.

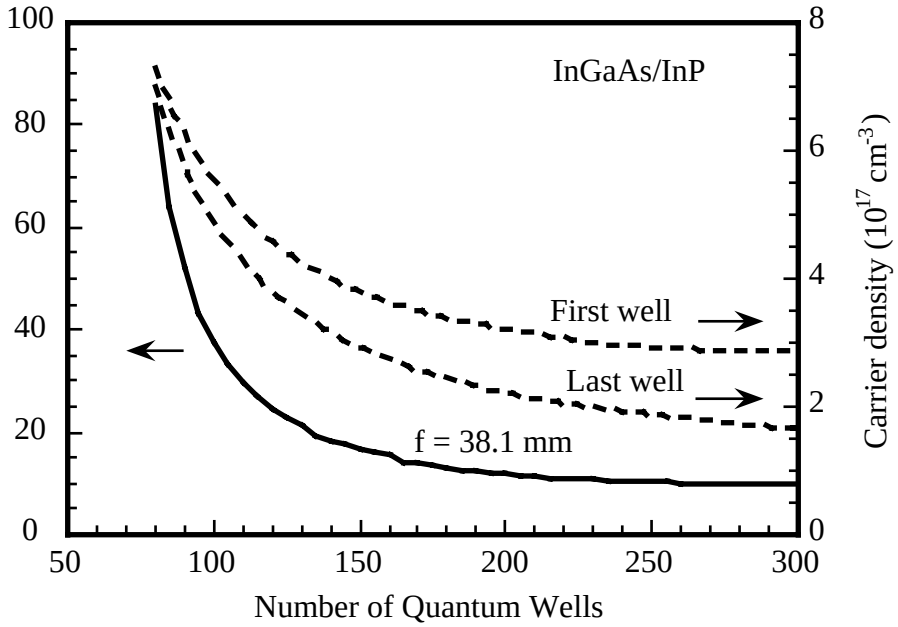

Figure 2.3.5 Threshold pump power as a function of number of quantum wells for the lens focal length of 38.1 mm (solid line), and the corresponding carrier density in the first quantum well and the last quantum well (dashed lines).

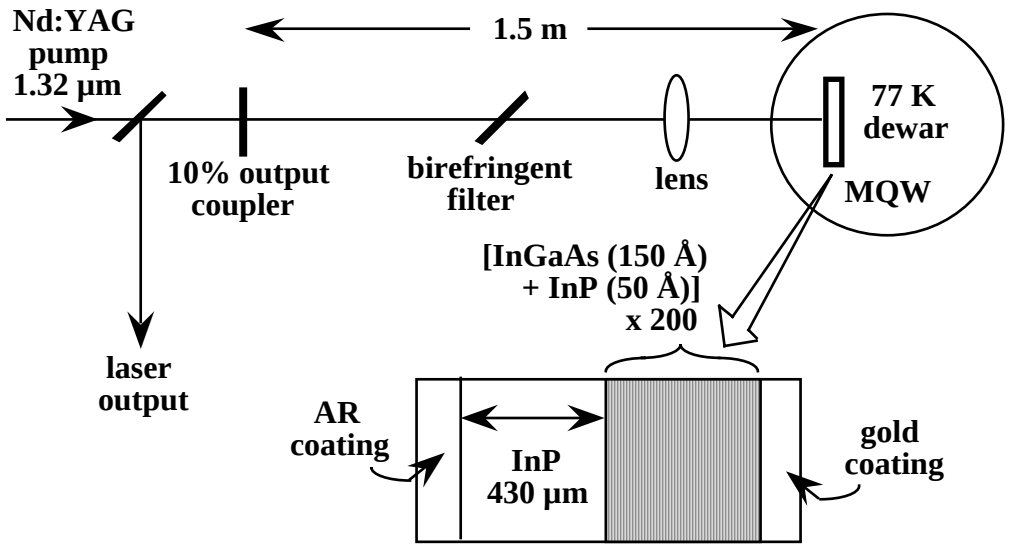

Figure 2.3.6 Cavity configuration of an InGaAs/InP mode-locked VCSEL.

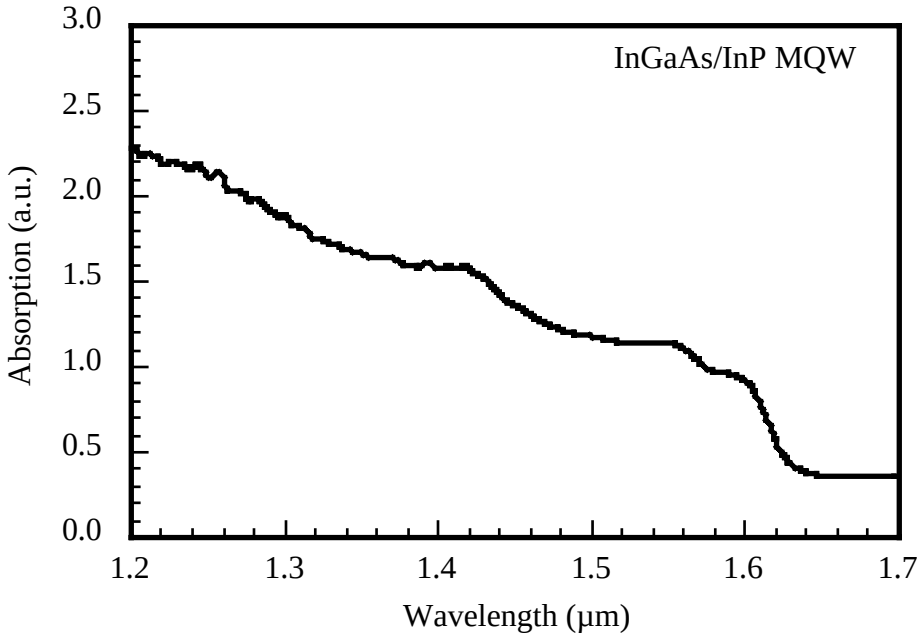

Figure 2.3.7 The absorption of the InGaAs/InP MQW sample as a function of wavelength at room temperature.

CW operation of the laser gives large output powers. Figure 2.3.9 (a) shows output powers as a function of pump power. The maximum output power is 190 mW at 1.3 W pump power, and the lasing threshold is at 40 mW pumping. These power levels are comparable to those of color-center lasers at this wavelength [14]. The absolute quantum efficiency of conversion from pump photons to lasing photons is as high as 18%, and the maximum differential quantum efficiency is 23%. Figure 2.3.9 (b) shows the center wavelength of the laser at peak powers, which shifts from 1.495 μm at threshold to 1.518 μm. Thermal loading, due to inadequate thermal contact of the MQW to the cryostat cold finger helped to prevent further increases of output power. The laser can be tuned from 1.44 μm to 1.53 μm with the birefringent tuning element, as shown in Figure 2.3.10 with the pump power of 850 mW. The sudden stop of lasing at wavelength of shorter than 1.44 μm is caused by the rapid deteriorating AR

coating at 1.44 μm as shown in Figure 2.3.2. The sudden stop of lasing at wavelength longer than 1.53 μm is caused by the bandgap limit.

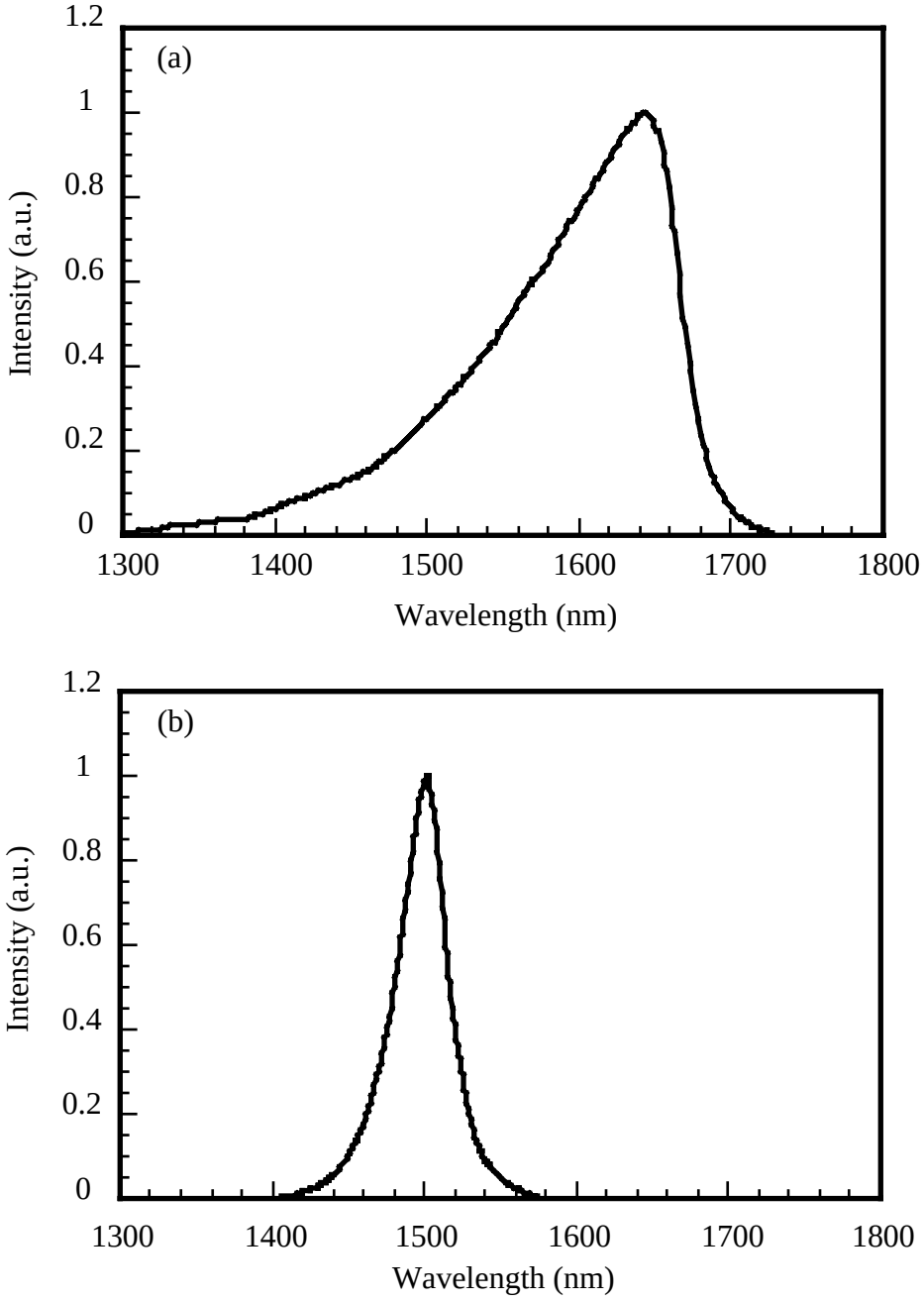

Figure 2.3.8 Photoluminescence spectrums of the InGaAs/InP MQW (a) at room temperature and (b) at 77 K.

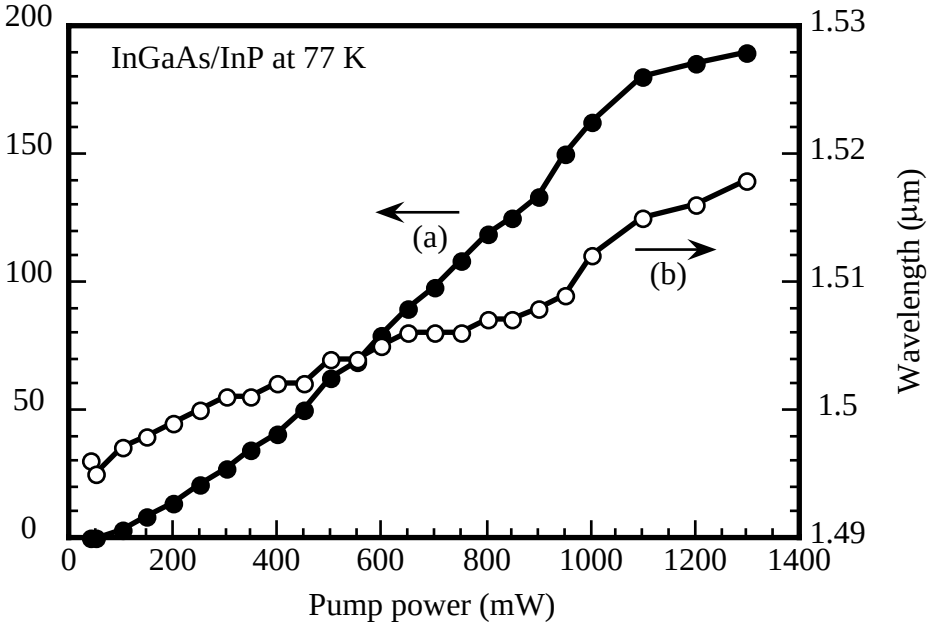

Figure 2.3.9 (a) Average output power from an InGaAs/InP external cavity SEL as a function of the pump power when the laser is operating at CW, and (b) The corresponding central wavelength varying with the pump.

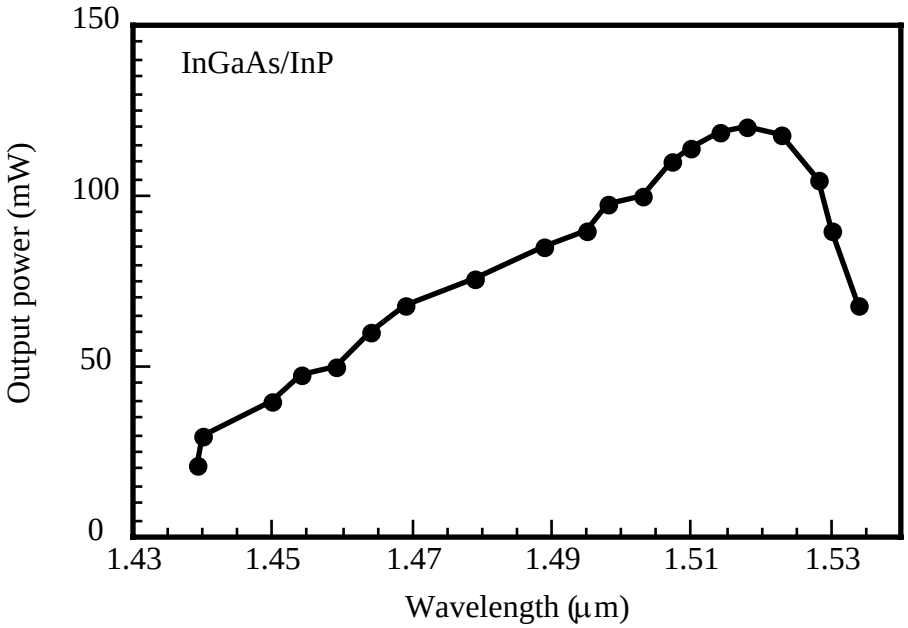

Figure 2.3.10 The wavelength tuning range of the InGaAs external-cavity SEL at 77 K.

The threshold pump power of 40 mW at CW is much larger than the predicted value of 12 mW as shown in Figure 2.3.5. Such a discrepancy is partly due to the difficulty in determining the actual active area and the pump area for the theoretical prediction. There may of cause be others causes.

Synchronous pumping at 100 MHz with 110 ps pulses from the 1.32 μm Nd:YAG gives 100 psec pulses and the average output powers nearly identical to the CW results, but with a reduced threshold pump power of 20 mW (See Figure 2.3.11). The predicted threshold pump power is 10 mW with the threshold carrier density of 2.8×10^{17} cm^{-3} and thus the absorption coefficient of -2400 cm^{-1} from Figures 2.3.3 and 2.3.5.

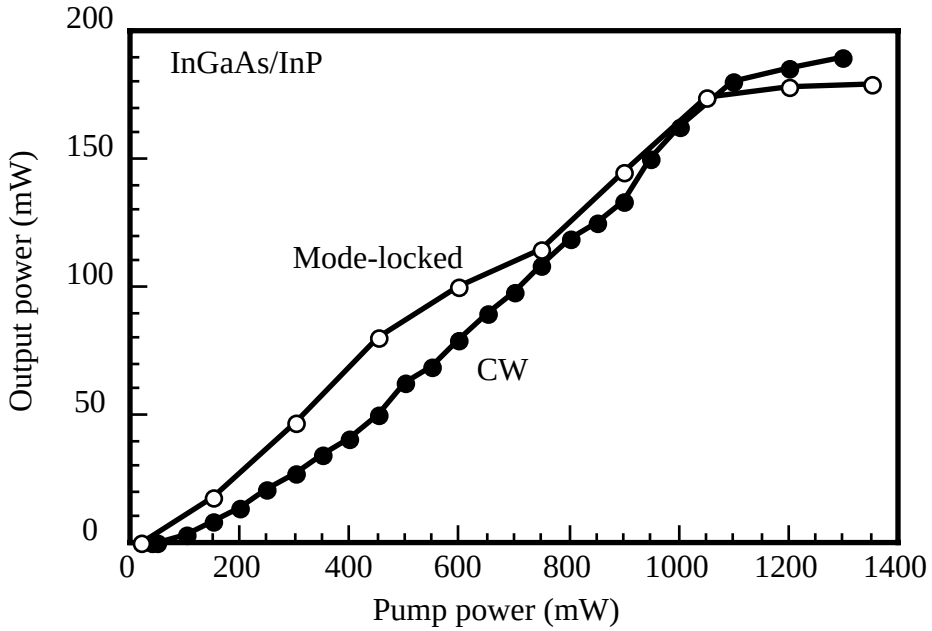

Figure 2.3.11 The average output power of the mode-locked InGaAs/InP VCSEL as a function of the pump power. The CW operating curve is shown for comparison.

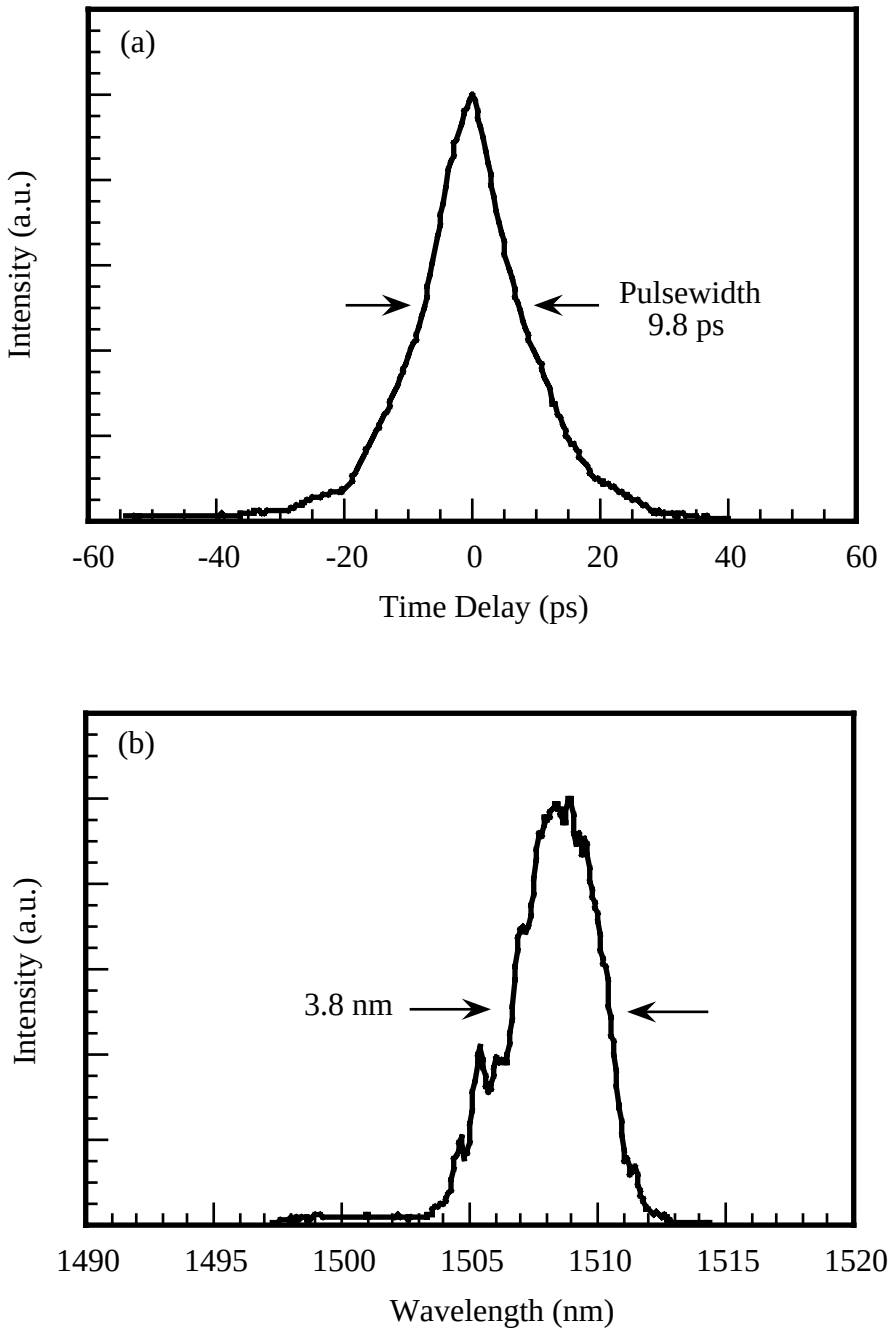

Figure 2.3.12 (a) The Intensity autocorrelation trace of pulses from a mode-locked InGaAs/InP VCSEL. Pulsewidth is 9.8 ps assuming a hyperbolic secant profile. (b) The corresponding power spectrum of the pulses.

2.3.3 Mode-locking operation

InGaAs/InP VCSELs can be mode-locked by synchronous pumping with a CW mode-locked 1.32 μm YAG laser. Residual reflection of AR coating on the InP substrate to both the pump and laser, however, prohibits shorter pulse generation. The output pulsewidth is very close to the pump pulsewidth of about 110 ps. To solve the problem, the YAG laser pulse is compressed to 6.0 ps using 80 meters of single-mode polarization-preserving optical fiber (GVD = 16 ps/km nm) and parallel grating-pair of 1200 lines/mm [15]. Masking is used to eliminate the pedestal [16]. The compressed pump has a power of 250 mW, which is limited by the Raman scattering in the fiber during the compression [17]. The average output power from the VCSEL is 15 mW at the maximum available pump power. The pulsewidth is measured with a FemtoChrone fast scan autocorrelator. Figure 2.3.12 (a) shows an autocorrelation trace, averaged 40 times, of the resulting pulses. Assuming a hyperbolic secant profile, the pulse has a FWHM of 9.4 ps. Single traces without averaging show pulses as short as 7.7 ps, though noisier. Figure 2.3.12 (b) shows the spectrum of the pulses, which has a FWHM spectral width of 3.8 nm. The measurement resolution is 2.5 nm, so the correspondent actual spectral width is 2.8 nm. The time-bandwidth product $\Delta\upsilon\Delta\tau$ (assuming 7.7 ps pulses) is 2.8, or roughly nine times of the transform limit, indicating that pulses are chirped.

Since the wavelength of the laser is around 1.5 μm, two methods can be used to shorten the pulsewidth, (1) grating-pair chirp compensation and (2) negative GVD fiber compression, if the laser pulse is upchirped. Soliton effect inside of fiber will further help in shortening the pulsewidth [18]. A parallel grating-pair is found capable of compressing the pulsewidth, which implies that the pulses are upchirped.

The compression is accomplished by double-pass transmission of pulses through a pair of identical 600 line/mm diffraction gratings separated by 36 cm. This yielded the (averaged) autocorrelation trace as shown in Figure 2.3.13. The pulsewidth is 1.6 ps if a secant hyperbolic pulse shape is assumed. Single-scan traces indicate that pulsewidth is as short as 1.1 ps, the discrepancy due to sweep to sweep jitter in the rotating-mirror autocorrelator. The spectral width (FWHM) of the pulse is reduced to 2.0 nm, with the time-bandwidth product of 0.29. The autocorrelation trace indicates that there is a small subsidiary pulse about 9.5 ps away from the main pulse, consistent with an etalon effect in the 430 μm-thick sample. The average power of the compressed pulses is 7 mW, implying a peak power of 64 W.

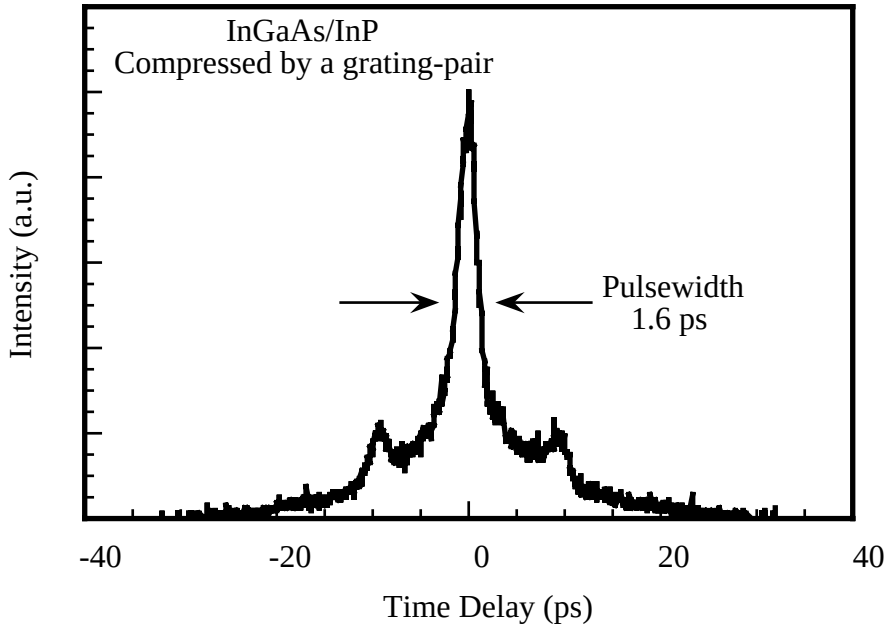

Figure 2.3.13 The intensity autocorrelation trace of the pulses from the mode-locked InGaAs VCSEL compressed by a grating-pair. Pulsewidth is 1.6 ps if assuming a hyperbolic secant profile.

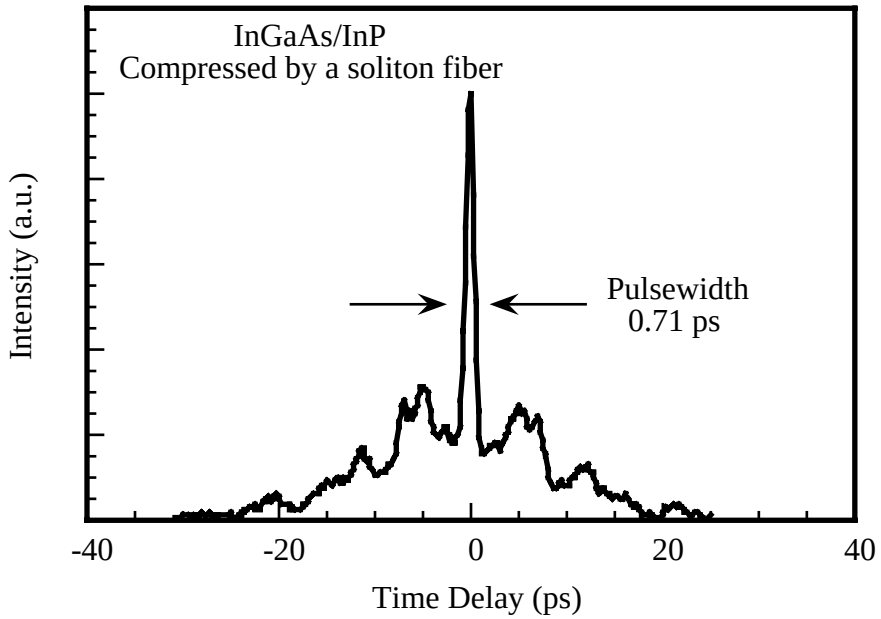

Figure 2.3.14 The intensity autocorrelation trace of the pulses from the mode-locked InGaAs VCSEL compressed by a grating-pair. Pulsewidth is 0.71 ps if assuming a hyperbolic secant profile.

Negative GVD in an optical fiber can also be utilized for the pulse chirp compensation. Pulses are coupled directly from the mode-locked VCSEL into a 400 m length of single-mode optical fiber with a negative GVD of 16 ps/km nm. The fiber dispersion compensates the pulse chirping. Due to the nonlinearity-induced self-phase modulation (SPM), additional pulse shortening can be produced through soliton effects. The compressed pulse has a duration of 710 fs with an average power of 10 mW as shown in Figure 2.3.14. The pedestal as wide as the uncompressed pulses shown by the autocorrelation can probably be reduced by tailoring the fiber length appropriately and by using polarization-preserving fiber. Higher order soliton effects are the cause of the multipeaks in Figure 2.3.14.

To completely solve the etalon problem due to the residual reflection from the AR-coating on the InP substrate, the substrate can be slanted by polishing, as shown

in Figure 2.3.15. Synchronous pumping the VCSEL with this 5□ slanted substrate by the mode-locked 1.32 μm YAG laser has been able to generate pulses of durations ranging from 5 to 30 ps with an average power over 200 mW [19]. The time-bandwidth product of the pulses is 100 times larger than the transform-limit. The subsequent pulse compression with a parallel grating-pair reduces the pulsewidth to 150 fs. The compressed pulse has a peak power over 3 kW, which is comparable to that from a mode-locked color center laser in this wavelength region. The second stage compression with a 400 m soliton fiber further reduces the pulsewidth from 150 fs to 21 fs [20].

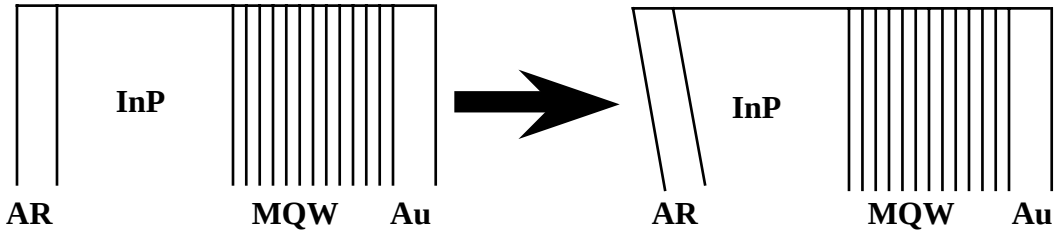

Figure 2.3.15 A schematic of slanting the InP substrate to reduce the reflection from the substrate surface into the cavity of a mode-locked InGaAs/InP VCSEL.

References

[1] A. Yariv, "*Quantum Electronics*," (John Wiley & Sons, Inc., 2nd Ed., 1975)

[2] M. Sargent III, M. O. Scully, and W. E. Lamb Jr., "*Laser physics*," (Addison-Wesley Pub. Co., Advanced Book Program, Mass., 1974)

[3] G. P. Agrawal, and N. K. Dutta, "*Long-wavelength semiconductor lasers*," (Van Nostrand Reinhold, New York, 1986)

[4] R. H. Yan, S. W. Corzine, L. A. Coldren and I. Suemune, "Corrections to the expression for gain in GaAs," *IEEE J. Quantum Electron.*, QE-26, 213 (1990)

[5] S. W. Corzine, "Design of vertical-cavity surface-emitting lasers with strained and unstrained quantum well active regions," (Ph.D dissertation, ECE Technical Report #93-09, UCSB, 1993)

[6] E. O. Kane, "Band structure of indium antimonide," *J. Phys. Chem. Solids*, **1**, 249 (1957)

[7] H. C. Casey, Jr., and M. B. Panish, "*Heterostructure lasers*," Part A, Chap. 3, (Academic Press, New York, 1978)

[8] H. A. Haus, "*Waves and Fields in optoelectronics*," Chap. 13, (Prentice-Hall, Inc, Englewood Cliffs, NJ, 1984)

[9] J. A. Giordmaine, M. A. Duguay, and J. W. Hansen, "Compression of optical pulses," *IEEE J. Quantum Electron.*, **QE-4,** 252 (1968)

[10] R. A. Fisher, and J. A. Fleck, "On the phase characteristics and compression of picosecond pulses," *Appl. Phys. Lett.*, **15**, 287 (1969) and R. A. Fisher, P. L. Kelley, and T. K. Gustafson, "Subpicosecond pulse generation using the optical Kerr effect," *Appl. Phys. Lett.*, **14**, 140 (1969)

[11] E. B. Treacy, "Optical pulse compression with diffraction gratings," *IEEE J. Quantum Electron.*, **QE-5**, 454 (1969)

[12] O. E. Martinez, "3000 times grating compressor with positive group velocity dispersion: application to fiber compensation in 1.3 - 1.6 μm region," *IEEE J. Quantum Electron.*, **QE-23**, 59 (1987)

[13] A. R. Beattie, P. T. Landsberg, "Auger effect in semiconductors," *Proc. R. Soc. London Ser.* A **249**, 16 (1959); Y. Horikoshi, and Y. Furukawa, "Temperature sensitive threshold current of InGaAsP-InP double heterostructure lasers," *Jpn. J. Appl. Phys.*, **18**, 809 (1979); G. H. B.

Thompson, and G. D. Henshall, "Nonradiative carrier loss and temperature sensitivity of threshold in 1.27 μm (GaIn)(AsP)/InP D. H. lasers," *Electron. Lett.*, **16**, 42 (1980); N. K. Dutta, and R. J. Nelson, "Temperature dependence of threshold of InGaAsP/InP double-heterostructure lasers and Auger recombination," *Appl. Phys. Lett.*, **38**, 407 (1981); A. Sugimura, "Band-to-band Auger recombination effect on InGaAsP laser threshold," *IEEE J. Quantum Electron.*, **QE-17**, 627 (1981)

[14] J. F. Pinto, L. W. Stratton, and C. R. Pollock, "Stable color-center laser in K-doped NaCl tunable from 1.42 to 1.76 μm," *Opt. Lett.*, **10**, 384 (1985)

[15] C. V. Shank, R. L. Fork, R. Yen, R. H. Stolen, and W. J. Tomlinson, "Compression of femtosecond optical pulses," *Appl. Phys. Lett.*, **40**, 761 (1982)

[16] J. P. Heritage, R. N. Thurston, W. J. Tomlinson, A. M. Weiner, and R. H. Stolen, "Spectral windowing of frequency-modulated optical pulses in a grating compressor," *Appl. Phys. Lett.*, **47**, 87 (1985)

[17] R. H. Stolen, E. P. Ippen, A. R. Tynes, "Raman oscillation in glass optical waveguide," *Appl. Phys. Lett.*, **20**, 62 (1972)

[18] L. F. Mollenauer, R. H. Stolen, and J. P. Gordon, "Experimental observation of picosecond pulse narrowing and solitons in optical fibers," *Phys. Rev. Lett.*, **45**, 1095 (1980)

[19] W. H. Xiang, S. R. Friberg, K. Watanabe, S. Machida, W. B. Jiang, H. Iwamura, and Y. Yamamoto, "Femtosecond external-cavity surface-emitting InGaAs/InP multiple-quantum-well laser," *Opt. Lett.*, **16**, 1394 (1991)

[20] W. H. Xiang, S. R. Friberg, K. Watanabe, S. Machida, Y. Sakai, H. Iwamura, and Y. Yamamoto, "Sub-100 femtosecond pulses from an external-cavity surface-emitting InGaAs/InP multiple quantum well laser with soliton-effect compression," *Appl. Phys. Lett.*, **59**, 2076 (1991)

Chapter 3 Femtosecond Periodic Gain Vertical-Cavity Semiconductor Lasers

3.1 Time-bandwidth product control and anti-gain-saturation

VCSELs can be mode-locked to generate picosecond pulses with a peak power of 100 times larger than that from a mode-locked in-plane semiconductor laser, as shown in the last chapter. Subpicosecond pulses are obtained by external cavity pulse compression. An equally interesting focus is to explore the shortest possible pulses that can be **directly** generated from VCSELs. This topic is discussed in this chapter.

An important factor that prevents subpicosecond pulse generation directly from the mode-locked VCSELs is significant laser pulse chirping, as to be discussed in Chapter 5. The time-bandwidth product of the pulses generated from this type of laser is usually 100 times larger than the Fourier transform limit. Grating-pair chirp compensation techniques have been employed to compress the laser pulses externally, thus the laser pulses have been compressed to 320 fs for the GaAs/AlGaAs system (Figure 2.2.14) and 150 fs for the InGaAs/InP system [1]. Intracavity chirp compensation with prism-pair is usually an efficient way for subpicosecond pulse generation directly from a laser oscillator, but is not very practical for such a laser with large pulse chirping. An intracavity filter is thus used to limit the extra bandwidth created by the pump induced XPM and the gain saturation induced SPM. This method is proved to be effective in controlling the time-bandwidth product of the laser pulses. The output laser pulsewidth usually remains unchanged or is sometimes shorter.

The experimental configuration is the same as that shown in Fig. 2.2.7 with a GaAs/AlGaAs multiple-quantum-well (MQW) active medium at room temperature.

To control the pulse chirping, a Brewster-angle placed birefringent filter is used in the laser cavity instead of the Brewster-angle glass plate. The filter thickness is 0.5 mm. With the pump pulse from the synchronously mode-locked dye laser, the laser pulsewidth from the VCSEL is 10 ps as shown in Fig. 3.1.1(a), as measured by a synchronous-scan streak camera. The specified resolution of the streak camera is 10 ps. The corresponding laser pulse spectrum is shown in Fig. 3.1.1(b). The actual pulsewidth should be shorter since the streak camera measurement averages hundreds of pulses. The timing jitter between pulses broadens the measured pulsewidth value. The time-bandwidth product of the pulses is 3.6, which is about one tenth of that shown earlier (Figure 2.2.10).

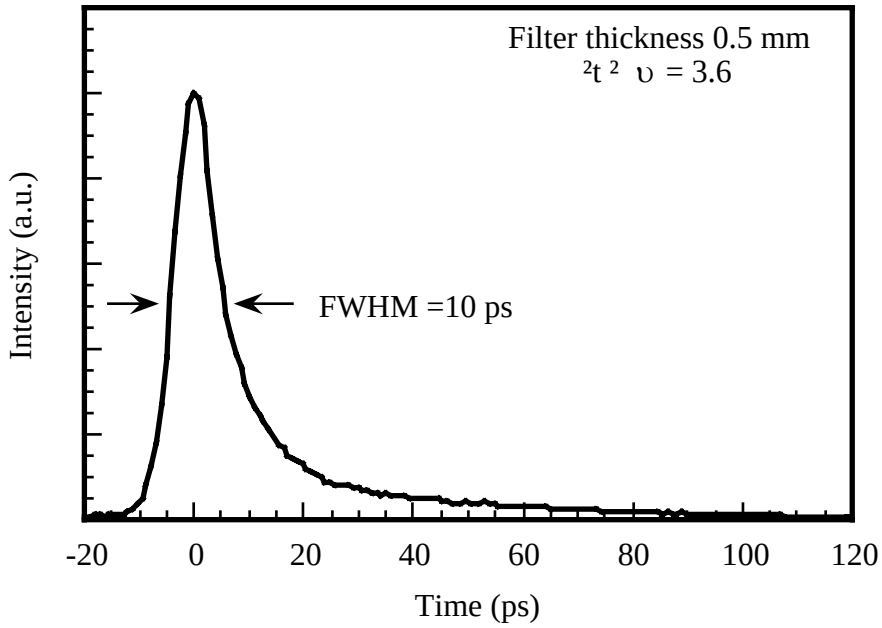

Figure 3.1.1 (a) Pulses from a mode-locked GaAs VCSEL with a birefringent filter of 0.5 mm in the cavity when pumped by a synchronously mode-locked dye laser. The measurement is conducted with a streak camera of 10 ps specified resolution.

For synchronous mode-locking, the leading edge of the laser pulse is shaped by the

rising edge of the pump pulse, and the trailing edge is shaped by the gain saturation. The measured laser pulse is asymmetrically shaped with a relatively long tail, which indicates poor gain saturation. On the other hand, the intracavity laser pulse energy is 4.1 nJ for a laser average output power of 10 mW at 80 MHz and an output coupler reflectivity of 97%. The gain saturation energy of GaAs/AlGaAs MQWs active medium is E_{sat} = 1.2 nJ (See Table 5.1). Since the intracavity laser pulse energy is more than 3 times larger than the gain saturation energy, the gain should have been deeply saturated by the laser pulse.

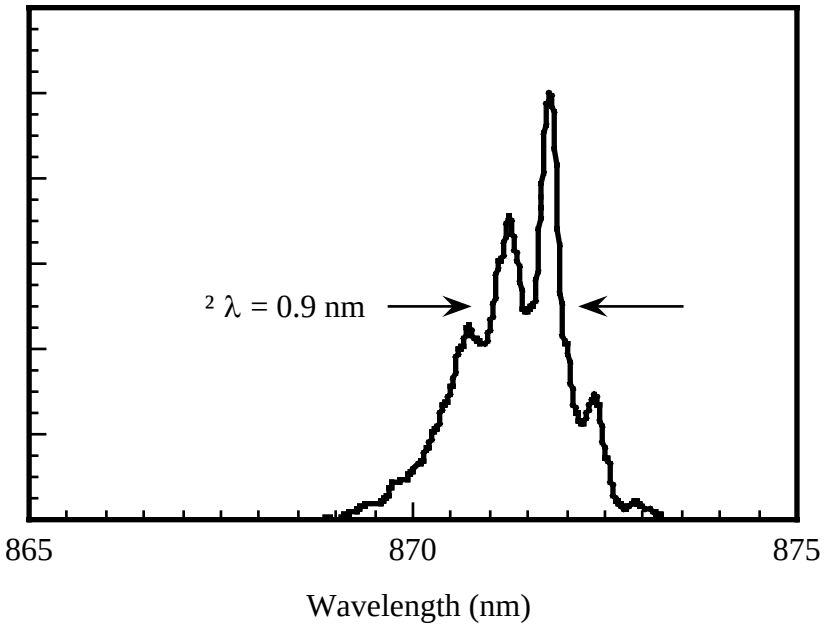

Figure 3.1.1 (b) Power spectrum of pulses shown in Fig. 3.1.1 (a).

To have a further insight into this contradiction, a mode-locked Ti: sapphire laser producing 100 - 200 fs pulses is used as the pump and the laser cavity is converted to 89 MHz to match the repetition rate of the Ti: sapphire laser. To decrease the intracavity pulse energy for the same amount of output power, thereby minimizing the gain-saturation-induced SPM, the reflectivity of the output coupler is reduced to 95%.

The intensity autocorrelation trace of the output pulse from the mode-locked VCSEL without the birefringent filter in the cavity is shown in Figure 3.1.2(a) and the corresponding power spectrum is shown in Figure 3.1.2(b). Assuming a hyperbolic secant pulse shape, the pulsewidth is 2.3 ps and the time bandwidth product is 2.3 for a spectrum width of 2.9 nm. The average output power is 13 mW at the pump power of 200 mW. It turns out that reducing the intracavity pulse energy does help in reducing the pulse chirping, as shown by the smaller time-bandwidth product.

When a birefringent filter with thickness of 0.5 mm is placed in the cavity, the shortest laser pulses directly from the laser oscillator are obtained as shown by the autocorrelation trace in Figure 3.1.3(a). Assuming a hyperbolic secant pulse shape, the laser pulsewidth is 0.92 ps. The average laser output power is 11 mW at the pump power of 200 mW. The side lobe at 5.5 ps away from the main peak in the autocorrelation trace indicates the existence of secondary pulses. This effect may be suppressed at the price of broadened laser pulsewidth by detuning the laser cavity length, as shown in Figure 3.1.3(b), in which the pulsewidth is 1.4 ps. The effect may also be strengthened by the cavity detuning in the other direction, as shown in Figure 3.1.3(c), in which more subpulses are observed. The pulsewidth in this case is 1.2 ps. The model proposed in Chapter 6 will theoretically reproduce these results. The spectrum of the 0.92 ps pulses is shown in Figure 3.1.3(d), in which the spectral width is 2.4 nm. The time-bandwidth product of the pulses is 0.85, which is a factor of 3 improvement over that without the filter. The ripple in the spectrum is the result of the interferences between the main pulses and the secondary pulses. The modulation mode spacing is 5 Å, so the time-spacing between the multiple pulses should be 5.2 ps, which is in good agreement with the autocorrelation measurement of 5.5 ps. Notice that the mode-locking operation is also more stable than that without the filter.

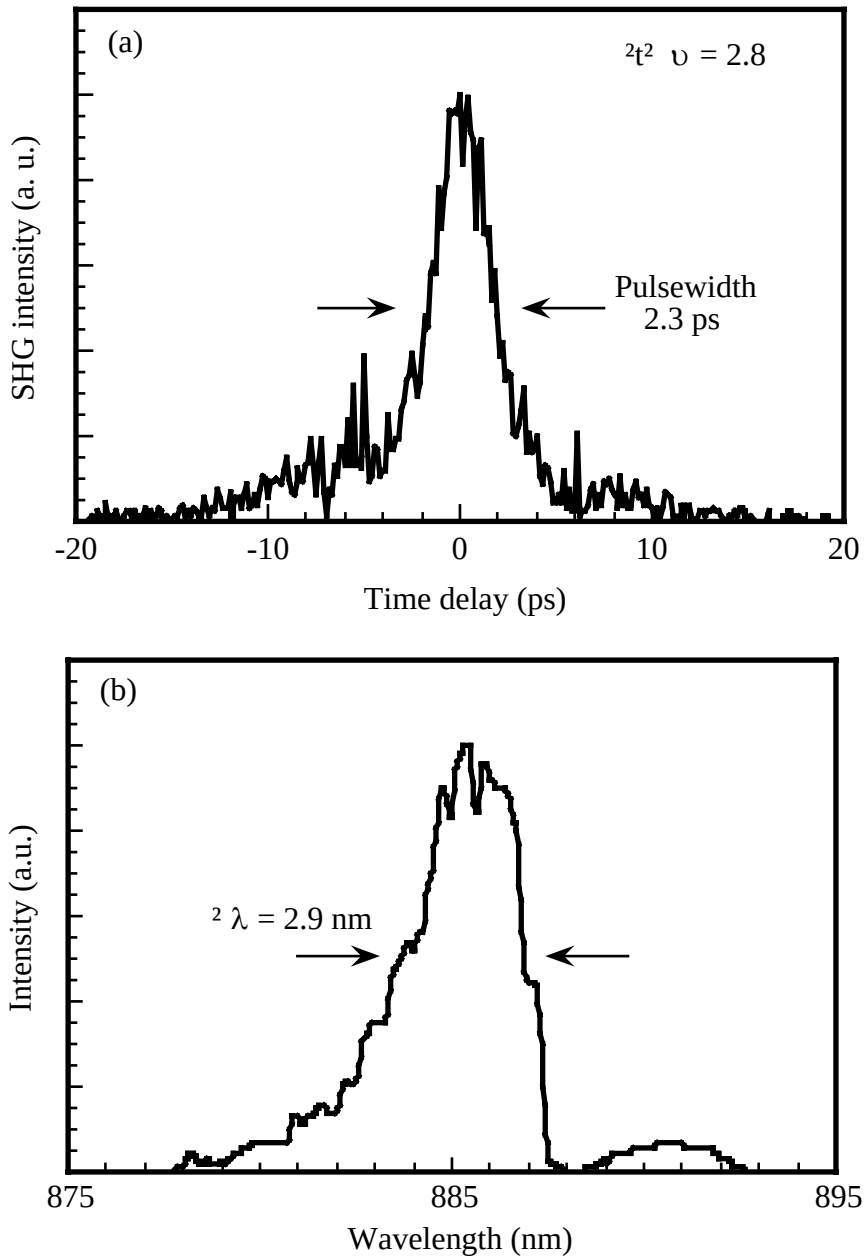

Figure 3.1.2 (a) The intensity autocorrelation trace of pulses from a mode-locked GaAs VCSEL pumped by a mode-locked Ti: sapphire laser. The pulsewidth is 2.3 ps when assuming a hyperbolic secant pulse shape. (b) The corresponding power spectrum.

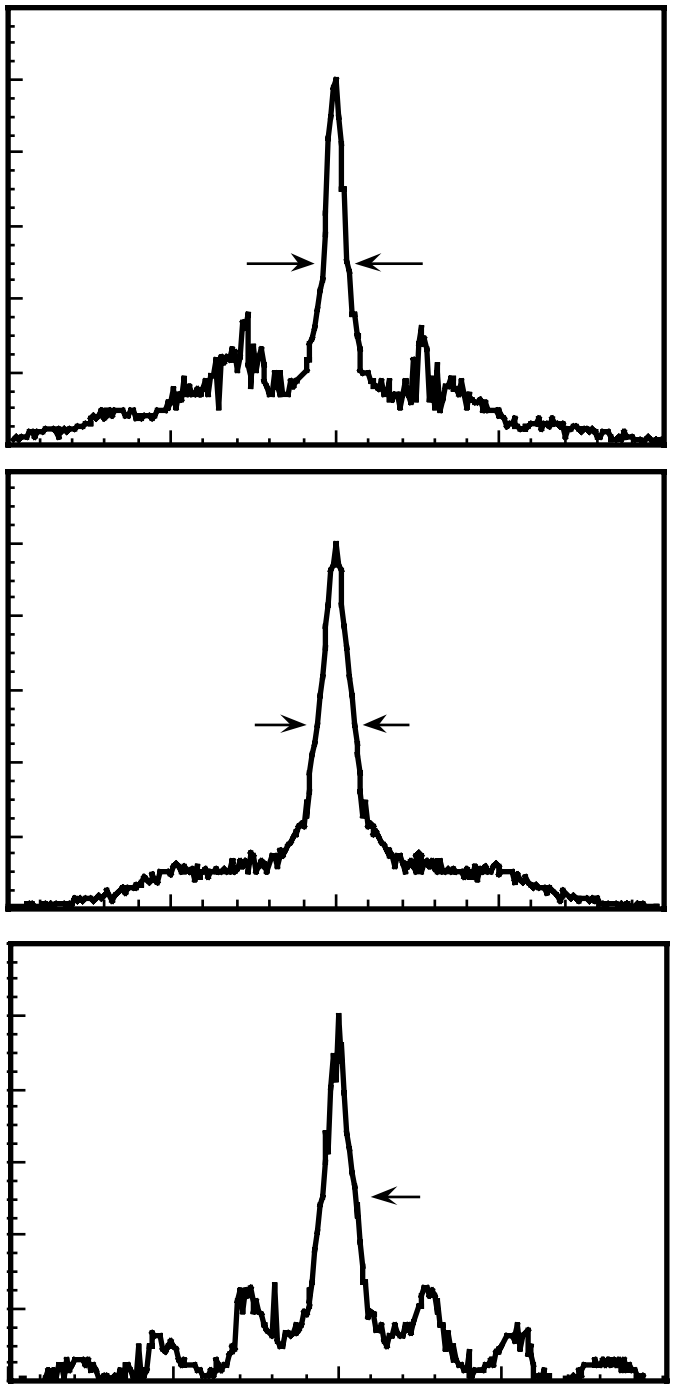

Figure 3.1.3 (a) - (c) The intensity autocorrelation traces of pulses from a mode-locked GaAs VCSEL under three different cavity detunings with a birefringent filter of 0.5 mm in the cavity when pumped by a mode locked Ti: sapphire laser.

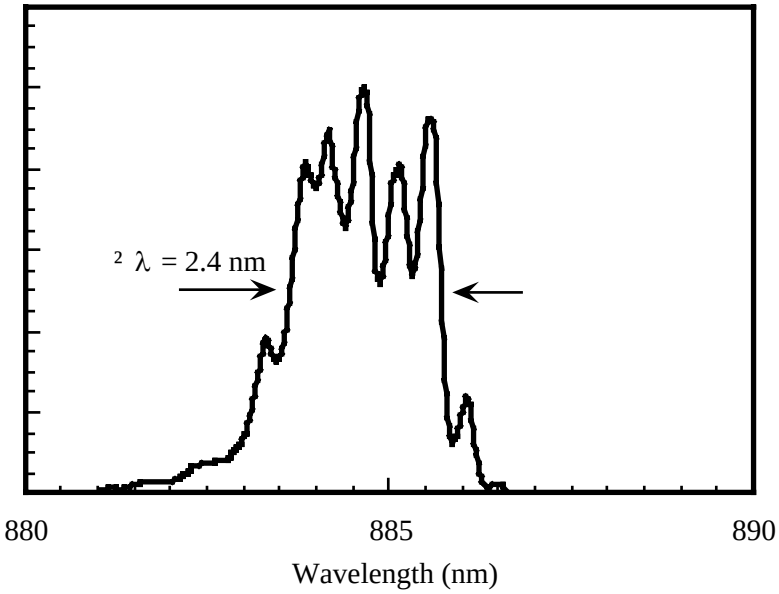

Figure 3.1.3 (d) Power spectrum of pulses corresponding to Fig. 3.1.3 (a).

To further suppress the pedestals and the subpulses, the 0.5 mm thick birefringent filter is replaced by a 1 mm thick birefringent filter. A thicker filter has a narrower bandpass. Figure 3.1.4(a) is the autocorrelation of the laser pulses from the laser cavity using this filter. The laser pulsewidth is 2.1 ps if a hyperbolic secant pulse shape is assumed. Although the laser pulsewidth is broadened, the pedestals are suppressed. More useful energy is included in the central lobe. The spectral width is 2.9 nm [Figure 3.1.4(b)], thus the time-bandwidth product is 2.3. This case is essentially similar to that without the filter, as shown in Figure 3.1.2(a), but the pulse is much more stable.

If the birefringent filter thickness is further increased to 5 mm, the pulsewidth is broadened to 3.4 ps, as shown in Figure 3.1.5(a). The pulsewidth is longer than that shown in Figure 3.1.2(a), indicating that the passband of the filter is too narrow that it starts to broaden the laser pulsewidth. The correspondent spectral width is 1.2 nm [Figure 3.1.5(b)], so the time-bandwidth product is 1.6. Obviously, there is a

compromise between minimum pulsewidth and minimum pedestals, i.e., there is an optimum birefringent filter thickness to produce relatively pedestal-free pulses with the shortest possible pulsewidth.

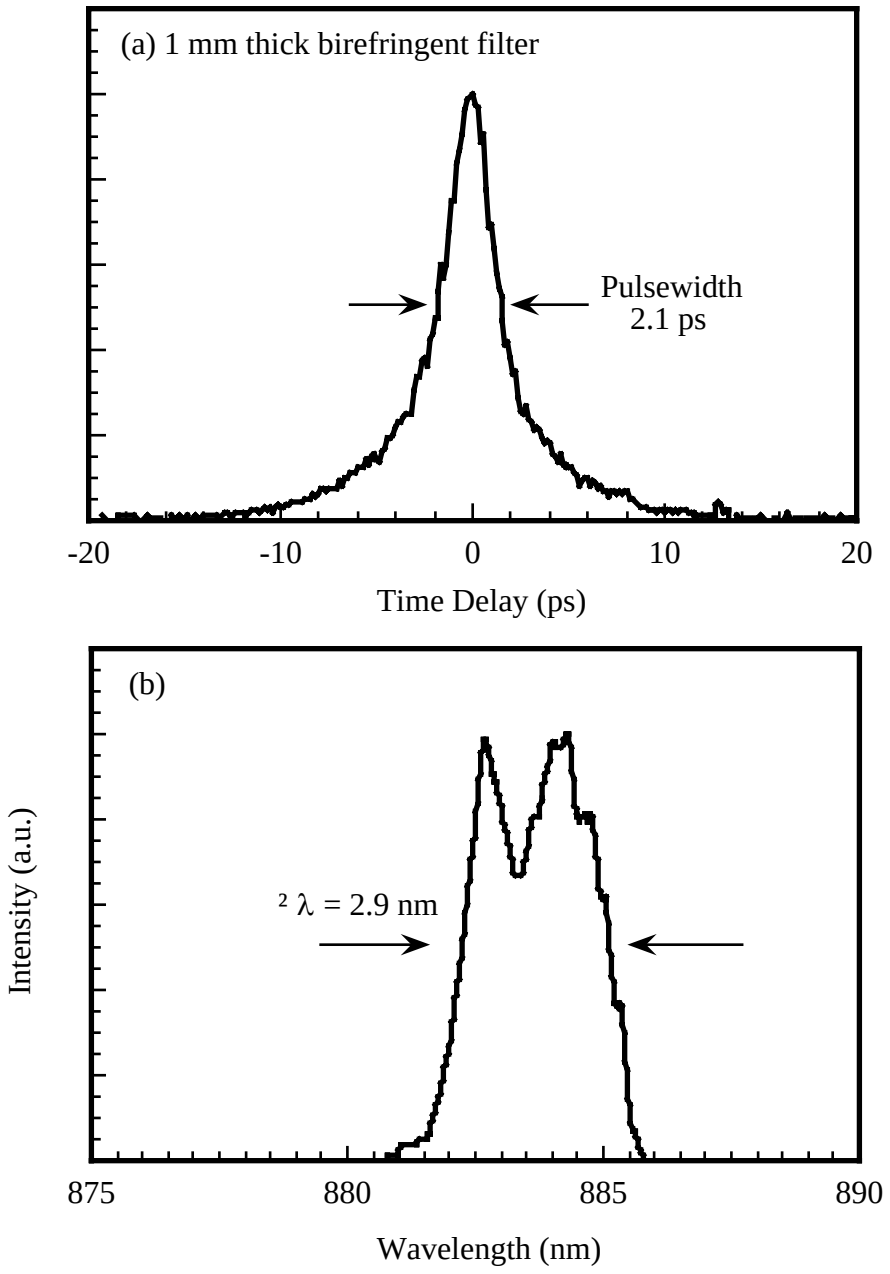

Figure 3.1.4 (a) Intensity autocorrelation of pulses from a mode-locked GaAs VCSEL with a birefringent filter of 1 mm thick in the cavity when pumped by a mode-locked Ti: sapphire laser. (b) The corresponding power spectrum of pulses.

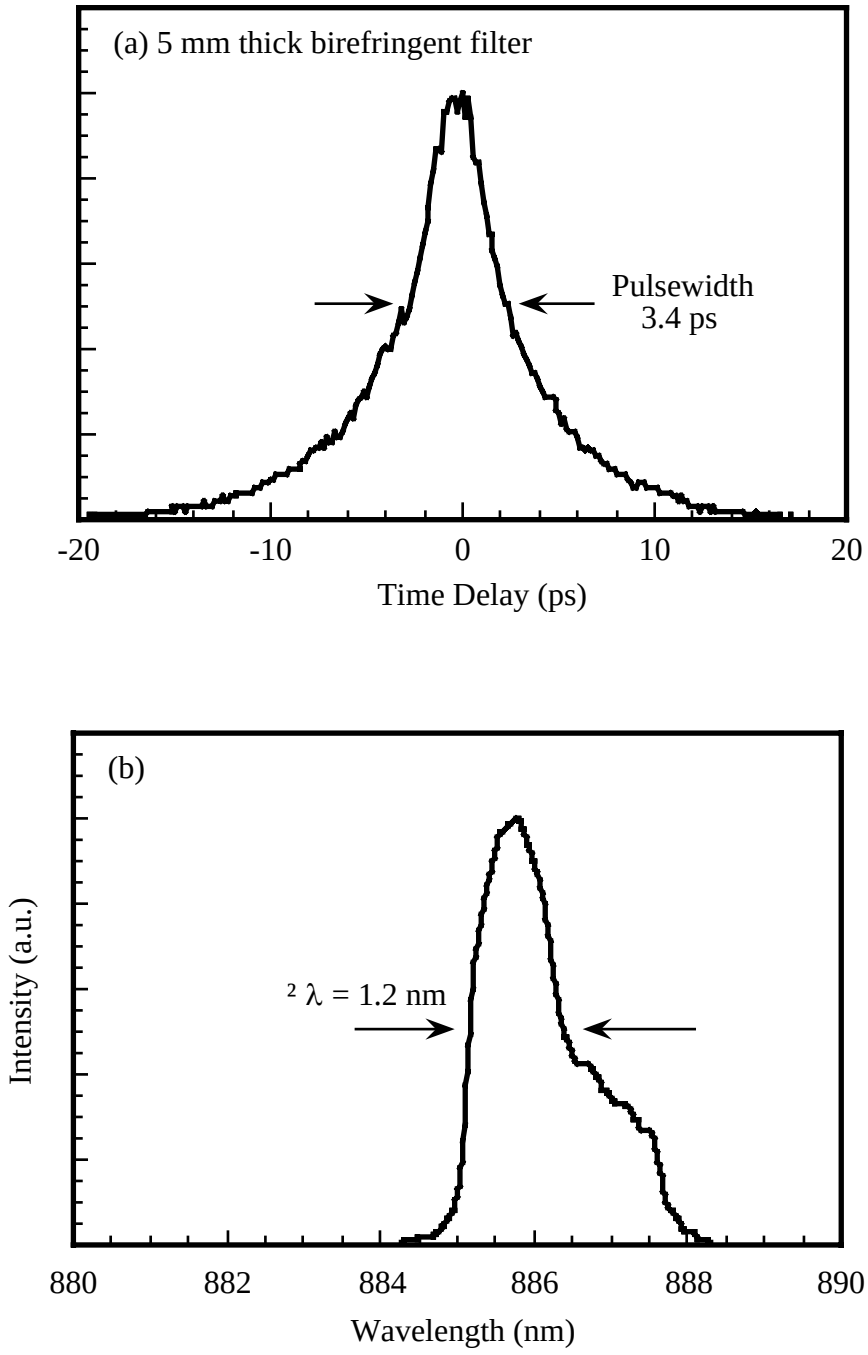

Figure 3.1.5 (a) Intensity autocorrelation of pulses from a mode-locked GaAs VCSEL with a birefringent filter of 5 mm thick in the cavity when pumped by a mode-locked Ti: sapphire laser. (b) The corresponding power spectrum of pulses.

The laser pulses in Figures 3.1.2 to 3.1.5 are much longer than the pump pulses, which again indicates the poor tail shaping, or in other words, poor gain saturation. The intracavity pulse energy in this case is actually around 2.3 nJ, larger than the gain saturation energy E_{sat}. How to explain this contradiction? There must be an anti-gain-saturation mechanism intrinsic to this laser. It is important to note that the gain medium in this laser is directly attached to one of the cavity mirrors. Spatial hole-burning occurred during the laser operation because of a standing wave in the gain medium formed by the incident and the reflected laser beams (Figure 3.1.6). The carriers in the quantum wells outside of the high intensity regions will transport into these regions through thermionic emission and recapturing, diffusion and tunneling. The carrier transport will not stop until the carrier densities become equal everywhere. The duration needed to reach such an equilibrium is the dominant limitation in obtaining femtosecond pulses, if the pulse chirping is carefully excluded.

To estimate the carrier transport time, the carrier diffusion time for the bulk active medium is a good reference. The diffusion equation to the problem is

$$\frac{\partial N(z,t)}{\partial t} = D\frac{\partial^2 N(z,t)}{\partial z^2} \tag{3.1.1}$$

where *N(z, t)* is the carrier density, and *D* is the diffusion coefficient. The solution to Equation (3.1.1) is

$$N(z,t) = N_0 + N_1 e^{-t/\tau}\left|\sin\left(\frac{2\pi n}{\lambda_0} z\right)\right| \tag{3.1.2}$$

where N_0 is initial carrier density at the peak of the standing wave in the gain medium (spatial hole), which equals to the carrier density at transparency to the laser central wavelength λ_0, $(N_0 + N_1)$ is the initial carrier density in the valley region of the

standing wave in the gain medium (outside of spatial hole), and n is the refractive index of the gain medium. The carrier diffusion time, τ, is given by

$$\tau = \frac{\lambda_0^2}{4\pi^2 n^2 D} \qquad (3.1.3)$$

where λ_0 = 0.88 μm and n = 3.5. If the ambipolar diffusion coefficient is taken as D = 5.0 $cm^2\ s^{-1}$, Equation (3.1.3) gives a diffusion time of τ = 3.2 ps.

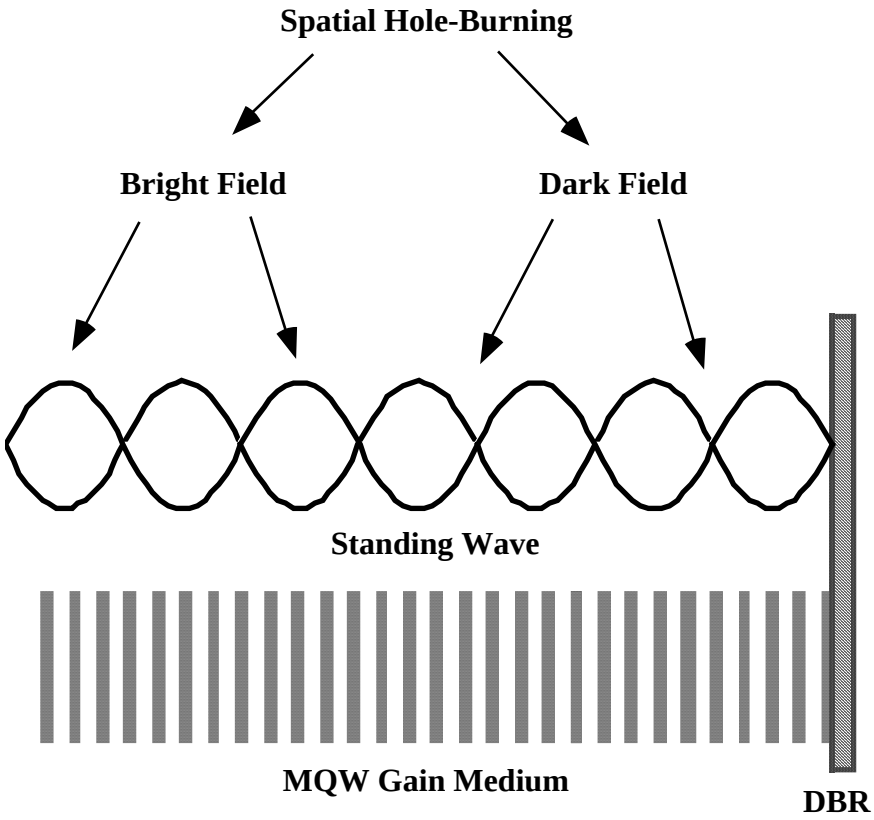

Figure 3.1.6 Spatial hole-burning caused by the standing wave pattern inside of the MQW gain medium.

The actual gain medium is a MQW sample, so the carrier diffusion time must be

longer. If the thermionic emission and recapturing, as well as the tunneling, are taken into account, the net carrier transport time is on the order of several picoseconds [2]. The gain in the MQW will thus remain high for this picosecond duration , within which the gain saturation is not complete even though the intracavity laser pulse energy is larger than the gain saturation energy. The laser pulses will either show a long tail extending over this duration, or be accompanied by subpulses if extra resonances are possible due to the residual Fabry-Perot effect. The pulse duration will also be limited to about a picosecond no matter how short the pump pulse is.

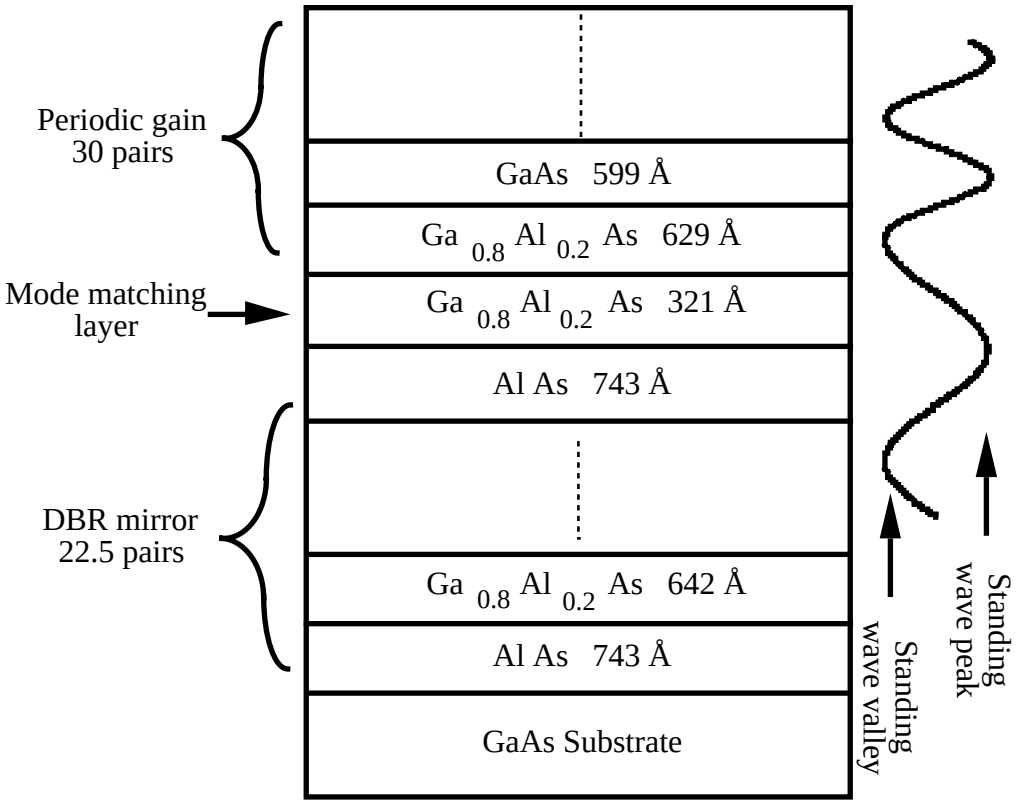

Figure 3.2.1 GaAs periodic gain structure for optical pumping. The standing wave peaks are located in the GaAs wells and the standing wave valleys are located in the GaAlAs barriers.

3.2 Mode-locked VCSEL with periodic gain structure

A solution to the carrier transport problem is to place the gain only at the peaks in the optical standing wave pattern. This periodic gain structure also has the advantage of lowering the lasing threshold [3]. Figure 3.2.1 schematically shows the gain design. On the GaAs substrate are 22 pairs of AlAs/$Ga_{0.8}Al_{0.2}As$ and an extra layer of AlAs, forming the distributed Bragg reflector (DBR) mirror. The AlAs thickness is 743 Å and the $Ga_{0.8}Al_{0.2}As$ thickness is 642 Å. The gain region is a periodic structure with $Ga_{0.8}Al_{0.2}As$/GaAs of 30 pairs. The barrier $Ga_{0.8}Al_{0.2}As$ is 629 Å thick and the well GaAs is 599 Å thick. Between the gain region and the DBR mirror is a 321 Å thick barrier $Ga_{0.8}Al_{0.2}As$ used for the mode matching between the standing waves in the DBR mirror and in the gain region. This structure is designed for a resonate wavelength of 883 nm. The standing wave pattern next to the periodic gain structure in the figure schematically shows that the peaks of the standing wave are located in the wells of the structure, while the valleys of the standing wave are located in the barriers.

The epitaxial side of the MBE grown wafer is AR coated. This wafer is mounted onto a heat sink in the laser cavity to replace the MQW sample used earlier. The designed reflectivity of DBR is shown in Figure 3.2.2(a), where the effect of the periodic gain structure is also included. The measured DBR reflective band is shown in Figure 3.2.2(b). The measurement is performed to the wafer edge where the epitaxial layer is about 3% thinner than that at the wafer center. The DBR mirror reflectivity band at the center portion of the wafer will thus center around 880 nm as designed. The output coupler has a reflectivity of 97%. Birefringent filters are not necessary in the cavity since the periodic gain structure itself effectively serves as a low-pass filter in the lasing wavelength region, as shown by the theoretically calculated transmission of

the periodic gain structure in Figure 3.2.3(a). Such an effect is also shown in Figure 3.2.3(b), which is an enlargement of Figure 3.2.2(a). During the laser operation, the shorter wavelength (higher frequency) part of the spectrum is attenuated by the filter effect of the periodic gain structure, while the longer wavelength (lower frequency) part of the spectrum is limited by the gain profile.

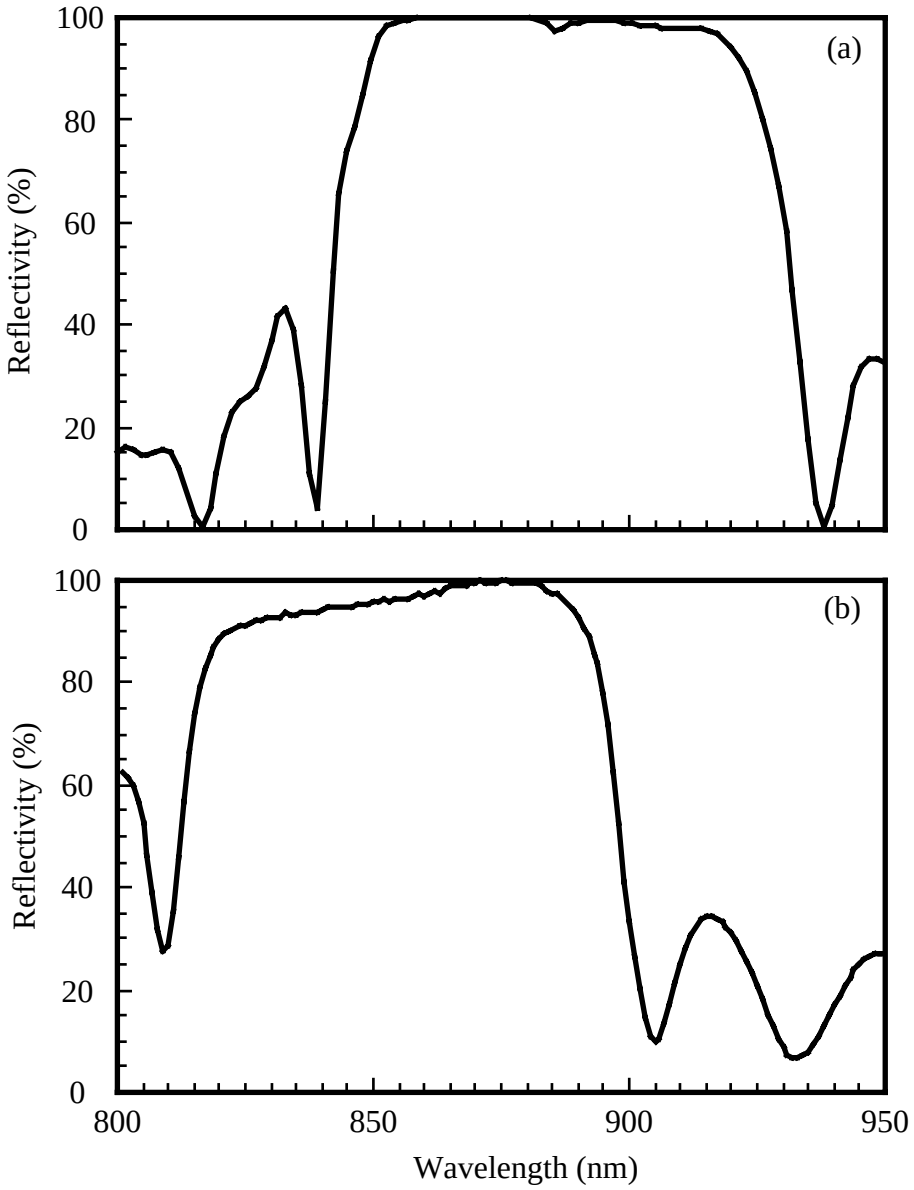

Figure 3.2.2 (a) The reflectivity of the designed DBR mirror used for the periodic gain structure and (b) the reflectivity of the DBR mirror measured at the edge of the wafer.

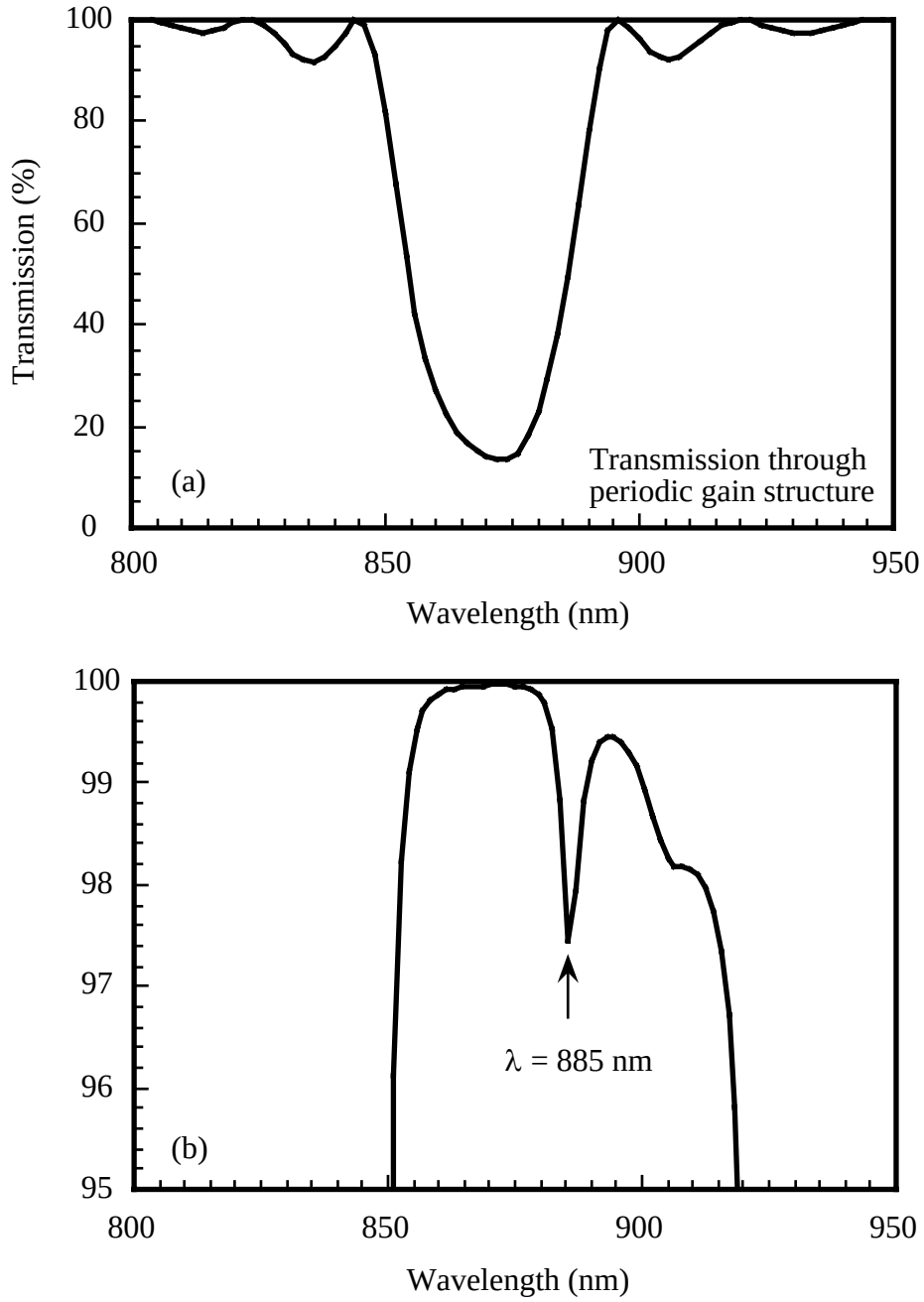

Figure 3.2.3 (a) Theoretical transmission of the GaAs periodic gain structure as a function of wavelength. (b) The reflectivity of the DBR mirror including the index difference effect of the periodic gain structure. The gain is assumed 0 in the calculation.

The VCSEL is mode-locked by matching the laser cavity length to that of the pump

laser, the CW mode-locked Ti: sapphire laser operating at 89 MHz with the wavelength at 800 nm. At the pump power of 200 mW, the output power from the mode-locked VCSEL is 6 mW. The intensity autocorrelation trace of the mode-locked pulses is shown in Figure 3.2.4(a). The full width at half maximum (FWHM) of the autocorrelation trace is 300 fs. The corresponding pulse spectrum is shown in Figure 3.2.4(b). The spectral width is 2.5 nm. If a pulse shape of hyperbolic secant were assumed, the laser pulsewidth would be 190 fs and the time-bandwidth product $\Delta\nu\Delta t$ become 0.18, which is smaller than the transform limited value of 0.32. If a pulse shape of single side exponential were assumed, the laser pulsewidth would be 150 fs and the time-bandwidth product $\Delta\nu\Delta t$ become 0.14, which is slightly larger than the transform limited value of 0.11. The actual pulse shape will probably have a very rapid rising edge close to the Gaussian shape, but a slow falling tail following the exponential shape, which is similar to the behavior measured by the streak camera in Figure 3.1.1(a). The large pedestals are probably due to the residual carrier transport effect, carrier heating, spectral hole-burning, etc. The carrier transport due to the lateral spatial hole-burning can not be eliminated with the periodic gain structure, which also contributes to the remaining pedestals.

In conclusion, the use of a periodic gain structure in the mode-locked VCSELs has successfully solved the problem of the longitudinal carrier transport from the valleys of the standing wave to the peaks (spatial hole), so that the laser pulsewidth directly generated from the VCSELs becomes much shorter than when a MQW structure is used as the gain. The periodic gain structure also acts as a spectral filter to curb the pulse chirping and increases the effective differential gain. The laser pulsewidth with its intensity autocorrelation FWHM of 300 fs is one of the shortest reported in any mode-locked semiconductor lasers. This pulsewidth is ultimately limited by the carrier heating and spectral hole-burning in the gain medium if only an active mode-locking

technique is used. Further shorter pulses generation directly from the mode-locked VCSELs relies on the implementation of passive mode-locking techniques.

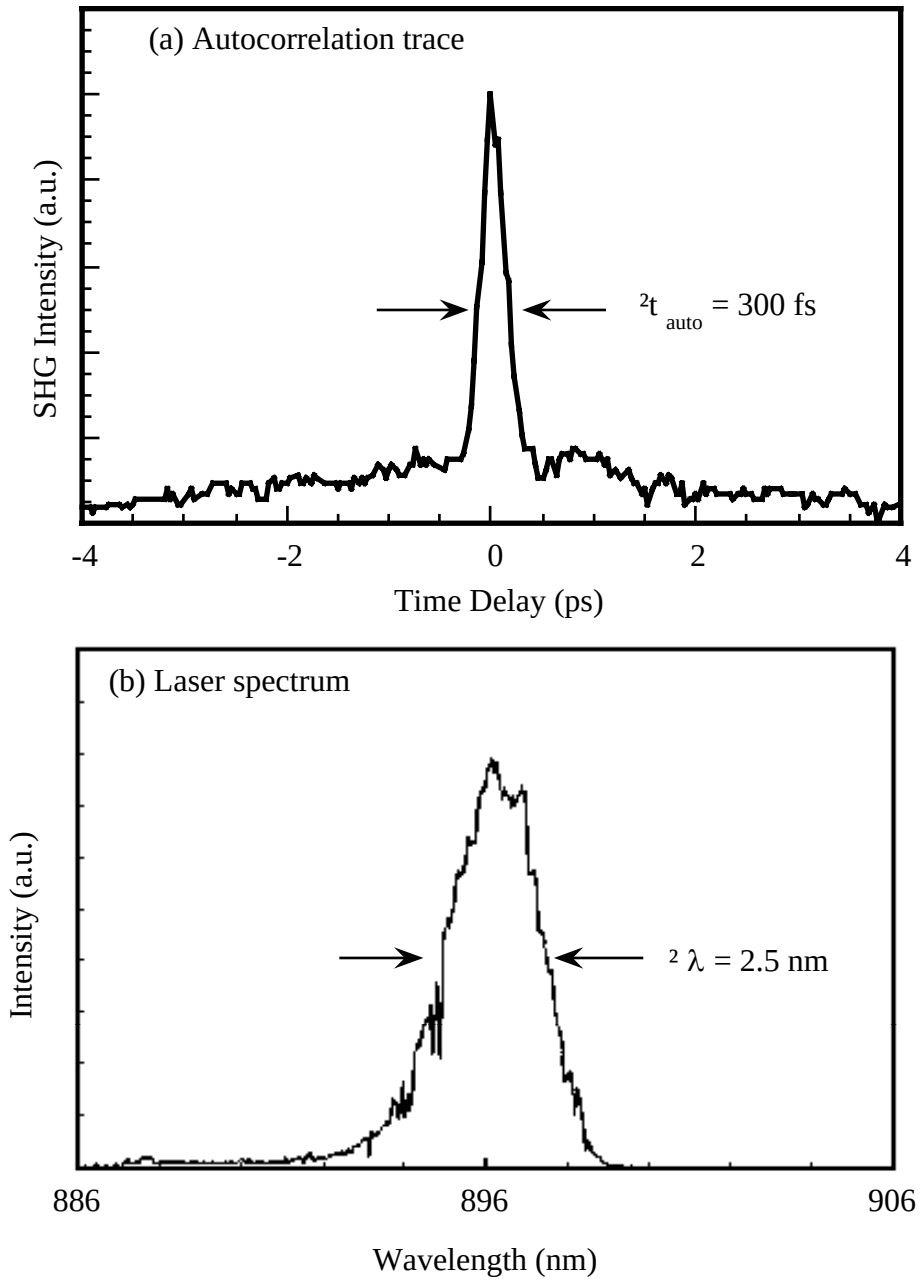

Figure 3.2.4 (a) The intensity autocorrelation of pulses from a mode-locked GaAs periodic gain VCSEL when pumped by a mode-locked Ti: sapphire laser. The autocorrelation width is 300 fs. (b) The corresponding power spectrum of the pulses.

References

[1] W. H. Xiang, S. R. Friberg, K. Watanabe, S. Machida, W. B. Jiang, H. Iwamura, and Y. Yamamoto, "Femtosecond external-cavity surface-emitting InGaAs/InP multiple-quantum-well laser," *Opt. Lett.*, 16, 1394 (1991)

[2] R. Nagarajan, M. Ishikawa, T. Fukushima, R. S. Geels, and J. E. Bowers, "High speed quantum-well lasers and carrier transport effects", *IEEE J. Quantum Electron.* 28, 1990 (1992)

[3] S. W. Corzine, R. S. Geels, J. W. Scott, R. H. Yan and L. A. Coldren, "Design of Fabry-Perot surface-emitting lasers with a periodic gain structure", *IEEE J. Quantum Electron.* 25, 1513 (1989)

Chapter 4 Electrically Pumped Mode-locked Semiconductor Lasers

Optically pumped vertical-cavity surface-emitting lasers have been mode-locked to generate subpicosecond laser pulses with very high peak powers, as shown in the previous chapters. The laser beam from the VCSELs can be controlled to be spatially single mode with nearly perfect Gaussian distribution [1]. The laser wavelength is also easily tunable with an intracavity birefringent filter. The peak powers from VCSELs are higher than in-plane lasers because of their larger gain cross sectional area and thus larger gain saturation energy. All the previously reported mode-locked VCSELs are optically pumped, and electrical pumping is important for compact mode-locked laser sources. In this chapter, the first operation of an electrically pumped actively mode-locked VCSEL will be demonstrated.

4.1 Gain consideration

The MQW gain structure as well as the periodic gain structure designed for optical pumping in the previous chapters is appropriate for electrical pumping only if the cavity loss is low and the required number of quantum wells is small, less than 20. It is difficult for injected carriers to cross over hundreds of quantum wells, as in the optically pumped lasers. Since the external cavity configuration of the mode-locked VCSEL requires a certain gain thickness to overcome the intracavity loss, bulk semiconductor materials are used as the active medium.

Holes are injected into the active region from p-side and electrons are injected from n-side. The finite diffusion lengths of holes and electrons limit the available length of

gain. The carrier density rate equation for holes N_h or electrons N_e in the active region under ambipolar approximation can be written as [2]

$$\frac{\partial N}{\partial t} = D_a \frac{\partial^2 N}{\partial x^2} - \frac{N}{\tau_a} \tag{4.1.1}$$

where D_a is the ambipolar diffusion coefficient, τ_a is the ambipolar carrier lifetime, $N_e \approx N_h = N$, and the electric field term is neglected. At steady state,

$$\frac{\partial N}{\partial t} = 0 \tag{4.1.2}$$

and the boundary conditions for the carriers are

$$-qD_a \left.\frac{\partial N}{\partial x}\right|_{x=0} = J_{th} = \frac{I_{th}}{\sigma} \tag{4.1.3a}$$

$$\left.\frac{\partial N}{\partial x}\right|_{x=L} = 0 \tag{4.1.3b}$$

where J_{th} is the threshold current density, I_{th} is the threshold current, σ is the active area and L is the total gain thickness. From Equations (4.1.1) to (4.1.3), it can be derived that [2]

$$J_{th} = \int_0^L e \frac{N(x)}{\tau_a} dx \tag{4.1.4}$$

Equation (4.1.4) has a physical meaning that all the injected carriers are recombined in the active medium. The solution to Equations (4.1.1) and (4.1.2) at steady state with the boundary conditions (4.1.3) is expressed by

$$N = \frac{I_{th}\tau_a}{e\sigma L_a}\frac{\cosh\left[(L-x)/L_a\right]}{\sinh\left(L/L_a\right)} \tag{4.1.5}$$

where $L_a = \sqrt{D_a\tau_a}$ is the ambipolar diffusion length. The threshold condition for gain is

$$\int_0^L g(N_e, N_h)dx = \alpha_{sa}L + \alpha_{sc}L_c + \frac{1}{2}\ln\left(\frac{1}{R_1R_2T}\right) \tag{4.1.6}$$

where α_{sa} is the scattering loss in the active medium, α_{sc} is the scattering loss in the cladding layer, L is the active thickness, L_c is the cladding thickness, R_1 and R_2 are the reflectivities of two end mirrors, respectively, and T accounts for the net transmission through all the intracavity passive optical components.

The absorption coefficient of the gain medium is expressed by [3]

$$\alpha(E) = \frac{e^2h|M_b|^2}{4\pi^2\varepsilon_0 m_0^2 c\bar{n}E}\left(\frac{2m_r}{h^2}\right)^{3/2}(E-E_g)^{1/2}\left[1 - f_c(E_c) - f_v(E_v)\right] \tag{4.1.7}$$

where E is the photon energy, $|M_b|^2$ is the matrix element as shown by Eq. (2.2.3), and

$$E_c = \frac{m_r}{m_c}(E - E_g)$$

$$E_v = \frac{m_r}{m_v}\left(E - E_g\right)$$

$$m_r = \frac{m_c m_v}{m_c + m_v}$$

where m_v is the effective hole mass with $m_v = m_{hh}$ for heavy hole and $m_v = m_{lh}$ for light hole. Fermi functions can be expressed by

$$f_c(E_c) = \frac{1}{\exp\left[\left(E_c - E_{fc}\right)/k_B T\right] + 1} \tag{4.1.8}$$

$$f_v(E_v) = \frac{1}{\exp\left[\left(E_v - E_{fv}\right)/k_B T\right] + 1} \tag{4.1.9}$$

where the quasi-Fermi energies are from Joyce and Dixon approximation [4]

$$E_{fc} = k_B T\left[\ln\left(\frac{N_e}{N_c}\right) + \sum_{i=1}^{\infty} A_i \left(\frac{N_e}{N_c}\right)^i\right] \tag{4.1.10}$$

$$E_{fv} = k_B T\left[\ln\left(\frac{p}{N_v}\right) + \sum_{i=1}^{\infty} A_i \left(\frac{p}{N_v}\right)^i\right] \tag{4.1.11}$$

with the first few coefficients $A_1 = 3.53553 \times 10^{-1}$, $A_2 = -4.95009 \times 10^{-3}$, $A_3 = 1.48386 \times 10^{-4}$, $A_4 = -4.42563 \times 10^{-6}$, and

$$N_c = 2\left(2\pi m_c k_B T / h^2\right)^{3/2} \qquad N_v = 2\left(2\pi k_B T / h^2\right)^{3/2}\left(m_{lh}^{3/2} + m_{hh}^{3/2}\right)$$

The gain $g(N_e, N_h)$ in Equation (4.1.6) is the addition of $\alpha(E)$ over both heavy-hole to electron and light-hole to electron transitions and expressed by

$$g(N_e, N_h) = -\sum_{i=hh,lh} \alpha(E)\Big|_i \qquad (4.1.12)$$

Table 4.1.1 Parameters used for threshold current calculation with bulk GaAs

Parameter	Value
Eff. electron mass in well m_e	0.067
Eff. heavy hole mass in well m_{hh}	0.45
Eff. light hole mass in well m_{lh}	0.082
Bandgap E_g (100 K)	1.5 eV
Bandgap E_g (300 K)	1.41 eV
Operating temperature	100 K or 300 K
Dielectric constant in active layer ε	13.1
Reflectivity of end mirror R_1	0.99
Reflectivity of coupler R_2	0.97
Intracavity optics transmission T	0.95
Active diameter d	15 μm
Spin-orbit split [2]	0.33 eV
Scattering loss in active layer α_{sa}	50 cm^{-1}
Scattering loss in cladding layer α_{sc}	10 cm^{-1}
Ambipolar diffusion coefficient D_a	5 $cm^2 s^{-1}$
Ambipolar carrier lifetime τ_a	3 ns
Cladding layer thickness L_c	3 μm

Figure 4.1.1 shows the threshold current I_{th} varying with the active thickness L at the temperature of T = 100 K and 300 K for a bulk GaAs gain medium using Equations (4.1.5), (4.1.6) and (4.1.12). The parameters used for calculations are listed in Table 4.1.1. As the first attempt for the experiment in the electrically pumped mode locked VCSEL, the gain thickness is taken as 1 μm, which is about the optimum thickness for operation at 100 K.

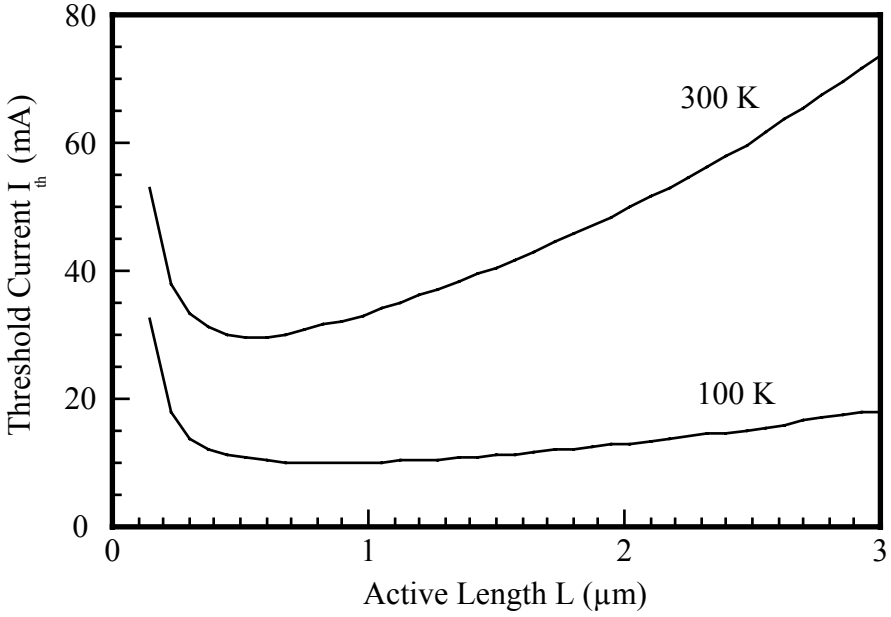

Figure 4.1.1 Threshold current as a function of active length at a temperature of 300 K and a temperature of 100 K, respectively.

To determine the doping of the active layer, stripe lasers are fabricated using the samples grown on n-GaAs substrates by the molecular-beam-epitaxial (MBE) method to compare the lasing thresholds and the quantum efficiencies. Sample A has an intrinsic GaAs active layer of 1 μm. Sample B has an n-GaAs active layer of 1 μm doped (Si) at 5×10^{17} cm^{-3}. Sample C has a p-GaAs active layer of 1 μm doped (Be) at 5×10^{17} cm^{-3}. The n-cladding layers of $Al_{0.3}Ga_{0.7}As$ are 1 μm thick and doped at 1×10^{19} cm^{-3}. The p-cladding layers of $Al_{0.3}Ga_{0.7}As$ are 1 μm and doped at 5×10^{18}

cm^{-3}. The cap layers of $Al_{0.1}Ga_{0.9}As$ are 100 nm and p-doped at a concentrations higher than 1×10^{-19} cm^{-3}. The stripe-widths are 50 μm.

Table 4.1.2 Results Measured from Stripe Lasers with Differently Doped Active Layers

	L (μm)	I_{th} (mA)	J_{th}(KA/cm^2)	η_d (%)	η_i (%)	α_i (cm^{-1})
A (Undoped)	200	556	5.6	16.0	N/A	N/A
	220	500	4.5	17.0		
	220	600	5.5	21.8		
	220	481	4.4	17.9		
	250	700	5.6	8.3		
B (n-doped)	185	430	4.6	15.5	N/A	N/A
	185	440	4.8	15.9		
	190	420	4.4	15.8		
	190	440	4.6	14.7		
	190	430	4.5	16.6		
	225	540	4.8	17.5		
	225	460	4.1	15.9		
C (p-doped)	220	614	5.6	14.1	24.9	36.8
	230	615	5.3	15.8		
	265	675	5.1	14.1		
	265	715	5.4	11.5		
	320	755	4.7	12.1		
	320	900	5.6	12.7		

Table 4.1.3 Stripe lasers with One facet AR coated

	L (μm)	I_{th} (mA)	J_{th}(KA/cm^2)	η_d (%)	η_i (%)	α_i (cm^{-1})
A (Undoped)	210	839	7.99	16.1	N/A	N/A
	210	964	9.17	17.3		
B (n-doped)	190	563	5.93	22.4	24.3*	4.7*
	200	759	7.59	13.7		
	215	642	5.97	22.6		
	410	1067	5.20	20.6		
	410	1083	5.28	21.1		
C (p-doped)	265	1553	11.02	11.9	21.3**	34**
	320	1210	7.57	10.9		
	320	1247	7.79	19.6		
	350	1474	8.42	26.6		
D (p-doped)	360	1610	8.95	5.9	N/A	N/A

*: Based on all the B samples but the second one.

**: Based on the first two samples.

Table 4.1.2 shows the lasing thresholds and the quantum efficiencies of the stripe lasers with several different laser lengths, where I_{th} is the threshold current, J_{th} is the threshold current density, η_d is the external differential quantum efficiency, η_i is the internal differential quantum efficiency, and α_i is the internal loss. η_i and α_i are interpolated from the relation [3]

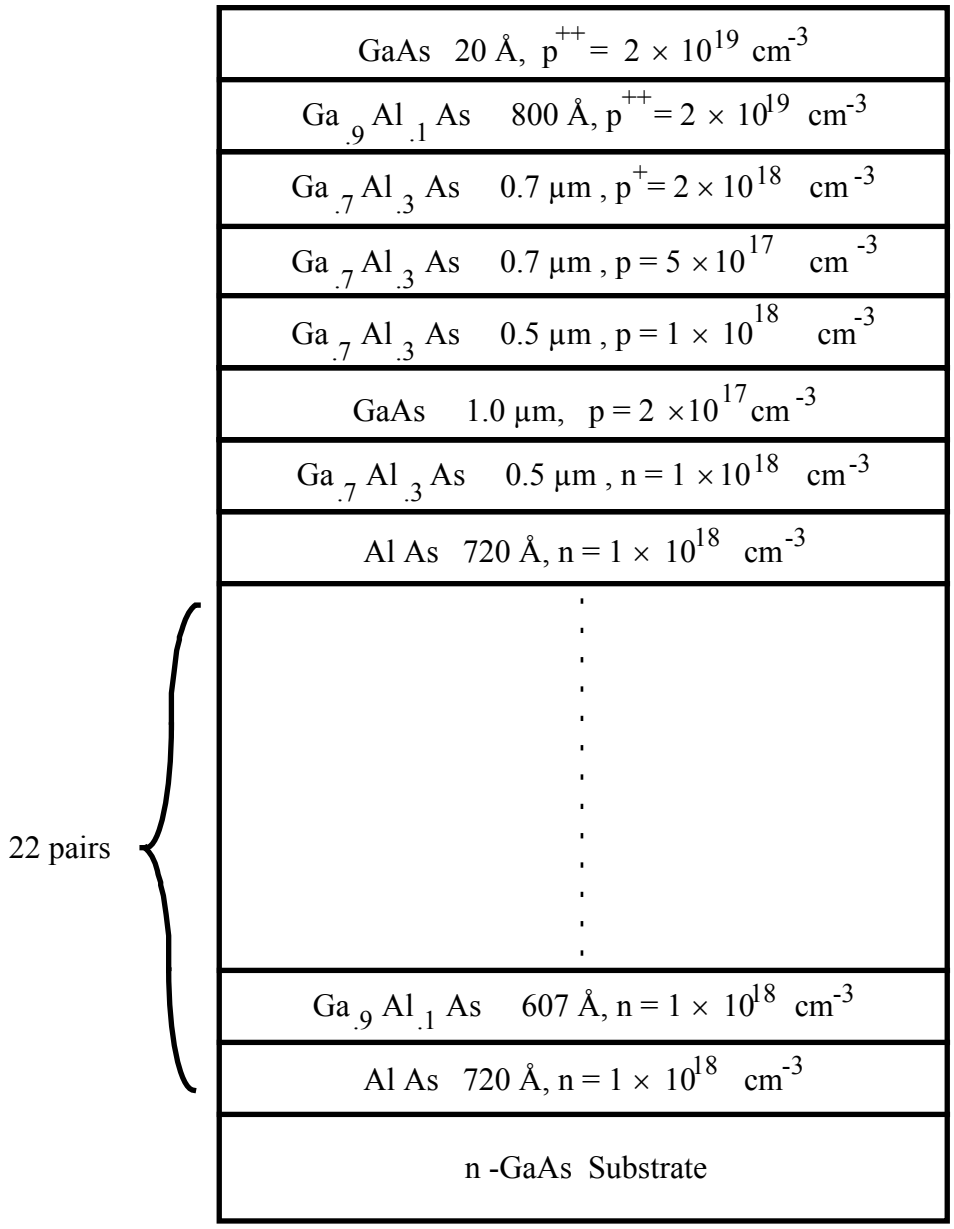

Figure 4.1.2 Wafer structure to be grown for electrical pumping.

$$\eta_d = \eta_i \left[1 + \frac{\alpha_i L}{\ln\left(1/R_m\right)} \right]^{-1} \tag{4.1.13}$$

with the groups of known data (L, η_d), where R_m is the reflectivity of the cleaved facets. Stripe lasers with n-doped active layer are found to have lower threshold current density and higher differential quantum efficiency in Table 4.1.2. A similar conclusion is drawn from the results with one facet of the stripe lasers AR coated, as shown in Table 4.1.3.

Figure 4.1.2 schematically shows the gain structure grown by MBE. A distributed-Bragg-reflector (DBR) mirror alternated with quarter wavelength thick n-doped (1×10^{18} cm^{-3}) AlAs and $Ga_{0.9}Al_{0.1}As$ is grown on an n-GaAs substrate. The interface of the two materials is linearly graded and selectively heavily doped to smooth the heterojunction, thus to decrease the series resistance [5]. On top of the DBR mirror is a $Ga_{0.7}Al_{0.3}As$ n-cladding of 0.5 μm thick with doping concentration of 1×10^{18} cm^{-3}. The active layer is 1 μm thick with n-doping of 2×10^{17} cm^{-3} to ease current spreading. In order that holes can be uniformly injected into the active region transversely under the ring p-contact, p^+p^-p structure is used as the p cladding. The p-layer of $Ga_{0.7}Al_{0.3}As$ is 0.5 μm thick and doped at $1 \infty 10^{18}$ cm^{-3}. The p^--layer and p^+-layer of $Ga_{0.7}Al_{0.3}As$ are both 0.7 μm thick and doped at 2×10^{17} cm^{-3} and 2×10^{18} cm^{-3}, respectively. Holes can thus be uniformly spread within the p^+ layer because of the higher resistive p^- layer. The p-contact layer of $Ga_{0.9}Al_{0.1}As$ is heavily doped at 2×10^{19} cm^{-3} with the thickness of 800 nm and a GaAs cap layer of 20 Å is grown to protect the layer of $Ga_{0.9}Al_{0.1}As$ from oxidizing.

4.2 Device processing

Before going into the process of device fabrication, it is necessary to characterize the grown wafer. The most important step is to characterize the reflectivity of DBR mirror, since it tends to be in the wrong wavelength region because of the changing

growth conditions. Chemical wet-etching is used to remove the absorptive p-cladding and the active layer for the appropriate reflectivity measurement. The etching procedure is described in Appendix II.

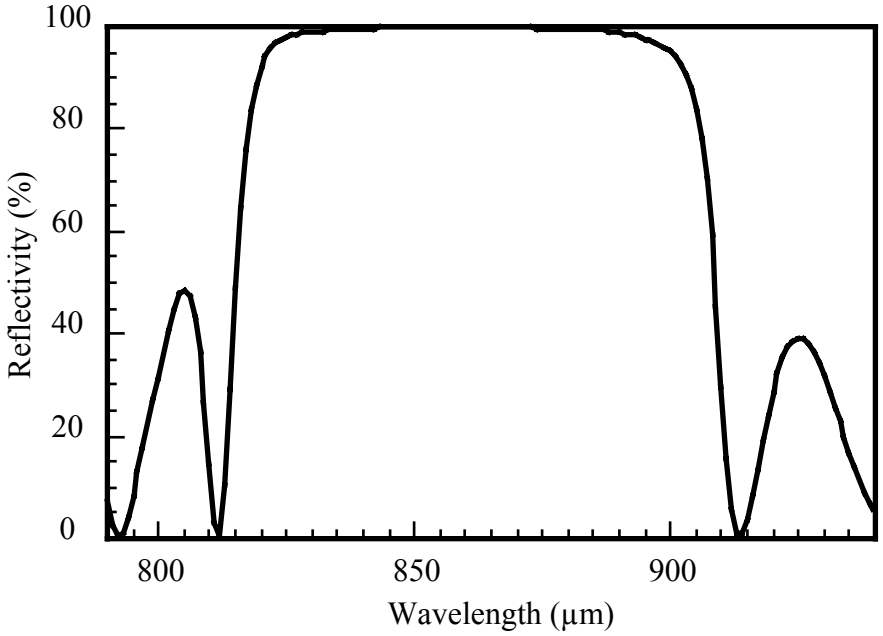

Figure 4.2.1 The designed reflectivity of semiconductor DBR mirror.

The wafer is ready for reflectivity measurement using the Lamda-9 Spectrometer after the etching. The designed reflectivity of DBR is centered at 860 nm with a bandwidth around 70 nm at room temperature (Figure 4.2.1). If the center wavelength of DBR varies by 1 Å for every degree of temperature variation [6], the DBR mirror should be centered at 840 nm at 100 K, and the bandwidth of the DBR should thus cover the laser operation from room temperature (λ = 890 nm) to 100 K (λ = 825 nm). The as-grown wafer, however, has a DBR with the reflectivity centered around 800 nm with a bandwidth of 60 nm at room temperature (Figure 4.2.2). The slight fall of the reflectivity from 820 nm to 775 nm is caused by the absorption of $Al_{0.1}Ga_{0.9}As$

material to the incident light. The minimum reflectivity of 30% is caused by the light reflected from the bulk GaAs surface when it is incident from the air. The measurement is performed using the edge part of the wafer. Since there is a 3% variation in thickness from the center to the edge of the wafer during the growth, the reflectivity of the DBR mirror at the wafer center should be centered around 825 nm, which is 35 nm shorter than the designed. The wafer is, nevertheless, good for 100 K operation, at which temperature the laser wavelength will be covered by the DBR bandwidth.

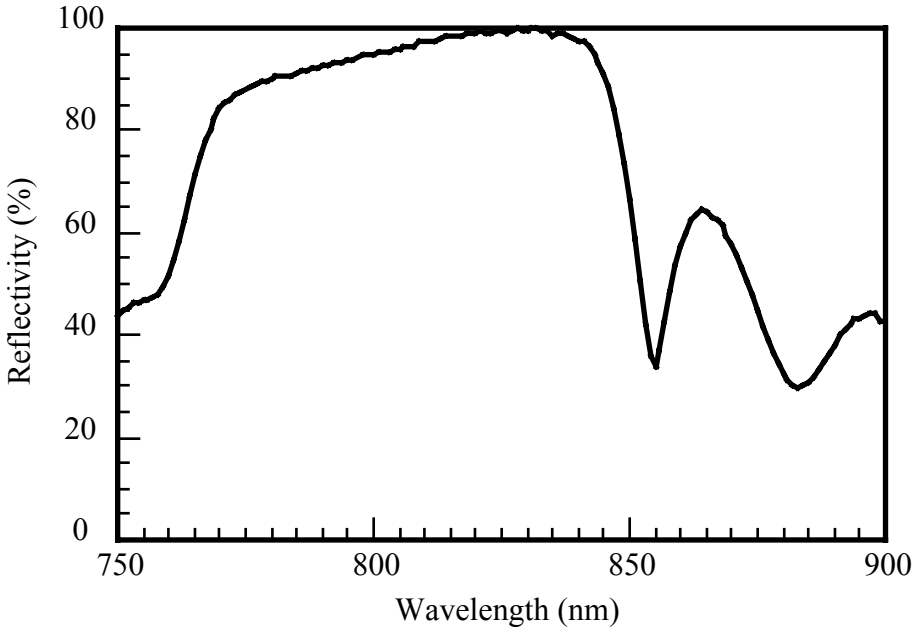

Figure 4.2.2 The actual measured reflectivity of monolithic semiconductor DBR mirror.

A good device will require a good metal contact to decrease the series resistance. The step to characterize the contact resistance is especially important to VCSELs for the less heat generation. The n-metal contact is not a problem for this device because of the

broad area contact on a n-GaAs substrate. The p-metal contact is the problem. Before the actual device process, the transmission line model (TLM) [7] is used to characterize the p-metal contact resistance on the grown wafer to ensure that a good metal contact on the p-side is possible.

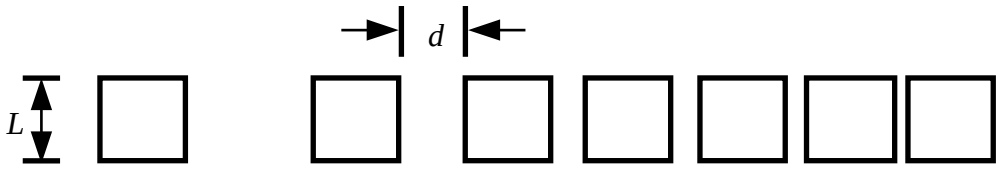

Figure 4.2.3 (a) Transmission line model (TLM) test pattern.

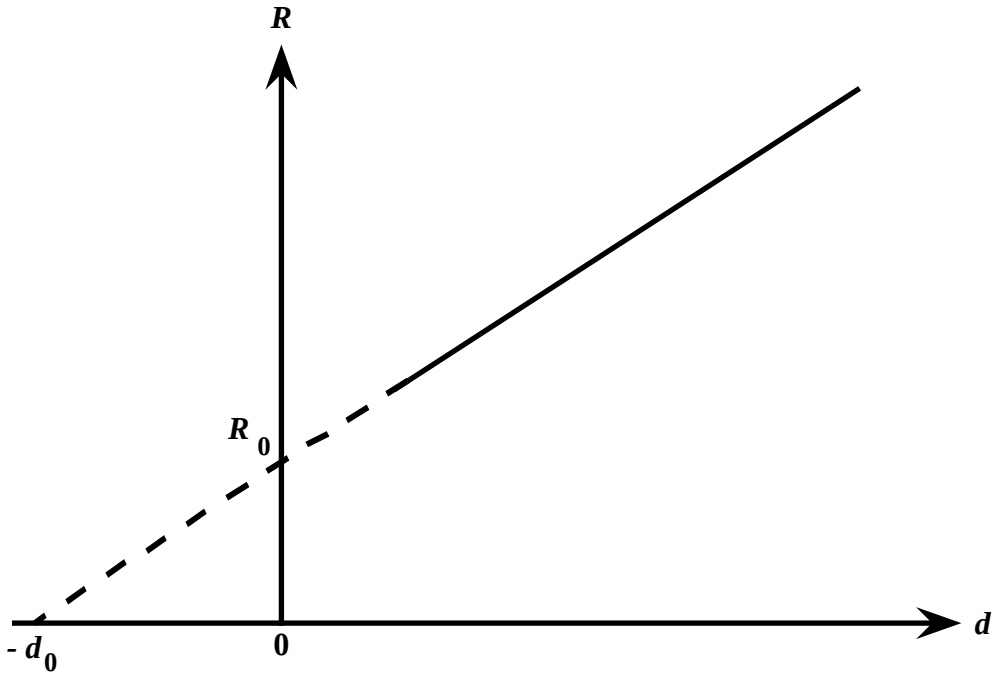

Figure 4.2.3 (b) Resistivity-spacing (*R* - *d*) relation related to TLM test pattern for contact resistance measurement.

The TLM test pattern is shown in Figure 4.2.3 (a), with an array of square metal contact (100 × 100 μm^2) separated by different spacings between each other onto the p-side of the wafer. Four-probe measurement is then used to measure the resistance

between the neighboring square contacts. The resistance R is a linear function of the spacing d between the neighboring contacts, which intersects with the y-axis at R_0 and intersects with the x-axis at $-d_0$ by interpolation [See Figure 4.2.3 (b)]. The contact resistance is expressed by

$$r_c = \frac{R_0}{2} \cdot \frac{d_0}{2} \cdot L \qquad (4.2.1)$$

where L is the length of one side of the square contact.

The metal lift-off technique is used to fabricate TLM pattern on the test wafer as described in Appendix III. The completed TLM pattern array has a spacing of 21 μm, 11 μm, 5.5 μm, 5 μm, 4 μm, 3 μm and 1.5 μm between the neighboring contacts. The annealing conditions are respectively 420 ˚C/30 s, 410 ˚C/30 s and 400 ˚C/30s. The four-probe method is used to measure the resistance of the annealed wafers as a function of the spacing. Using Equation (4.2.1), the contact resistance r_c is 3.6×10^{-4} Ω cm^2 at the annealing condition of 420 ˚C for 30 seconds, 4.8×10^{-4} Ω cm^2 at annealing condition of 410 ˚C for 30 seconds, and 2.3×10^{-4} Ω cm^2 at annealing condition of 400 ˚C for 30 seconds. These results are one to two orders of magnitude larger than a good p-metal contact resistance. A separate TLM pattern processing with HCl:H_2O = 1:10 instead of NH_4OH:H_2O = 1:10 to remove the oxidization gives no improvement in the contact. In that case, the contact resistance r_c is 3.8×10^{-4} Ω cm^2 at the annealing condition of 410 ˚C for 60 seconds, 2.8×10^{-4} Ω cm^2 at the annealing condition of 410 ˚C for 30 seconds, 3.8×10^{-4} Ω cm^2 at the annealing condition of 400 ˚C for 60 seconds, and 2.6×10^{-4} Ω cm^2 at the annealing condition of 400 ˚C for 30 seconds.

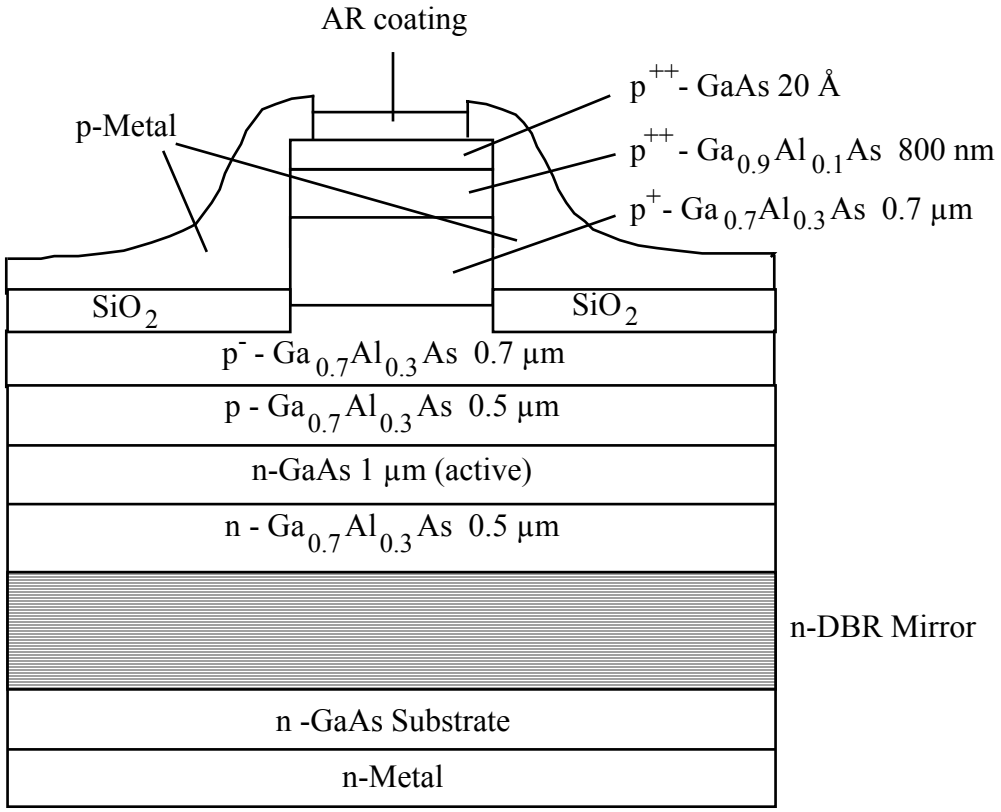

Figure 4.2.4 The schematic diagram of completed device structure used for electrically pumped mode-locked VCSEL.

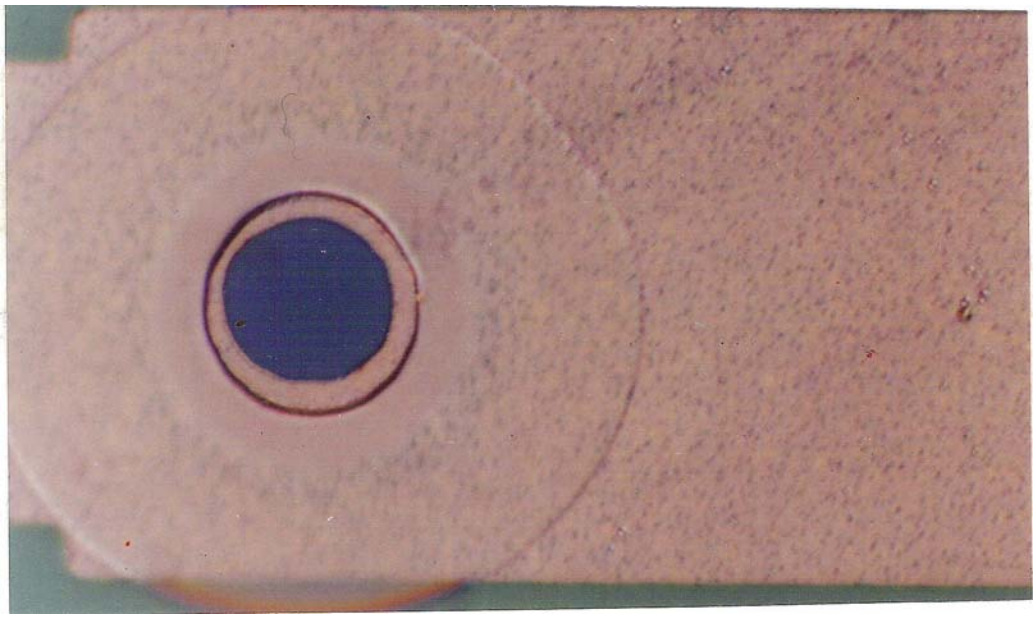

Figure 4.2.5 Top view of the device for electrically pumped mode-locked VCSEL.

It turns out that the beryllium (Be) doping concentration in the wafer contact layer is not high enough to ensure a good p-contact. The exact cause is not very clear. One possible explanation may be the forming of BeO at the wafer surface, or the Be out-diffusion during the cool-down of the wafer growth and the subsequent processing, which results in a lower doping concentration right at the wafer surface. To solve the problem, a closed ampule Zn-diffusion is used to raise the p-doping concentration at the contact surface. The diffusion source is ZnAs and the diffusion proceeds at the temperature of 620 ˚C for 5 minutes. A TLM pattern characterization to the Zn-diffused wafer shows the contact resistance of $r_c = 4.8 \times 10^{-6}\ \Omega\ \text{cm}^2$ at the annealing condition of 400 ˚C for 30 seconds, and $r_c = 6.6 \times 10^{-6}\ \Omega\ \text{cm}^2$ at the annealing condition of 410 ˚C for 30 seconds, which is a great improvement to that without the Zn-diffusion.

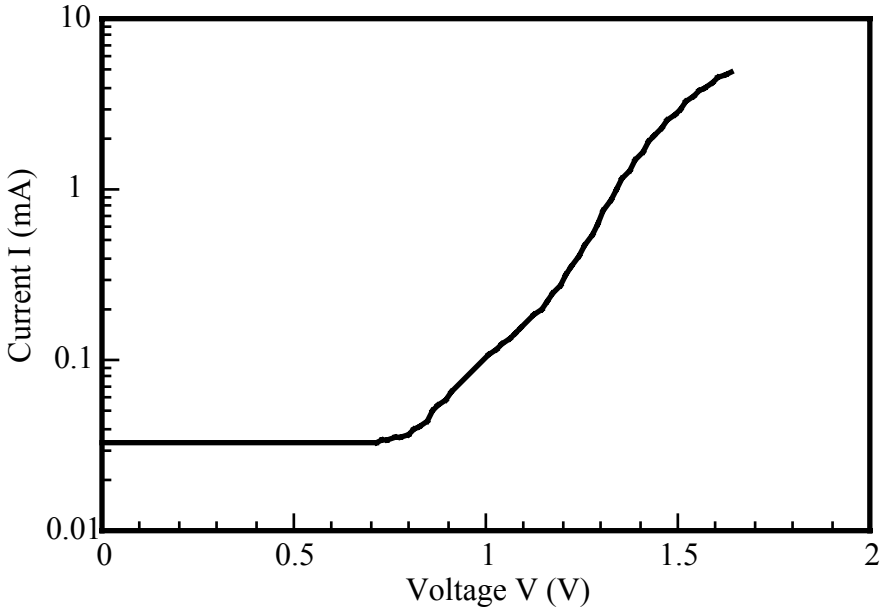

Figure 4.3.1 *I* - *V* characteristics of the devices used for mode-locked VCSEL.

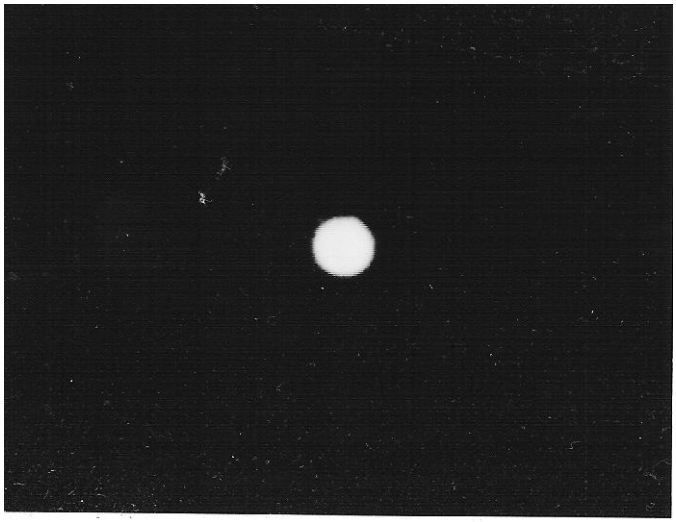

(a)

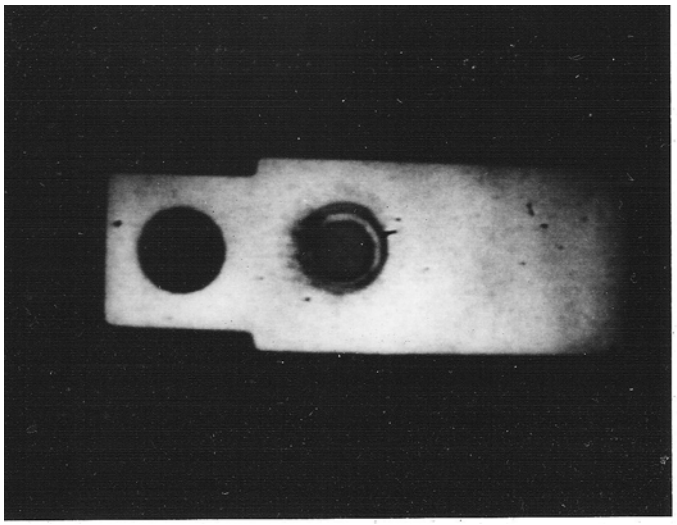

(b)

Figure 4.3.2 (a) The homogeneity of the near field of the device spontaneous emission implies the uniform current spreading transversely in the active layer. (b) The corresponding device spontaneous emission window.

After going through the wafer characterization, it is now ready for device fabrication. The standard device processing steps are listed in Appendix IV. The completed device structure is shown in Figure 4.2.4, and the top view of the devices is shown by the photo in Figure 4.2.5.

4.3. Device characterization

After the devices are fabricated, the first test is to look at the *I* - *V* curve to see if the device has the right electrical characteristics. *I* - *V* curve measurement is also one of the device screening procedures. A typical *I* - *V* curve of the fabricated devices is shown in Figure 4.3.1. Two kinks are shown by the *I* - *V* characteristics in Log-scale, one at a voltage of 0.8 V, and the other is at a voltage of 1.2 V. The first kink is due to the leakage current, and the second kink of 1.2 V is the device turn-on voltage. The contact resistance is 65 Ω. The best device has a contact resistance of about 50 Ω.

Near field of the spontaneous emission will tell the transverse uniformity of the current spreading in the active region. The uniformity is important in lowering the lasing threshold with transverse TEM00 spatial mode. The near field is measured on a probe station with a microscope imaged into an IR sensitive TV camera. The almost perfect circular near field as shown in the photo (Figure 4.3.2) implies that the p^+p^-p structure for p-cladding does work in uniformly spreading the current transversely in the active region under the ring p-metal contact.

An easy way to examine if the devices have the right lasing capability is to further fabricate a conventional monolithic VCSEL out of those fabricated devices used for constructing external cavity VCSELs. This can be done by evaporating a layer of gold on top of the AR-coating of the devices. The gold mirror should be thin enough to allow the light coupling out of the cavity, but thick enough to allow sufficiently high

reflectivity for the laser to reach threshold. Thermal evaporation is used to deposit 660 Å gold at over 10 Å/sec deposition rate on the p-side of the device. The laser is then mounted on a copper finger and cooled down with liquid N_2 inside a dewar. The actual temperature of the cold finger is maintained at -172 ˚C during the measurement.

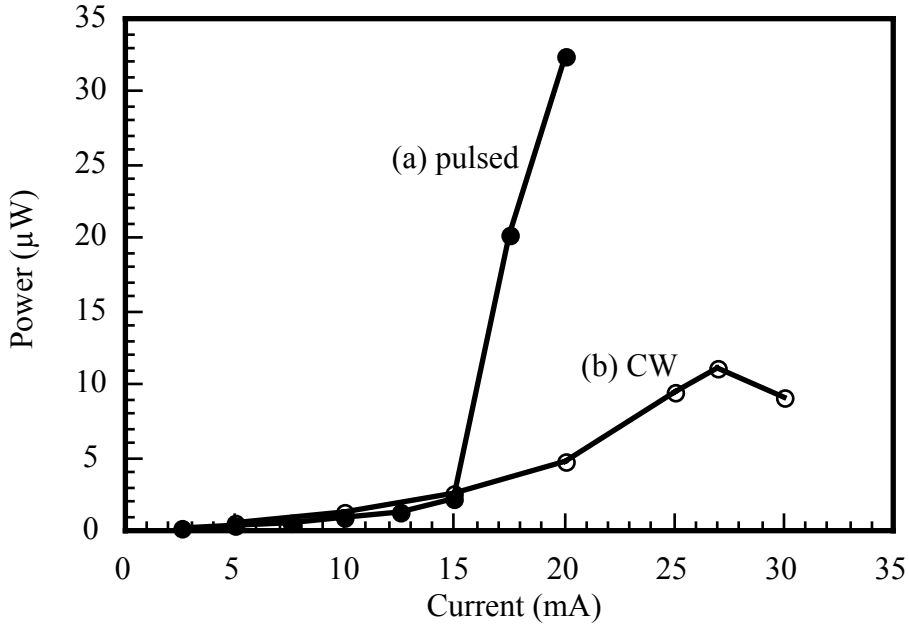

Figure 4.3.3 *L - I* characteristics of a monolithic VCSEL with a Au mirror at one side and a semiconductor DBR mirror at the other side when operating at a temperature of 100 K.

Figure 4.3.3 (a) shows the *L - I* curve of the monolithic VCSEL with a Au mirror pumped by a pulsed current source with a pulsewidth of 0.1 μs at a repetition rate of 10 kHz and Figure 4.3.3 (b) shows the *L - I* curve of the laser pumped by a CW current source. For pulsed pumping, the lasing threshold is 15 mA. At the current of 40 mA, the output power reaches 342 μW. The corresponding power spectrum of the laser is shown in Figure 4.3.4 (a). The lasing wavelength is not at the gain peak as shown by the spontaneous emission spectrum [Figure 4.3.4 (b)] measured without the gold mirror

at p-side when pumped by a CW current of 10 mA. The deviation of the laser wavelength from the gain peak is caused by the wide longitudinal cavity mode separation in this microcavity laser. It is verified by the fact that when the cold finger temperature rises to -100 ˚C, the lasing threshold goes up to 40 mA, but the wavelength maintains the same. Under CW pumping, there is no obvious lasing threshold and the output power drops at the pump current over 25 mA. Heat dissipation is obviously a big problem for this device.

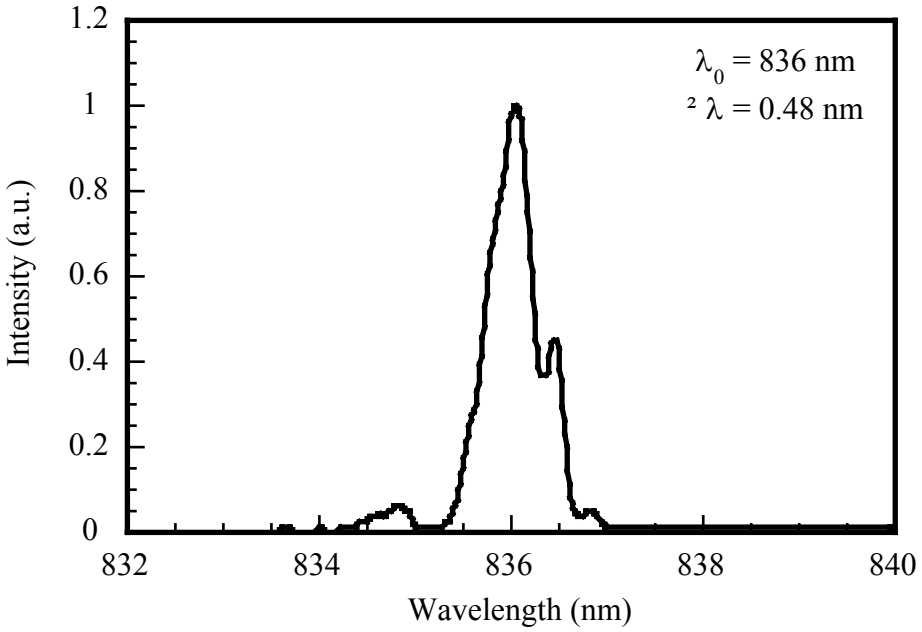

Figure 4.3.4 (a) The power spectrum of the laser from a monolithic VCSEL corresponding to Fig. 4.3.3.

4.4. Mode-locked vertical cavity lasers

After going through a series of characterizations, the device is now placed in an external cavity for mode-locking operation. The device is mounted on a copper cold finger that is placed in a dewar maintained at liquid N_2 temperature. The temperature

of the cold finger is -172 ˚C during the laser operation. Both sides of the dewar window are AR coated. The monolithic DBR mirror forms one end of the laser. The external cavity laser is finished by an output coupler and an intracavity 19-mm-focal-length lens that has the same AR coating as that of the dewar window (Figure 4.4.1). The laser cavity round-trip length is 31.25 cm, which corresponds to a mode-locking frequency of 0.96 GHz. This is the twelfth harmonic of the trigger rate of 80 MHz of the synchronous-scan streak camera. When a square pulsed current is applied to the device, the laser starts to lase at the current of 15 mA with a 1% output coupler.

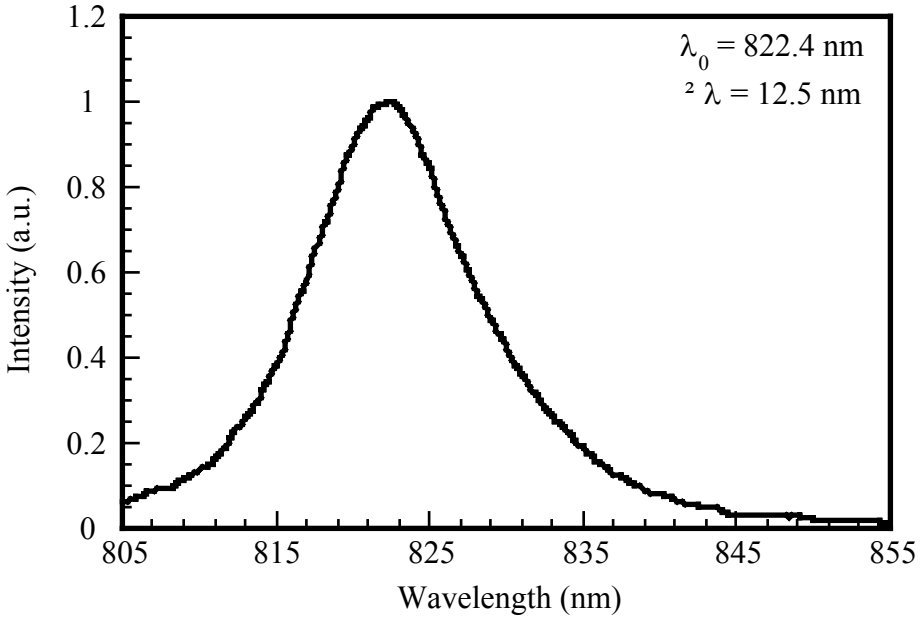

Figure 4.3.4 (b) The power spectrum of the spontaneous emission from the VCSEL device at 100 K.

Figure 4.4.2 shows the *L* - *I* curves of this laser with output couplers of three different reflectivities from 95% to 99%. The current pulsewidth is 2 μs and the repetition rate of the current source can be increased to 100 kHz without degrading the laser operation. Device heating occurs when the repetition rate goes over 100 kHz or

the current pulsewidth increases, which prohibits the CW operation of this device. The laser wavelength is between 825 nm to 830 nm, depending on the injected current level. The laser beam has a circular TEM_{00} transverse mode for all three cases (See photo in Figure 4.4.3). The roll-off in curve (c) is due to the device heating. The maximum external differential quantum efficiency is 9.2 %.

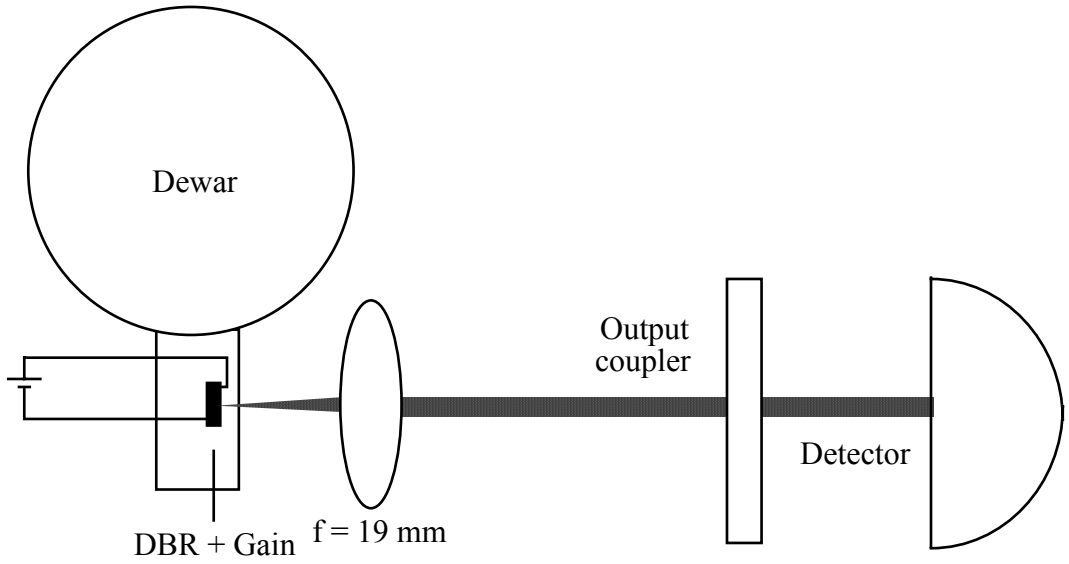

Figure 4.4.1 External-cavity surface-emitting laser configuration.

Active modulation on top of the DC bias is used to actively mode-lock the electrically pumped GaAs VCSEL. An amplified RF signal at 0.96 GHz from a synthesized RF signal generator is used to drive a step-recovery-diode (SRD). The negative electrical pulse of 200 ps from the SRD is sent into a broadband pulse inverter and is then applied onto the VCSEL device through a microwave bias-Tee (Figure 4.4.4). The mode-locked pulsewidth from the VCSEL is measured with a synchronous-scan streak camera that is triggered at 80 MHz. The quasi-DC bias has a pulsewidth of 2 μm at the repetition rate variable from 100 Hz to 100 kHz.

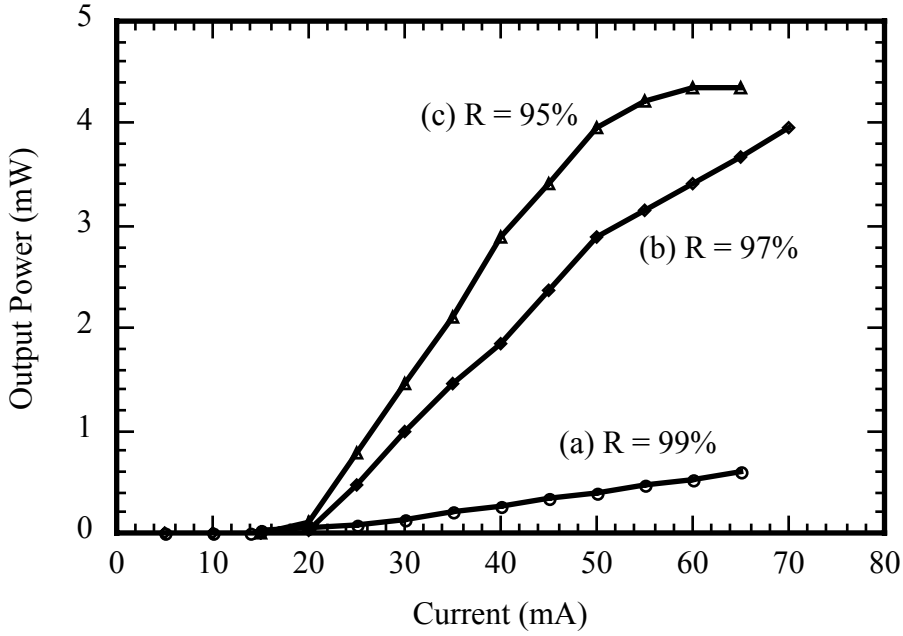

Figure 4.4.2 *L* - *I* characteristics of the external-cavity VCSEL for three different output couplers with reflectivities from 95% to 99%.

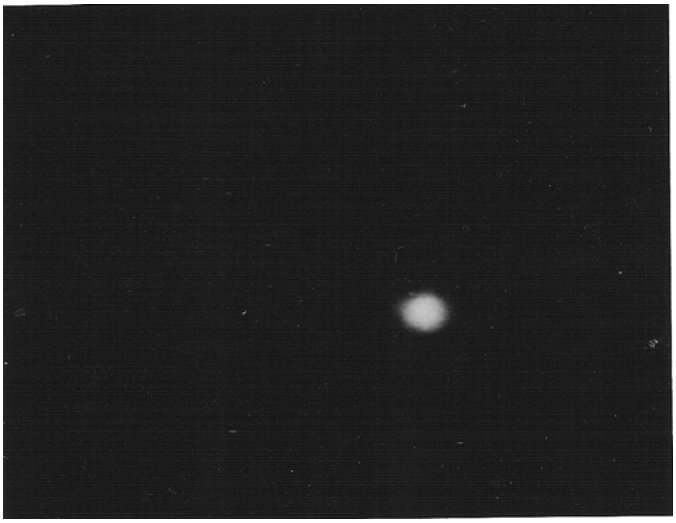

Figure 4.4.3 Photo of the laser beam spot taken at 1 m away from the output coupler of the external-cavity VCSEL shows that the laser beam is transversely single mode.

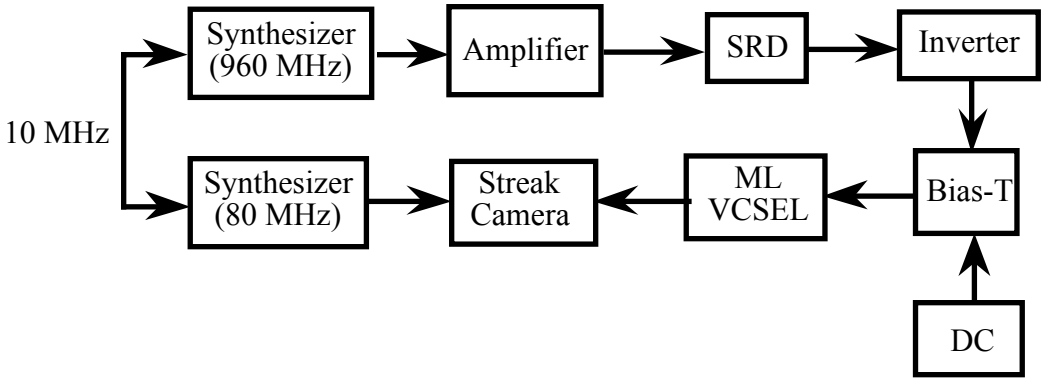

Figure 4.4.4 Diagram of current bias and pulse measurement configuration.

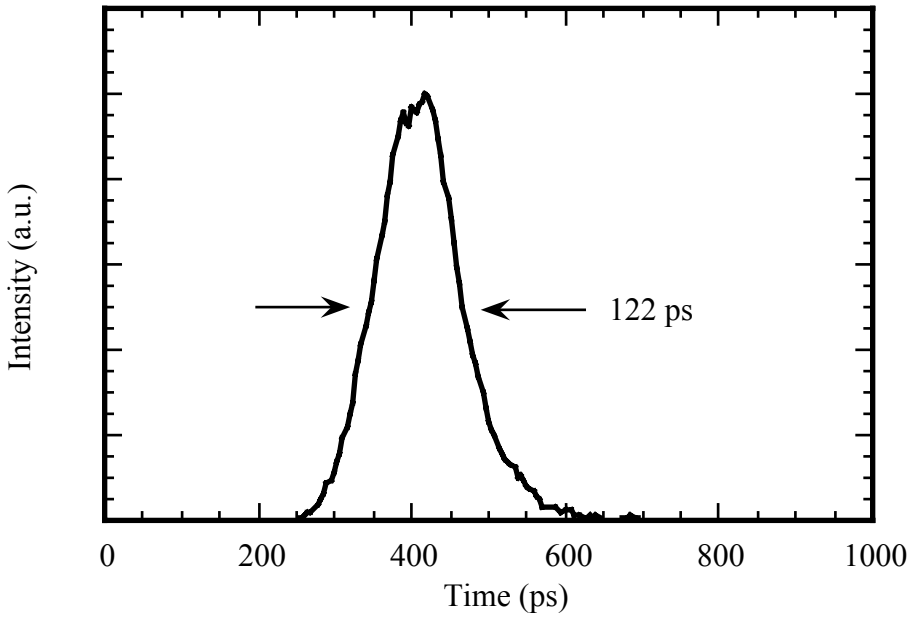

Figure 4.4.5 Pulses at a quasi-DC bias of 50 kHz measured with a synchronous scan streak camera at an integration time of 100 ms.

Figure 4.4.5 shows a typical streak camera pulsewidth measurement, which is conducted with the streak camera integration time at 100 ms and a device quasi-DC bias of 30 mA at the repetition rate of 50 kHz. The pulsewidth is 122 ps. A wider pulsewidth value is measured if the streak camera integration time is set longer than

100 ms. For example, the measured pulsewidth is 137 ps at an integration time of 193 ms, as shown in Figure 4.4.6. This is because the measurement averages over many pulses during one scan. Timing jitter between pulses is included during the averaging. More pulses are averaged during the measurement for longer streak camera integration time, and thus more timing jitter influence is added onto the measured pulsewidth. The severe timing jitter is partly due to the fact that the quasi-DC bias pulses and the modulation pulses are not synchronized.

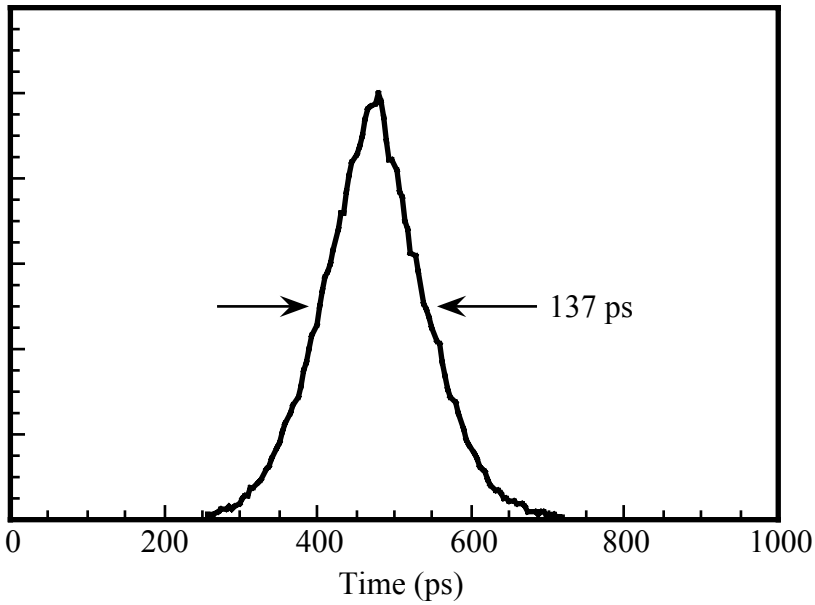

Figure 4.4.6 Pulses at a quasi-DC bias of 50 kHz measured with a synchronous scan streak camera at an integration time of 193 ms.

To decrease the timing jitter influence on the pulsewidth measurement, we need to decrease the streak camera integration time, so that the number of pulses to be averaged per measurement can be decreased. Single shot streak camera measurements would be more preferred [8]. Since the specified minimum integration time of the synchronous-scan streak camera is 100 ms, the repetition rate of the quasi-DC bias may be decreased to further decrease the number of pulses to be averaged per measurement.

Figure 4.4.7 (a) shows the measured pulse shape with the repetition rate of the quasi-DC bias at 1 kHz. The pulsewidth is 81 ps. The corresponding power spectrum is shown in Figure 4.4.7 (b). The spectral width is 0.5 nm, so the time-bandwidth product is 17.7. Less timing jitter influence in the measurement contributes to the decreased pulsewidth. Note that the mode-locked pulse build-up time is around 1 μs, and the quasi-DC bias has a pulsewidth of 2 μs. The synchronous-scan streak camera measurement also averages all the pulses including the initial portion of the pulses. Due to this reason, the measured pulsewidth of 81 ps is still wider than the actual stabilized laser pulsewidth. A single-shot measurement should be able to identify this process and to more precisely determine the stabilized pulsewidth. To fundamentally solve the problem, however, it is necessary to run the laser CW mode-locked, which is prohibited by device heating in this case.

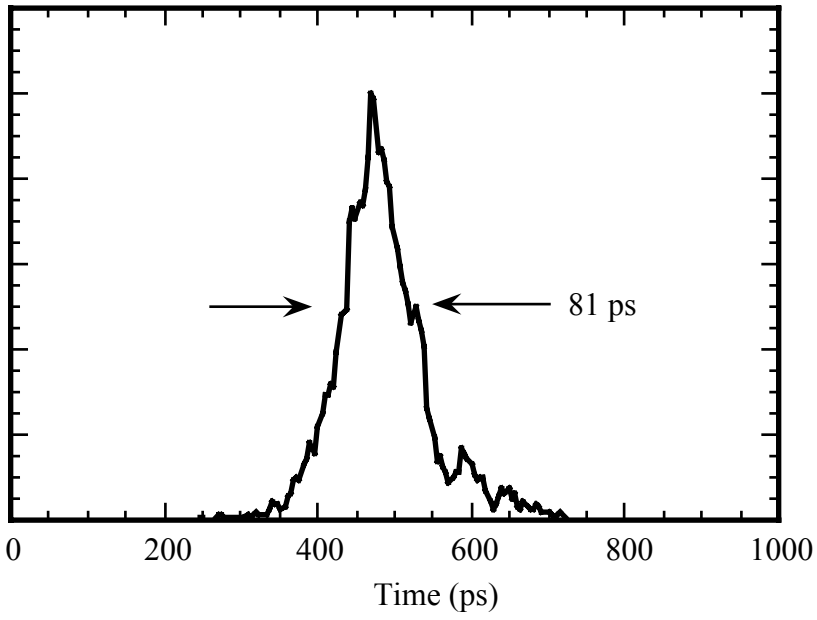

Figure 4.4.7 (a) Pulses at a quasi-DC bias of 1 kHz measured with a synchronous scan streak camera at an integration time of 100 ms.

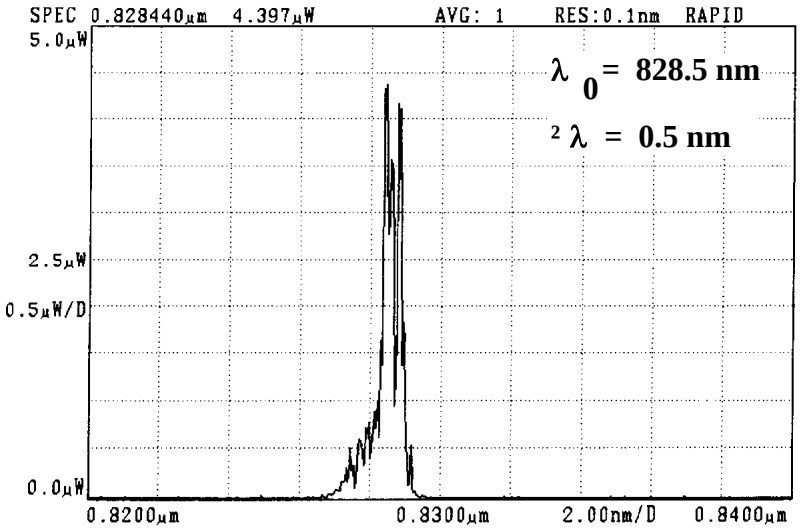

Figure 4.4.7 (b) Power spectrum of pulses corresponding to Fig. 4.4.7 (a). The modulation to the spectrum is due to the low repetition rate of quasi-DC bias.

The laser pulsewidth is dependent on the quasi-DC bias level. When the quasi-DC bias is increased, the pulsewidth is increased, and the pulse energy is increased as well. Figure 4.4.8 shows the pulsewidths and the corresponding output pulse energy for several different quasi-DC biases at 50 kHz, measured with the shortest possible streak camera integration time. The maximum output pulse energy is 4.6 pJ at a bias of 60 mA. The output coupler has a reflectivity of 95%, thus the maximum intracavity pulse energy is 92 pJ. The gain saturation energy is expressed by Equation (1.4.1). If a differential gain of 5×10^{-16} cm^2 is assumed for the bulk GaAs at 100 K, the gain saturation energy is 840 pJ for a gain diameter of 15 μm with a confinement factor of unity. Since the ultimate limitation to the intracavity pulse energy is the gain saturation energy, as usually observed for in-plane lasers, at least a factor of nine increase in the intracavity pulse energy should be expected from this mode-locked VCSEL. At present, the output from the laser is limited by heating.

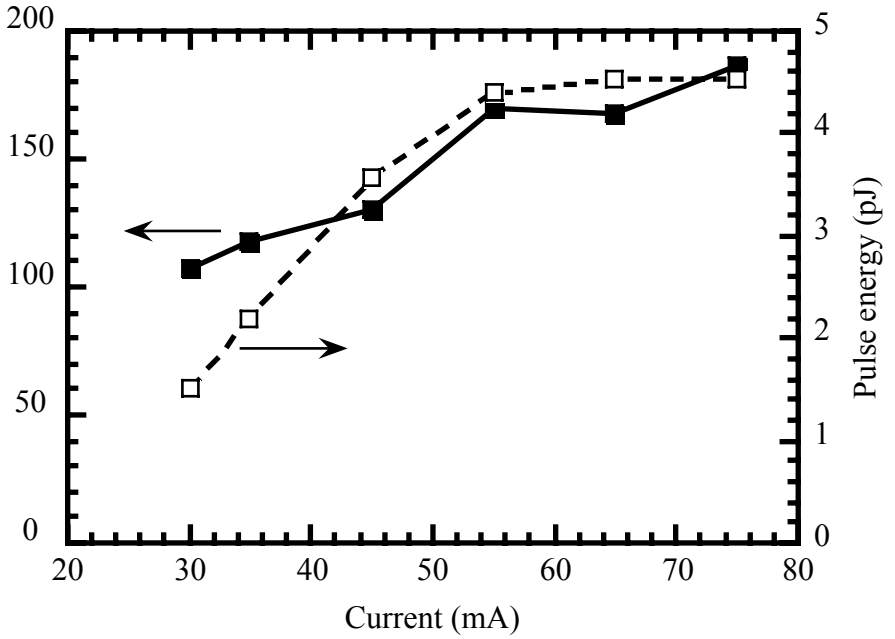

Figure 4.4.8 Pulsewidth as a function of the quasi-DC bias at a repetition rate of 50 kHz (solid line) and the corresponding output laser pulse energy (dashed line).

In conclusion, an electrically pumped actively mode-locked vertical cavity surface emitting laser has been successfully demonstrated. To make the device working CW mode-locked at room temperature, the device structure design needs improved for better heat dissipation and higher quantum efficiency. Reports on monolithic VCSELs have shown that high power-conversion efficiency of 14.9% can be achieved with a better p-DBR mirror design [9]. Greater than 100 mW CW output power at room temperature has also been achieved with a p-side down device mounted on a diamond heat sink for better heat dissipation [10]. An electrically pumped CW mode-locked VCSEL operating at room temperature should thus be promising if those techniques are implemented. The excellent beam quality and the potential high output power from such a laser should make it an attractive candidate for a compact short laser pulse source.

References

[1] D. C. Sun, S. R. Friberg, K. Watanabe, S. Machida, Y. Horikoshi, and Y. Yamamoto, "High power and high efficiency vertical cavity surface emitting GaAs laser," *Appl. Phys. Lett.*, **61**, 1502 (1992)

[2] S. M. Sze, "*Physics of semiconductor devices*", John Wiley & Sons, New York, 2nd Ed., Ch. 2, 1981

[3] G. P. Agrawal, and N. K. Dutta, "*Long wavelength semiconductor lasers*," Van Nostrand Reinhold, New York, 1986

[4] W. B. Joyce, and R. W. Dixon, "Analytic approximations for the Fermi energy of an ideal Fermi gas," *Appl. Phys. Lett.*, **31**, 354 (1977)

[5] R. S. Geels and L. A. Coldren, "Low threshold, high power, vertical-cavity surface-emitting lasers," *Electron. Lett.*, **27**, 1984 (1991)

[6] J. J. Dudley, D. L. Crawford, and J. E. Bowers, "Temperature dependence of the properties of DBR mirrors used in surface normal optoelectronic devices," *IEEE Photon. Tech. Lett.*, **4**, 311 (1992)

[7] H. H. Berger, "Models for contacts to planar devices," *Solid-State Electron.*, **15**, 145 (1972)

[8] K. Watanabe, H. Iwamura, and Y. Yamamoto, "The effect of an additive pulse mode-locking on an external-cavity surface-emitting InGaAs semiconductor laser," *Opt. Lett.*, **18**, Oct. (1993)

[9] M. G. Peters, F. H. Peters, D. B. Young, J. W. Scott, B. J. Thibeault, and L. A. Coldren, "High wallplug efficiency vertical-cavity surface-emitting lasers using lower barrier DBR mirrors," *Electron. Lett.*, **29**, 170 (1993)

[10] F. H. Peters, M. G. Peters, D. B. Young, J. W. Scott, B. J. Thibeault, S. W. Corzine, and L. A. Coldren, "High-power vertical-cavity surface-emitting lasers," *Electron. Lett.*, **29**, 200 (1993)

Chapter 5 Analysis of laser pulse chirping in mode-locked VCSELs

5.1. Introduction

Mode-locking of vertical cavity surface emitting lasers (VCSEL) has been discussed in the previous chapters with either GaAs or InGaAs semiconductor active materials using synchronous optical pumping or electrical pumping. For optically pumped VCSELs, pulses with a peak power over 100 W have been obtained because of the large active cross sectional area in the VCSELs. This peak power is about two orders of magnitude larger than that directly from mode-locked edge emitting semiconductor lasers. External cavity chirp compensation of mode-locked VCSELs has been able to produce sub-picosecond laser pulses [1, 2, 3]. The high peak power has allowed the use of soliton compression techniques, in which the pulses have been shortened to 21 fs [4]. For electrically pumped system, the pulse energy is still low. Work remains to improve the device structure designing to optimize the active doping, heat dissipation, current injection, etc. Nevertheless, a new generation of electrically pumped mode-locked semiconductor lasers using vertical cavity structures arranged into 2-dimensional array will be very promising in generating short optical pulses with a peak power of kilowatts.

It has been found that the pulses generated in the optically pumped VCSELs are usually highly chirped and have a large time-bandwidth product, as shown in Chapter 2. This large chirping makes it difficult to directly generate sub-picosecond pulses from the lasers. With the employment of a birefringent filter into the laser cavity to limit the spectral width, the time-bandwidth product is improved by a factor of 10

(Chapter 3). However, the laser pulsewidth is not shorter. The use of a periodic gain structure instead of the MQW in the laser cavity, as well as the shorter pump pulses, results in subpicosecond pulses directly generated from the mode-locked VCSEL.

In this chapter, the origin and the magnitude of the laser pulse chirp will be discussed theoretically. The analysis is applicable to both optically pumped GaAs and InGaAs systems, but the GaAs laser will specifically be analyzed as an example.

The laser configuration used for the mode-locked GaAs VCSEL has been shown in Figure 2.2.7. The laser is synchronously pumped at 800 nm by a mode-locked dye laser. The repetition rate of the pump is 80 MHz and the pump pulsewidth is 10 ps with the average pump power up to 200 mW. Within this mode-locked laser, the following mechanisms will affect the laser pulse chirp:

(a) the self-phase-modulation (SPM) due to the gain saturation and the cross-phase-modulation (XPM) due to the pulsed optical pumping.

(b) the phase dispersion due to the finite gain shape.

(c) the dispersion due to the DBR structure of both the semiconductor mirror and the dielectric mirrors.

(d) the material dispersion of the intracavity components.

The dispersion caused by DBR mirrors has been well analyzed [5, 6] and is on the order of 10^{-28} s^2. It varies depending on the design and the layer uniformity. The material dispersion for the related semiconductor materials in the transparent region and other intracavity components like fused silica glass is also known [7, 8]. They are on the order of 10^{-28} s^2 for 2 μm thick GaAs/AlGaAs [7] or for 5 mm thick fused silica [8]. The main purpose of this chapter is to analyze the laser pulse chirping caused by (a) and (b) after a single pass through the cavity . In Section 5.2 the laser SPM due to the gain saturation and the XPM due to the pulsed optical pumping will be discussed. The phase dispersion due to the finite gain shape will be discussed in

Section 5.3. The laser pulse evolution in the laser cavity will be discussed in Section 5.4. The experimental results will be compared with the theoretical results in Part Section 5.5 and the chapter will be concluded in Section 5.6.

5.2. SPM and XPM of laser pulses

In this section the SPM due to the gain saturation and the XPM due to the pulsed optical pumping are discussed. Agrawal's treatment of pulse propagation in a semiconductor laser amplifier[9] has been modified to include an optical pulse pumping term. The wave propagation equation is

$$\frac{\partial A(z,t)}{\partial z}+\frac{1}{v_g}\frac{\partial A(z,t)}{\partial t}+\frac{i}{2}\beta_2\frac{\partial^2 A(z,t)}{\partial t^2}=\frac{1}{2}(1-i\alpha)g(z,t)A(z,t)-\frac{1}{2}\alpha_{\text{int}}A(z,t) \tag{5.2.1}$$

where *A(z, t)* is the slowly varying pulse amplitude envelope of the electric field

$$\mathbf{E}(z,t)=\mathbf{e}_x\frac{A(z,t)}{\sqrt{\sigma}}\exp\left[i(k_0 z-\omega_0 t)\right] \tag{5.2.2}$$

with *A(z, t)* normalized so that $|A(z,t)|^2$ stands for the instantaneous laser power, v_g is the group velocity, β_2 is the material dispersion parameter, *g(z, t)* is the amplifier power gain, α_{int} is the internal scattering loss and α is the linewidth enhancement factor. In Equation (5.2.2), $\mathbf{e}_x$ is the polarization unit vector, σ is the active cross sectional area, k_0 is the free space wave vector of the laser pulse and ω_0 is the optical central frequency. Although the relationship between the gain and the carrier density is closer to logarithm in MQW, it is modeled to be linear as given by

$$g(z,t) = a\left[N(z,t) - N_0\right] \tag{5.2.3}$$

where a is the differential gain coefficient and N_0 is the carrier density value at transparency. This linear relationship is valid around the lasing threshold. The transverse mode confinement factor Γ is taken as unity, which is reasonable for VCSELs.

The carrier density variation with time at position z in the gain medium is determined by the rate equation

$$\frac{\partial N(z,t)}{\partial t} = \frac{\alpha_p(z,t)}{\hbar\,\omega_p \sigma} P_p(z, t+\Delta t) - \frac{N(z,t)}{\tau_c} - \frac{g(z,t)}{\hbar\,\omega_0 \sigma}\left|A(z,t)\right|^2 + D\frac{\partial^2 N(z,t)}{\partial z^2} \tag{5.2.4}$$

where $P_p(z, t+\Delta t)$ is the pump laser power, $\alpha_p(z, t)$ is the absorption of the active material to the pump pulse at pump frequency ω_p, τ_c is the carrier lifetime, and D is the carrier diffusion coefficient. Δt determines the position of the pump pulse relative to the laser pulse. If $\Delta t > 0$, the pump pulse arrives earlier than the laser pulse, and if $\Delta t < 0$, the laser pulse arrives earlier than the pump pulse. $\alpha_p(z, t)$ is also assumed to be linearly proportional to the carrier density $N(z, t)$, as shown by

$$\alpha_p(z,t) = -b\left[N(z,t) - N_{p0}\right] \tag{5.2.5}$$

where b is the differential gain coefficient at the pumping frequency, ω_p, and N_{p0} is the transparency carrier density value at ω_p.

The effect due to the β_2 term in Equation (5.2.1) will temporally be neglected in this section and the phase dispersion effect on the chirp formation of the laser pulse due to

the finite gain shape will be addressed in Section 5.3. $\alpha_{int} << g(z, t)$ is assumed, so the term including α_{int} is neglected in Equation (5.2.1). The carrier density is assumed nearly uniform in the z direction in this chapter for the ease of discussion, so the diffusion term in Equation (5.2.4) is ignored. It has been demonstrated in the experiment that the carrier transport effects including the carrier diffusion do affect the laser pulsewidth (Chapter 3). The effects of the carrier transport on the laser pulse will be addressed theoretically in Chapter 6. The term including τ_c in Equation (5.2.4) can be ignored when the optical pulsewidths are much shorter than the carrier recombination lifetime. Under these conditions, Equations (5.2.1) and (5.2.4) are simplified to

$$\frac{\partial A(z,\tau)}{\partial z} = \frac{1}{2}(1 - i\alpha)g(z,\tau)A(z,\tau) \tag{5.2.6}$$

$$\frac{\partial N(z,\tau)}{\partial \tau} = \frac{\alpha_p(z,\tau)P_p(z,\tau+\Delta\tau)}{\hbar\omega_p\sigma} - \frac{g(z,\tau)}{\hbar\omega_0\sigma}\left|A(z,\tau)\right|^2 \tag{5.2.7}$$

where the local time $\tau = t - z/v_g$ has been introduced. Similar to the derivation of Equation (5.2.6) for $A(z, \tau)$ from Equation (5.2.1), the equation for the pump $P_p(z, \tau + \Delta\tau)$ can be expressed by

$$\frac{\partial P_p(z,\tau+\Delta\tau)}{\partial z} = -\alpha_p(z,\tau)P_p(z,\tau+\Delta\tau) \tag{5.2.8}$$

Equation (5.2.7) can be rewritten as

$$\frac{\partial g(z,\tau)}{\partial \tau} = \frac{\alpha_p(z,\tau)P_p(z,\tau+\Delta\tau)}{\gamma E_{psat}} - \frac{g(z,\tau)}{E_{sat}}\left|A(z,\tau)\right|^2 \tag{5.2.9}$$

using Equation (5.2.3), where

$$E_{sat} = \frac{\hbar \omega_0 \sigma}{a} \tag{5.2.10}$$

$$E_{psat} = \frac{\hbar \omega_p \sigma}{b} \tag{5.2.11}$$

are the saturation energies of the gain medium at laser frequency ω_0 and pump frequency ω_p, respectively, and

$$\gamma = b / a \tag{5.2.12}$$

is the ratio between the differential gain coefficients at ω_p and ω_0. From Equations (5.2.3) and (5.2.5), $\alpha_p(z, \tau)$ and $g(z, \tau)$ can be related by

$$\alpha_p(z,\tau) = -\gamma g(z,\tau) + b\left(N_{p0} - N_0\right) \tag{5.2.13}$$

The following discussions will be based on Equations (5.2.3), (5.2.6), (5.2.8), and (5.2.9). Both the pump and the laser input pulses will be assumed to be Gaussian, $E_0 / \left(\sqrt{\pi}\tau_0\right)\exp\left[-\left(\tau/\tau_0\right)^2\right]$, where E_0 is the pulse energy and $2\sqrt{\ln 2}\tau_0$ is the FWHM (full width at half maximum) pulsewidth.

The normalized complex electric field $A(z, \tau)$ is rewritten in terms of the real values $P(z, \tau)$, the laser power, and $\phi(z, \tau)$, the phase,

$$A(z,\tau) = \sqrt{P(z,\tau)}\exp\left[i\phi(z,\tau)\right] \tag{5.2.14}$$

so that Equation (5.2.6) becomes

$$\frac{\partial P(z,\tau)}{\partial z} = g(z,\tau)P(z,\tau) \tag{5.2.15}$$

$$\frac{\partial \phi(z,\tau)}{\partial z} = -\frac{\alpha(z,\tau)}{2} g(z,\tau) \tag{5.2.16}$$

Equations (5.2.15) and (5.2.16) can be analytically solved, as given by

$$P_{out}(\tau) = P_{in}(\tau)e^{G(\tau)} \tag{5.2.17}$$

$$\phi_{out}(\tau) = \phi_{in}(\tau) - \frac{1}{2}\alpha G(\tau) \tag{5.2.18}$$

where $P_{in}(\tau)$ and $P_{out}(\tau)$ stand for the power of the input and output laser pulses from the gain medium, $\phi_{in}(\tau)$ and $\phi_{out}(\tau)$ stand for the phase of the input and output laser pulses, and $G(\tau)$ is the total gain experienced by the laser after passing through the gain medium, as defined by

$$G(\tau) = \int_0^L g(z,\tau)dz \tag{5.2.19}$$

Equation (5.2.8) can also be solved, as shown by

$$P_p(L,\tau + \Delta\tau) = P_p(\tau + \Delta\tau)\exp\left[-\int_0^L \alpha_p(z,\tau)zdz\right] \tag{5.2.20}$$

where $P_p(\tau + \Delta\tau) = P_p(0,\ \tau + \Delta\tau)$ is the input pump power and $P_p(L,\ \tau + \Delta\tau)$ is the output pump power. By integrating Equation (5.2.9) over z from 0 to L, using Equations (5.2.8), (5.2.13), (5.2.15), (5.2.17), (5.2.19) and (5.2.20),

$$\frac{dG(\tau)}{d\tau} = \frac{P_p(\tau+\Delta\tau)}{\gamma E_{psat}} \left\{ -\exp\left[\gamma G(\tau) - b\left(N_{p0} - N_0\right)L\right]\right\} - \frac{P_{in}(\tau)}{E_{sat}} \left\{\exp\left[G(\tau)\right] - 1\right\} \tag{5.2.21}$$

is obtained. By solving this differential equation, the output pulse information may be obtained using Equations (5.2.17) and (5.2.18).

The instantaneous frequency sweep $\Delta\omega$ of the laser pulse after passing through the gain medium is related to $G(\tau)$ by

$$\Delta\omega_{out}(\tau) = -\frac{d\phi_{out}(\tau)}{d\tau} = \Delta\omega_{in} + \frac{1}{2}\alpha\frac{dG(\tau)}{d\tau} \tag{5.2.22}$$

from Equation (5.2.18). If the input laser pulse is non-chirped ($\Delta\omega_{in} = 0$), $\Delta\omega_{out}$ may be expressed by

$$\Delta\omega_{out}(\tau) = \frac{\alpha P_p(\tau+\Delta\tau)}{2\gamma E_{psat}} \left\{ -\exp\left[\gamma G(\tau) - b\left(N_{p0} - N_0\right)L\right]\right\} - \frac{\alpha P_{in}(\tau)}{2E_{sat}} \left\{\exp\left[G(\tau)\right] - 1\right\} \tag{5.2.23}$$

Take a look at Equation (5.2.21) or Equation (5.2.23). The first term on the right-hand side is related to the pulsed optical pumping, which induces XPM to the pulses. The second term is related to the gain saturation, which induces SPM to the pulses. Before going through the detailed numerical evaluation, two extreme cases that have analytical solutions are examined here.

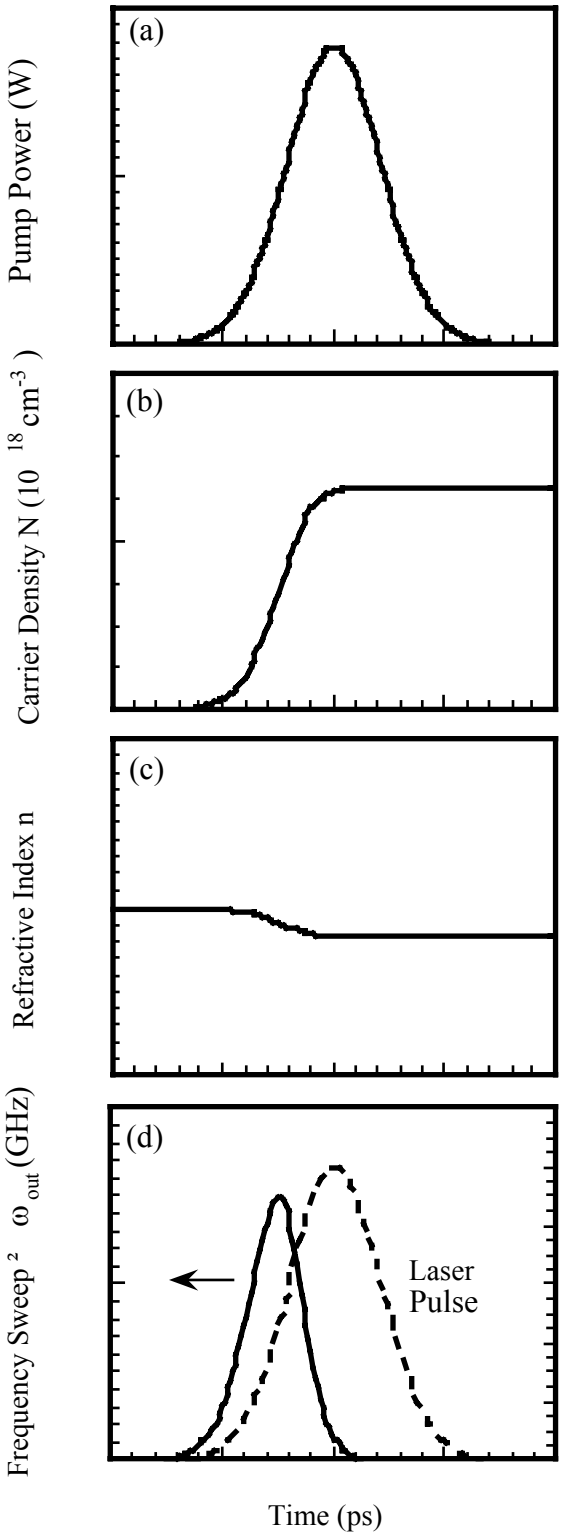

Figure 5.2.1 XPM induced pulse chirping due to the pulsed optical pumping.

Table 5.2.1 Parameters used for calculation

Laser center wavelength λ_0 (μm)	0.86
Pump center wavelength λ_p (μm)	0.8
Effective length of gain medium L (μm)	1.8
Diameter of active medium d (μm)	19
Differential gain at ω_0 a (cm^2)	5.27×10^{-16}
Differential gain at ω_p b (cm^2)	3.57×10^{-15}
Differential gain ratio γ	6.77
Transparent carrier density at ω_0 N_0 (cm^{-3})	6.97×10^{17}
Transparent carrier density at ω_p N_{p0} (cm^{-3})	1.98×10^{18}
Carrier lifetime τ_c (ns)	3
Intraband relaxation time T_2 (ps)	0.1
Linewidth enhancement factor α	5
Saturation energy at ω_0 E_{sat} (nJ)	1.24
Saturation energy at ω_p E_{psat} (nJ)	0.20
Pump pulsewidth τ_{p0} (ps)	10

(a) The first case is for no gain saturation, but including the pump bleaching effect. In this case, $E_{in} << E_{sat}$, where

$$E_{in} = \int_{-\infty}^{+\infty} P_{in}(\tau) d\tau \tag{5.2.24}$$

is the input laser pulse energy, the second term on the right-hand side of Equation (5.2.21) or Equation (5.2.23) may thus be neglected. From Equation (5.2.21), the gain $G(\tau)$ can be re-expressed as

$$G(\tau) = a\left(N_{p0} - N_0\right)L - \frac{1}{\gamma} \ln\left\{1 + \left(e^{bN_{p0}L} - 1\right)\exp\left[-\frac{E_p(\tau + \Delta\tau)}{E_{psat}}\right]\right\} \tag{5.2.25}$$

where

$$E_p(\tau + \Delta\tau) = \int_{-\infty}^{\tau} P_p(\tau + \Delta\tau) d\tau \tag{5.2.26}$$

It is clear from Equation (5.2.23) that the frequency sweep $\Delta\omega_{out}$ of the output pulse follows the shape of the pump pulse $P_p(\tau + \Delta\tau)$ and is modified by the gain $G(\tau)$ as given by

$$\Delta\omega_{out}(\tau) = R(\tau + \Delta\tau)\frac{P_p(\tau + \Delta\tau)}{\gamma E_{psat}} \tag{5.2.27}$$

where

$$R(\tau+\Delta\tau)=\frac{1}{2}\alpha\frac{\left(e^{bN_{p0}L}-1\right)\exp\left[-\dfrac{E_p(\tau+\Delta\tau)}{E_{psat}}\right]}{1+\left(e^{bN_{p0}L}-1\right)\exp\left[-\dfrac{E_p(\tau+\Delta\tau)}{E_{psat}}\right]} \tag{5.2.28}$$

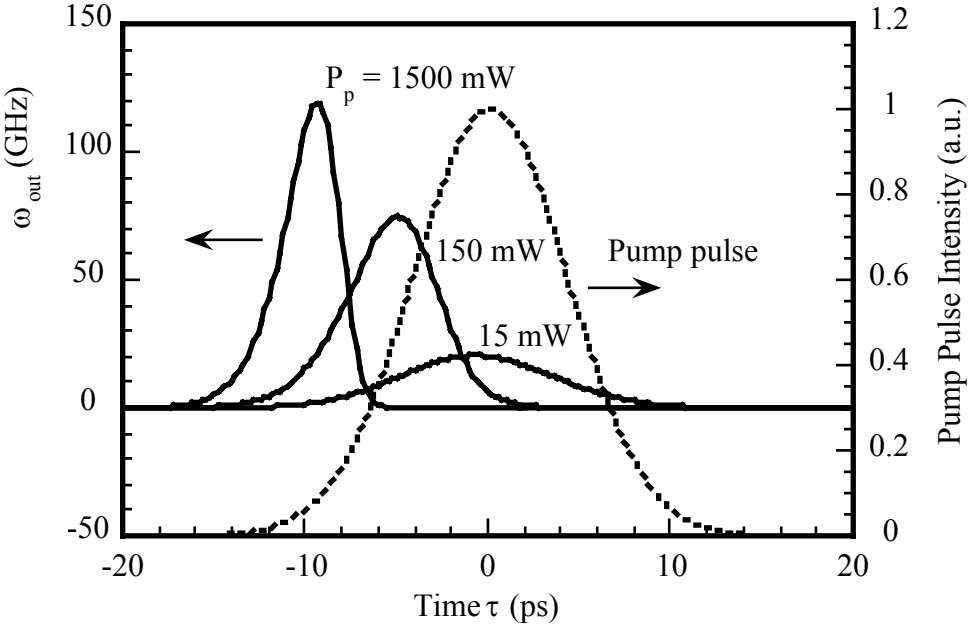

Figure 5.2.2 (a) The instantaneous frequency sweep $\Delta\omega_{out}$ of a weak laser pulse relative to the position of the pump pulse after a single pass through a 120 GaAs-AlGaAs multiple quantum-well (MQW) sample at three different pump power 1.5 W, 150 mW, and 15 mW. The pump pulse of the 10 ps is shown by the dashed line. The laser pulse can be positioned anywhere depending on $\Delta\tau$.

The case can be physically pictured in this way. A very weak laser pulse passes through a gain medium pumped by an optical pulse [Figure 5.2.1(a)]. The absorption to the pump causes the variation of carrier density, as shown in Figure 5.2.1(b). The variation of carrier density causes the variation of refractive index, as shown in Figure 5.2.1(c), thus causes the modulation to the phase of the laser pulse, as shown in Figure 5.2.1(d), where the laser pulse is assumed to enter the gain medium simultaneously

with the pump. This cross-phase-modulation (XPM) is solely caused by the pulsed pumping. How much the laser pulse phase is affected by the XPM depends on when the laser pulse is launched into the gain medium. In other words, the laser pulse can be positioned anywhere in Figure 5.2.1(d), but the phase variation of the laser pulse is as it is in the figure.

Figure 5.2.2(a) shows the instantaneous frequency sweep $\Delta\omega_{out}$ of the weak laser pulse passing through the gain medium under the average pump power of 150 mW (E_p = 1.875 nJ), which is a typical pump level for the GaAs mode-locked VCSEL. The cases for the average pump power of 1.5 W and 15 mW are also shown in the same figure for comparison. The pump pulse is shown by the dashed line. All other data needed for the calculation can be found in Table 5.2.1. The laser pulse can be positioned anywhere depending on $\Delta\tau$, the relative time difference between the pump and the laser pulses.

When the pump pulse energy, E_p, is comparable to or smaller than the pump saturation energy E_{psat} = 0.2 nJ, the laser frequency sweep $\Delta\omega_{out}$ will follow exactly the shape of the pump pulse $P_p(\tau + \Delta\tau)$ as in the case of pump power of 15 mW. Depending on the laser pulse position relative to the pump pulse $\Delta\tau$, the laser will acquire either upchirp or downchirp. If the laser pulsewidth is smaller than the pump pulsewidth, the laser chirp can be linear for certain $\Delta\tau$.

When E_p is larger than E_{psat} as in the cases of pump power of 150 mW and 1.5 W, $\Delta\omega_{out}$ will rise at the leading edge of the pump pulse. Because of absorption bleaching, $\Delta\omega_{out}$ will immediately fall so that most parts of the laser pulse will acquire little frequency sweep if $\Delta\tau > 0$. Figure 5.2.2(b) shows the instantaneous frequency sweep $\Delta\omega_{out}$ of the laser pulse for a pump power of 150 mW at various values of $\Delta\tau$. The laser pulse acquires significant chirp from the pump pulse only for the case of the laser pulse arriving in the gain region earlier than the pump pulse ($\Delta\tau < 0$). For a

synchronously pumped laser in stable operation, the laser pulses usually arrive in the gain region later than the pump pulses ($\Delta\tau > 0$) [10].

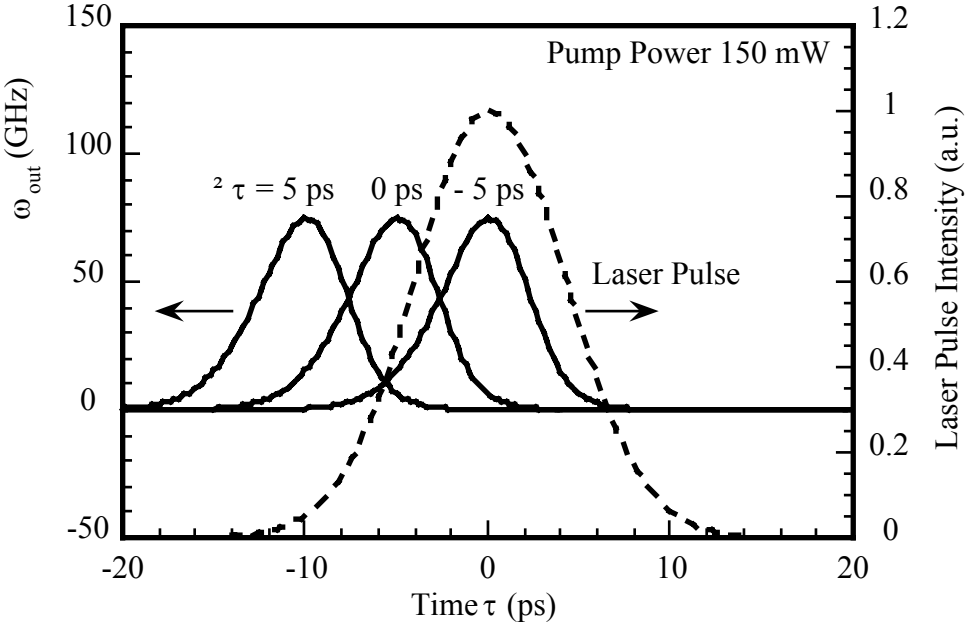

Figure 5.2.2 (b) The instantaneous frequency sweep $\Delta\omega_{out}$ of a weak laser pulse after a single pass through a 120 GaAs-AlGaAs multiple quantum-well (MQW) sample for three different positions relative to the pump pulse, $\Delta\tau$. The pump power is 150 mW and its pulse width is 10 ps. The laser pulse is shown by the dashed line.

(b) The second case is for the absence of the pump, but with an initial gain G_0. By ignoring the first term in Equation (5.2.21) and assuming $G_0 << 1$,

$$G(\tau) = G_0 \exp\left[-\frac{E(\tau)}{E_{sat}}\right] \tag{5.2.29}$$

is obtained, where

$$E(\tau) = \int_{-\infty}^{\tau} P_{in}(\tau) d\tau \tag{5.2.30}$$

The frequency sweep of the output laser pulse $\Delta\omega_{out}$ follows the profile of the input laser pulse and is modified by the gain $G(\tau)$ as given by

$$\Delta\omega_{out}(\tau) = -\frac{1}{2}\alpha G_0 \exp\left[-\frac{E(\tau)}{E_{sat}}\right]\frac{P_{in}(\tau)}{E_{sat}} \tag{5.2.31}$$

This case is essentially similar to that discussed in Ref. 9. Physically it can be pictured in this way. A high energy laser pulse [Figure 5.2.3(a)] passes through a pre-amplified gain medium and creates a carrier density variation as shown in Figure 5.2.3(b). The refractive index of the gain medium will vary as shown in Figure 5.2.3(c). Such an index variation introduces a SPM to the laser pulse, as shown in Figure 5.2.3(d).

Figure 5.2.4(a) shows the instantaneous frequency sweep $\Delta\omega_{out}$ of the laser pulse for various input pulse energies using the parameters given in Table 5.2.1 with $G_0 = a\,(N_{p0} - N_0)L$, the initial gain at which the gain medium is transparent to the pump pulse. When $E_{in} << E_{sat}$, $\Delta\omega_{out}$ shifts toward the negative following the laser pulse shape, so the chirp will be nonlinear over the central portion of the laser pulse. When $E_{in} > E_{sat}$, however, the saturation of the gain will alter the laser chirp. At the leading edge, the frequency sweep $\Delta\omega_{out}$ decreases following the rise of the laser pulse. The gain will then be saturated during the rise of the laser pulse so that $\Delta\omega_{out}$ will return immediately. Depending on the pulse energy level, the chirp acquired may be very linear over the main portion of the laser pulse as shown by the curve for E_{in} = 5 nJ.

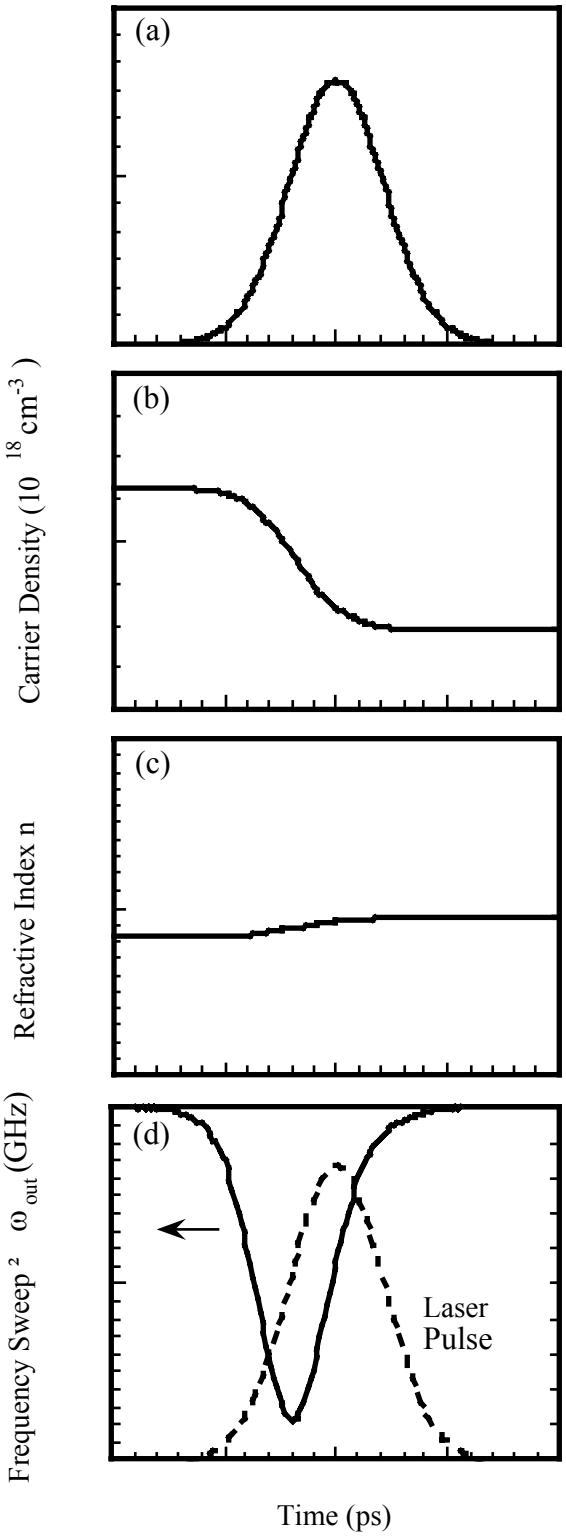

Figure 5.2.3 SPM induced pulse chirping due to the gain saturation.

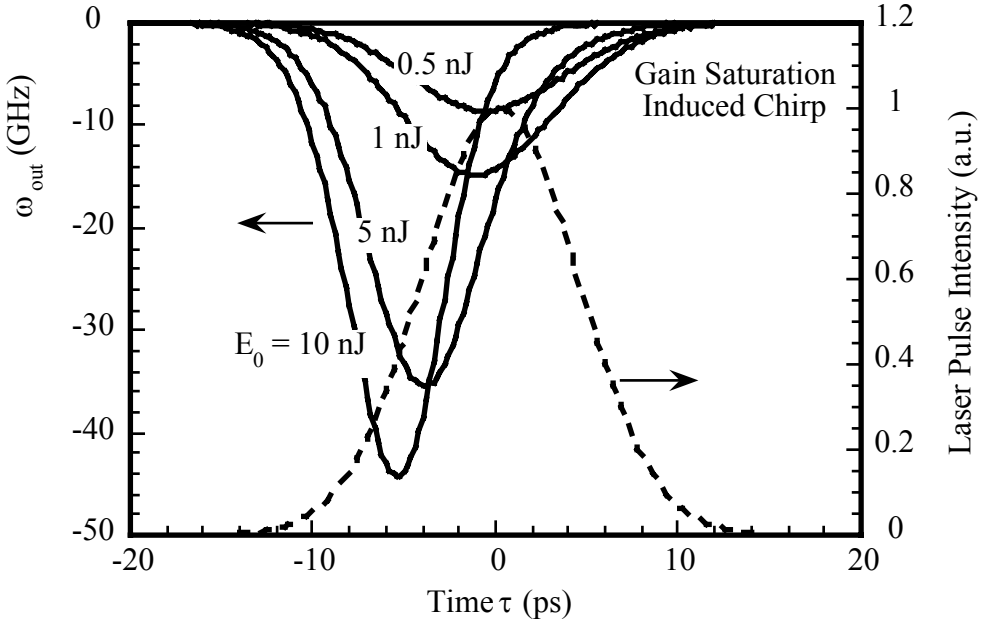

(a)

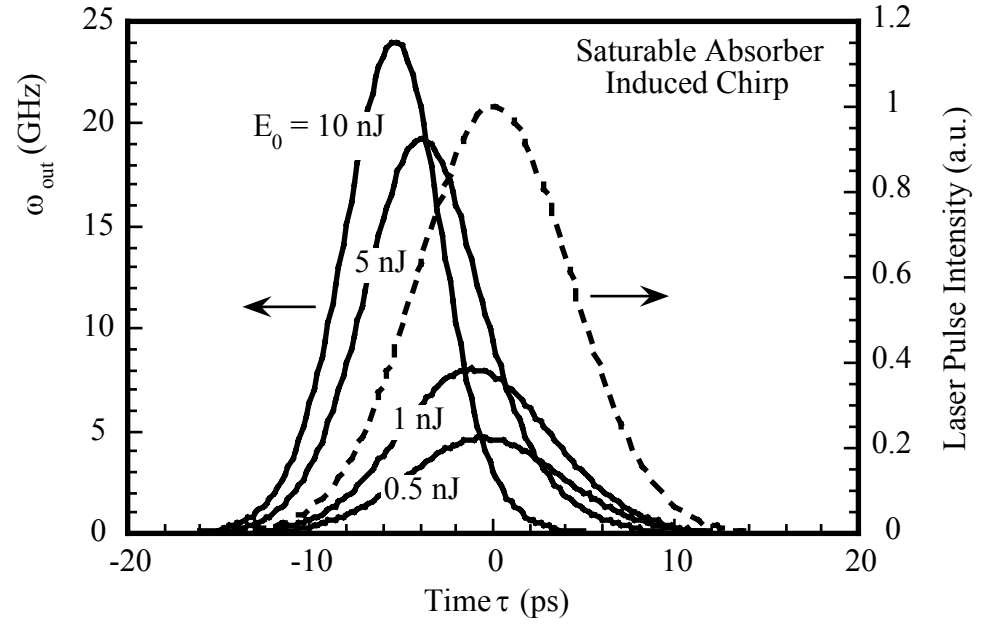

(b)

Figure 5.2.4 The instantaneous frequency sweep $\Delta\omega_{out}$ of a laser pulse with several different pulse energies after a single pass through a 120 GaAs-AlGaAs multiple quantum-well (MQW) sample without the pump, but with an initial gain (a) $G_0 = a(N_{p0} - N_0)L$, and (b) $G_0 = -aN_0L$.

A saturable absorber case worth mentioning is when $G_0 = - aN_0L$, as shown in Figure 5.2.4(b). When $E_{in} << E_{sat}$, $\Delta\omega_{out}$ simply follows the laser pulse shape. When $E_{in} > E_{sat}$, the saturation of the absorption will alter the laser chirp similar to the case of Figure 5.2.4(a). At the leading edge, the frequency sweep $\Delta\omega_{out}$ increases following the rise of the laser pulse. The absorption will then be saturated during the rise of the laser pulse so that $\Delta\omega_{out}$ will fall immediately. Depending on the pulse energy level, the chirp acquired may also be very linear over the main portion of the laser pulse, as shown by the curve for E_{in} = 5 nJ. The sign of the chirp acquired by the laser pulse from the saturable absorber is opposite to that acquired from the gain medium.

Concluding the discussions of (a) and (b), for a pump power of 150 mW and laser pulse energy of 5 nJ, the pulsed optical pumping causes a downchirp to the laser pulse because of the absorption bleaching, while the gain saturation causes an upchirp to the laser pulse. To quantitatively evaluate the laser pulse chirp for the actual case of the mode-locked VCSEL, both effects should be lumped together. $G(\tau)$ is first obtained numerically from Equation (5.2.21) with both of the two right-hand side terms involved. The frequency sweep $\Delta\omega_{out}$ can then be calculated from Equation (5.2.23). Under certain circumstances, either linear downchirp or linear upchirp can be obtained, which is important for laser pulse compression.

Figure 5.2.5 shows the instantaneous frequency sweep $\Delta\omega_{out}$ of a 15 ps pulse with a pulse energy of 5 nJ after passing through a sample with 120 GaAs/AlGaAs multiple quantum wells (MQWs). The pulse energy of 5 nJ corresponds to 12 mW average output power if the coupling mirror has a 97% reflectivity in the mode-locked VCSEL [1]. The typical pump power is 150 mW with 10 ps pulsewidth at 80 MHz repetition rate. The rest of the necessary parameters can be found in Table 5.2.1. When $\Delta\tau$ is small, the XPM induced pulse chirping due to the pulsed optical pumping dominates. When $\Delta\tau$ is large, the SPM induced pulse chirping due to the gain

saturation dominates. An appropriate $\Delta\tau$ will create a linear downchirp to the central portion of the laser pulses because of the balance between the XPM and the SPM.

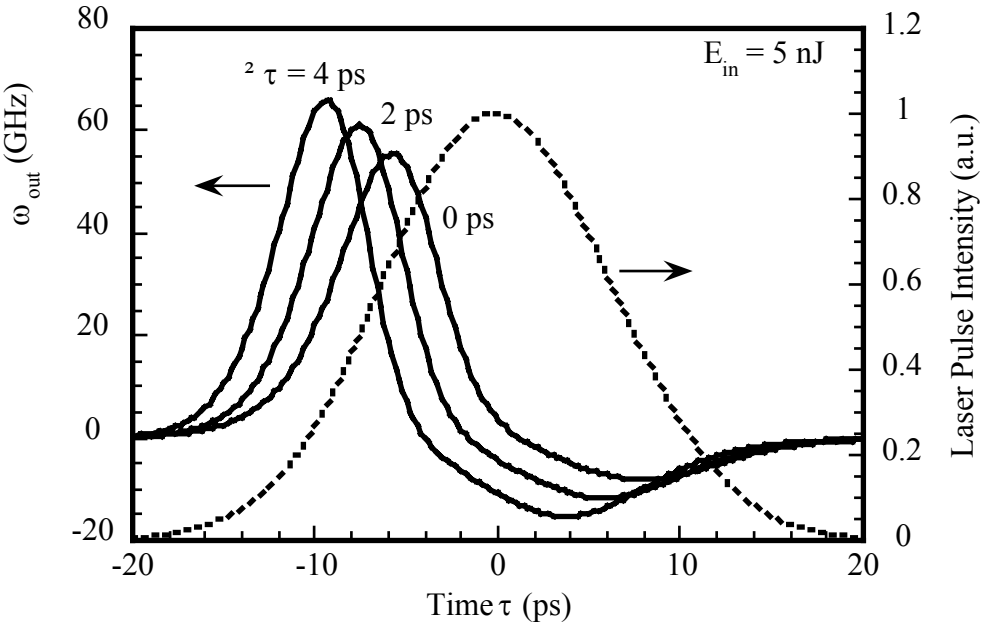

Figure 5.2.5 The instantaneous frequency sweep $\Delta\omega_{out}$ of a 15 ps pulse with a pulse energy of 5 nJ after a single pass through a 120 GaAs-AlGaAs MQW sample with $\Delta\tau$ as a varying parameter. The pump pulsewidth is 10 ps and pump power is 150 mW.

The sign of the chirp on a single pass through the laser has a strong dependence on the laser pulsewidth if the pump pulsewidth is fixed. Figures 5.2.6(a) and 5.2.6(b) show the instantaneous frequency sweep $\Delta\omega_{out}$ of a 5 nJ laser pulse with different pulsewidths for $\Delta\tau$ = 0 and 2 ps, respectively. The pump pulsewidth is 10 ps, and pump power is 150 mW. When $\Delta\tau$ = 0, the laser pulse chirp at its peak is negative if its pulsewidth is longer than 8 ps and becomes positive if its pulsewidth is shorter. When $\Delta\tau$ = 2 ps, there is a similar tendency, but the chirp will flip its sign for a laser pulsewidth of about 10 ps.

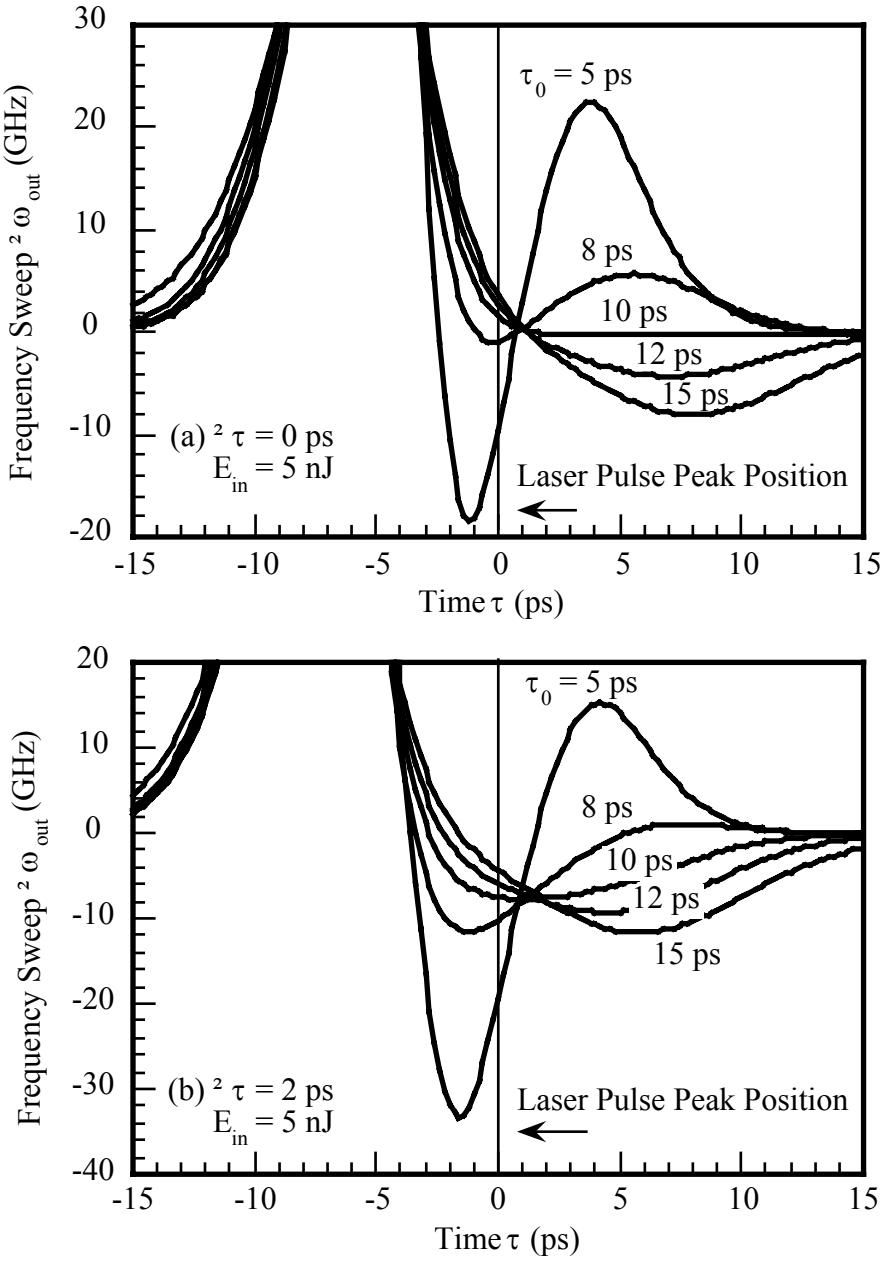

Figure 5.2.6 The instantaneous frequency sweep $\Delta\omega_{out}$ of a 5 nJ laser pulse with its pulsewidth τ_0 as a varying parameter after a single pass through a 120 GaAs-AlGaAs MQW sample under (a) $\Delta\tau = 0$ and (b) $\Delta\tau = 2$ ps. The pump pulsewidth is 10 ps and pump power is 150 mW. The laser pulse peak position is shown by the vertical line in the center.

The instantaneous frequency sweep $\Delta\omega_{out}$ and the chirp C at the pulse peak varying with the laser pulsewidth are shown in Figure 5.2.7. The laser pulse energy is 5 nJ and $\Delta\tau = 0$. The chirp C is defined by

$$C = -\frac{d^2\phi_{out}(\tau)}{d\tau^2} \tag{5.2.32}$$

When the laser pulse is downchirped ($C < 0$), the frequency sweep at the pulse peak $\Delta\omega_{out} > 0$. When the laser pulse is upchirped ($C > 0$), the frequency sweep at the pulse peak $\Delta\omega_{out} < 0$. Similar chirp behavior relating to the laser pulsewidth can be found for the wider pump pulsewidth.

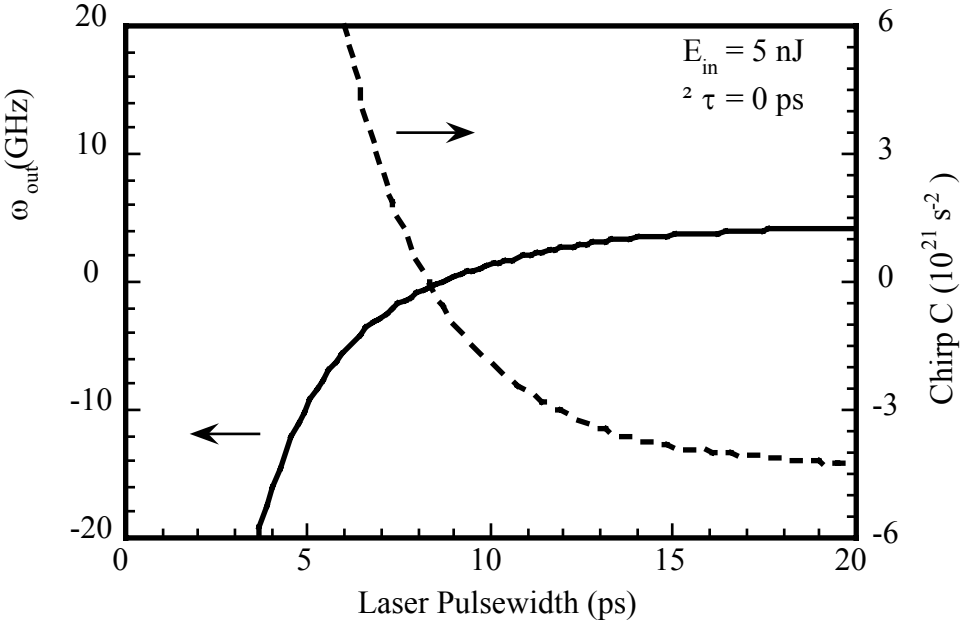

Figure 5.2.7 The instantaneous frequency sweep $\Delta\omega_{out}$ of a pulse and its chirp C at the pulse peak after the single pass through a 120 GaAs-AlGaAs MQW sample varying with the laser pulsewidth. The laser pulse energy is 5 nJ and $\Delta\tau = 0$. The pump pulsewidth is 10 ps and pump power is 150 mW.

To gain knowledge on how much linear group velocity dispersion (GVD) is needed to compensate for the laser pulse chirping because of the gain saturation and the pulsed pumping, the phase of the output pulse obtained using Equations (5.2.17), (5.2.18) and (5.2.21) in the frequency domain is examined. The phase function $\Phi(\omega)$ in the frequency domain is defined by $\Phi(\omega) = \beta(\omega)L$, where $\beta(\omega)$ is the wave propagation constant. $\Phi(\omega)$ can be expanded into the Taylor series,

$$\Phi(\omega) = \Phi(\omega_0) + \frac{d\Phi(\omega_0)}{d\omega}(\omega - \omega_0) + \frac{1}{2}\frac{d^2\Phi(\omega_0)}{d\omega^2}(\omega - \omega_0)^2 + \frac{1}{6}\frac{d^3\Phi(\omega_0)}{d\omega^3}(\omega - \omega_0)^3 + O(\omega - \omega_0)^4 \tag{5.2.33}$$

The first derivative of the pulse phase with regard to the frequency $d\Phi(\omega_0)/d\omega$ is defined as the group delay. The net effect of this group delay is to create a local time shift $\Delta\tau$ for the whole pulse in the time domain. It can be compensated by varying the laser cavity length. The second derivative of the pulse phase $d^2\Phi(\omega_0)/d\omega^2$ is related to the dispersion parameter β_2 by $\beta_2 = d^2\Phi(\omega_0)/d\omega^2 /L$. Figure 5.2.8(a) shows the variation of $d^2\Phi(\omega_0)/d\omega^2$ with $\Delta\tau$ for the laser pulse energy of 5nJ and laser pulsewidth of 15 ps. Also shown in the figure is the gain $G(L)$ experienced by the laser pulse after it passes through the gain medium. When $d^2\Phi(\omega_0)/d\omega^2 > 0$, the pulse is upchirped, and the pulse is downchirped when $d^2\Phi(\omega_0)/d\omega^2 < 0$. For a laser to reach the lasing threshold, certain cavity gain is needed to overcome the cavity loss. For example, if the round-trip cavity loss is 5%, a round-trip gain of 1.05 will be needed to sustain the laser operation. Because of this extra gain requirement, the allowance of $\Delta\tau$ will be limited. For the example illustrated here, the laser will be able to operate at certain range of $\Delta\tau > 0$ so that $G(L) > 1.05$. The laser pulse in this region will be downchirped with $d^2\Phi(\omega_0)/d\omega^2$ between - 9 x 10^{-24} ~ - 5 x 10^{-24} s^2. **This value is**

four orders of magnitude as large as the GVD caused by the intracavity material dispersion or the semiconductor DBR mirror and the dielectric mirrors.

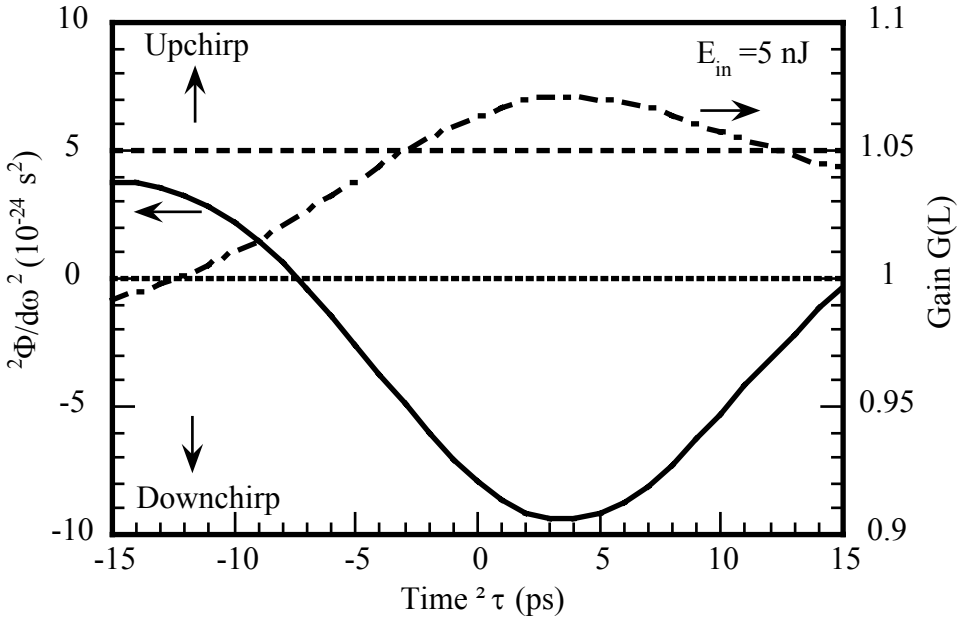

Figure 5.2.8 (a) $d^2\Phi(\omega_0)/d\omega^2$ varying with $\Delta\tau$ after the laser pulse passing through a 120 GaAs-AlGaAs MQW sample (solid line). Also shown in the figure are the gain *G(L)* experienced by the laser pulse after its pass through the sample (dash-dotted line). The laser pulse energy is 5 nJ and the pulsewidth is 15 ps. The pump pulsewidth is 10 ps and the pump power is 150 mW. The short dashed line specifies the gain level of 1 and the chirp level of 0. The long dashed line specifies the gain level of 1.05.

The magnitude of $d^2\Phi(\omega_0)/d\omega^2$ induced by the gain saturation and the pulsed optical pumping may be compared with that generated by a grating-pair. The dispersion from the grating-pair can be expressed by [11]

$$\frac{1}{2}\frac{d^2\Phi(\omega_0)}{d\omega^2} = -\frac{4\pi^2 c b_0}{\omega_0^3 a_c^2 \cos^2\theta_{r0}} \tag{5.2.34}$$

where c is the speed of light, b_0 is the center to center distance between the gratings, a_c is the grating constant (line spacing). The diffraction angle θ_{r0} is related to the incident angle θ_i by

$$\sin\theta_{r0} = \frac{2\pi c}{\omega a} - \sin\theta_i \qquad (5.2.35)$$

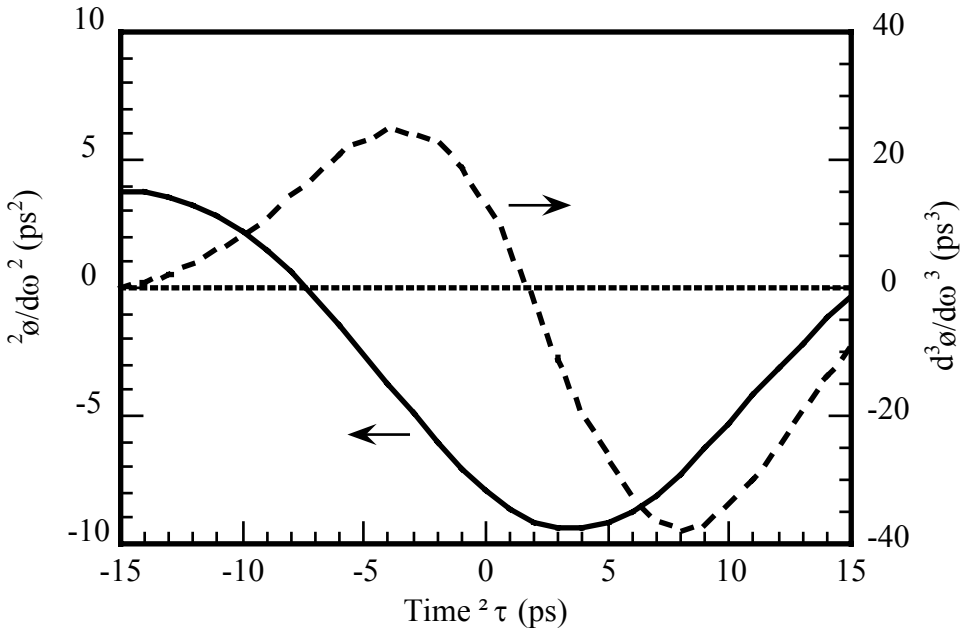

Figure 5.2.8 (b) The variation of $d^3\Phi(\omega_0)/d\omega^3$ with $\Delta\tau$ for the laser pulse energy of 5 nJ and pulsewidth of 15 ps (dashed line). The pump power is 150 mW and the pump pulsewidth is 10 ps. The correspondent $d^2\Phi(\omega_0)/d\omega^2$ (solid line) is shown for comparison.

Both θ_{r0} and θ_i are assumed on the same side of the grating normal. If assuming that the grating has 1200 lines/mm, λ is 0.88 μm, and $\cos\theta_{ro} \sim 1$, $d^2\Phi(\omega_0)/d\omega^2 \sim -5 \times 10^{-24}$ s^2 will be equivalent to a b_0 of ~ 1 m. Since the dispersion obtainable from a prism-pair is much smaller than that from a grating-pair, such a large equivalent intracavity dispersion would be difficult to be compensated by the usual intracavity

prism-pair dispersion compensation method [12] widely adopted in the colliding pulse mode-locking (CPM) [13] and Ti: Sapphire laser [14] systems, while the high loss of grating-pair compressors [11, 15] prevents them from being used within the VCSEL cavity.

The third order derivative of phase to the frequency $d^3\Phi(\omega_0)/d\omega^3$ reveals the nonlinearity of the chirp. Figure 5.2.8(b) shows the variation of $d^3\Phi(\omega_0)/d\omega^3$ with $\Delta\tau$ for the laser pulse energy of 5 nJ and pulsewidth of 15 ps. The pump power is 150 mW and the pump pulsewidth is 10 ps. For comparison, $d^2\Phi(\omega_0)/d\omega^2$ is also shown in the same figure. Notice that $d^3\Phi(\omega_0)/d\omega^3 = 0$ at the position of $\Delta\tau = 1.7$ ps. Physically it means that the chirp around the peak of the laser pulse has the best linearity at this position. The consequence is that the chirp of the output pulse can thus be ultimately compensated by a grating-pair that has the linear GVD.

5.3 Gain dispersion

The chirp due to the SPM and the XPM will broaden the spectrum of the pulse. It will eventually reach such a width that the finite gain shape of the gain material or other magnitude filtering elements may limit its further broadening. In this section, the effect of the phase dispersion due to the finite gain shape will be discussed. The gain saturation and the linewidth enhancement factor α will be ignored during the discussion since their role related to the pulse chirping has been taken into account in Section 5.2. This procedure is similar to the split-step Fourier method [8] that has been used in the analysis of light transmitting in the optical fiber.

The gain shape of the semiconductor materials is assumed Lorenzian so that the complex power gain coefficient can be written as [16]

$$\tilde{g}(\omega-\omega_0)=\frac{g_p}{1-iT_2(\omega-\omega_0)} \tag{5.3.1}$$

where g_p is the peak power gain coefficient, ω_0 is the peak frequency, and T_2 is a bandwidth parameter. The exact gain shape of the semiconductor materials is somewhat different in that the gain shape is closer to the Gaussian shape on the higher frequency side [17]. The difference will, however, not affect the discussion here.

In the frequency domain, Equation (5.2.6) may be written as

$$\frac{\partial\tilde{A}(z,\omega)}{\partial z}=\frac{1}{2}\tilde{g}(\omega-\omega_0)\tilde{A}(z,\omega) \tag{5.3.2}$$

where $\tilde{A}(z, \omega)$ is related to $A(z, \tau)$ by the inverse Fourier transform

$$A(z,\tau)=\int_{-\infty}^{\infty}\tilde{A}(z,\omega)e^{-i(\omega-\omega_0)\tau}d\omega \tag{5.3.3}$$

After a single pass through the gain medium of length L, the electric field $\tilde{A}(z, \omega)$ can be solved in terms of the input $\tilde{A}(0, \omega)$ from Equation (5.3.2), as given by

$$\tilde{A}(L,\omega)=\tilde{A}(\omega)\exp[i\Phi(\omega)] \tag{5.3.4}$$

with the real amplitude

$$\tilde{A}(\omega)=\tilde{A}(0,\omega)\exp\left(\frac{\frac{1}{2}g_pL}{1+T_2^2(\omega-\omega_0)^2}\right) \tag{5.3.5}$$

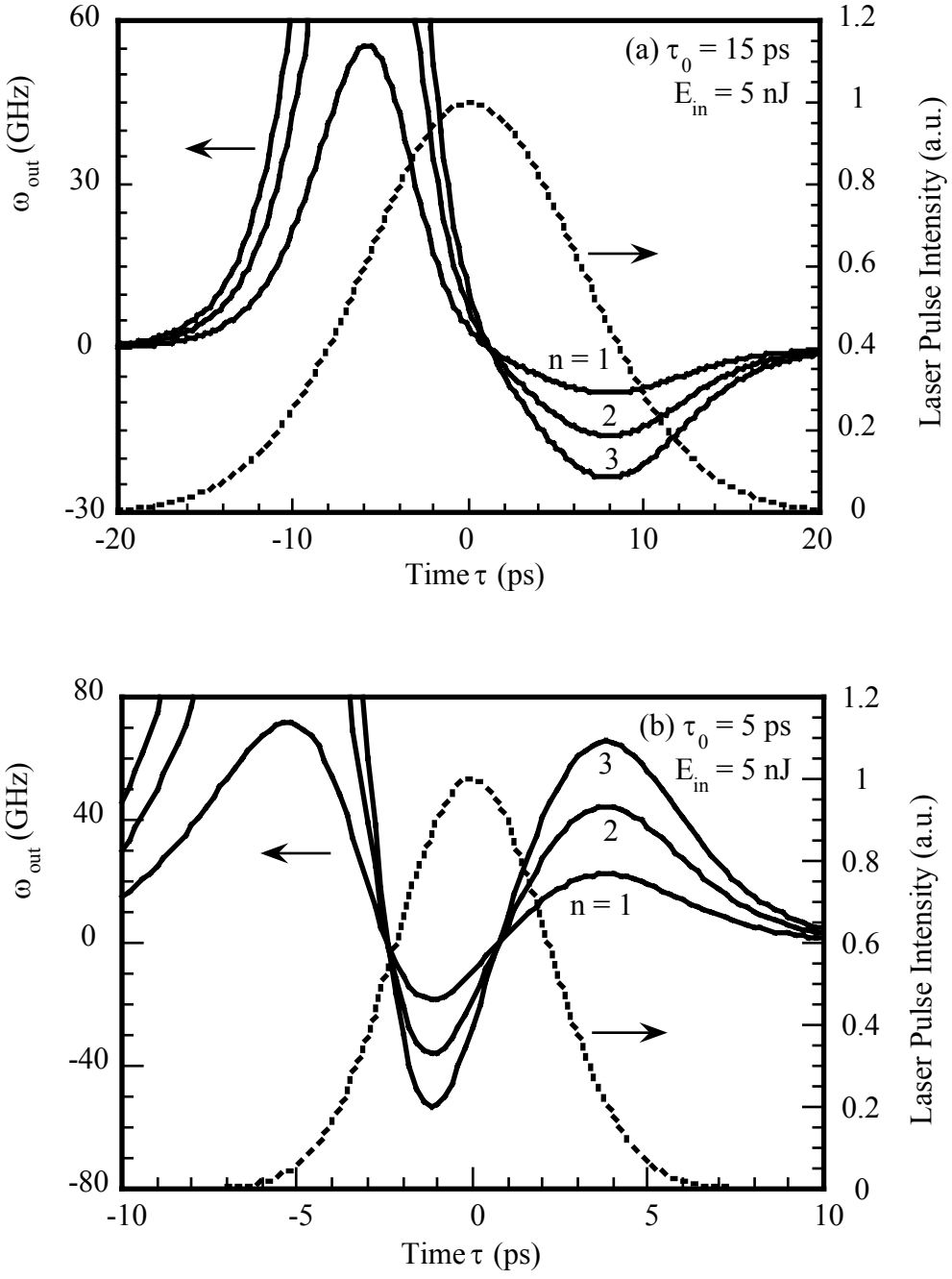

Figure 5.4.1 The instantaneous frequency sweep $\Delta\omega_{out}$ (solid lines) of a laser pulse after the first three passes through a 120 GaAs-AlGaAs MQW sample. The laser pulsewidth τ_0 is (a) 15 ps and (b) 5 ps, and laser pulse energy E_{in} is 5 nJ (short dashed line). The pump pulsewidth is 10 ps and the pump power is 150 mW.

and the phase

$$\Phi(\omega) = \frac{\frac{1}{2} g_p L T_2 (\omega - \omega_0)}{1 + T_2^2 (\omega - \omega_0)^2} \tag{5.3.6}$$

The peak gain g_p can be obtained from Equation (5.2.25) as

$$g_p = a(N_{p0} - N_0) \tag{5.3.7}$$

by assuming $E_p >> E_{psat}$, which is true for the optically pumped mode-locked VCSELs. From Equation (5.3.6), the maximum value of the second derivative of the phase, $\Phi''_{max}(\omega)$, can be expressed by

$$\Phi''_{\max} = 0.73 g_p L T_2^2 \tag{5.3.8}$$

Using the data in Table 5.2.1, $\Phi''_{max}(\omega)$ is ~ 1 x 10^{-27} s^2. **This is three orders of magnitude smaller than the $\Phi''(\omega)$ caused by the gain saturation and the pulsed pumping**. In other words, the phase dispersion caused by the finite gain shape will have little effect on the formation of the laser pulse chirping in an mode-locked VCSEL. The main effect of the finite gain shape on the laser pulse is its amplitude modulation to the spectrum of the pulses.

5.4. Discussion of laser pulse evolution

Laser pulse evolution in a laser cavity involves pulse shortening mechanisms and pulse broadening mechanisms. In the frequency domain, it is a balance between

spectral broadening and spectral narrowing. In a synchronously pumped laser system, the leading edge of the laser pulse is shortened by the rising of the gain, the trailing edge is confined by saturation of the gain. This gain modulation mechanism causes pulse shortening. In the frequency domain, pulse shortening is represented by spectral broadening. For the mode-locked VCSEL, strong SPM and XPM will cause extra spectral broadening, thus the time-bandwidth product will be larger than the Fourier transform-limit. With the shortening of the pulsewidth and the broadening of the spectrum, the dispersive elements in the laser cavity start to act on the laser pulse. These dispersive elements include material dispersion, phase dispersion of gain, DBR structure related dispersion, and other intentionally introduced filters. The dispersion can be a pulse shortening factor or pulse broadening factor, depending on the relative sign between the pulse chirping and the dispersion. The phase dispersion factor is small, however, compared to the SPM and XPM effects in the mode-locked VCSEL, as shown in the discussions in Sections 5.2 and 5.3. One of the dominant pulse broadening or spectral narrowing mechanisms is thus the amplitude modulation to the pulse spectrum from a spectral filter with a finite filter bandwidth within the laser cavity. This filter can be an intracavity birefringent plate, an etalon, or can be caused by the Fabry-Perot effect of an imperfect intracavity element , the finite gain bandwidth, the band edge of the DBR mirror, or something else related to the laser cavity design. Carrier transport because of the non uniform carrier distribution within the gain medium also plays an important role in limiting the laser pulse shortening, as demonstrated in Chapter 3.

Take a look at what will happen if an initially unchirped pulse of 15 ps is launched into a GaAs VCSEL. The pulse will become down-chirped due to the gain saturation and the pulsed optical pumping (Figure 5.2.7) after one round trip traveling in the cavity. During the second round trip, the down-chirped input pulse becomes more

down-chirped at the output [Figure 5.4.1(a)]. This process will continue so that the laser pulse will be shortened and the laser spectrum will be broadened. Interestingly, the down-chirp acquired by the laser pulse during the following each round trip around the laser cavity tends to decrease after several passes because of the pulse shortening (Figure 5.2.7). Two important cases of the equilibrium pulse formation processes are examined here.

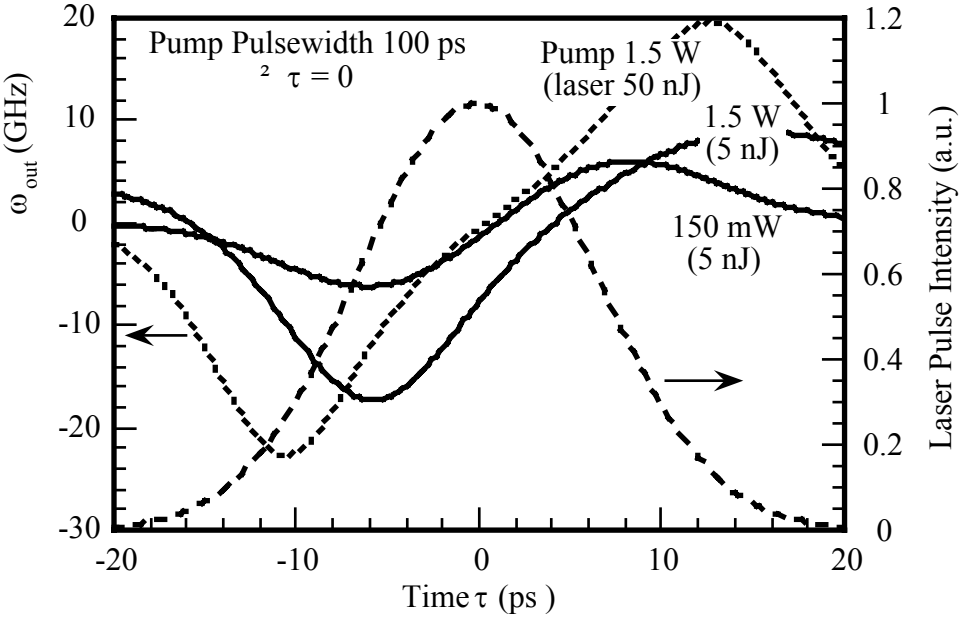

Figure 5.4.2 (a) The instantaneous frequency sweep $\Delta\omega_{out}$ of a 15 ps pulse with a pulse energy of 50 nJ or 5 nJ after a single pass through a 120 GaAs-AlGaAs MQW sample at $\Delta\tau = 0$. The pump pulsewidth is 100 ps and the pump power is 1.5 W, or 150 mW. The SPM due to the gain saturation dominates and the laser pulse acquires upchirp.

In the first case, the filter bandwidth is not very wide, but the spectrum of the laser pulses has become as wide as that of the spectral width of a Fourier transform limited subpicosecond pulse. The actual pulsewidth is still more than 8 ps though since the pulse is strongly chirped. Further spectral broadening is suppressed by the amplitude

modulation of the filter within the cavity. On each additional pass through the gain medium, the laser pulse will acquire extra bandwidth because of the gain modulation, the SPM and the XPM. The acquired extra bandwidth will be curtailed by the filter so that after a round trip, the pulse spectrum remains unchanged. In the time domain, this will be the case that the pulse shortening is balanced by the pulse broadening. The output pulse will be down-chirped. This is the case of the mode-locked GaAs VCSEL in Chapter 2.2.3.

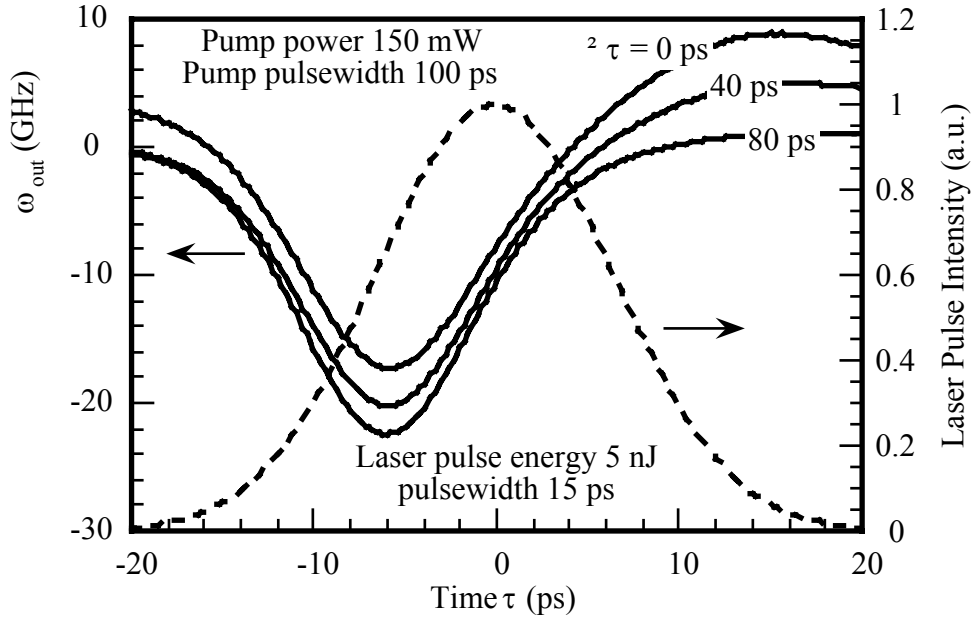

Figure 5.4.2 (b) The instantaneous frequency sweep $\Delta\omega_{out}$ of a 15 ps pulse with a pulse energy of 5 nJ after a single pass through a 120 GaAs-AlGaAs MQW sample at different $\Delta\tau$. The pump pulsewidth is 100 ps and the pump power is 150 mW. The SPM due to the gain saturation dominates and the laser pulse acquires upchirp.

In the second case, the filter bandwidth is very wide and the gain modulation induced pulse shortening is strong enough to obtain a pulsewidth shorter than 8 ps. The sign of the laser pulse chirp acquired during each additional pass through the gain medium will thus be positive as shown in Figure 5.2.7. This will counter-act the down-chirp

acquired by the laser pulse in the former trips so that the laser pulse will soon become up-chirped. As the laser pulse becomes more and more up-chirped [Figure 5.4.1(b)], the spectral broadening caused by the gain modulation and the phase modulation will be offset by the filter. The laser pulsewidth will thus be stabilized, and the laser pulse will be up-chirped. This case is not able to be constructed experimentally with the pump pulsewidth of 10 ps or shorter. It can be done, however, with a pump pulsewidth over 100 ps [2, 3]. In that case, a laser pulse of shorter than 30 ps acquires a positive chirp when passing through the gain medium, rather than the down-chirp in the case of the pump pulsewidth of 10 ps (Figure 5.4.2). The laser pulse will thus have an upchirp when it is stabilized in the laser cavity.

According to the above discussions, the laser pulse can be made unchirped with the insertion of matched filter in the cavity to limit extra bandwidth (Chapter 3). This approach has also been reported by Sun and Yamamoto [18], who have utilized the coupled-cavity characteristics that works like a filter in the cavity. Another possibility will be to utilize the downchirp characteristics of a saturable absorber [Figure 5.2.4(b)]. This approach involves how to choose parameters of saturable absorbers and is only appropriate for the compensation of pulses with upchirp.

It should be pointed out that in some occasions the intracavity filter effect may not be the mechanism in limiting the laser pulse shortening, but the finite carrier transport time within the gain medium. Such a difference, however, does not affect the basic idea of the pulse formation discussion. To conclude the discussion of this section, it is worth mention that the laser chirp is linearly proportional to the linewidth enhancement factor α according to Equation (5.2.18). The optimum way to decrease the laser chirp is to have a smaller α, which is possible by tuning the laser λ_0.

5.5. Discussions of experimental results

It is shown in Chapter 2.2.3 that the pulse is downchirped in a GaAs mode-locked VCSEL. A grating-pair with a telescope set-up is used to generate positive dispersion to compensate for the chirp. The pulses from InGaAs/InP mode-locked VCSELs are, however, upchirped [2, 3]. The variation of the chirp sign can be explained from Figures 5.2.6 and 5.2.7. In the GaAs VCSEL, the laser pulse is always longer than 10 psec while the pump laser pulsewidth is only 5 - 10 ps. Accordingly, the laser pulse must have been downchirped --- the first case discussed in Section 5.4. In the InGaAs/InP VCSEL, the pump pulsewidth is over 100 ps [3] and the laser pulses varied from 5 ps to 40 ps, which are shorter than the pump pulsewidth, thus the laser pulses are upchirped (Figure 5.4.2) --- the second case discussed in Section 5.4. In the case of Chapter 2.3.3, although the laser pulse is about 7 ps, longer than the pump pulsewidth, it is actually the addition of several pulses very close to each other. The actual pulsewidth of the individual pulses may well be shorter than the pump pulse. Also, the pump comes from the compression of a 120 ps pulse by a fiber grating-pair compressor, so that the compressed pulse has a relatively long tail, which differs from the pump pulse profile of a Gaussian that is assumed through out the discussions in this chapter. Different shapes of the pump pulse will make the laser pulse to change its chirp sign at different laser pulsewidth, but will not change the basic discussions made.

It has been found experimentally that the laser chirp is tunable by varying the laser cavity length [3]. It is understandable from Figures 5.2.5 and 5.2.8 that the variation of $\Delta\tau$ will change not only the magnitude of chirp, but also the linearity of the chirp. More importantly, the laser pulsewidth is critically dependent on the matching of the laser cavity length and the pump cavity length in a synchronously pumped laser

system. The variation of the laser cavity length will vary the relative position between the laser and the pump pulses $\Delta\tau$, thus severely varying the laser pulsewidth and altering the pulse chirp as shown by Figures 5.2.6 and 5.2.7.

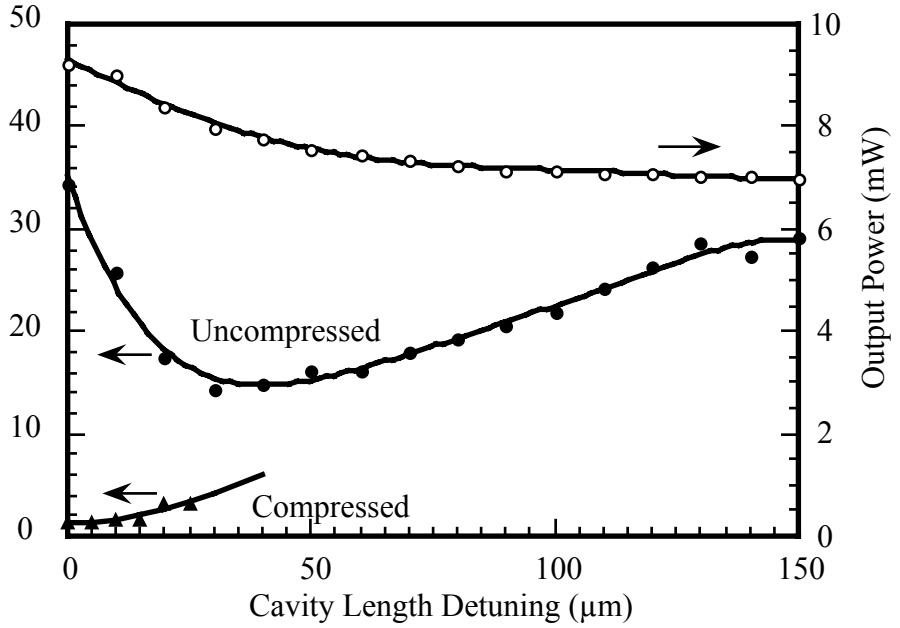

Figure 5.5.1 The laser pulsewidth and its output power versus the cavity detuning in a mode-locked GaAs VCSEL. Also shown is the variation of the compressed pulsewidth with the cavity detuning. The solid lines are a guide to the eye.

Figure 5.5.1 shows the laser pulsewidth as a function of the detuning of the laser cavity in a mode-locked GaAs VCSEL. The pump pulsewidth is 10 ps and the pump power is 150 mW. Also shown in the figure is the compressed pulsewidth. Note that efficient pulse compression occurs where the uncompressed pulsewidth is not at the minimum. A similar observation was found in the InGaAs/InP system [3] where the maximum compression occurred when the uncompressed pulsewidth was 30 ps, rather than the shortest pulsewidth of 5 ps.

The phenomena can be explained using Figures 5.2.8(a) and 5.2.8(b). In Figure 5.2.8(a), the maximum available gain happens at $\Delta\tau \sim 3$ ps for the laser pulsewidth of 15 ps and laser pulse energy of 5 nJ, rather than the cavity length matching case of $\Delta\tau = 0$ ps. As the laser pulse chirping is more linear at this maximum gain position than at larger $\Delta\tau$ [Figure 5.2.8(b)], the pulse compression is more effective. The corresponding uncompressed laser pulsewidth is, however, not necessary at its minimum at the maximum gain position. The optimum laser pulsewidth in a synchronously pumped laser system is usually obtained at a cavity length of longer than that of the maximum gain position, so that the gain saturation can be fully used to suppress the trailing edge of the laser pulse [10]. Because the chirp linearity deteriorates for a larger $\Delta\tau$, the pulse compression becomes less effective.

5.6 Conclusions:

The origin of the laser pulse chirp in mode-locked VCSELs has been discussed. Gain saturation and pulsed optical pumping are the dominant causes of the pulse chirping. The adjustment of the chirp value can be realized mainly through tuning the laser cavity length thus varying the laser pulsewidth. The sign of the laser chirp is closely related to the laser pulsewidth and the pump pulsewidth, as well as the relative importance of the gain saturation and the pulsed optical pumping. The magnitude of the chirp is so large that the usual intracavity prism-pair chirp compensation becomes impractical. This problem is intrinsic to higher power operation, as in the synchronously pumped VCSEL system, since larger pulse energy is always related to a larger variation of carrier density, producing larger chirp. External cavity chirp compensation seems efficient [1, 2, 3], but the compressed pulses often contain a large amount of energy in wings due to the difficulty in compensation for the nonlinear chirp

over the part other than the central portion of the pulses. An extra intracavity filter is a useful way to limit the spectral width so that the time bandwidth product of pulses can be made closer to the Fourier transform-limit, but it will also limit the minimum pulsewidth to be achieved. Saturable absorbers will probably be a candidate for the intracavity chirp compensation if the laser is up-chirped as in the case of InGaAs mode-locked VCSELs. They will not be useful for the chirp compensation purpose if the laser is downchirped as in the case of GaAs mode-locked VCSEL.

Before the chapter is brought into conclusion, it should be pointed out that although the discussion made in this chapter is for an optically pumped mode-locked VCSEL, it can be easily extended to discuss the chirping for an electrically pumped mode-locked VCSEL by replacing the optical pump pulse with an electrical pump pulse. Typically an electrical pulse has a pulsewidth on the order of 100 ps, the pulse chirping due to the pump pulse is thus sufficiently less than that due to the gain saturation if the laser pulse energy is comparable to that from an optically pumped laser, similar to that shown by Figures 5.4.2 (a) and (b). For the case demonstrated in Chapter 4, the laser pulse energy is about one-tenth of the gain saturation energy and the pulsewidth is long, while the electrical pump pulse is only a slight modulation on top of the quasi-DC bias. The pulse chirping due to the pulsed pumping and the gain saturation should thus be considerably smaller than that from an optically pumped laser and be comparable to the phase dispersion due to the finite gain profile. This is confirmed by the narrow power spectral width of no more than 0.5 nm shown in Figure 4.4.7 (b).

References

[1] W. B. Jiang, R. Mirin, and J. E. Bowers, "Mode-locked GaAs vertical cavity surface emitting lasers," *Appl. Phys. Lett.*, **60**, 677 (1992)

[2] W. B. Jiang, S. R. Friberg. H. Iwamura, and Y. Yamamoto, "High powers and subpicosecond pulses from an external-cavity surface-emitting InGaAs/InP multiple quantum well laser," *Appl. Phys. Lett.*, **58**, 807 (1991)

[3] W. H. Xiang, S. R. Friberg, K. Watanabe, S. Machida, W. B. Jiang, H. Iwamura, and Y. Yamamoto, "Femtosecond external-cavity surface-emitting InGaAs/InP multiple-quantum-well laser," *Opt. Lett.*, **16**, 1394 (1991)

[4] W. H. Xiang, S. R. Friberg, K. Watanabe, S. Machida, Y. Sakai, H. Iwamura, and Y. Yamamoto, "Sub-100 femtosecond pulses from an external-cavity surface-emitting InGaAs/InP multiple quantum well laser with soliton-effect compression," *Appl. Phys. Lett.*, **59**, 2076 (1991)

[5] S. de Silvestri, P. Laporta, and O. Svelto, "The role of cavity dispersion in CW mode-locked lasers," *IEEE J. Quantum Electron.*, **QE-20**, 533 (1984)

[6] P. Laporta and V. Magni, "Dispersive effects in the reflection of femtosecond optical pulses from broadband dielectric mirrors," *Appl. Opt.*, **24**, 2014 (1985)

[7] A. N. Pikhtin and A. D. Yas'kov, "Dispersion of the refractive index of semiconductors with diamond and zinc-blende structures," *Sov. Phys. Semicond.*, **12**, 622 (1978)

[8] G. P. Agrawal, *Nonlinear Fiber Optics* , Ch. 1 & 2. (Academic Press, 1989)

[9] G. P. Agrawal and N. A. Olsson, "Self-phase modulation and spectral broadening of optical pulses in semiconductor laser amplifiers," *IEEE J. Quantum Electron.*, **QE-25**, 2297 (1989)

[10] D. M. Kim, J. Kuhl, R. Lambrich and D. von der Linde, "Characteristics of picosecond pulses generated from synchronously pumped CW dye laser system," *Opt. Comm.,* **27**, 123 (1978)

[11] E. B. Treacy, "Optical pulse compression with diffraction gratings," *IEEE J. Quantum Electron.*, **QE-5**, 454 (1969)

[12] R. L. Fork, O. E. Martinez, and J. P. Gordon, "Negative dispersion using pairs of prisms," *Opt. Lett.*, **9**, 150 (1984)

[13] W. H. Xiang, W. B. Jiang, and Y. Ishida, "Femtosecond pulses generated from non-colliding pulse mode-locked ring dye lasers," *Opt. Comm.*, **86**, 70 (1991)

[14] N. Sarukura, Y. Ishida, and H. Nakano, "Generation of 50-fsec pulses from a pulse-compressed, cw passively mode-locked Ti:sapphire laser," *Opt. Lett.*, **16**, 153 (1991)

[15] O. E. Martinez, "3000 times grating compressor with positive group velocity dispersion: application to fiber compensation in 1.3-1.6 μm region," *IEEE J. Quantum Electron.*, **QE-23**, 59 (1987)

[16] A. E. Siegman, *Lasers* , Ch. 8. (University Science Books, 1986)

[17] A. Yariv, *Quantum Electronics*, Ch. 21. (John Wiley & Sons, 3rd Ed., 1989)

[18] D. C. Sun and Y. Yamamoto, "Passive stabilization of a synchronously pumped external-cavity surface-emitting InGaAs/InP multiple quantum well laser by a coherent photon-seeding technique," *Appl. Phys. Lett.*, **60**, 1286 (1992)

Chapter 6 Effect of carrier transport on mode-locked vertical-cavity semiconductor lasers

Vertical-cavity semiconductor laser mode-locking can generate ultrashort pulses with very high pulse energy because of the higher gain saturation energy in the vertical cavity configuration, as discussed in previous chapters. Those high energy pulses directly from the laser oscillators are usually highly chirped because of the cross-phase-modulation (XPM) induced by the high pump power and self-phase-modulation (SPM) induced by the gain saturation (Chapter 5). The pulsewidth of the pulses is thus limited to several picoseconds. Grating-pair compressors have been used for chirp compensation so that the laser pulsewidth has been reduced to subpicosecond (Chapter 2). A second stage compressor with a soliton fiber has reduced the pulsewidth to 21 fs [1].

In order to directly generate subpicosecond pulses from the laser oscillators, birefringent filters have been introduced to confine the pulse spectrum, thus to control the pulse chirping (Chapter 3). The pulsewidth of the laser pulses is, however, still around 1 ps. Some other methods to shorten the pulsewidth have been suggested, but have not been successful [2, 3]. The hypothesis was proposed that the carrier transport within the gain medium due to the spatial hole-burning was the cause of the long pulsewidth and the pedestals (Chapter 3). A periodic gain structure was then used to decrease this effect and pulses with an intensity autocorrelation width of 300 fs were generated (Chapter 3).

In this chapter, a model to simulate the laser pulse build-up in the synchronously pumped mode-locked VCSEL is proposed. The model takes into account the finite carrier transport time. How the carrier transport affects the laser pulse shape,

pulsewidth and pulse energy is analyzed. The simulation model is finally used to reproduce the experimental observations.

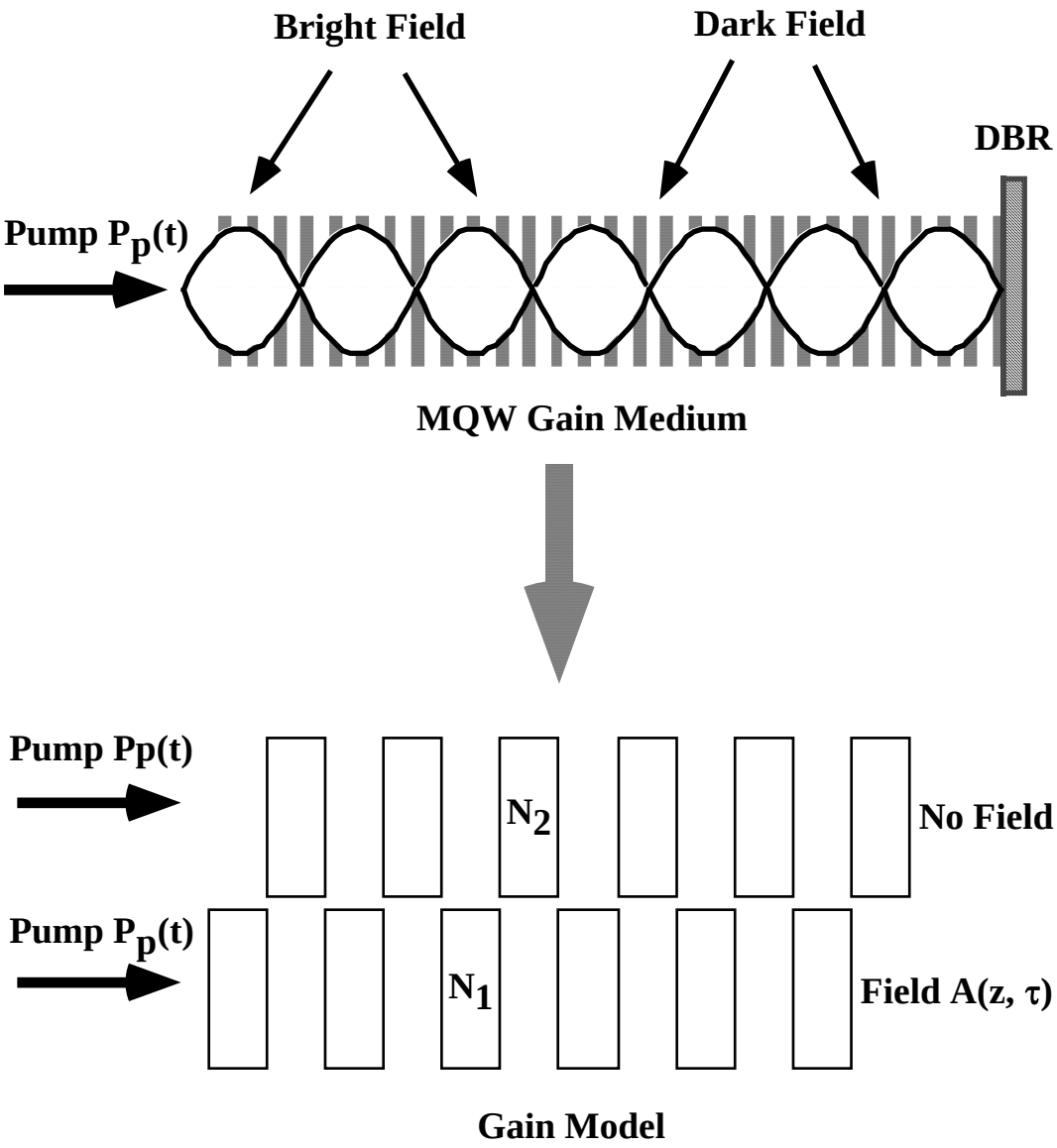

Figure 6.1 Standing wave pattern in the gain medium and the corresponding gain model used for simulation.

Examine the standing wave pattern established in the gain medium during the lasing action, as shown in Figure 6.1. Spatial hole-burning occurs because of this standing

wave pattern. Those spatial holes are caused by the rapid carrier depletion because of the strong field at those locations. The excited carriers outside of the high intensity regions can only be depleted by transporting into these spatial holes through thermionic emission, diffusion and tunneling, or by a slow process of spontaneous emission. As an approximation to simplify the simulation process, the gain medium is separated into two parts. One part accounts for the gain medium seeing the lasing field, the other part accounts for the gain medium seeing no lasing field. The rate equations for the carrier densities in the two regions can be written as

$$\frac{\partial N_1(z,\tau)}{\partial \tau} = \frac{\alpha_{p1}(z,\tau)}{\hbar\,\omega_p \sigma} P_p(z,\tau+\Delta\tau) - \frac{g_1(z,\tau)}{\hbar\,\omega_0 \sigma}\left|A(z,\tau)\right|^2 - \frac{N_1(z,\tau)}{\tau_c} + \frac{N_2(z,\tau)-N_1(z,\tau)}{\tau_d} \tag{6.1a}$$

$$\frac{\partial N_2(z,\tau)}{\partial \tau} = \frac{\alpha_{p2}(z,\tau)}{\hbar\,\omega_p \sigma} P_p(z,\tau+\Delta\tau) - \frac{N_2(z,\tau)}{\tau_c} - \frac{N_2(z,\tau)-N_1(z,\tau)}{\tau_d} \tag{6.1b}$$

where $N_1(z, \tau)$ is the carrier density in the gain region seeing the lasing field, $N_2(z, \tau)$ is the carrier density in the gain region seeing no lasing field, $\alpha_{p1}(z, \tau)$ and $\alpha_{p2}(z, \tau)$ are the absorption coefficient to the pump at frequency ω_p in the two regions, respectively, $P_p(z, \tau + \Delta\tau)$ is the pump power, σ is the active cross sectional area, τ_c is the carrier lifetime, and ω_0 is the optical central frequency of the lasing field. $A(z,\tau)$ is the normalized lasing field so that $|A(z,\tau)|^2$ stands for the instantaneous laser power. τ_d stands for the effective carrier transport time from the dark field region to the bright field region in the gain medium. The gain coefficient is assumed to be linear with carrier density so that

$$g_1(z,\tau) = a\left[N_1(z,\tau) - N_0\right] \tag{6.2a}$$

where

$$a = \frac{dg(z,\tau)}{dN(z,\tau)} \tag{6.2b}$$

is the differential gain coefficient and N_0 is the carrier density value at transparency. Equations (6.1) can be rewritten as

$$\frac{\partial g_1(z,\tau)}{\partial \tau} = \frac{\alpha_{p1}(z,\tau)}{\gamma E_{psat}} P_p(z,\tau+\Delta\tau) - \frac{g_1(z,\tau)}{E_{sat}} \left|A(z,\tau)\right|^2 - \frac{g_1(z,\tau)}{\tau_c} - \frac{aN_0}{\tau_c} + \frac{g_2(z,\tau) - g_1(z,\tau)}{\tau_d} \tag{6.3a}$$

$$\frac{\partial g_2(z,\tau)}{\partial \tau} = \frac{\alpha_{p2}(z,\tau)}{\gamma E_{psat}} P_p(z,\tau+\Delta\tau) - \frac{g_2(z,\tau)}{\tau_c} - \frac{aN_0}{\tau_c} - \frac{g_2(z,\tau) - g_1(z,\tau)}{\tau_d} \tag{6.3b}$$

where the gain saturation energy at ω_0 and ω_p are respectively,

$$E_{sat} = \frac{h\,\omega_0 \sigma}{a} \tag{6.4a}$$

$$E_{psat} = \frac{h\,\omega_p \sigma}{b} \tag{6.4b}$$

The gain coefficient $g_2(z,\ \tau)$ is expressed by

$$g_2(z,\tau) = a\left[N_2(z,\tau) - N_0\right] \tag{6.5}$$

and γ is defined by

$$\gamma = b/a \tag{6.6}$$

The differential gain coefficient at the pumping frequency ω_p is

$$b = -\frac{d\alpha(z,\tau)}{dN(z,\tau)} \tag{6.7a}$$

and the absorption coefficient at frequency ω_p is

$$\alpha_p(z,\tau) = -b\left[N(z,\tau) - N_{p0}\right] \tag{6.7b}$$

where N_{p0} is the transparency carrier density value at ω_p. The equation for the pump $P_p(z, \tau + \Delta\tau)$ can be expressed by

$$\frac{\partial P_p(z,\tau+\Delta\tau)}{\partial z} = -\alpha_p(z,\tau)P_p(z,\tau+\Delta\tau) \tag{6.8}$$

Following Chapter 5, Equations (6.3a) and (6.3b) are integrated separately over length L, as shown by

$$\frac{dG_1(\tau)}{d\tau} = \frac{P_p(\tau+\Delta\tau)}{\gamma E_{psat}}\left\{-\exp\left[\gamma G_1(\tau) - b\left(N_{p0} - N_0\right)L\right]\right\} - \frac{P_{in}(\tau)}{E_{sat}}\left\{\exp\left[G_1(\tau)\right]-1\right\}$$

$$-\frac{G_1(\tau)}{\tau_c} - \frac{aN_0L}{\tau_c} + \frac{G_2(\tau)-G_1(\tau)}{\tau_d} \tag{6.9a}$$

$$\frac{dG_2(\tau)}{d\tau} = \frac{P_p(\tau+\Delta\tau)}{\gamma E_{psat}} \left\{ -\exp\left[\gamma G_2(\tau) - b\left(N_{p0} - N_0\right)L\right]\right\}$$

$$- \frac{G_2(\tau)}{\tau_c} - \frac{aN_0L}{\tau_c} - \frac{G_2(\tau) - G_1(\tau)}{\tau_d} \tag{6.9b}$$

where

$$G_1(\tau) = \int_0^L g_1(z,\tau)dz \tag{6.10a}$$

$$G_2(\tau) = \int_0^L g_2(z,\tau)dz \tag{6.10b}$$

and L is the length of the gain in the two regions, and $P_{in}(\tau)$ is the input laser power. The initial conditions to solve Equation (6.9) are

$$G_1(-\infty) = -aN_0L \tag{6.11a}$$

$$G_2(-\infty) = -aN_0L \tag{6.11b}$$

The fourth-order Runge-Kutta method is used to integrate Equation (6.9) and to obtain $G_1(\tau)$. The output laser power $P_{out}(\tau)$ and corresponding phase of the field $\phi_{out}(\tau)$ can be expressed by the input power $P_{in}(\tau)$ and phase $\phi_{in}(\tau)$ using $G_1(\tau)$ following Chapter 5, as shown by

$$P_{out}(\tau) = P_{in}(\tau)e^{G_1(\tau)} \tag{6.12a}$$

$$\phi_{out}(\tau) = \phi_{in}(\tau) - \frac{1}{2}\alpha G_1(\tau) \tag{6.12b}$$

The dispersion effect because of the finite gain shape has been discussed in Chapter 5, and the related equations are as follows,

$$\tilde{A}(L,\omega) = \tilde{A}(\omega)\exp\left[i\Phi(\omega)\right] \tag{6.13}$$

where

$$\tilde{A}(\omega) = \tilde{A}(0,\omega)\exp\left(\frac{\frac{1}{2}g_p L}{1+T_2^2(\omega-\omega_0)^2}\right) \tag{6.14a}$$

$$\Phi(\omega) = \frac{\frac{1}{2}g_p L T_2(\omega-\omega_0)}{1+T_2^2(\omega-\omega_0)^2} \tag{6.14b}$$

In Equation (6.14), T_2 is a bandwidth parameter and the peak gain g_p is expressed by

$$g_p = a\left(N_{p0} - N_0\right) \tag{6.15}$$

The laser pulse build-up in the cavity follows the route as shown in Figure 6.2. The laser pulse starts from a field $E_1(\tau)$. On the laser pulse traveling route, it is amplified by the gain medium and the relation between $E_2(\tau)$ and $E_1(\tau)$ is governed by Equation (6.12) in the form of the amplitudes and the phases. The linear loss comes from the output coupler and whatever optical components within the laser cavity. If the net intensity loss is Λ,

$$E_3(\tau) = \sqrt{1-\Lambda}E_2(\tau) \tag{6.16}$$

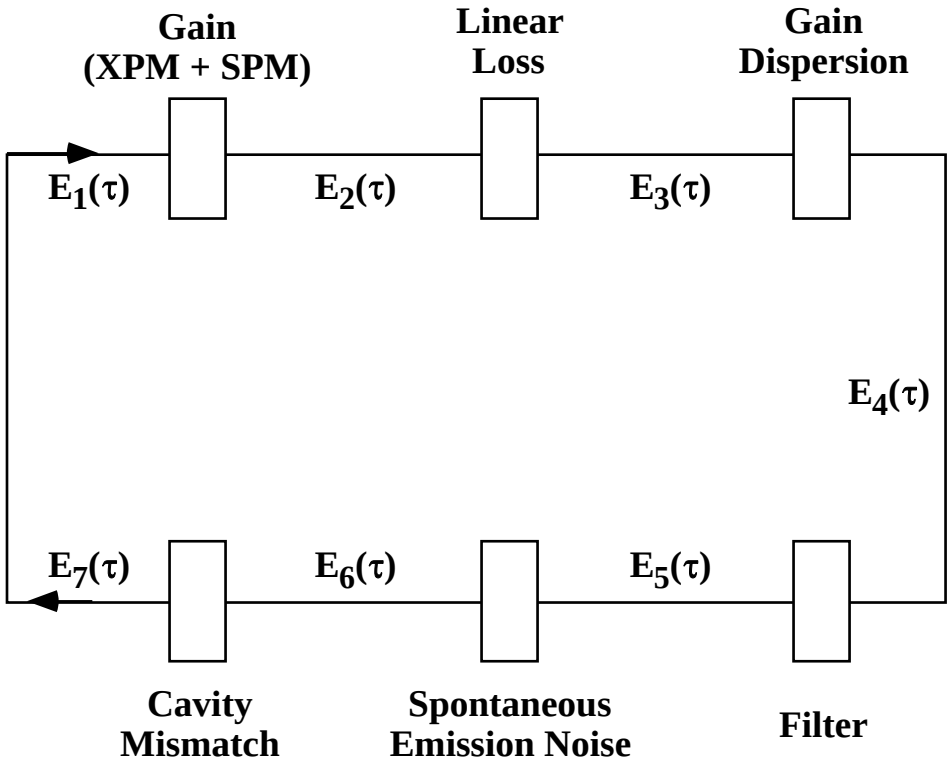

Figure 6.2 Laser pulse traveling route used in the pulse build-up modeling.

The gain dispersion is due to the finite gain bandwidth and the relation between $E_4(\tau)$ and $E_3(\tau)$ are governed by Equation (6.13) in the frequency domain. If there is any filter in the cavity, it can be expressed in the frequency domain by $\exp[-(\omega-\omega_{f0})^2/\Delta\omega_f^2]$ in terms of the intensity transmission so that

$$\tilde{E}_5(\omega) = \tilde{E}_4(\omega)\exp\left[-\left(\omega-\omega_{f0}\right)^2 \Big/ \left(2\Delta\omega_f^2\right)\right] \tag{6.17}$$

where ω_{f0} is the center frequency of the filter and $\Delta\omega_f$ is the filter bandwidth [4]. The influence of the filter on the pulse phase is neglected. Spontaneous emission noise usually exists among semiconductor lasers and is taken into account during the simulation [5]. The spontaneous noise can be obtained using a noise generator for the random phase generation, while the amplitude observes the Gaussian distribution with a bandwidth equal to the gain bandwidth in the frequency domain. $\tilde{E}_6(\omega)$ is obtained by adding this noise to $\tilde{E}_5(\omega)$. Finally, the VCSEL cavity and the pump laser cavity will not always match in length. The difference in cavity lengths will introduce a time-shift $\Delta\tau$ so that

$$E_7(\tau) = E_6(\tau - \Delta\tau) \tag{6.18}$$

where $\Delta\tau > 0$ if the VCSEL cavity is longer than the pump laser cavity. This concludes one of the many pulse round-trips within the laser cavity. The following round-trip will start with the output pulse $E_7(\tau)$ to replace the input $E_1(\tau)$ until a steady state is reached.

The mode-locked VCSEL starts initially from the spontaneous noise. It takes many round-trips for the noise signal to evolve into a laser pulse. If the change in the intensity in one round trip is small,

$$\sqrt{\left|\frac{\sum_j I_j^2(n+1) - \sum_j I_j^2(n)}{\sum_j I_j^2(n)}\right|} \le \delta \tag{6.19}$$

the mode-locked VCSEL is considered to have reached the steady state, where $I_j(n)$ is the laser pulse intensity at the j-th sampling point after the n-th round-trip in the cavity.

The required round-trips to reach the steady state depend on the choice of δ. For example, it may take around 350 round-trips to have a pulse to converge if δ is taken as 0.5%, but it will take around 2950 round-trips if δ is 0.1%. Even though Equation (6.19) is satisfied, the laser pulse may include fine structures that keep changing, as well as its phase. Since the experimentally measurable values are usually the intensity autocorrelation traces of laser pulses and the power spectrums that average over many pulses, only those autocorrelation traces and their power spectrums will be examined in the simulation to compare with the experiment. During the simulation, the pump pulse is 200 fs at a wavelength of 800 nm. The average pump power is 200 mW at 89 MHz. Other parameters used for the simulation can be found in Table 6.1. Both the intensity autocorrelation traces and the power spectrums of the pulses are obtained by averaging the corresponding pulses over the 1000-th to the 1500-th round-trips. The averaging corresponds to an integration time of 5.6 μs for a laser cavity of 89 MHz.

Although the model used for simulation is simplified, some featured predictions are verified in the experiment. Figure 6.3(a) shows the average autocorrelation traces at a carrier transport time τ_d of 4 ps for several different cavity mismatch time $\Delta\tau$. No intracavity filter is included during this simulation. Most of the pulse energy is contained in the side-lobes or pedestals if the pulsewidth is narrow. The problem is not so severe for a gain medium without the carrier transport, as shown by Figure 6.4(a) with a carrier transport time τ_d of infinite. Pulses are generally narrower in Figure 6.4(a) than in Figure 6.3(a). With the carrier transport effect, pulses are also noisier as shown by the corresponding power spectrums in Figure 6.3(b) than those pulses without the carrier transport, as shown by the corresponding power spectrums in Figure 6.4(b). Experiments using a periodic-gain structure in a mode-locked VCSEL have supported those predictions (Chapter 3).

Table 6.1 Parameters used for simulation

Pump pulse energy (nJ)	2.25
Pump pulsewidth (fs)	200
Pump wavelength (nm)	800
Central wavelength of gain (nm)	860
Effective length of gain medium (μm)	1.8
Diameter of active medium d (μm)	19
Transparent carrier density at ω_0 N_0 (cm^{-3})	6.97×10^{17}
Transparent carrier density at ω_p N_{p0} (cm^{-3})	1.98×10^{18}
Differential gain at ω_0 a (cm^2)	5.27×10^{-16}
Differential gain at ω_p b (cm^2)	3.57×10^{-15}
Differential gain ratio γ	6.77
Intraband relaxation time T_2 (ps)	0.1
Carrier life time τ_c (ns)	1
Linewidth enhancement factor α	5
Saturation energy E_{sat} (nJ)	1.24
Saturation energy E_{psat} (nJ)	0.20
Net cavity loss Λ	7%
Spontaneous emission energy (fJ)	50
Spontaneous emission bandwidth (s^{-1})	50×10^{12}

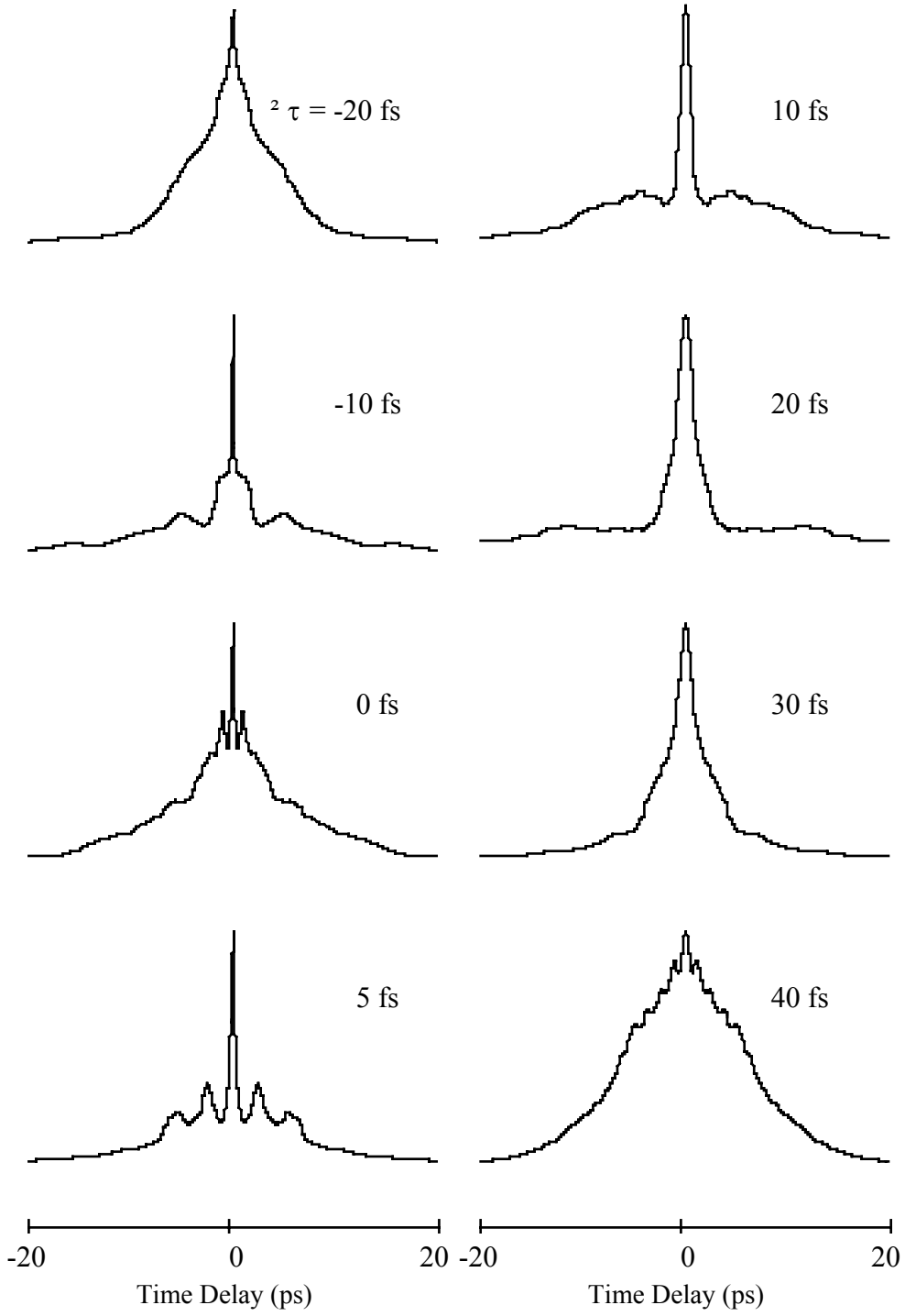

Figure 6.3(a) Average intensity autocorrelation traces of pulses from simulation at a carrier transport time of 4 ps for different cavity mismatch times $\Delta\tau$ and without any filter in the cavity.

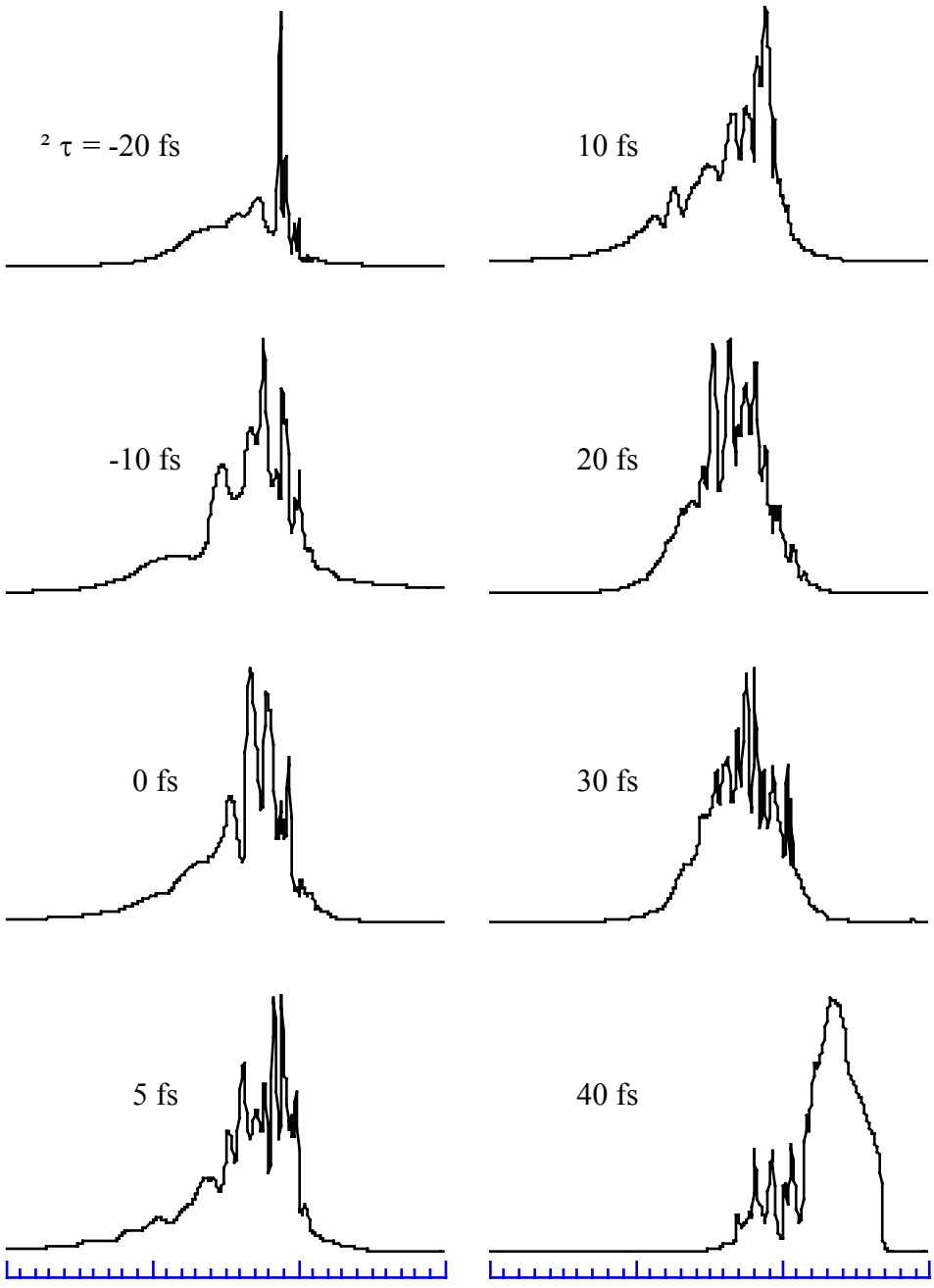

Figure 6.3(b) Average power spectrums of pulses from simulation at a carrier transport time of 4 ps for different cavity mismatch times $\Delta\tau$ and without any filter in the cavity.

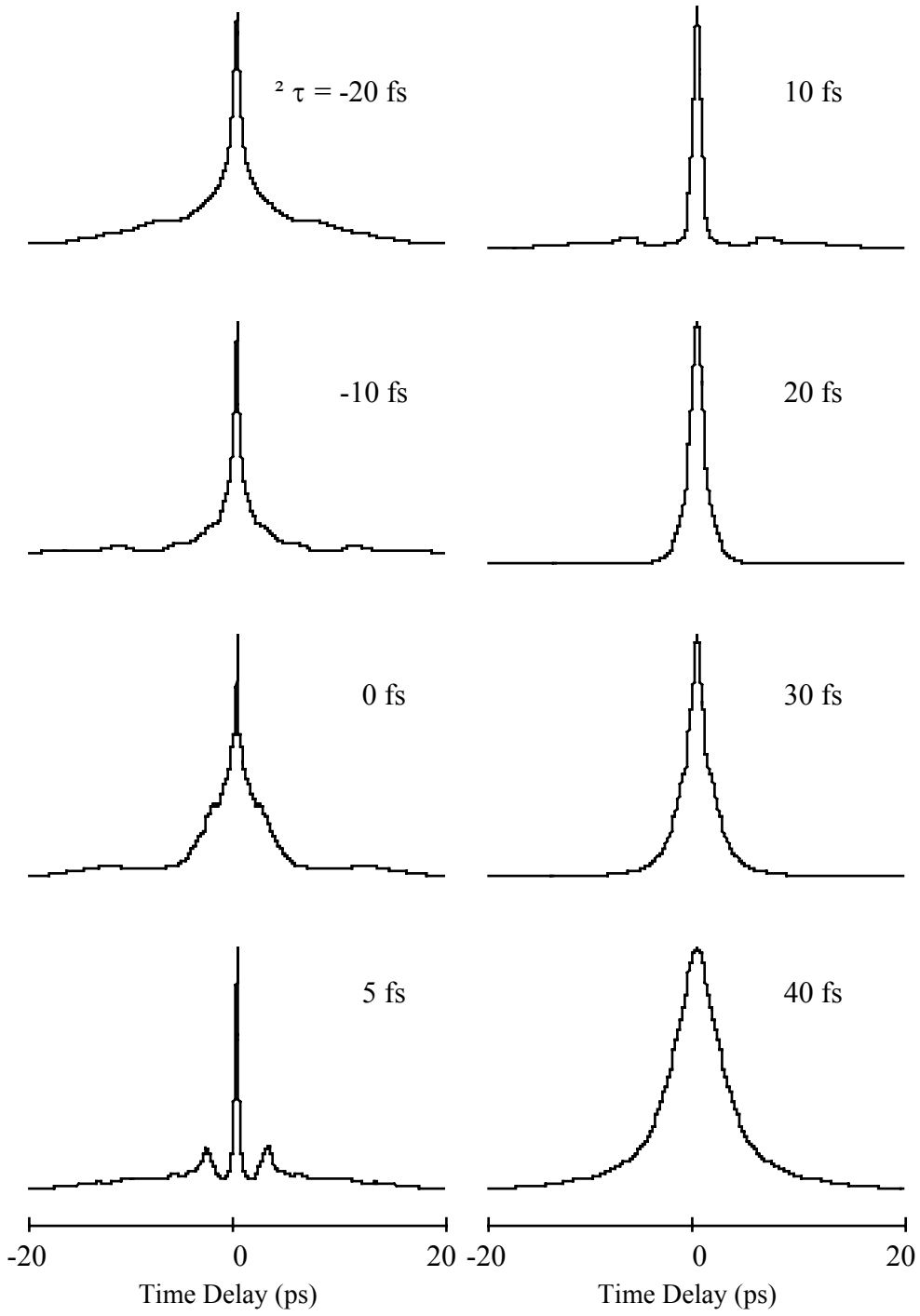

Figure 6.4(a) Average intensity autocorrelation traces of pulses obtained from simulation at an infinite carrier transport time for several different cavity mismatch times $\Delta\tau$ and without any filter in the cavity.

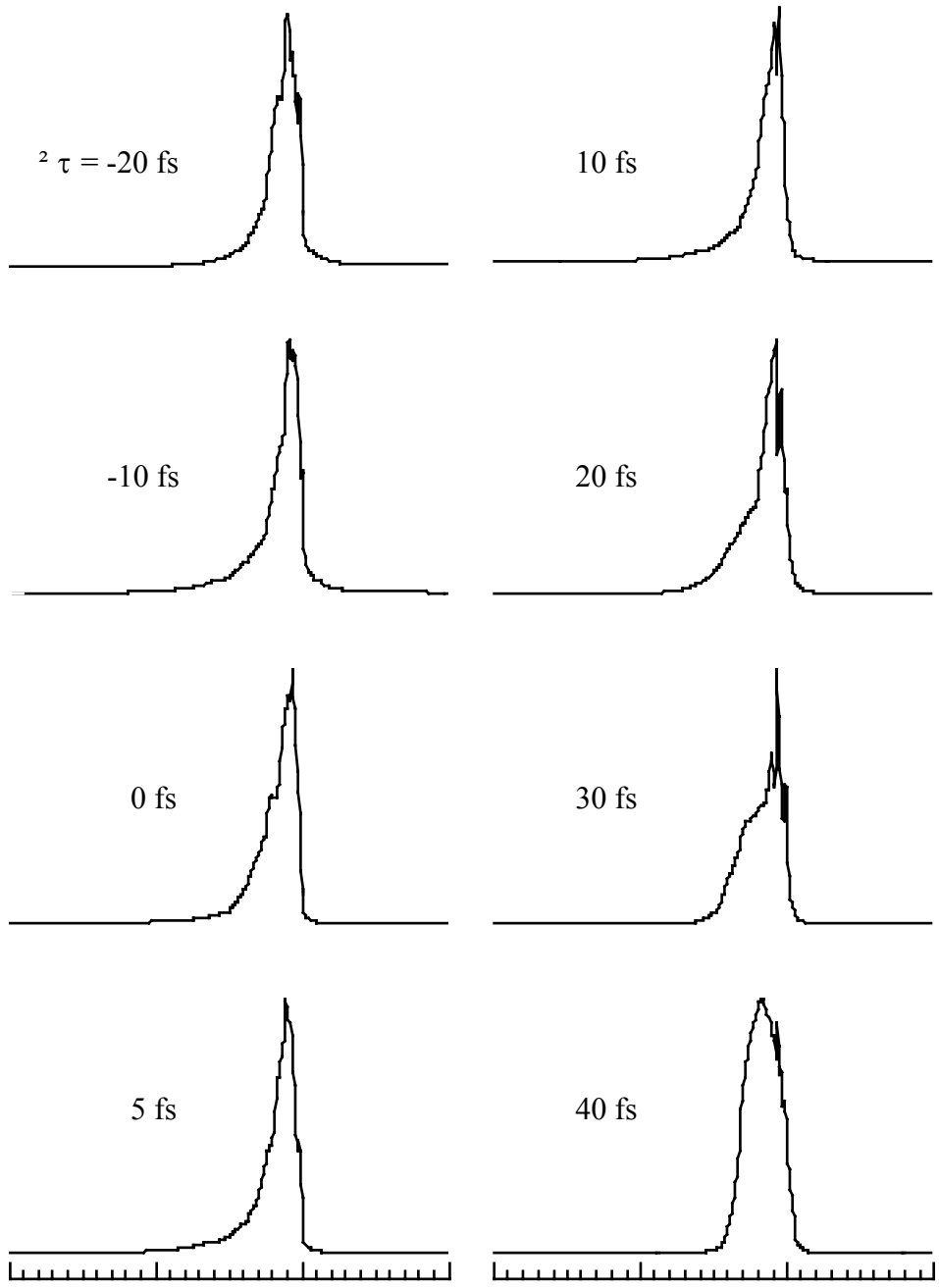

Figure 6.4(b) Average power spectrums of pulses from simulation at an infinite carrier transport time for different cavity mismatch times $\Delta\tau$ and without any filter in the cavity.

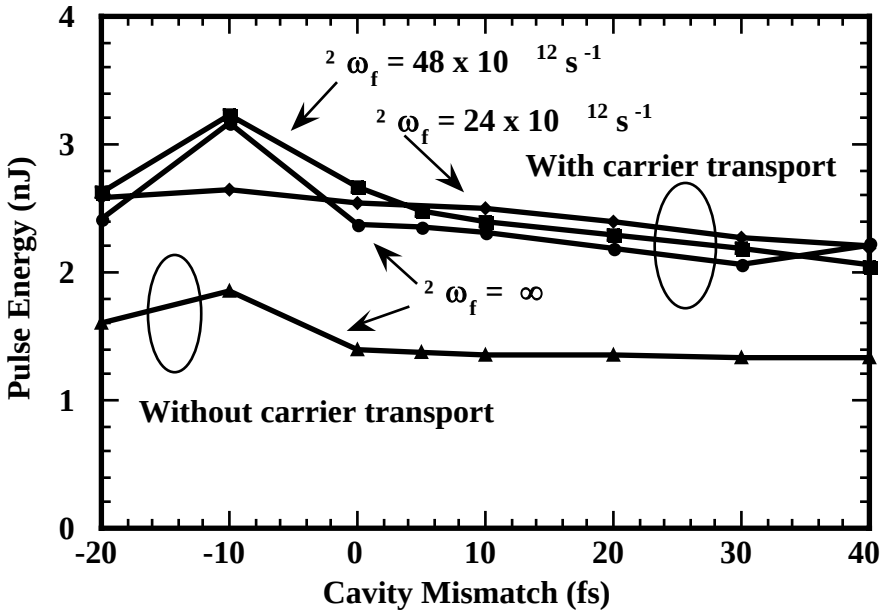

Figure 6.5 Pulse energy varying with cavity mismatch time from simulation for a gain with carrier transport and a gain without carrier transport. $\Delta\omega_f$ stands for the filter bandwidth.

The pulse energy is predicted larger for the case with the carrier transport than without the carrier transport (Figure 6.5). This is understandable as those carriers transported into the area seeing the strong lasing field will contribute to the gain. The maximum average output power in the experiment for the case with carrier transport is 13 mW (See Chapter 3), which converts to an intracavity pulse energy of 2.9 nJ for a cavity frequency of 89 MHz and an output coupler of 95% reflectivity. This pulse energy is consistent with the simulation in Figure 6.5. The maximum average output power in the experiment for the case without carrier transport is 6 mW (See Chapter 3), which converts to an intracavity pulse energy of 2.2 nJ for a cavity frequency of 89 MHz and an output coupler of 97% reflectivity. The pulse energy of 2.2 nJ is slightly lager than the predicted value in Figure 6.5, partly due to the residual carrier transport

since the periodic gain structure is not perfect in completely eliminating the carrier transport effect. Lateral carrier transport also contributes to the higher pulse energy. It should be noted that bulk material is used for the periodic gain structure in the experiment instead of the MQW. A bulk semiconductor gain medium has a smaller differential gain, and thus a larger gain saturation energy, which allows larger pulse energy in the experiment.

To examine how effective the model is in simulating the laser pulse formation, it is necessary to examine if the experimental results can be reproduced using the model. The comparison of the intensity autocorrelations of pulses between the experiment and the simulation is a straightforward approach. The mode-locked laser with a MQW gain medium when pumped by 200 fs pulses from a Ti: sapphire laser is very unstable during the experiment, as demonstrated in Chapter 3. This is also demonstrated in the simulation, as shown by the spectrums in Figure 6.3(b). No extensive data are therefore available for comparison in this case. The laser becomes, however, stable when a birefringent filter with a thickness of 0.5 mm is mounted into the laser cavity to replace a Brewster-angle-placed glass plate. A series of intensity autocorrelation traces of pulses are obtained by varying the laser cavity length and by rotating the filter, as shown by the solid curves in Figure 6.6. Those curves are reproducible in simulation with the filter included. The 0.5 mm filter corresponds to a filter bandwidth $\Delta\omega_f$ of about 48 x 10^{12} s^{-1}. The central frequency of the filter can be tuned around the gain peak. To reduce the computing time, only cases involving the filter central frequency of 0 and $\pm$ 10 x 10^{12} s^{-1} away from the gain peak are simulated. Those results are shown by the dashed lines in Figure 6.6. In the simulation, every 10 fs cavity mismatch time corresponds to a cavity mismatch length of 1.5 μm. The central frequency of the filter is tuned 10 x 10^{12} s^{-1} larger than the gain peak in Figure 6.6(a). In Figure 6.6(b), the central frequency of the filter is aligned to the gain peak, and the

central frequency of the filter is 10×10^{12} s^{-1} smaller than the gain peak in Figure 6.6(c). The results from the simulation fit very well with the experiment in terms of the pulsewidth. The difference in the details of the pulse substructure is also within the acceptable range. Better fitting can be expected if finer filter tuning is used in simulation.

It has to be pointed out that the model used for the simulation has neglected any effects of two-photon absorption, spectral hole burning and carrier heating. The time constant for those effects is typically within 300 fs. Those effects must be taken into account to more precisely predict the laser pulse behavior [6] when the laser pulsewidth falls into that regime. Namely, the model discussed in this Chapter remains to be improved to fully reproduce the experimental results when using the periodic-gain structure in the mode-locked VCSEL to generate pulses with the pulsewidth of shorter than 300 fs.

In conclusion, carrier transport effects have been included in simulating the laser pulse formation in an optically pumped mode-locked VCSEL. The multiple-pulse structures and the strong pedestals shown in the pulses from the mode-locked VCSELs are attributed to the existence of the carrier transport. Shorter and cleaner pulses can be generated by decreasing those carrier transport effect. Pulse energy is accordingly decreased, as well. The experimental results using a MQW gain in the mode-locked VCSEL are reproducible using the simulation model discussed in this chapter.

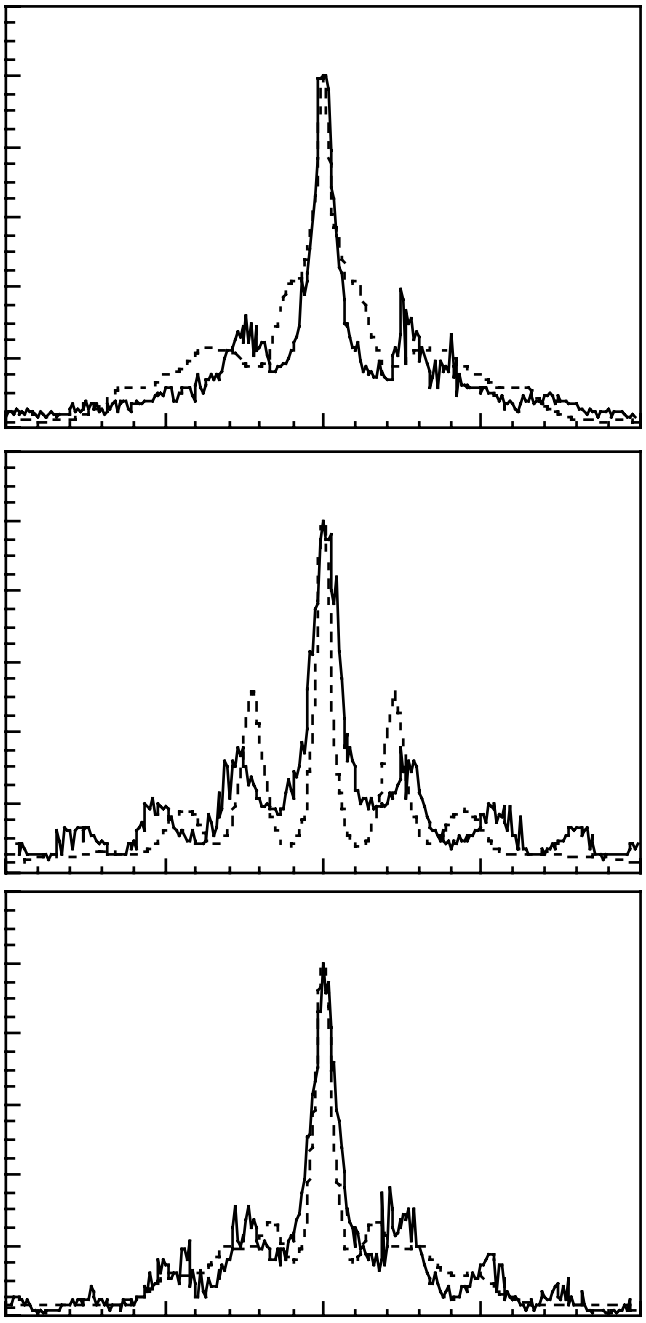

Figure 6.6(a) Intensity autocorrelation traces of pulses measured in the experiment (solid lines) and reproduced in the simulation using a filter of a bandwidth of 48 x 10^{12} s^{-1} and a central frequency of 10 x 10^{12} s^{-1} larger than the gain peak (dashed lines).

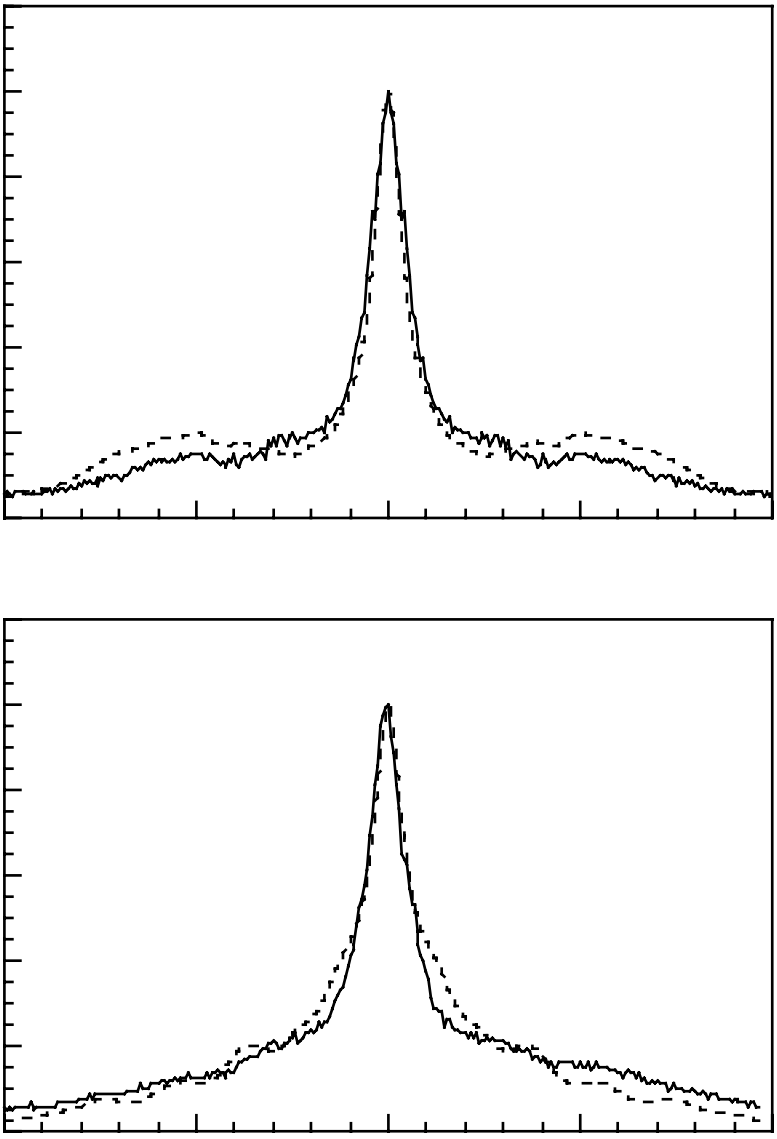

Figure 6.6(b) Intensity autocorrelation traces of pulses measured in the experiment (solid lines) and reproduced in the simulation using a filter of a bandwidth of 48 x 10^{12} s^{-1} and a central frequency aligned with the gain peak (dashed lines).

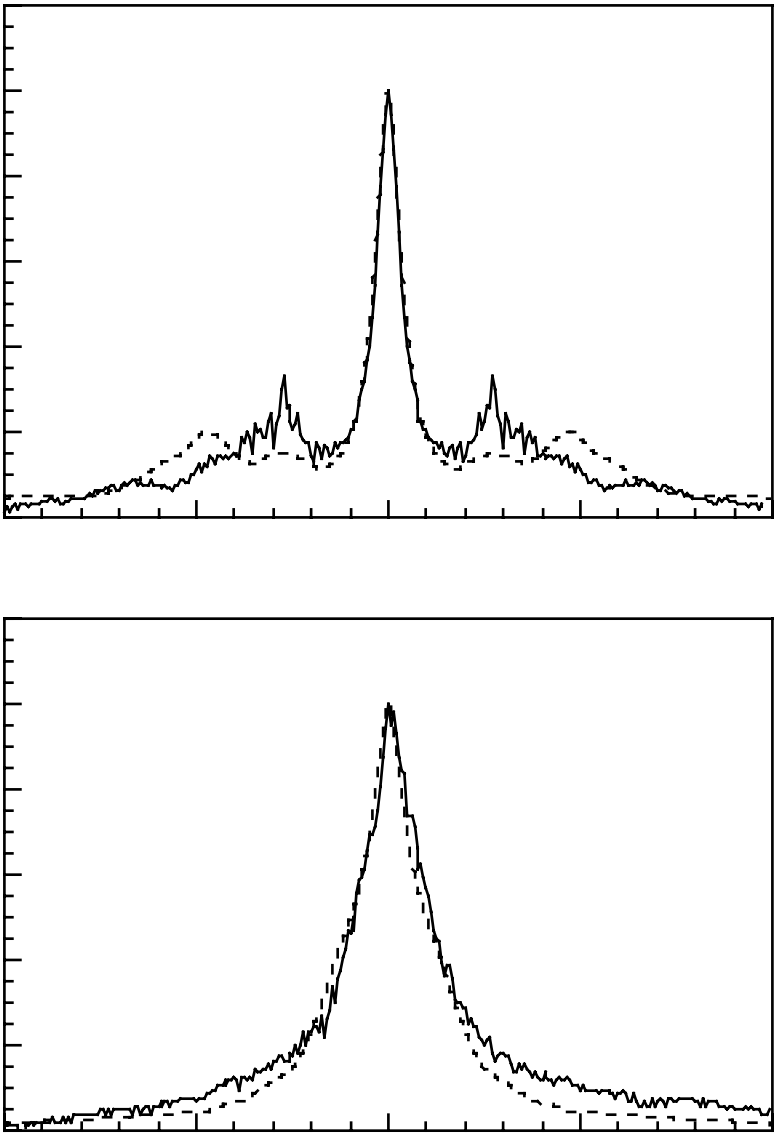

Figure 6.6(c) Intensity autocorrelation traces of pulses measured in the experiment (solid lines) and reproduced in the simulation using a filter of a bandwidth of 48 x 10^{12} s^{-1} and a central frequency of 10 x 10^{12} s^{-1} smaller than the gain peak (dashed lines).

References

[1] W. H. Xiang, S. R. Friberg, K. Watanabe, S. Machida, Y. Sakai, H. Iwamura, and Y. Yamamoto, "Sub-100 femtosecond pulses from an external-cavity surface-emitting InGaAs/InP multiple quantum well laser with soliton-effect compression," *Appl. Phys. Lett.*, **59**, 2076 (1991)

[2] D. C. Sun and Y. Yamamoto, "Passive stabilization of a synchronously pumped external-cavity surface-emitting InGaAs/InP multiple quantum well laser by a coherent photon-seeding technique," *Appl. Phys. Lett.*, **60**, 1286 (1992)

[3] K. Watanabe, H. Iwamura, and Y. Yamamoto, "The effect of an additive pulse mode-locking on an external-cavity surface-emitting InGaAs semiconductor laser," *Opt. Lett.*, **18**, Oct., (1993)

[4] D. M. Kim, J. Kuhl, R. Lambrich, and D. von der Linde, "Characteristics of picosecond pulses generated from synchronously pumped CW dye laser system," *Opt. Comm.*, **27**, 123 (1978)

[5] T. Urisu, and Y. Mizushima, "Transient pulse buildup mechanisms in a synchronously-pumped mode-locked dye laser," *J. Appl. Phys.*, **57**, 1518 (1985)

[6] A. Dienes, J. P. Heritage, M. Y. Hong, Y. H. Chang, "Time-domain and spectral-domain evolution of subpicosecond pulses in semiconductor optical amplifiers," *Opt. Lett.*, **17**, 1602 (1992)

Chapter 7 Conclusion and Prospects

Vertical cavity surface emitting semiconductor lasers have been mode-locked using synchronous optical pumping. A GaAs/AlGaAs MQW surface emitting laser is mode-locked to generate 10 ps pulses at room temperature when pumped by a mode-locked dye laser. Pulses generated from the mode-locked VCSEL are severely chirped due to the XPM caused by pulsed optical pumping and the SPM caused by the gain saturation. After the chirp compensation using a grating-pair-telescope configuration outside of the laser cavity, the pulsewidth is reduced to 320 fs at a peak power of 64 W. An intracavity birefringent filter is effective in limiting the time-bandwidth product of the pulses directly from the laser oscillator. When the laser with the MQW gain is pumped by a mode-locked Ti: sapphire laser, the output pulsewidth is reduced to around 1 ps. Carrier transport is responsible in preventing shorter pulse generation from the mode-locked VCSEL. A periodic gain structure is used to eliminate the source of carrier transport, so that pulses with the intensity autocorrelation width of 300 fs (FWHM) are generated directly from the VCSEL oscillator. This represents the shortest pulsewidth directly generated from any semiconductor lasers. Passive mode-locking techniques will be necessary if further shorter pulses are desired from the semiconductor laser.

A vertical cavity surface emitting laser with InGaAs/InP MQW gain is mode-locked at 77 K when synchronously pumped by a mode-locked 1.32 μm YAG laser. The output laser pulsewidth is around 10 ps before chirp compensation with the compressed pulse pumping. After chirp compensation outside of the laser cavity, the pulsewidth is again reduced to around 1 ps. Best results have been reported with a pulsewidth of 150 fs at a peak power over 3 kW after one stage chirp compensation. The second

stage pulse compression reduces the pulsewidth to 21 fs.

The results from the mode-locked VCSELs have clearly demonstrated that the surface emitting lasers can be mode-locked to generate picosecond or even subpicosecond pulses at much higher output power than that of edge emitting in-plane semiconductor lasers. Another advantage is the good laser beam quality from the VCSELs.

Several techniques have been used to improve the VCSEL mode-locking, such as the coherent photon seeding [1] and APM [2]. A bulk GaAs external cavity surface emitting laser pumped by a Kr^+ laser has generated over 700 mW CW power at 77 K [3], highest ever reported from any SELs. Questions remain, however, that which mode-locking technique is the most appropriate for the VCSELs.

An optically pumped mode-locked VCSEL works fine as a lab tool, but is not very cost effective compared to an electrically pumped in-plane semiconductor laser. It is possible that a future mode-locked VCSEL will be pumped by an arrayed edge emitting diode laser. The laser will then be passively mode-locked with a semiconductor saturable absorber. In some sense, a mode-locked VCSEL will work like a coherent beam converter that converts a transverse-mode-uncorrelated laser beam from the arrayed laser into a correlated beam. Since semiconductor materials can be tailored to satisfy different wavelength requirements, the mode-locking method will be an efficient way to build a compact short pulse source for various applications.

One of the advantages of semiconductor lasers is the capability of being electrically pumped. An electrically pumped external cavity bulk GaAs surface-emitting laser is mode-locked at 0.96 GHz when operating at liquid N_2 temperature. The measurement shows a pulsewidth of 80 ps when measured with a synchronous-scan streak camera. The intrinsic pulsewidth should be shorter if timing jitter between pulses can be eliminated during the measurement.

More work remains in improving the electrically pumped mode-locked device operation. First, better heat dissipation is necessary to have the mode-locked VCSEL operating at room temperature. A possible technique is to mount the device p-side down onto a diamond heat sink. This requires a good p-DBR mirror with a low series resistance. Successful work has been demonstrated in reducing the series resistance of p-DBR mirror [4]. A p-side down broad area monolithic SEL has been shown to generate 120 mW average power [5], and the device with wall-plug efficiency of 15% has been demonstrated [4].

Second, the doping of active area should be optimized. The current device has an n-doped active layer (2×10^{17} cm^{-3}). Other work on monolithic SELs suggests that slightly p-doped active layer has more advantage over n-doped active layer. Further work remains to compare the different doping to justify the choice. The active thickness also needs to be optimized. The current device has an active thickness of 1 μm. Devices with thinner active layer will probably perform better (Figure 4.1.1).

Third, the maximum possible external quantum efficiency for this device is 50% due to the ring p-metal contact. To improve the device efficiency, some improvement to the device design is necessary. A possible approach is to regrow a p-n structure on top of the etched blocking area to replace the SiO_2, such that the blocking area has a thyrister structure of p-n-p-n, while maintaining a p-i-n structure in the mesa area. The p-metal contact will be on the regrown p layer. Such an approach is not necessary for a p-side down device, where etching has to be used to form a well in the substrate to couple the light out since the GaAs substrate is absorptive to the output light. Etching is not needed if the active layer is an InGaAsP layer grown on an InP substrate.

Finally, an appropriate mode-locking scheme is necessary to generate the shortest possible pulses from an electrically pumped mode-locked VCSEL. Active modulation is generally the easiest way, but not the most efficient way. Passive mode-locking,

either through the use of a saturable absorber, or a nonlinear auxiliary cavity (such as APM), or the use of other nonlinear element in the cavity, may generate shorter pulses. Extensive investigation is needed to bring the electrically pumped mode-locked VCSEL to the same performance level as that of an optically pumped mode-locked VCSEL. The ultimate goal is an electrically pumped CW mode-locked VCSEL with subpicosecond pulses and high peak powers.

In conclusion, the advantages of mode-locked VCSELs have been demonstrated. The future looks promising.

Reference

[1] D. C. Sun and Y. Yamamoto, "Passive stabilization of a synchronously pumped external-cavity surface-emitting InGaAs/InP multiple quantum well laser by a coherent photon-seeding technique," *Appl. Phys. Lett.*, Vol. 60, 1286 (1992)

[2] K. Watanabe, H. Iwamura, and Y. Yamamoto, "The effect of an additive pulse mode-locking on an external-cavity surface-emitting InGaAs semiconductor laser," *Opt. Lett.*, **18**, Oct. (1993)

[3] D. C. Sun, S. R. Friberg, K. Watanabe, S. Machida, Y. Horikoshi, and Y. Yamamoto, "High power and high efficiency vertical cavity surface emitting GaAs laser," *Appl. Phys. Lett.*, **61**, 1502 (1992)

[4] M. G. Peters, F. H. Peters, D. B. Young, J. W. Scott, B. J. Thibeault, and L. A. Coldren, "High wallplug efficiency vertical-cavity surface-emitting lasers using lower barrier DBR mirrors," *Electron. Lett.*, **29**, 170 (1993)

[5] F. H. Peters, M. G. Peters, D. B. Young, J. W. Scott, B. J. Thibeault, S. W. Corzine, and L. A. Coldren, "High-power vertical-cavity surface-emitting lasers," *Electron. Lett.*, **29**, 200 (1993)

Appendix I Comparison on Gain Expressions

Agrawal's expressions on absorption coefficient α and spontaneous emission rate R_{sp} for the MQW structure are as follows [1],

$$\alpha(E) = \frac{e^2 m_r |M_b|^2}{\varepsilon_0 m_0^2 c h \overline{n} E L_w} \left[1 - f_c(E_c) - f_v(E_v)\right] \tag{A.1.1}$$

$$R_{sp} = \frac{16\pi^2 \overline{n} e^2 m_r |M_b|^2}{m_0^2 \varepsilon_0 h^4 c^3 L_w} \int_{E_q}^{\infty} E f_c(E_c) f_v(E_v) dE \tag{A.1.2}$$

where

$$E_c = \frac{m_r}{m_c}(E - E_q) \qquad E_v = \frac{m_r}{m_v}(E - E_q)$$

$$m_r = \frac{m_c m_v}{m_c + m_v}$$

E_q is the separation between the levels in the conduction band and in the valence band, f_c and f_v denote the Fermi factors for the electron at energy E_c and the hole at energy E_v, m_c and m_v are the effective mass of an electron and the effective mass of a hole respectively. The matrix element in the equation is given by

$$|M_b|^2 = \frac{m_0(E_g + \Delta)}{12 m_c (E_g + 2\Delta/3)} m_0 E_g = \xi m_0 E_g \tag{A.1.3}$$

where m_0 is the free-electron mass, E_g is the band gap, and Δ is the spin-orbit splitting. ξ lies between 1 and 2 for most semiconductors. The uncertainty in the value of ξ

represents the accuracy of the results. E in Equation (A.1.1) denotes the photon energy. If E is the VCSEL photon energy, $-\alpha(E)$ will be the gain $g(N)$, where the carrier density variable N is implicitly included in the Fermi function f_c and f_v since the quasi-Fermi energies of both electrons and holes vary with carrier density N. If E is the pump photon energy, the summation of $\alpha(E)$ over all possible transitions between the various subbands in the conduction and valence bands will be the absorption to the pump $\alpha(N)$. A complete expression of radiative recombination rate should also include summation over all possible transitions between the various subbands in the conduction and valence bands, but the transition from the lowest level in the conduction band (level 1c) to the lowest level in the heavy-hole band (level 1hh) has the most contribution to the spontaneous emission rate $R_{sp}(N)$.

Now take a look at Corzine's expressions to gain g and spontaneous emission rate R_{sp} [2],

$$g(\hbar\omega) = \left(\frac{1}{\hbar\omega}\right)\frac{\pi e^2 \hbar}{\varepsilon_0 c m_0^2}\frac{\overline{n}_g}{\overline{n}^2}\left|M_T\right|^2 \rho_{red}\left(E_{eh} - E_g'\right)\left(f_c - f_v\right) \tag{A.1.4}$$

$$R_{sp}(\hbar\omega) = \int_{\hbar\omega}^{\infty}\left(\frac{1}{\hbar\omega}\right)\frac{\pi e^2 \hbar}{\overline{n}^2 \varepsilon_0 m_0^2}\left|M_{ave}\right|^2 \rho_{red}\left(E_{eh} - E_g'\right)\rho_{opt}(\hbar\omega)\cdot f_c(1-f_v)\; d(\hbar\omega) \tag{A.1.5}$$

where M_T is the matrix element, and

$$\rho_{red}\left(E_{eh} - E_g'\right) = \frac{m_r}{2\pi\hbar^2}\left(\frac{1}{L_w}\right)$$

$$\left|M_{ave}\right|^2 \equiv \frac{1}{3}\sum_{\substack{all\ three \\ polarization}}\left|M_T\right|^2$$

$$\rho_{opt}(\hbar\omega) = \frac{1}{\pi^2}\frac{\bar{n}^2 \bar{n}_g'}{(\hbar c)^3}(\hbar\omega)^2$$

If the notation difference for Fermi functions f_c and f_v is discounted, and all the indices $\bar{n}$, $\bar{n}_g$ and $\bar{n}_g'$ are assumed to be equal, Agrawal's expressions and Corzine's expressions are the same except that the matrix elements $|M_b|^2$ in the former case are replaced by $|M_T|^2/2$ for the gain expression and $|M_{ave}|^2/2$ for the spontaneous emission in the later case. The difference of this 2 in the denominator is from the fact that the spin contribution is not included in the gain and spontaneous emission rate expressions, but counted in the matrix element calculation in the later case. The important difference between Agrawal's and Corzine's expressions lies in the choice of matrix element value.

Agrawal's expressions to the absorption coefficient $\alpha(E)$ and spontaneous emission rate R_{sp} for bulk semiconductor materials are [1]

$$\alpha(E) = \frac{e^2 h|M_b|^2}{4\pi^2 \varepsilon_0 m_0^2 c\bar{n}E}\left(\frac{2m_r}{\hbar^2}\right)^{3/2}(E-E_g)^{1/2}\left[1-f_c(E_c)-f_v(E_v)\right] \qquad \text{(A.1.6)}$$

$$R_{sp} = \frac{2\bar{n}e^2 E|M_b|^2}{\pi m_0^2 \varepsilon_0 h^2 c^3}\left(\frac{2m_r}{\hbar^2}\right)^{3/2}\int_{E_g}^{\infty}(E-E_g)^{1/2} f_c(E_c) f_v(E_v) dE \qquad \text{(A.1.7)}$$

where E is the photon energy, $|M_b|^2$ is the matrix element as shown by Eq. (A.1.3), and

$$E_c = \frac{m_r}{m_c}(E-E_g)$$

$$E_v = \frac{m_r}{m_v}(E-E_g)$$

$$m_r = \frac{m_c m_v}{m_c + m_v}$$

m_v is the effective hole mass with $m_v = m_{hh}$ for heavy hole and $m_v = m_{lh}$ for light hole.

The gain $g(N)$ is the addition of $\alpha(E)$ over both heavy-hole to electron and light-hole to electron transitions and expressed by

$$g(N) = -\sum_{i=hh,lh} \alpha(E)\big|_i \qquad \text{(A.1.8)}$$

Similarly, the spontaneous emission $R_{sp}(N)$ is the addition of R_{sp} over both heavy-hole to electron and light-hole to electron transitions and expressed by

$$R_{sp}(N) = \sum_{i=hh,lh} R_{sp}\big|_i \qquad \text{(A.1.9)}$$

Corzine's expressions can be obtained again by replacing the matrix element $|M_b|^2$ in Eq. (2.4.1) with $|M_T|^2/2$ and in Eq. (2.4.2) with $|M_{ave}|^2/2$. The difference of this 2 in the denominator comes from the fact that the spin is not included until the consideration of the matrix element in Corzine's expressions.

References

[1] G. P. Agrawal, and N. K. Dutta, "*Long wavelength semiconductor lasers*," (Van Nostrand Reinhold, New York, 1986)

[2] S. W. Corzine, "Design of vertical-cavity surface-emitting lasers with strained and unstrained quantum well active regions," (Ph.D dissertation, ECE Technical Report #93-09, UCSB, 1993)

Appendix II Wet Etching for DBR Mirror Characterization

To measure the reflectivity of the monolithically grown DBR mirror, it is necessary to remove the p-cladding layer and the active layer using wet etching. The etching procedures are as follows:

1. Take a piece of MBE grown wafer and have it cleaned through acetone, isopropanol, methanol and DI water. Blow dry.

2. Dip the sample into H_2SO_4:H_2O_2:H_2O = 1:1:20 mixture solution. Carefully watch the wafer color changing from silver -> black, or sometimes other colors like green, yellow, or brown -> silver. Stop etching and rinse with DI water as soon as the color is back to silver. Blow dry. It takes 2 - 3 minutes for this process. At this moment, the p-cladding is all removed. What's left is the active GaAs layer.

3. This step is to remove the GaAs active layer. Selective wet etching is used that will stop at AlGaAs with Al concentration over 30%. Dip the sample into NH_4OH:H_2O_2 = 1:20 mixture solution at 40 ˚C. Watch for the wafer color changing. As soon as the color becomes uniformly green or brown, stop etching and rinse with DI water. Blow dry. It usually takes less than 1 minute for this process.

4. The color will sometimes turn into black after blow drying because of the Al oxidization. Dip the wafer into buffered HF for 30 seconds to remove the oxidized Al, and rinse with DI water. Blow dry. This step is not necessary if the wafer is not oxidized after the third step.

5. The wafer is now ready for reflectivity measurement using the Lamda-9 Spectrometer.

Appendix III Metal Lift-off Technique for TLM Test Pattern Fabrication

The metal lift-off technique is used to fabricate TLM pattern on the test wafer as follows for the contact resistance characterization:

1. Take a piece of MBE grown wafer and have it cleaned through acetone, isopropanol, methanol and DI water. Blow dry, and bake the cleaned wafer for 5 minutes at 120 ˚C.

2. One drop of HMDS onto the wafer and spin the wafer for 10 seconds. Spin the photoresist AZ4110 onto the wafer at 6K per minute for 30 seconds.

3. Bake the wafer covered with photoresist on a hot plate at 95 ˚C for 1 minute.

4. With a TLM pattern mask, expose the wafer for 8 seconds.

5. Dip the wafer in toluene for 5 minutes. This is important to ensure a successful lift-off. Develop the wafer in a AZ400K:H_2O = 1:4 solution for 45 seconds. Rinse with DI water after developing. Blow dry.

6. Dip the wafer into NH_4OH:H_2O = 1:10 (or HCl:H_2O = 1:10) solution for 20 seconds right before loading the sample into a thermal evaporator for p-metal evaporation. The purpose of this step is to remove the oxidized stuff on the wafer surface that might hurt to form a good contact. Rinse with DI water and blow dry.

7. Thermal evaporating Cr/AuZn (with 5% Zn)/Cr/Au = 30 Å/500Å/200Å/2000Å onto the wafer.

8. Metal lift-off in acetone, and clean the wafer with acetone -> isopropanol -> methanol -> DI water. Blow dry.

9. Cleave the wafer into several pieces for annealing under different conditions.

After the annealing, the samples are ready for the resistivity measurement using the four-probe method.

Appendix IV VCSEL Device Fabrication Procedure

The standard device processing steps are listed below with the corresponding sketches.

1. Clean the wafer with TCE -> acetone -> isopropanol -> methanol -> DI water. Blow dry and bake for 5 minutes at 120 ˚C [Figure A.4.1(a)].

2. Closed ampule Zn-diffusion with ZnAs source of 20 - 30 mg at 620 ˚C for 5 minutes. After diffusion, rapidly cool down the whole ampule to avoid the As deposition on the wafer surface.

3. Repeat Step 1.

4. Spin HMDS onto the wafer for 10 seconds. Spin photoresist AZ 4110 onto the wafer at 6K for 30 seconds [Figure A.4.1 (b)]. The photoresist thickness is around 1 μm.

5. Bake the wafer covered with photoresist on a hot plate at 95 ˚C for 1 minute.

6. Expose the wafer for 8 seconds with a bright field mask of 20 μm diameter circles spaced by 1 mm between the neighbors.

7. Develop with AZ 400 K: DI water = 1:4 for 40 seconds. Rinse thoroughly. A photoresist mask of 20 μm diameter is formed for the following wet-etching [Figure A.4.1 (c)].

8. O_2 plasma for 2 minutes to descum the photoresist.

9. H_2SO_4:H_2O_2:H_2O = 1:1:20 mixture solution wet-etching for 1 minute and 25 seconds. The mesa height is about 1.2 μm [Figure A.4.1 (d)].

10. Remove the photoresist mask on the top of the mesa [Figure A.4.1 (e)].

11. Deposit 3000 Å SiO_2 using PECVD. Test sample shows that the actual thickness is about 2500 Å with an index of 1.39 [Figure A.4.1 (f)].

12. Photolithography (Steps 3 - 8) to form 20 μm diameter dark field circle mask on the mesa top [Figure A.4.1 (g)].

13. Buffered HF to etch the SiO_2 on the mesa top. The undesired under cutting happens during the etching. It won't affect the following ring metal contact because it is difficult to have a good metal contact on the under-cutting area that is $Al_{0.3}Ga_{0.7}As$ with relatively low p-doping [Figure A.4.1 (h)].

14. Remove the photoresist [Figure A.4.1 (i)] in acetone.

15. Photolithography (Steps 3 - 6) to form a ring p-metal contact with the opening window diameter of 15 μm.

16. Dip the wafer in toluene for 5 minutes and then develop the wafer in a AZ400K:H_2O = 1:4 solution for 45 seconds. Rinse with DI water after developing. Blow dry [Figure A.4.1 (j)].

17. O_2 plasma for 1 minutes to descum the photoresist.

18. Dip the wafer into NH_4OH:H_2O = 1:10 solution for 20 seconds right before loading the sample into a thermal evaporator for p-metal evaporation. The purpose of this step is to remove the oxidized stuff on the wafer surface that might hurt the contact. Blow dry.

19. Thermal evaporating Cr/AuZn (with 5% Zn)/Cr/Au = 30 Å/500Å/200Å/2000Å onto the wafer for p-metal contact [Figure A.4.1 (k)].

20. Metal lift-off in acetone, and clean the wafer with acetone -> isopropanol -> methanol -> DI water. Blow dry [Figure A.4.1 (l)].

21. Annealing the p-metal contact at 400 ˚C for 30 seconds with N_2 as forming gas in the rapid thermal annealer (RTA).

22. Lapping the substrate to 125 μm.

23. E-beam evaporator to deposit Ni/AuGe/Ni/Au = 50 Å/1000 Å/150 Å/1500 Å on the n-GaAs substrate side for n-metal contact [Figure A.4.1 (m)].

24. Annealing the n-metal contact at 380 ˚C for 30 seconds with N_2 as forming gas in the RTA.

25. SiN_xO_y AR-coating with sputtering machine on the p-side [Figure A.4.1 (n)].

26. Cleave the wafer.

27. Wire bonding.

Usually it is not necessary to remove the AR-coating on the contact metal after Step 25 because the AR-coating is thin enough for the Au wire to penetrate the coating during the wire bonding.

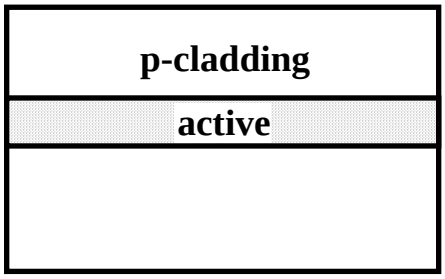

(a)

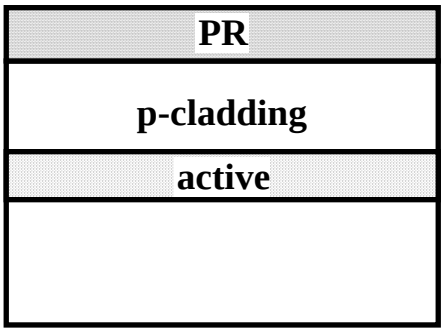

(b)

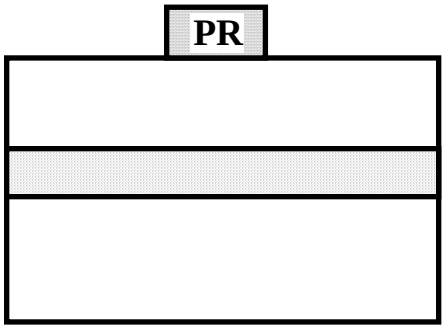

(c)

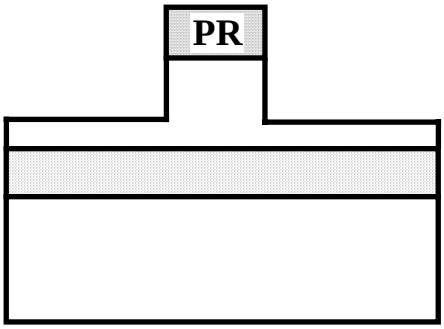

(d)

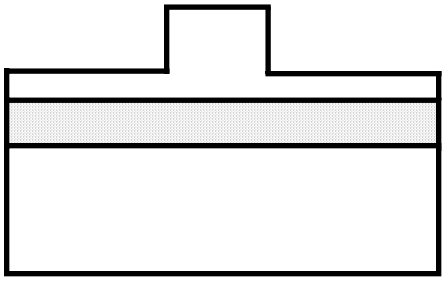

(e)

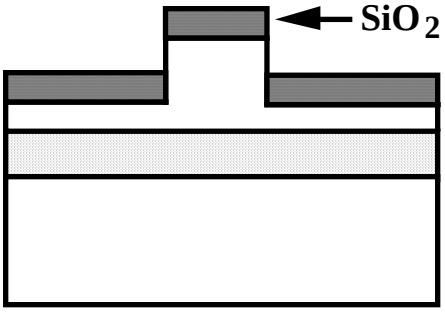

(f)

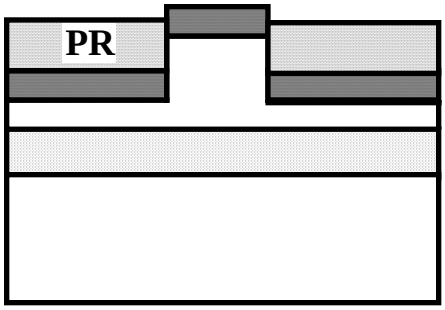

(g)

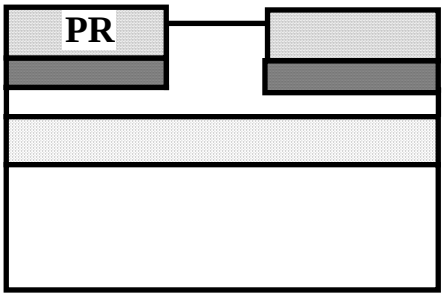

(h)

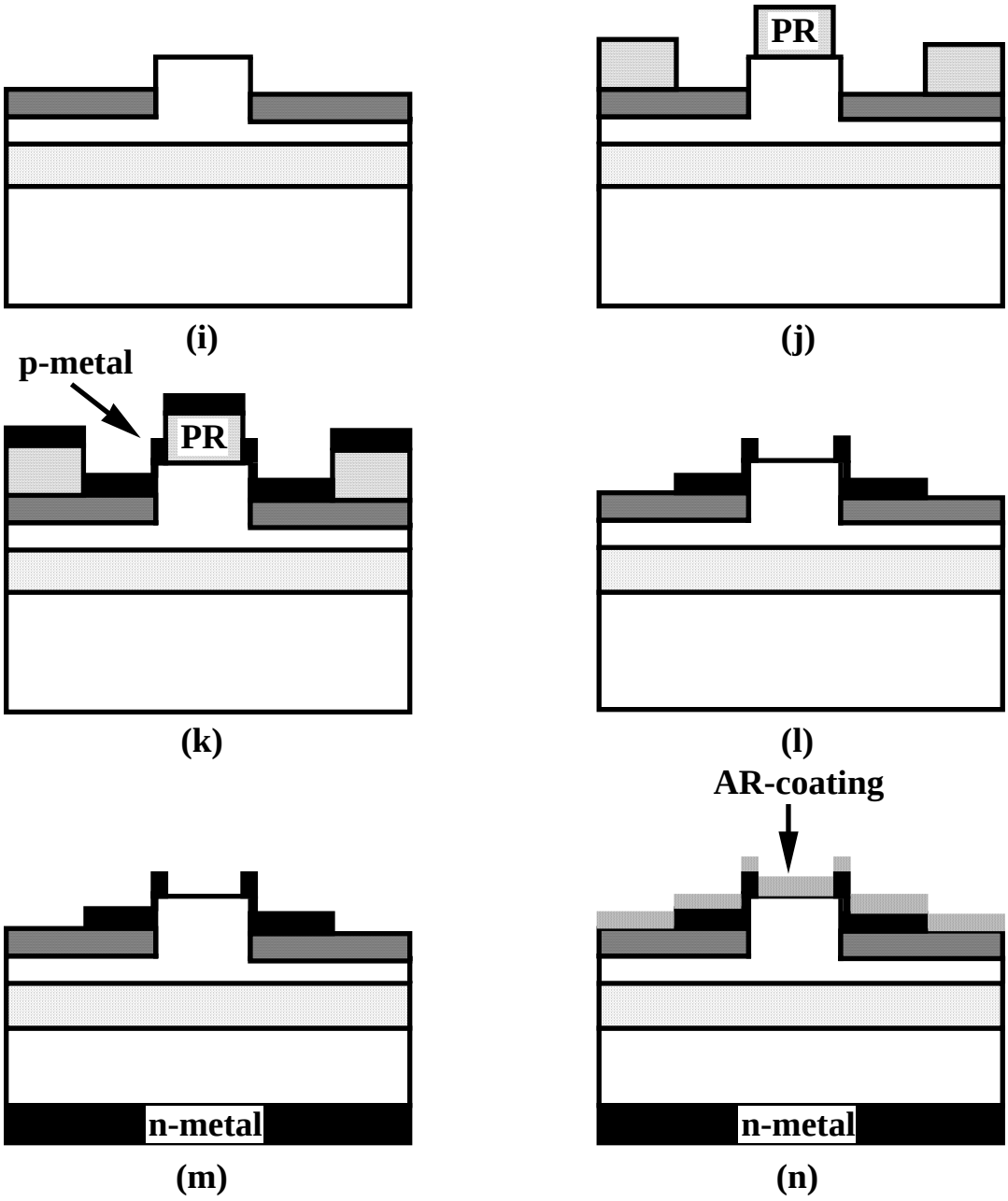

Figure A.4.1 Sketches on device processing procedure.